



Doctoral Thesis

**Study on Intelligent Prediction Models of
Geological Conditions ahead of Tunnel Face using
Measurement-While-Drilling Data**

March 2021

**Graduate School of Engineering
Nagasaki University**

Jiankang Liu

Acknowledgements

I would like to express my gratitude to all those who helped me during my study at Nagasaki University.

My deepest gratitude goes first and foremost to Professor **Yujing Jiang**, my supervisor in the faculty of civil engineering, Nagasaki University, for his kind advice, great guidance and constant support throughout my studies in a master course in China and a doctoral course in Nagasaki University in the last 6 years. Many of the ideas in this thesis would not have taken shape without his incisive thinking and insightful suggestions. What I learned from him will benefit me greatly in the rest of my life.

Second, I am incredibly grateful to thank Professor **Kiyoshi Omine**, Assistant Professor **Satoshi Sugimoto** at Nagasaki University for their generous help and continuous supports during my daily life and research. I would like to express my heartfelt gratitude to Professor **Richeng Liu** at China University of Mining and Technology, for his kind supports and valuable friendship. He was always generous in helping me, and was willing to read my manuscripts and provide useful suggestions. Also, I would like to thank Assistant Professor **Xuezhen Wu** in Fuzhou University, Professor **Wang Gang**, Professor **Lianjun Chen**, Dr. **Hengjie Luan**, Dr. **Xuepeng Zhang**, and Dr. **Bin Gong** in Shandong University of Science and Technology, Assistant Professor **Qiang Zhang** and Assistant Professor **Qian Yin** in China University of Mining and Technology, Assistant Professor **Na Huang** in China University of Petroleum, for their generous help and supports for my research.

Third, I would like to thank my friends in Nagasaki, Dr. **Changsheng Wang**, Mr. **Sodai Ishizu**, Mr. **Osamu Sakaguchi**, Mr. **Ningbo Li**, Mr. **Yuanchao Zhang**, Mr. **Wei Han**, Mr. **Xinshuai Si**, Mr. **Zichen Zhang**, Ms. **Cui Li**, and all others who helped make my stay in Japan an enjoyable one.

Finally, I would like to thank my wife **Minmin Zhao**, who always supported and encouraged me. I also want to thank my other family members, for their everlasting love, patience and support over my entire lifetime.

Jiankang Liu
Nagasaki, Mar. 2021

Abstract

Prediction of geological conditions ahead of tunnel face is one of the main issues that affect the support design and operation cost of tunnel engineering. Inaccurate prediction may cause the failure of support and even lead to irreparable disasters such as water/mud gushing and collapse of a tunnel. Measurement-while-drilling (MWD) technology that are rapidly developed since 1980s have been adopted as one of the effective methodologies to predict the geological conditions of ahead of tunnel face. The prediction results obtained by this technique are objective and direct with high reliability. However, there are still many problems that are not solved when processing the MWD data, due to the numerous uncertainties such as huge data, existence of abnormal values, and the limitation of computing power. This thesis is focused on contributing to three aspects: predictions of tunnel support pattern, rock mass quality score (RQS) and uniaxial compressive strength (UCS), which is based on MWD data using artificial neural network (ANN) and optimized ANN technologies.

First, the feasibility of using specific energy (a composite parameter of the MWD parameter) in the drilling process to evaluate the geological conditions ahead of tunnel face was analyzed and the relationship between specific energy, RQS, tunnel buried depth and tunnel deformation were compared. As indicated by the results, although the geological conditions of the four intervals of the new Nagasaki tunnel (east) are different, the difference between the average values of specific energy of these intervals is not very large, within 100 J/cm^3 . According to the distributions of specific energy, RQS and buried depth with the mileage of this tunnel, it can be observed that certain correlations exist between these items. In addition, a high correlation exists between specific energy and RQS but the feasibility of employing this correlation to evaluate the geological conditions ahead of the tunnel face is limited. Additionally, although the correlation coefficient values obtained are small and widely dispersed, the geological conditions can be evaluated by comparing the correlation coefficient values and the distribution trend of each variable. The results of comparative analysis show that compared with the distribution of buried depth, a high probability of large tunnel deformation occurs in the region with extensive low specific energy values. The specific energy can reflect the strength of rock and the strength state of rock mass. If the distribution of the specific energy in some areas deviates from the distribution of buried depth, it is considered that abnormal geological conditions exist in this area with a higher probability.

Second, ANN models were established to estimate support pattern selection ahead of tunnel face based on MWD data. Controlled trials were conducted considering different input sample sizes and hidden layer sizes. The results show that strong correlation exists between MWD data and support patterns, with the optimal prediction results of the average accuracy values corresponding to six classes of support patterns are 0.884, 0.866,

0.819, 0.742, 0.805 and 0.920, respectively. The prediction performance of ANN is affected by the input sample sizes and the hidden layer sizes. An input sample size greater than 6000 samples and a hidden layer size greater than 30 neurons do not have an optimizing effect on the performance. Additionally, comparative ANN models were established to investigate the influence of different input feature parameters and different hidden layer sizes on the prediction performance. The results indicate that the prediction performance of the ANN is affected by the different input feature parameters and hidden layer sizes. The combination of 6 feature parameters outperforms the subset of the entire feature parameters in terms of average accuracy, sensitivity, and stability. The computing-time increases with the number of feature parameters, there is on huge difference for 2 to 6 feature parameters. A hidden layer size greater than 30 neurons has no optimizing effect on the prediction performance. The sensitivity of the 6 feature parameters is ordered as hammer pressure > feed pressure > hammer frequency > rotation pressure > penetration rate > specific energy.

Finally, optimized ANN models: GA-ANN (genetic algorithm), PSO-ANN (particle swarm optimization) and ICA-ANN (imperialist competition algorithm), regression models: multiple linear regression (MLR) and multiple nonlinear regression (MNR), and ANN models were established to investigate the best prediction model of RQS values. The results show that the developed PSO-ANN and ICA-ANN models have higher accuracy and efficiency than other models. However, among the two hybrid models, PSO-ANN hybrid model has slightly higher performance in predicting RQS. In addition, an optimization algorithm of GA, was employed to develop hybrid model of GA-ANN to estimate the UCS value ahead of tunnel face. To evaluate the prediction performance of the hybrid models, MLR and ANN models were also developed to estimate the UCS. The results indicate that the ANN and GA-ANN models have a high degree of accuracy and efficiency. The hybrid GA-ANN model has slightly higher prediction performance for predicting the UCS compared with other models. The results of $R^2 = 0.881$ and 0.819 , $RMSE = 6.641$ and 8.102 and $VAF = 0.881$ and 0.815 for the training sets and testing sets were obtained for the GA-ANN model, respectively. The findings demonstrate that the GA-ANN model is better than MLR and ANN model. Based on the determined best prediction models of RQS and UCS, comparative tests were carried out for four intervals with different geological conditions. The comparison results show that the prediction performance is affected by geological conditions.

Keywords: Tunnel face; Measurement-while-drilling; Support pattern; Rock mass quality; Uniaxial compressive strength; Artificial neural network; Genetic algorithm; Particle swarm optimization; Imperialist competition algorithm; Multiple linear regression; Multiple nonlinear regression; Machine learning

Contents

ACKNOWLEDGEMENTS.....	I
ABSTRACT.....	II
LIST OF CONTENTS	IV
1 Introduction.....	1
1.1 Background	1
1.1.1 Measurement-while-drilling technology.....	3
1.1.2 Intelligent prediction ahead of tunnel face.....	4
1.2 Objective and thesis structure.....	5
References	7
2 The criterion for evaluating geological conditions ahead of tunnel face based on specific energy	15
2.1 Introduction	15
2.2 Case study.....	17
2.2.1 Description of the new Nagasaki tunnel (east)	17
2.2.2 The deformation.....	21
2.2.3 The specific energy	23
2.2.4 Rock mass quality score of tunnel face.....	26
2.3 Evaluation methods and results	26
2.3.1 Evaluation methods.....	26
2.3.2 Evaluation results and discussion	26
2.4 Conclusions	37
References	38
3 Prediction models of tunnel support patterns using artificial neural network.....	42
3.1 Introduction	42
3.2 Case description	45
3.3 Model development.....	49
3.3.1 The input and output layer sizes	52
3.3.2 The hidden layer sizes.....	52
3.3.3 The learning rate and the momentum term	53
3.4 Results and discussion.....	53
3.5 Conclusions	57
References	58
4 Influence of different combinations of MWD parameters on prediction of tunnel support patterns	67

4.1 Introduction	67
4.2 Data collection.....	69
4.3 Experimental setup.....	73
4.3.1 Basic ANN parameter setting.....	73
4.3.2 Setting of the experiments	74
4.4 Results and discussion.....	75
4.4.1 Performance of ANN with different experimental conditions	75
4.4.2 Sensitivity analysis of each feature parameter	78
4.4.3 Stability of prediction performance	82
4.5 Conclusions	84
References	85
5 Optimized artificial neural network model for predicting of rock mass quality ahead of tunnel face.....	92
5.1 Introduction	92
5.2 Case study and dataset collection	94
5.3 Methods.....	99
5.3.1 Multiple linear/nonlinear regression	99
5.3.2 Artificial neural network.....	100
5.3.3 Genetic algorithm.....	101
5.3.4 Particle swarm optimization	102
5.3.5 Imperialist competition algorithm.....	103
5.4 Determination of prediction models.....	103
5.4.1 Multiple linear regression statistical model	103
5.4.2 Artificial neural network models.....	104
5.4.3 Optimized ANN models by genetic algorithm.....	105
5.4.4 Optimized ANN models by particle swarm optimization	110
5.4.5 Optimized ANN models by imperialist competition algorithm	112
5.5 Results and discussion.....	116
5.6 Conclusion.....	123
References	124
6 Prediction models of unconfined compressive strength ahead of tunnel face using machine learning technology	131
6.1 Introduction	131
6.2 Data collection and regression analysis.....	133
6.2.1 Project description	133
6.2.2 Data collection	134

6.2.3 Regression analysis	136
6.3 Establish prediction models.....	139
6.3.1 Multiple regression	139
6.3.2 Artificial neural network models.....	140
6.3.3 Optimized ANN models by genetic algorithm.....	144
6.3.4 Classification and regression tree models	146
6.4 Results and discussion.....	147
6.5 Conclusions	153
References	154
7 Summaries	165

1 Introduction

1.1 Background

Most of the mountain tunnels need to pass through the fault fracture zone, weak surrounding rock and other complex geological conditions (Roy and Sarkar 2017; Zhong et al. 2020). Under such complex geological conditions, tunnel engineering construction is prone to encounter water inrush, mud burst, landslide and other engineering disasters, resulting in casualties and property losses (Zhao et al. 2013; Wang et al. 2020a). In order to ensure the safety and stability of rock mass in the process of tunnel construction, it is necessary to scientifically design the tunnel support parameters according to the complex conditions ahead of the tunnel face (Oreste 2005; Ramoni and Anagnostou 2011; Oke et al. 2014). Therefore, a rapid and accurate prediction technology of geological conditions and tunnel support patterns is needed to provide a basis for surrounding rock support design of tunnel engineering under complex conditions, so as to solve the problem that the existing mountain tunnel design is based on similar engineering analogy and previous design experience, and can not be designed according to site rock mass characteristics.

The selection of tunnel support patterns heavily relies on the detailed detection of engineering rock mass characteristics (El-Naqa 2001; Marinos et al. 2006; Kaya et al. 2011; Morelli 2015). Under normal conditions, the preliminary design of the support patterns is mainly based on empirical calculations and standardized rock mass classification systems. Due to the uncertainties in the rock mass behavior, the final selection of the support patterns is determined in construction process according to the exposed geological characteristics. The instability of such support patterns often occurs because of the sudden change of geological conditions ahead of the tunnel face (Kontogianni et al. 2004; Li et al. 2012). Rock mass quality and uniaxial compressive strength are important factors to evaluate geological conditions ahead of tunnel face. In recent decades, the most commonly employed rock mass quality assessment system is the rock quality designation (RQD) system (Deere 1964), Norwegian geotechnical institute Q-system (Q) (Barton et al. 1974), rock mass rating (RMR) system (Bieniawski 1973) and geological strength index (GSI) system (Hoek and Brown 1997). In Japan, the Japan Highway Public Corporation (JH) system, which is based on the RMR system, is commonly used to quantitatively evaluate the rock mass quality (Masahiro et al. 1999;

Akagi et al. 2001; Yuji et al. 2006). Similar to other assessment systems (e.g., Q system, RMR system, and GSI system), when the JH system is utilized, the rock mass quality score (RQS), the scores of tunnel face observation items (e.g., compressive strength, weathering, and spacing of joints), is used to evaluate and grade the rock mass quality. Although these proposed assessment systems are extensively employed in rock engineering and tunnel engineering, the objectivity of the evaluation is insufficient due to subjective judgments that are based on the engineer's experience observation items (Palmstrom 2005; Rahmati et al. 2014; Zolfaghari et al. 2015; Wang et al. 2020b). Additionally, laboratory test is commonly used to determine uniaxial compressive strength, which requires field coring to obtain a number of complete core specimens meeting the standard (Karaman et al. 2015; Asem 2020). Coring changes the natural structure and environmental state of rock mass, and cannot directly and accurately characterize the mechanical properties of rock mass (Mišćević and Vlastelica 2014). Due to excavation disturbance, the rock mass in the construction area is relatively broken, which makes coring difficult. At the same time, it takes a lot of time and manpower to transport the complete core specimens from the site to the laboratory and to prepare the standard specimens. However, the commonly used in-situ measurement methods, such as point load method and scratch method, can only approximately determine the uniaxial compressive strength (Suarez-Rivera et al. 2002; Ahmadi Sheshde and Cheshomi 2015; Tripathy et al. 2015).

Measurement-while-drilling (MWD) technology (Schunnesson 1998; Schunnesson et al. 2011; Ghosh et al. 2017b; Van Eldert et al. 2020) is an exploration technology developed rapidly in recent years. This method does not need sampling and can continuously control and real-time monitor MWD parameters (e.g. penetration rate, hammer pressure, rotation pressure) during drilling. Many scholars have carried out laboratory and field tests of digital drilling for different types of rock masses. The test results show that there is an obvious response relationship between MWD parameters and rock mass mechanical parameters (Kahraman et al. 2003; Mostofi et al. 2011). It is proved that it is feasible to predict the geological conditions ahead of tunnel face by MWD data. At the same time, applications of intelligence algorithm (e.g., artificial neural network (ANN), ANN optimization algorithms, and classification and regression tree (CART)) in decision-making and prediction of engineering problems have been attracted substantial interest to various computation sciences and engineering disciplines, since these algorithms have the strong non-linear analysis capabilities and can provide engineers with

scientific methods for optimal decision-making (Caglar and Arman 2007; Sarkar et al. 2010; Gordan et al. 2016; Ozer et al. 2019).

1.1.1 Measurement-while-drilling technology

In tunnel construction, although the site survey including rough prediction of geological conditions ahead of tunnel face is generally carried out, unexpected anomalies (e.g., cavities or water bearing, fractured, or relatively stronger zones) that may influence construction safety often exist (Otto et al. 2002; Ryu et al. 2011; Park et al. 2017; Liu et al. 2018). Such anomalies can be detected by MWD technology (Schunnesson 1997), which records the data information of operational parameters involved in drilling. For rotary drilling, Teale (1965) defined the concept of specific energy (SE) as the energy required to excavate unit volume of rock. Rabia (1985) compared different bit selections based on both cost per foot and SE and presented a simplified approach to bit selection that uses the principle of SE. Zhou et al. (2011) proposed an adaptive unsupervised approach based on MWD data to estimate the rock types and demonstrated that the proposed approach has a satisfactory performance in identification of rock types by experiments on actual data. Leung and Scheduling (2015) proposed a novel measure called modulated specific energy (SEM) for characterizing drilled material in open-pit coal mining, which can overcome the problems of low specificity and high variability observed in existing MWD approaches. Khorzoughi et al. (2018) correlated drill performance variables (MWD parameters) with measured fracture logs and identified that drill performance variables can accurately determine open versus closed fractures. In relation to studies developed for percussive and rotary-percussive drilling, Aoki et al. (1999) reported that a drill logging system had been developed in 1995 to evaluate the ground conditions at various depths by the data obtained while boring through the rock with a hydraulic drill. Yue et al. (2004) presented a methodology for identifying zones of volcanic weathering and decomposition grades in the ground through the MWD data monitored from rotary-percussive drilling. Factual data showed that the penetration rate parameter had a close correlation with decomposition grades in the ground. Peng et al. (2005) and Tang (2006) investigated the characteristics of void/fracture and the rock mass properties in roof rocks. The clear correlation between such geological properties and drilling parameters was confirmed. They found that the feed pressure can be used to detect the anomalies or discontinuities in the rock and to estimate the rock mass strength.

Laudanski et al. (2012) evaluated the drilling measurements individually as well as combined into compound parameters to further enhance the ability of MWD to identify strata characteristics. It demonstrated that MWD can clearly provide qualitative evaluation of soil types, density and permeability using both rotary and percussion drilling methods. Ghosh et al. (2015) used MWD data to evaluate data trends among logged parameters and calculated average SE. They found that the prediction of SE through penetration rate and feed force was affected greatly by the hole length. From the correlation of MWD data with rock mass geo-mechanical features, Ghosh et al. (2017a) suggested a method for distinguishing solid rock, fracture zones, cavities and damaged rock, based on the responses from the drill monitoring system. Navarro et al. (2018) investigated the mutual relation between MWD parameters. They determined that the feed pressure is a lead parameter that drives the adjustment of other parameters. The MWD method is usually implemented to quantify and visualize the geological conditions ahead of the tunnel face, yet it still needs further exploration and in-depth study on the fast prediction of support patterns and rock mechanical parameters based on MWD data.

1.1.2 Intelligent prediction ahead of tunnel face

In the last few years, intelligence algorithms (e.g., ANN, ANN optimization algorithms, and CART) have been proved to be a powerful tool to settle geotechnical engineering problems (Alimoradi et al. 2008; Ocaik and Seker 2012; Hasanipanah et al. 2017; Khandelwal et al. 2017; Esmailzadeh et al. 2018; Salimi et al. 2018). Kanamoto et al. (2005) and Kimura et al. (2005) accurately estimated the different rock mass rating of a part of one tunnel using ANN based on partial MWD parameters. Mahdevari and Torabi (2012) developed a method based on ANN for prediction of convergence in tunnels and carried out a correlation analysis of the convergence data sets with geo-mechanical and geological parameters. They determined that cohesion, internal friction angle, Young's modulus and uniaxial compressive strength are the most effective factors and uniaxial tensile strength is the least effective one. Ghorbani and Firouzi Niavol (2017) applied ANN and evolutionary polynomial regressions to propose a method which can accurately reflect both static and coupled static-dynamic settlements. Ghorbani et al. (2018) used two different classes of ANNs to estimate the prediction of the support pressure of circular tunnels in elasto-plastic, strain-softening rock mass. Xu et al. (2007) used a back-propagation neural network to assess the rock mass quality. The RMR values were

estimated by Hussain et al. (2016), who compared ANN technology with multiple regression technology. Karlaftis (2018) proposed an ANN model to classify rock masses using data from tunnels in Greece. The results demonstrated that the ANN can place a rock mass in the classification ratings very quickly and with very high accuracy with a smaller number of input variables. According to the research of Meulenkamp and Grima (1999), in contrast to the statistical regression analysis, the UCS value predicted by artificial neural network (ANN) is not force to be the average value, so the existing variance of measurement data can be retained and employed. ANN is one of the most innovative research fields in the field of science and engineering, with strong nonlinear mapping ability. However, slow learning speed and easy to fall into local minima are some defects of ANN (Armaghani et al. 2018; Armaghani et al. 2019). Applications of population-based evolutionary algorithms, such as genetic algorithm (GA), particle swarm optimization (PSO) and imperialist competitive algorithm (ICA), are helpful to overcome these shortcomings. Using these algorithms to optimize artificial neural network can solve complex engineering problems and become a research hotspot (Hasanipanah et al. 2017; Khandelwal et al. 2017; Liu et al. 2020).

1.2 Objective and thesis structure

The objective of this thesis is to investigate the predication performance of geological conditions and support pattern ahead of tunnel face using intelligent algorithm based on MWD data. The outline of this thesis is shown in Fig. 1.1.

Chapter 1 gives a brief introduction of the background, the objective and the structure of this thesis.

In Chapter 2, a comparative analysis is conducted on the relationship among specific energy, rock mass quality score (RQS, an index used in Japan to evaluate the quality of tunnel rock mass), buried depth of the tunnel, and tunnel deformation. The criterion of the evaluation of the geological conditions ahead of the tunnel face is proposed based on this comparative analysis.

In Chapter 3, the feasibility of using ANN based on MWD data to predict the support patterns ahead of tunnel face is investigated. Contrast models with different input sample sizes and different ANN structures are developed to analyze the influence of the number of input sample and the hidden layer nodes on prediction performance. The input sample sizes and topological structure of the best ANN model used to predict the support patterns

are proposed.

In Chapter 4, the ANN model was used to predict the support patterns ahead of the tunnel face based on the MWD data. The effects of all possible combinations of different MWD parameters on the prediction performance are investigated. The sensitivity of each MWD parameter to the prediction performance of the ANN is compared. The stability of the prediction performance of the superior ANN models are analyzed as well. Finally, the ANN model with optimal prediction performance is proposed.

Chapter 5 propose three hybrid ANN models, including GA-ANN, PSO-ANN and ICA-ANN, to predict the RQS (a rock mass quality index used in Japan) using the MWD data obtained from the new Nagasaki tunnel (east) of the West Kyushu line of the high-speed railway project in Japan. A conventional regression model and simple ANN model are developed. Three hybrid ANNs are established and compared with the developed regression model and ANN model. Through comparative analysis, the best model to predict RQS value is determined. Based on the determined best model, comparative tests are carried out for four intervals with different geological conditions, and the influence of geological conditions on prediction performance is investigated.

In Chapter 6, the feasibility analysis of using WMD data to predict the UCS of rock mass ahead of tunnel face is conducted. For this purpose, the correlation among MWD parameters and the correlation between MWD parameters and UCS are investigated. And, a machine learning method: ANN, GA-ANN, and CART, to predict of UCS utilizing the MWD data is proposed. As a contrast, the traditional multiple linear/nonlinear regressions models are developed to evaluate the prediction performance of machine learning models. Through comparative analysis, the best model to predict UCS value is determined. The influence of geological conditions on prediction performance is investigated.

Chapter 7 summarizes the major conclusions obtained from the studies of this thesis.

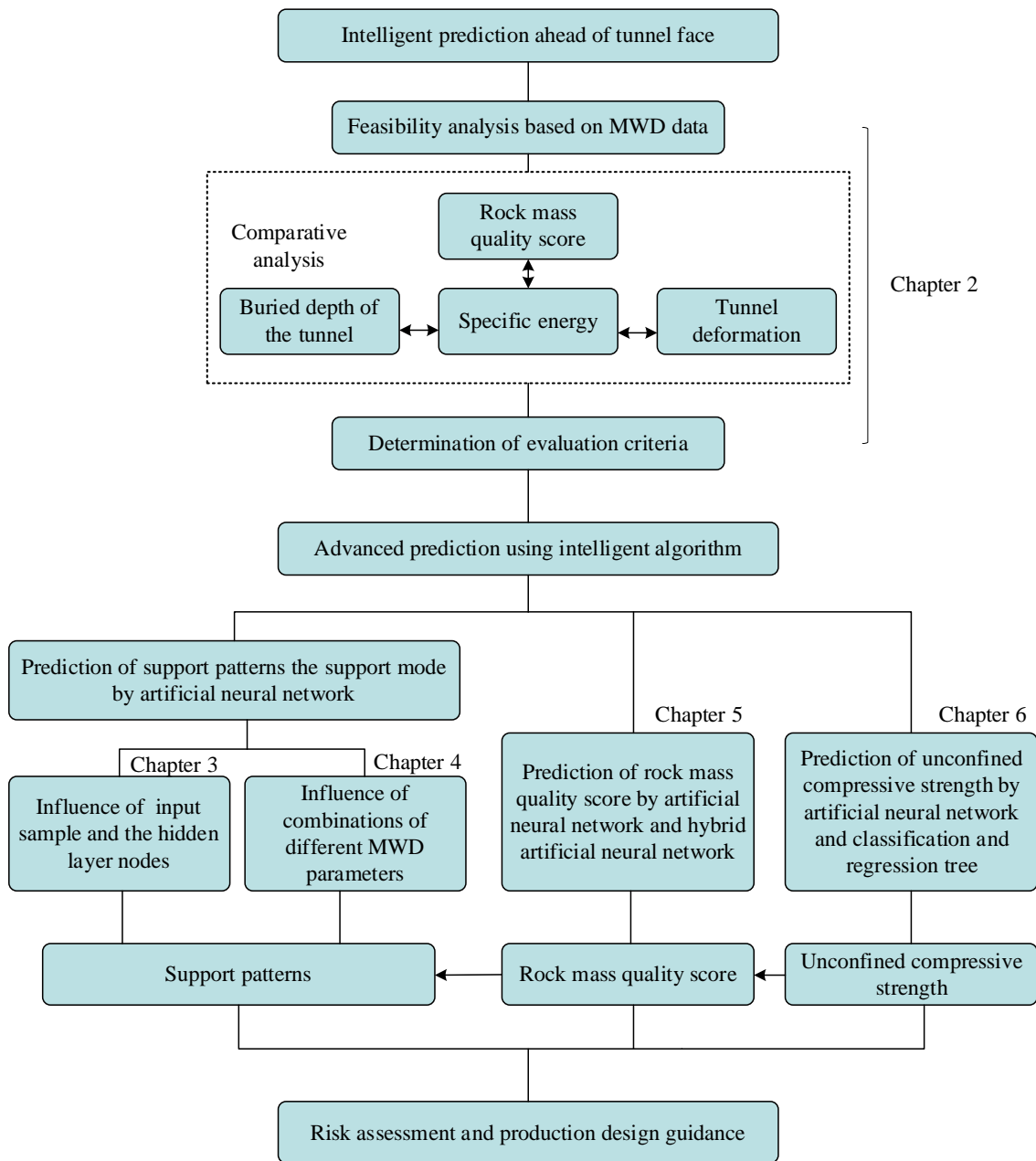


Fig. 1.1 Thesis structure

References

- Ahmadi Sheshde E, Cheshomi A (2015), New method for estimating unconfined compressive strength (UCS) using small rock samples. *Journal of Petroleum Science and Engineering*, 133:367-375. <https://doi.org/10.1016/j.petrol.2015.06.022>
- Akagi W, Sano A, Shinji M, Nishi T, Nakagawa K (2001), A new rock mass classification

- method at tunnel face for tunnel support system. *Doboku Gakkai Ronbunshu*, 2001:121-134. (In Japanese)
- Alimoradi A, Moradzadeh A, Naderi R, Salehi MZ, Etemadi A (2008), Prediction of geological hazardous zones in front of a tunnel face using TSP-203 and artificial neural networks. *Tunn Undergr Space Technol*, 23:711-717. <https://doi.org/10.1016/j.tust.2008.01.001>
- Aoki K, Shirasagi S, Yamamoto T, Inou M, Nishioka K (1999), Examination of the application of drill Logging to predict ahead of the tunnel face. In: *Proceedings of the 54th Annual Conference of the Japan Society of Civil Engineers*, Tokyo, Japan, September 1999. pp 412-413. (In Japanese)
- Armaghani DJ, Hasanipanah M, Mahdiyar A, Abd Majid MZ, Bakhshandeh Amnieh H, Tahir MMD (2018), Airblast prediction through a hybrid genetic algorithm-ANN model. *Neural Computing and Applications*, 29:619-629. <https://doi.org/10.1007/s00521-016-2598-8>
- Armaghani DJ, Koopialipour M, Marto A, Yagiz S (2019), Application of several optimization techniques for estimating TBM advance rate in granitic rocks. *J Rock Mech Geotech Eng*, 11:779-789. <https://doi.org/10.1016/j.jrmge.2019.01.002>
- Asem P (2020), Prediction of unconfined compressive strength and deformation modulus of weak argillaceous rocks based on the standard penetration test. *Int J Rock Mech Min Sci*, 133:104397. <https://doi.org/10.1016/j.ijrmms.2020.104397>
- Barton N, Lien R, Lunde J (1974), Engineering classification of rock masses for the design of tunnel support. *Rock mechanics*, 6:189-236. <https://doi.org/10.1007/bf01239496>
- Bieniawski Z (1973), Engineering classification of jointed rock masses. *Civil Engineer in South Africa*, 15
- Caglar N, Arman H (2007), The applicability of neural networks in the determination of soil profiles. *Bull Eng Geol Environ*, 66:295-301. [10.1007/s10064-006-0075-9](https://doi.org/10.1007/s10064-006-0075-9)
- Deere DU (1964), Technical description of rock cores for engineering purpose. *Rock Mechanics and Engineering Geology*, 1:17-22.
- El-Naqa A (2001), Application of RMR and Q geomechanical classification systems along the proposed Mujib Tunnel route, central Jordan. *Bull Eng Geol Environ*, 60:257-269.

- Esmailzadeh A, Mikaeil R, Shafei E, Sadegheslam G (2018), Prediction of rock mass rating using TSP method and statistical analysis in Semnan Rooziyeh spring conveyance tunnel. *Tunn Undergr Space Technol*, 79:224-230. <https://doi.org/10.1016/j.tust.2018.05.001>
- Ghorbani A, Firouzi Niavol M (2017), Evaluation of induced settlements of piled rafts in the coupled static-dynamic loads using neural networks and evolutionary polynomial regression. *Applied Computational Intelligence and Soft Computing*, 2017
- Ghorbani A, Hasanzadehshooiili H, Sadowski Ł (2018), Neural prediction of tunnels' support pressure in elasto-plastic, strain-softening rock mass. *Applied Sciences*, 8:841.
- Ghosh R, Danielsson M, Gustafson A, Falksund H, Schunnesson H (2017a), Assessment of rock mass quality using drill monitoring technique for hydraulic ITH drills. *Int J Min Miner Process Eng*, 8:169-186.
- Ghosh R, Danielsson M, Gustafson A, Falksund H, Schunnesson H (2017b), Assessment of rock mass quality using drill monitoring technique for hydraulic ITH drills. 8:169-186. 10.1504/ijmme.2017.085830
- Ghosh R, Schunnesson H, Kumar U (2015), The use of specific energy in rotary drilling: the effect of operational parameters. In: *Proceedings of the 37th International Symposium, May 2015. Application of Computers and Operations Research in the Mineral Industry*. pp 713-723.
- Gordan B, Jahed Armaghani D, Hajihassani M, Monjezi M (2016), Prediction of seismic slope stability through combination of particle swarm optimization and neural network. *Eng Comput*, 32:85-97. <http://10.1007/s00366-015-0400-7>
- Hasanipanah M, Jahed Armaghani D, Bakhshandeh Amnieh H, Majid MZA, Tahir MMD (2017), Application of PSO to develop a powerful equation for prediction of flyrock due to blasting. *Neural Computing Applications*, 28:1043-1050. <https://doi.org/10.1007/s00521-016-2434-1>
- Hoek E, Brown ET (1997), Practical estimates of rock mass strength. *Int J Rock Mech Min Sci*, 34:1165-1186. [https://doi.org/10.1016/S1365-1609\(97\)80069-X](https://doi.org/10.1016/S1365-1609(97)80069-X)
- Hussain S, Mohammad N, Khan M, Rehman ZU, Tahir M (2016), Comparative analysis of rock mass rating prediction using different inductive modeling techniques. *International Journal of Mining Engineering Mineral Processing*, 5:9-15.
- Kahraman S, Bilgin N, Feridunoglu C (2003), Dominant rock properties affecting the

- penetration rate of percussive drills. *Int J Rock Mech Min Sci*, 40:711-723. [https://doi.org/10.1016/S1365-1609\(03\)00063-7](https://doi.org/10.1016/S1365-1609(03)00063-7)
- Kanamoto T, Ohnishi Y, Nishiyama S, Uehara S, Kimura T, Yamashita M (2005), Study on application of neural network to evaluation of geological condition using drilling survey system. Paper presented at the Proceedings of the 60th JSCE Annual Meeting, 2005.
- Karaman K, Cihangir F, Ercikdi B, Kesimal A, Demirel S (2015), Utilization of the Brazilian test for estimating the uniaxial compressive strength and shear strength parameters. *J South Afr Inst Min Metall*, 115:185-192.
- Karlaftis A (2018), Classifying rock masses using artificial neural networks. In: *Geoecology and Computers*. Routledge, pp 279-284.
- Kaya A, Bulut F, Sayin A (2011), Analysis of support requirements for a tunnel portal in weak rock: A case study from Turkey. *Scientific Research and Essays*, 6:6566-6583.
- Khandelwal M, Mahdiyar A, Armaghani DJ, Singh TN, Fahimifar A, Faradonbeh RS (2017), An expert system based on hybrid ICA-ANN technique to estimate macerals contents of Indian coals. *Environmental Earth Sciences*, 76:399. <https://doi.org/10.1007/s12665-017-6726-2>
- Khorzoughi MB, Hall R, Apel D (2018), Rock fracture density characterization using measurement while drilling (MWD) techniques. *International Journal of Mining Science and Technology*, 28:859-864. <https://doi.org/10.1016/j.ijmst.2018.01.001>
- Kimura T, Ohnishi Y, Nishiyama S, Ishiyama K (2005), Study on prediction ahead of tunnel face by using drilling survey method. *Geoinformatics*, 16:191.
- Kontogianni V, Tzortzis A, Stiros S (2004), Deformation and failure of the Tymfristos tunnel, Greece. *J Geotech Geoenviron Eng*, 130:1004-1013.
- Laudanski G, Reiffsteck P, Tacita J, Desanneaux G, Benoît J (2012), Experimental study of drilling parameters using a test embankment. In: *Proceedings of the Fourth International Conference on Geotechnical and Geophysical Site Characterization, Pernambuco, Brazil, September 2012*. CRC Press Porto de Galinhas-Pernambuco, pp 435-440.
- Leung R, Scheduling S (2015), Automated coal seam detection using a modulated specific energy measure in a monitor-while-drilling context. *Int J Rock Mech Min Sci*, 75:196-209. <https://doi.org/10.1016/j.ijrmms.2014.10.012>

- Li L et al. (2012), Spatial deformation mechanism and load release evolution law of surrounding rock during construction of super-large section tunnel with soft broken surrounding rock masses. *Chin J Rock Mech Eng*, 10:2109-2118.
- Liu B, Chen L, Li S, Xu X, Liu L, Song J, Li M (2018), A new 3D observation system designed for a seismic ahead prospecting method in tunneling. *Bull Eng Geol Environ*, 77:1547-1565. [10.1007/s10064-017-1131-3](https://doi.org/10.1007/s10064-017-1131-3)
- Liu J, Luan H, Zhang Y, Sakaguchi O, Jiang Y (2020), Prediction of unconfined compressive strength ahead of tunnel face using Measurement-While-Drilling data based on hybrid genetic algorithm. *Geotech Eng*, 22 <https://doi.org/10.12989/gae.2020.22.1.000>
- Mahdevari S, Torabi SR (2012), Prediction of tunnel convergence using artificial neural networks. *Tunn Undergr Space Technol*, 28:218-228. <https://doi.org/10.1016/j.tust.2011.11.002>
- Marinos P, Hoek E, Marinos V (2006), Variability of the engineering properties of rock masses quantified by the geological strength index: the case of ophiolites with special emphasis on tunnelling. *Bull Eng Geol Environ*, 65:129-142. <http://10.1007/s10064-005-0018-x>
- Masahiro N, Koji M, Hiroshi Y, Takuro N, Kazuo N, Koji N (1999), A New Proposal of Evaluation System for Tunnel Face Based on the Analysis of the Observation Records. *Journal of Japan Society of Civil Engineers*, 623:131-141.
- Meulenkamp F, Grima MA (1999), Application of neural networks for the prediction of the unconfined compressive strength (UCS) from Equotip hardness. *Int J Rock Mech Min Sci*, 36:29-39. [https://doi.org/10.1016/S0148-9062\(98\)00173-9](https://doi.org/10.1016/S0148-9062(98)00173-9)
- Miščević P, Vlastelica G (2014), Impact of weathering on slope stability in soft rock mass. *Journal of Rock Mechanics Geotechnical Engineering*, 6:240-250.
- Morelli GL (2015), Variability of the GSI index estimated from different quantitative methods. *Geotech Geol Eng*, 33:983-995. <http://10.1007/s10706-015-9880-x>
- Mostofi M, Rasouli V, Mawuli E (2011), An estimation of rock strength using a drilling performance model: a case study in blacktip field, Australia. *Rock mechanics rock engineering*, 44:305.
- Navarro J, Sanchidrian JA, Segarra P, Castedo R, Paredes C, Lopez LM (2018), On the mutual relations of drill monitoring variables and the drill control system in tunneling

- operations. *Tunn Undergr Space Technol*, 72:294-304.
<https://doi.org/10.1016/j.tust.2017.10.011>
- Ocak I, Seker SE (2012), Estimation of elastic modulus of intact rocks by artificial neural network. *Rock Mech Rock Eng*, 45:1047-1054. <http://10.1007/s00603-012-0236-z>
- Oke J, Vlachopoulos N, Marinos V (2014), Umbrella Arch Nomenclature and Selection Methodology for Temporary Support Systems for the Design and Construction of Tunnels. *Geotech Geol Eng*, 32:97-130. 10.1007/s10706-013-9697-4
- Oreste P (2005), A probabilistic design approach for tunnel supports. *Comput Geotech*, 32:520-534. <https://doi.org/10.1016/j.compgeo.2005.09.003>
- Otto R, Button E, Bretterebner H, Schwab P (2002), The application of TRT-true reflection tomography-at the Unterwald Tunnel. *Felsbau*, 20:51-56.
- Ozer U, Karadogan A, Ozyurt MC, Sahinoglu UK, Sertabipoglu Z (2019), Environmentally sensitive blasting design based on risk analysis by using artificial neural networks. *Arabian J Geosci*, 12:60. 10.1007/s12517-018-4218-7
- Palmstrom A (2005), Measurements of and correlations between block size and rock quality designation (RQD). *Tunn Undergr Space Technol*, 20:362-377.
<https://doi.org/10.1016/j.tust.2005.01.005>
- Park J, Lee KH, Kim BK, Choi H, Lee IM (2017), Predicting anomalous zone ahead of tunnel face utilizing electrical resistivity: II. Field tests. *Tunn Undergr Space Technol*, 68:1-10. <https://doi.org/10.1016/j.tust.2017.05.017>
- Peng S, Tang D, Sasaoka T, Luo Y, Finfinger G, Wilson G (2005), A method for quantitative void/fracture detection and estimation of rock strength for underground mine roof. In: *Proceedings of 24th International Conference on Ground Control in Mining*, Morgantown, USA, August 2005. pp 195-197.
- Rabia H (1985), Specific energy as a criterion for bit selection. *Journal of petroleum technology*, 37:1,225-221,229.
- Rahmati A, Faramarzi L, Sanei M (2014), Development of a new method for RMR and Q classification method to optimize support system in tunneling. *Frontiers of Structural Civil Engineering*, 8:448-455. <https://doi.org/10.1007/s11709-014-0262-x>
- Ramoni M, Anagnostou G (2011), The Interaction Between Shield, Ground and Tunnel Support in TBM Tunnelling Through Squeezing Ground. *Rock Mech Rock Eng*, 44:37-61. 10.1007/s00603-010-0103-8

- Roy N, Sarkar R (2017), A review of seismic damage of mountain tunnels and probable failure mechanisms. *Geotechnical Geological Engineering*, 35:1-28.
- Ryu HH, Cho GC, Yang SD, SHIN HK (2011), Development of tunnel electrical resistivity prospecting system and its applicaton. *Geoelectric Monitoring*:179.
- Salimi A, Faradonbeh RS, Monjezi M, Moormann C (2018), TBM performance estimation using a classification and regression tree (CART) technique. *Bull Eng Geol Environ*, 77:429-440. 10.1007/s10064-016-0969-0
- Sarkar K, Tiwary A, Singh TN (2010), Estimation of strength parameters of rock using artificial neural networks. *Bull Eng Geol Environ*, 69:599-606. 10.1007/s10064-010-0301-3
- Schunnesson H (1997), Drill process monitoring in percussive drilling for location of structural features, lithological boundaries and rock properties, and for drill productivity evaluation. Dissertation, Luleå tekniska universitet.
- Schunnesson H (1998), Rock characterisation using percussive drilling. *Int J Rock Mech Min Sci*, 35:711-725. [https://doi.org/10.1016/S0148-9062\(97\)00332-X](https://doi.org/10.1016/S0148-9062(97)00332-X)
- Schunnesson H, Elsrud R, Rai P (2011), Drill monitoring for ground characterization in tunnelling operations. Paper presented at the International Symposium on Mine Planning and Equipment Selection : 12/10/2011 - 14/10/2011, 2011.
- Suarez-Rivera R, Stenebråten J, Dagrain F (2002), Continuous Scratch Testing on Core Allows Effective Calibration of Log-Derived Mechanical Properties for Use in Sanding Prediction Evaluation. Paper presented at the SPE/ISRM Rock Mechanics Conference, Irving, Texas, January 2002.
- Tang X (2006), Development of real time roof geology detection system using drilling parameters during roof bolting operation. Dissertations, West Virginia University.
- Teale R (1965), The concept of specific energy in rock drilling. In: *International Journal of Rock Mechanics and Mining Sciences & Geomechanics Abstracts*, 1965. vol 1. Elsevier, pp 57-73.
- Tripathy A, Singh TN, Kundu J (2015), Prediction of abrasiveness index of some Indian rocks using soft computing methods. *Measurement*, 68:302-309. <https://doi.org/10.1016/j.measurement.2015.03.009>
- Van Eldert J, Schunnesson H, Saiang D, Funehag J (2020), Improved filtering and normalizing of Measurement-While-Drilling (MWD) data in tunnel excavation. *Tunn*

- Undergr Space Technol, 103:103467. <https://doi.org/10.1016/j.tust.2020.103467>
- Wang X, Lai J, Qiu J, Xu W, Wang L, Luo Y (2020a), Geohazards, reflection and challenges in mountain tunnel construction of China: a data collection from 2002 to 2018. *Geomatics, Natural Hazards Risk*, 11:766-784.
- Wang X, Yuan W, Yan Y, Zhang X (2020b), Scale effect of mechanical properties of jointed rock mass: A numerical study based on particle flow code. *Geotech Eng*, 21:259-268.
- Xu J, Wang J, Ma Y (2007), Rock mass quality assessment based on BP artificial neural network (ANN) A case study of borehole BS03 in Jiujing segment of Beishan, Gansu. *Uranium Geology*, 23:243,249-256.
- Yue ZQ, Lee CF, Law KT, Tham LG (2004), Automatic monitoring of rotary-percussive drilling for ground characterization—illustrated by a case example in Hong Kong. *Int J Rock Mech Min Sci*, 41:573-612. <https://doi.org/10.1016/j.ijrmms.2003.12.151>
- Yuji W, Tatsuo K, Masaki K, Kenichi H (2006), Solution with modified perceptron to tunnel cutting face evaluation problems. *Geoinformatics*, 17:61-70.
- Zhao Y, Li P, Tian S (2013), Prevention and treatment technologies of railway tunnel water inrush and mud gushing in China. *J Rock Mech Geotech Eng*, 5:468-477. <https://doi.org/10.1016/j.jrmge.2013.07.009>
- Zhong Z, Wang Z, Zhao M, Du X (2020), Structural damage assessment of mountain tunnels in fault fracture zone subjected to multiple strike-slip fault movement. *Tunn Undergr Space Technol*, 104:103527. <https://doi.org/10.1016/j.tust.2020.103527>
- Zhou H, Hatherly P, Ramos F, Nettleton E An adaptive data driven model for characterizing rock properties from drilling data. In: 2011 IEEE International Conference on Robotics and Automation, Shanghai, China, May 2011. IEEE, pp 1909-1915.
- Zolfaghari A, Sohrabi Bidar A, Maleki Javan MR, Haftani M, Mehinrad A (2015), Evaluation of rock mass improvement due to cement grouting by Q-system at Bakhtiary dam site. *Int J Rock Mech Min Sci*, 74:38-44. <https://doi.org/10.1016/j.ijrmms.2014.12.004>

2 The criterion for evaluating geological conditions ahead of tunnel face based on specific energy

2.1 Introduction

Evaluation of geological conditions ahead of a tunnel face is of major importance for safe and economic tunnel building (Lee et al. 2009; Djogo et al. 2011; Mahdevari and Torabi 2012). The inaccurate evaluation of geological conditions may lead to the failure of the support design, which will significantly reduce the safety of tunnel construction and operation, and even bring irreparable disaster such as water and mud gushing (Lu and Liu 2009; Gong et al. 2013; Li et al. 2017b) and sudden collapse of tunnel (Shin et al. 1999; Chen et al. 2012; Li et al. 2014). Consequently, detection of weak zones and other geological features affecting the construction work ahead of the tunnel face is highly desirable (Janda et al. 2018).

The purpose of detection ahead of a tunnel face is to avoid unexpected collapses at a tunnel face. Conventional horizontal boring conducted from a tunnel face can detect weak zones directly. However, it is time-consuming and often interferes with tunneling works (Li et al. 2017a; Bu et al. 2019). Geophysical methods can also offer several principal possibilities to achieve this goal. One of them is seismic imaging ahead of a tunnel face, which is based on vertical seismic profiling (Swinnen et al. 2007; Tzavaras et al. 2012; Bellino et al. 2013). This method has been developed in the field of hydrocarbon exploration and uses seismic wave fields generated by surface sources and observed by geophone arrays in boreholes (Dix 1952; Robertson and Pritchett 1985; Stewart et al. 2002). Tunnel Seismic Prediction (TSP), the first technique for searching ahead of a tunnel face using seismic reflection, was proposed by Sattel et al. (1996) in 1996. This technique was introduced in Japan, and various application tests have been carried out by Inaba et al. (1996), KASA et al. (1996) and Yamamoto et al. (2011). Several drawbacks were pointed out, such as that the strike of the strata must be assumed, and small variations in analytical accuracy appear from person to person and based on experience. Additionally, in order to simplify the analysis, the results obtained are still two-dimensional, and only the reflection surface on the tunnel line is generated. On the other hand, a three-dimensional seismic image was created by Ashida (2001) to interpret the

image of reflector planes using the equi-travel time plane algorithm. Furthermore, the required precision was improved by using seismic signals from three-component geophones in the tunnel. However, a great amount of boring is required with these methods for probing ahead of a tunnel face due to the fact that they involve special blasting work and geophone installation. Not only does the continuous measurement have to be carried out when the excavation work is interrupted, but also a great quantity of time for preparation and analysis is required.

In recent decades, advanced measure-while-drilling (MWD) technology has been rapidly developed to create the opportunities to assess the geological conditions ahead of a tunnel face in broad tunneling projects (Schunnesson 1996; Sugawara et al. 2003; Høien and Nilsen 2014; Galende-Hernández et al. 2018). The MWD technology can therefore be considered as a robust technique for detailed characterizing of large rock masses provided that the raw data are treated properly and effective analysis is applied. In geological engineering, many researchers have carried out the study of evaluating geological conditions by MWD technology. For example, the MWD system was first developed by Aoki et al. (1999) in 1995 to evaluate the geological conditions at various ground depths by the data obtained while boring through the rock with a hydraulic drill. A methodology was presented by Yue et al. (2004) to identify zones of volcanic weathering and decomposition grades in the ground through the MWD data monitored from rotary percussive drilling. Results showed that the penetration rate parameter had a close correlation with decomposition grades in the ground. As a composite MWD parameter, specific energy was proposed by Teale (1965) to correlate drill performance parameters in rotary drilling. Drilling monitoring devices installed on the drilling rigs provide systematic records of the main drilling parameters (e.g., penetration rate, hammer pressure, rotation pressure, hammer frequency) from which the specific energy can be easily derived and expressed in terms of the mechanical energy necessary to drill a determined volume of rock (J/cm^3). Leung and Scheduling (2015) proposed a novel measure called modulated specific energy for characterizing drilled material in open-pit coal mining, which can overcome the problems of low specificity and high variability observed in existing MWD approaches. Celada et al. (2009) found that the values of specific energy can be correlated with the main quality indexes as rock mass rating. Laboratory tests also have been carried out measuring uniaxial compressive strength, Young's modulus, and obtained results indicating that the relationship exists between the specific energy of drilling and these rock mechanical parameters. As the result of onsite

applications of the MWD technology the obtained indices have been validated to be reliable for evaluating geological conditions. However, due to the complexity of analyzing and processing the MWD data, the existing methods of utilizing specific energy to evaluate geological conditions ahead of tunnel face have limited practical guidance for onsite applications.

To the authors' knowledge, little research on the relationship between the specific energy of the mechanical drilling rig in the region ahead of the tunnel face derived from MWD data, rock mass quality index, buried depth of the tunnel, and tunnel deformation has been reported, if any. In this study, a new method was proposed to evaluate the geological conditions ahead of a tunnel face based on the comparative analysis of the relationship among specific energy, rock mass quality score (RQS, an index used in Japan to evaluate the quality of tunnel rock mass), buried depth of the tunnel, and tunnel deformation. The measurement of the specific energy, RQS, buried depth, and tunnel deformation were firstly carried out with the excavation of a tunnel, and then the correlations among these measurement data were subsequently compared and analyzed. Finally, the criterion for evaluating geological conditions ahead of the tunnel face was determined. The proposed method can contribute to the accurate and effective evaluation of the geological conditions ahead of the tunnel face.

2.2 Case study

2.2.1 *Description of the new Nagasaki tunnel (east)*

Many mountains exist in Japan. The construction cost will increase when building a highway or railway bypass the mountains. Therefore, quantities of tunnels are inevitably required for the construction of a highway or railway. Unpredictable geological conditions such as water inrush, mud inrush, and cavity are abundant in mountain tunnels, especially in the south of Japan. The case study was carried out on the new Nagasaki tunnel of West Kyushu Line with a total length of 7.46 km. Its construction was started in March 2013, and it connects the cities of Nagasaki and Isahaya in the southeast and center of Nagasaki province, respectively. As shown in Fig. 2.1, this tunnel has been designed and built with two phases, east and west phases, with lengths of 3.885 and 3.575 km, respectively. The shape of the tunnel is a horseshoe with 9.3 m height and 10.4 m width. For the both east and west phases of the tunnel, the New Austrian Tunneling Method was

used. The excavation of the new Nagasaki tunnel (east) was completed in 2017, and the data measured from this tunnel were used for the analysis and research of this study. The stratum that this tunnel passes through is volcanic rock. The rock type is roughly pyroxene andesite. The geological conditions of the surrounding rock of this tunnel are not very good, with the elastic wave velocity of 2.5–3.5 km/sec.

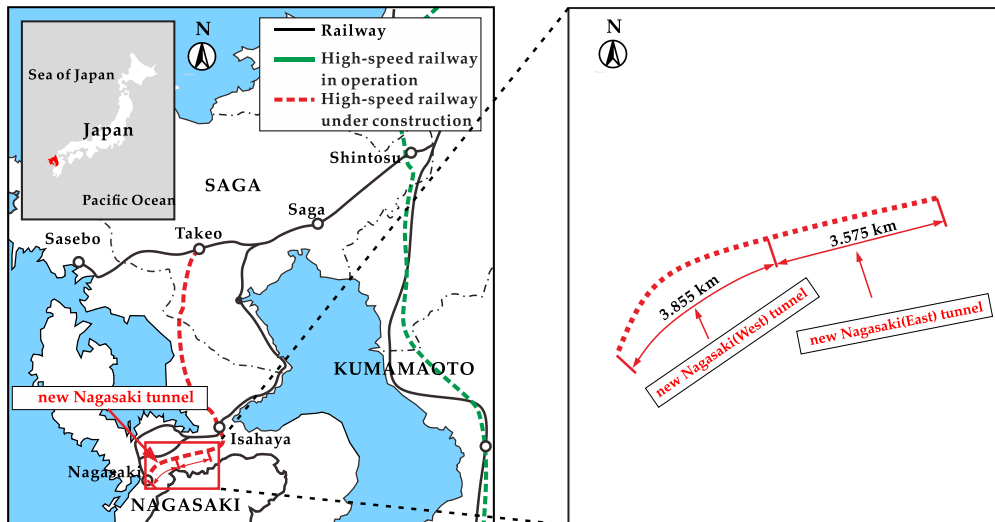


Fig. 2.1 The location of the new Nagasaki tunnel

The data used for the evaluation of the geological conditions ahead of the tunnel face are the data obtained during the construction of the tunnel, including the MWD data and the data (e.g., RQS, buried depth of the tunnel, and tunnel deformation) recorded in the observation report of the tunnel face. The specific energy is one of the MWD data obtained by drilling ahead of the tunnel face in the drilling process. In this study, the drilling data of every 1 m length are processed averagely. The specific energy, buried depth of tunnel and RQS are compared, and their correlation is analyzed to evaluate the factors closely related to the geological conditions ahead of tunnel face.

In this study, the new Nagasaki tunnel (east) with a total length of about 4 km is divided into four intervals for investigation, as shown in Fig. 2.2 and Table 2.1. The geological conditions at a certain mileage of the tunnel are determined according to the corresponding deformations of the tunnel recorded in the investigation report. The deformations of the tunnel include convergences in the top and lower half of the tunnel and crown settlement of the tunnel. The large deformation value of the tunnel indicates that the geological conditions are poor. It should be noted that due to the reason that some

field measurements are difficult to carry out, the specific energy and RQS measurement data used in this paper have not been obtained from all tunnel sections. At the same time, in order to be able to clearly compare and analyze the relationship between the measurement data under different geological conditions, part of the measurement data is applied to analyze four representative tunnel sections (intervals 1 to 4). The geological conditions in intervals 1 and 3 are good, while poor in interval 2 and fair in interval 4. As for the burial depth of tunnel, intervals 1, 2, and 4 have common burial depth, while interval 3 has large burial depth. As for the water inflow of the tunnel face, there is a small amount of water inflow in intervals 1 and 3 and a large amount in intervals 2 and 4. Descriptive statistical distribution of the values of the specific energy, buried depth, and RQS is summarized in Table 2.2. Additionally, Fig. 2.3 compares the range and distribution of the parameters. As can be observed from Fig. 2.3 and Table 2.2, all the three parameters have a certain degree of discrimination.

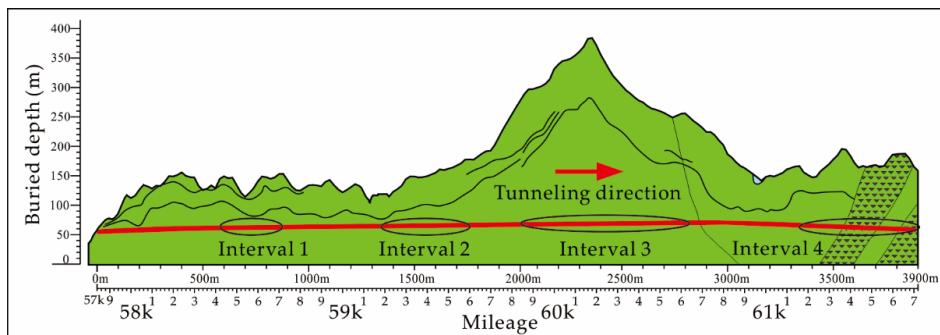


Fig. 2.2 Distribution of four intervals of the new Nagasaki tunnel (east)

Table 2.1 Geological conditions, buried depth, and water inflow of four intervals

Interval	Mileage	Geological conditions	Buried depth	Water inflow	Remarks
1	58K424.4–58K724.3 m	Good	Common < 150m	Small	Small deformation of surrounding rock
2	59K178.4–59K611.0 m	Poor	Common < 150m	Large	Most of the surrounding rock has a large amount of deformation
3	59K847.3–60K652.1 m	Good	Large 150m-400m	Small	Most of the surrounding rock has a small deformation
4	61K192.3–61K714.1 m	Fair	Common < 150m	Large	Small deformation of the surrounding rock, but the water inflow is large

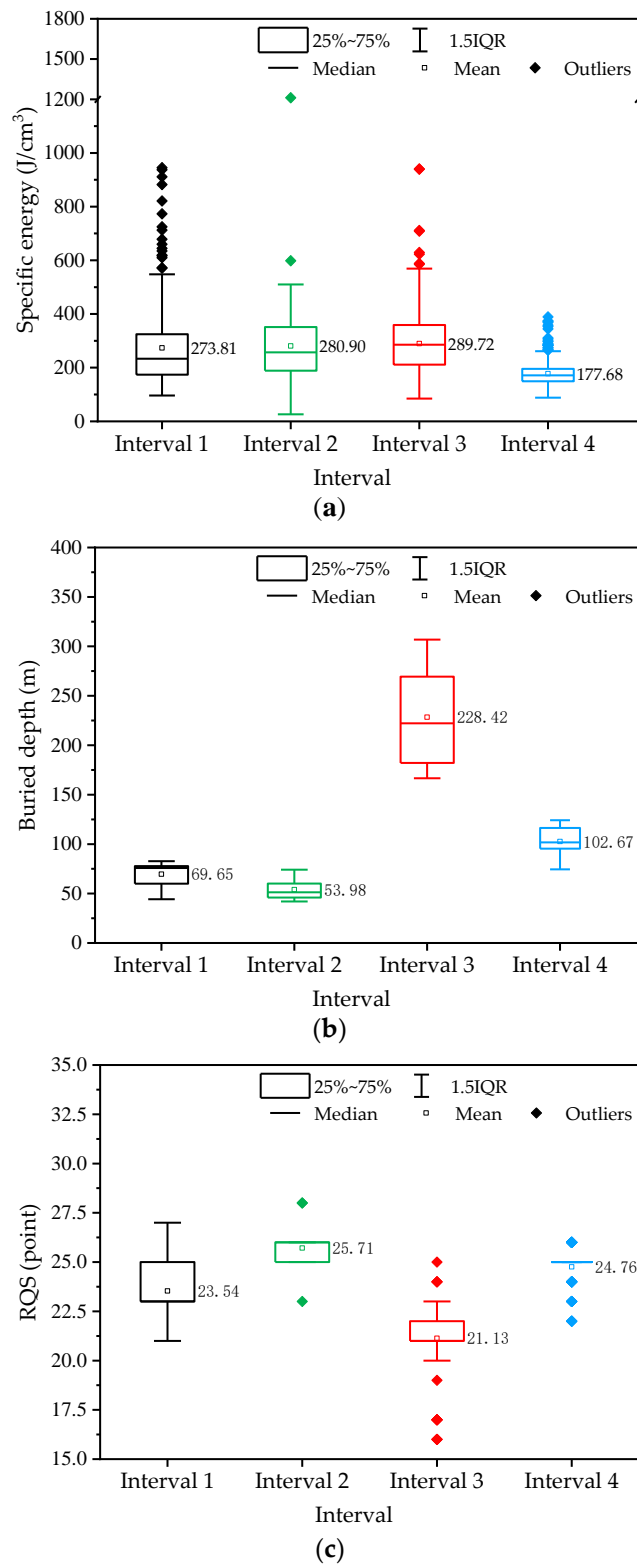


Fig. 2.3 The range and distribution of the values of the specific energy, buried depth, and rock mass quality score (RQS). (a) The value of the specific energy; (b) The value of the buried depth; (c) The value of the RQS

Table 2.2. Basic statistical description of the values of the specific energy, buried depth, and RQS

Interval	Item	Specific energy (J/cm ³)	Buried depth (m)	RQS (point)
1	Maximum	945.06	82.70	27
	Minimum	96.42	44.30	21
	Average	273.81	69.64	23.54
2	Maximum	1211.42	74.10	28
	Minimum	26.50	42.00	23
	Average	280.90	53.92	25.71
3	Maximum	940.65	306.80	25
	Minimum	84.99	166.60	16
	Average	289.72	228.42	21.13
4	Maximum	389.22	124.20	26
	Minimum	88.49	74.50	22
	Average	177.61	102.61	24.75

2.2.2 The deformation

Deformation monitoring is an important part of the tunnel construction process and has been used extensively in tunnel engineering (Schubert et al. 2002). The data provided by the monitoring process can not only be used to determine whether the tunnel structure is stable but also to reflect the geological conditions of the surrounding rock of the tunnel (Bizjak and Petkovšek 2004). In addition, the trend of tunnel deformation monitoring is vital to determine the reasonable support design to adapt to the unforeseen geological conditions ahead of tunnel face. Tunnel deformation includes wall convergence (horizontal displacement) and crown settlement (vertical displacement). Many measuring technologies have been developed for these processes, such as tape extensometers, total station survey (or other geodetic methods), photogrammetric devices, and laser profilers (laser scanners). The total station measurement has the advantages of being simple, fast, and non-contact. Therefore, in this study, the total station was applied to measure the deformation of the tunnel. Horizontal convergence and crown settlement are measured mainly using a total station and a reflective film; the accuracy of the measurement could reach 0.5–1 mm.

In this paper, the deformation measurement of the entire length of the new Nagasaki tunnel (east) was carried out by the measuring technology of total station survey. Through the trigonometry relation among total station, rear viewpoint, and measuring point, the settlement displacement of a measuring point can also be obtained (as shown in Fig. 2.4).

Fig. 2.5 depicts the measuring points layout of cross section. Two measuring lines B–C and D–E were set to measure the horizontal convergence during tunnel excavation. In addition, point A was set to measure the crown settlement.

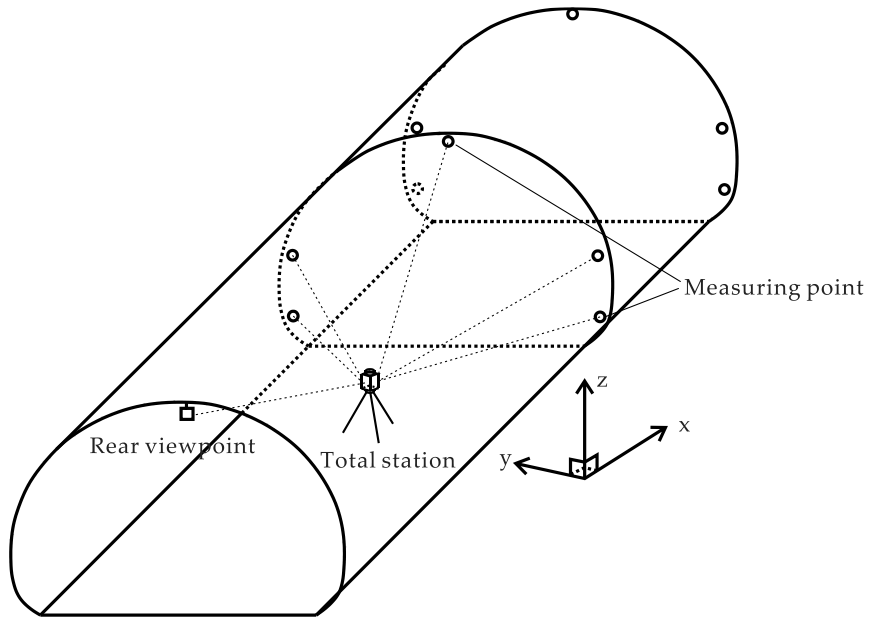


Fig. 2.4 The sketch of deformation measurement with total station

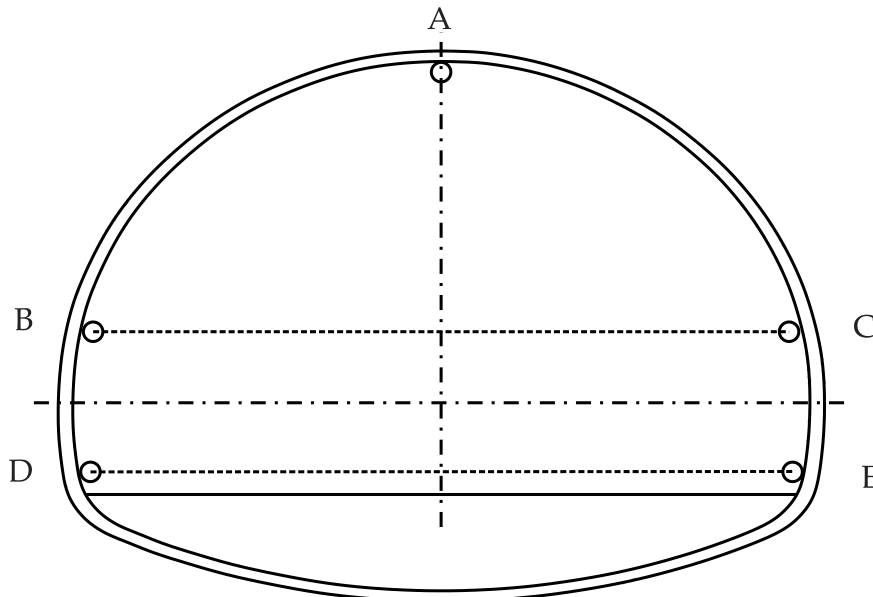


Fig. 2.5 Measuring points layout of cross section

Table 2.3 and Table 2.4 illustrate the monitoring interval and frequency applied in this

site, respectively, which was set according to the technical code for monitoring measurement of railway tunnels. It should be noted that the deformation data (wall convergence and crown settlement) used for the relationship analysis with specific energy and RQS are the final data after the tunnel deformation was basically stable after support. The detailed discussion of the measured data is given in the next section.

Table 2.3 The deformation monitoring interval applied in this site

Rock grade	$L^1 < 50$ m	50 m $< L < 200$ m	200 m $< L$	Buried depth $< 2D^2$
C I, C II	10 m	20 m	30 m	10 m
D I, D II	10 m	20 m	20 m	10 m

¹ L is the distance from the tunnel portal. ² D is the diameter of the tunnel

Table 2.4 The deformation monitoring frequency applied in this site.

Monitoring frequency	T^3	Convergence speed
Twice a day	0–0.5 day	>10 mm/day
Once a day	0.5–2.0 day	5–10 mm/day
Once every two days	2.0–5.0 day	1–5 mm/day
Once a week	>5.0 day	<1 mm/day

³ T is the time from the tunnel face passing through the measured position

2.2.3 The specific energy

In this study, during the tunnel excavation, the advance drilling work ahead of the tunnel face was carried out utilizing a hydraulic rotary percussion drill (as shown in Fig. 2.6). The parameters of MWD data (the data obtained from a 30 m borehole as shown in Fig. 2.7) obtained from the data collection device include the penetration rate, hammer pressure, hammer frequency, and specific energy. The specific energy is a fundamental parameter in the drilling of rocks and is defined as the amount of mechanical energy required to break a unit volume of rock, calculated as equation (1) (Masayuki et al. 2001):

$$E_s = \frac{ALN_s f}{vS} \times k, \quad (2-1)$$

where E_s is the specific energy (J/cm³), f is hammer frequency (1/min), v is penetration

rate (cm/min), S is cross-sectional area of the drill hole(cm^2), k is loss coefficient, A is piston compression area (cm^2), L is piston stroke (cm), and N_s is the hammer pressure (MPa). The role of loss coefficient k in this equation is mainly to compensate the energy loss caused by the friction between drill pipe and borehole. The determination of loss coefficient k is based on the laboratory test of drilling different lithology rocks. The drilling data obtained from the field in this study are directly measured using the drilling guidance system "Drill Navi" developed by Konoike Construction Co., Ltd of Japan. The calculation equation of the specific energy is embedded in the system.



Fig. 2.6 The hydraulic rotary percussion drill

Table 2.5 Geomechanics classification of rock masses

Item	Description	Evaluation score			
		1	2	3	4
1	Total state	Stable	Rock fall	Pressed	Collapse or outflow
2	Self-stability	Able	Gradual instability	Unable, primary support	Unable, pre-support
3	Intact rock strength, MPa	>100	20–100	5–20	<5
4	Weathering	Unweathered	Slightly weathered	Moderately weathered	Highly weathered

5	Joints proportion	<5%	5%–20%	20%–50%	>5%
6	Spacing of joints	>1 m	0.2–1 m	50–200 mm	<50 mm
7	Joint aperture	Highly closed	Moderately closed	Slightly closed	Unclosed
8	Morphology of joints	Random square	Columnar	Layered	Psammitic
9	Ground water inflow	None	Slight	Moderate	Heavy
10	Ground Water corrosion	Uncorroded	Slightly corroded	Moderately corroded	Heavily corroded

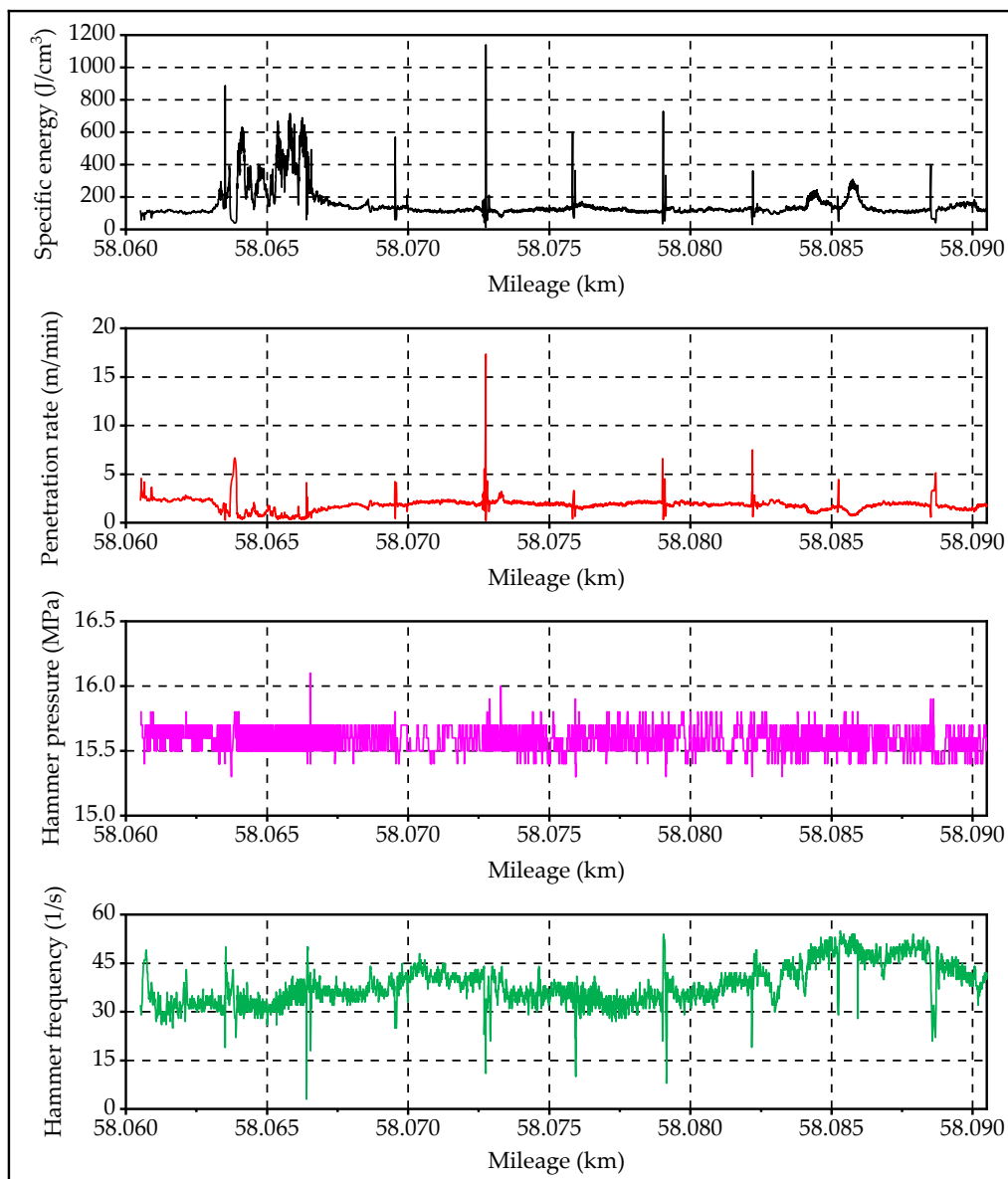


Fig. 2.7 Visualization of the measure-while-drilling (MWD) data obtained from a 30 m borehole

2.2.4 Rock mass quality score of tunnel face

In this tunnel construction, the observation report of tunnel face is implemented for rock mass assessment. A tunnel rock mass classification method, JH method, proposed by Akagi et al. (2001), is employed to classify the rock mass. This method uses ten rock parameters of overall state, self-stability, intact rock strength, weathering, joints proportion, spacing of joints, joint aperture, morphology of joints, ground water inflow, and ground water corrosion to assess rock mass quality. Based on the above parameters, an engineering classification of rock masses, termed the geomechanics classification, is shown in Table 2.5. As shown in Table 2.5, all observation items are configured with four values from 1 to 4. The RQS (the final rock class rating) value will be the sum of each item value, with lower numbers reflecting better conditions and, hence, lesser support requirements in the case of tunnels.

2.3 Evaluation methods and results

2.3.1 Evaluation methods

This section contains the comparison and analysis between specific energy, RQS, and deformation. In addition, the feasibility of utilizing the correlation between these data to evaluate the geological conditions ahead of tunnel face is also discussed. In this study, the correlation coefficient (R^2) index was calculated to evaluate the correlation between variables, as employed by Grima and Babuška (1999):

$$R^2 = 1 - \frac{\sum_{i=1}^n (y - y')^2}{\sum_{i=1}^n (y - \bar{y})^2}, \quad (2-2)$$

2.3.2 Evaluation results and discussion

2.3.2.1 Interval 1

Fig. 2.8 shows the deformation of the convergences (top and lower half) and crown settlement of interval 1. As shown in Fig. 2.8, for interval 1, although a small amount of water inflow is visible, the deformations are quite small. The maximum deformation is less than 10 mm with the 58.65 km mileage. Comparing intervals 1–4, interval 1 has the

best geological conditions among the four intervals.

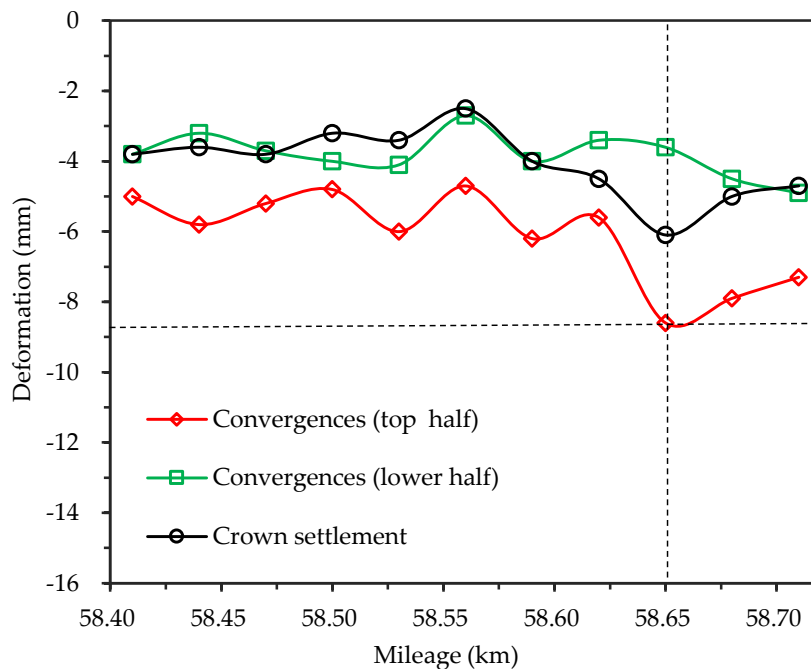


Fig. 2.8 Measured deformation of the convergences and crown settlement of interval 1.

The distributions of specific energy and RQS with mileage are shown in Fig. 2.9. As can be seen, higher singular values of specific energy exist near 58.45 km mileage. After removing these singular values, the specific energy is roughly distributed between 100–500 J/cm³. It can be concluded that the specific energy of interval 1 varies little with the mileage. The relationship between specific energy and RQS was analyzed by comparing Fig. 2.8 with Fig. 2.9a and Fig. 2.10a. In theory, high specific energy values and low RQS values indicate that the rock mass is harder. As displayed in Table 2.2 and Fig. 2.9a, it can be seen that RQS of interval 1 is 27 points at the highest, 21 points at the lowest, and 23.5 points on average. As mentioned above, interval 1 has the best geological condition with the smallest deformation. However, if only RQS is considered, the average RQS of interval 3 is smaller than that of interval 1, which means that the geological condition of interval 3 is the best. It is not matched with the fact that interval 1 has the best geological conditions. As shown in Fig. 2.9a, when the points of specific energy and RQS overlap, the distribution trends of specific energy and RQS points look similar, but it is not consistent at 58.424–58.500 km mileage. The R^2 values of specific energy and RQS are also smaller at this mileage. In addition, the largest RQS exists at 58.63 km and 58.73 km

mileage, rather than at 58.65 km mileage where the deformation is the largest. From these results, it can be concluded that a reasonable correlation exists between specific energy and RQS for interval 1, but there is low correlation between RQS and deformation.

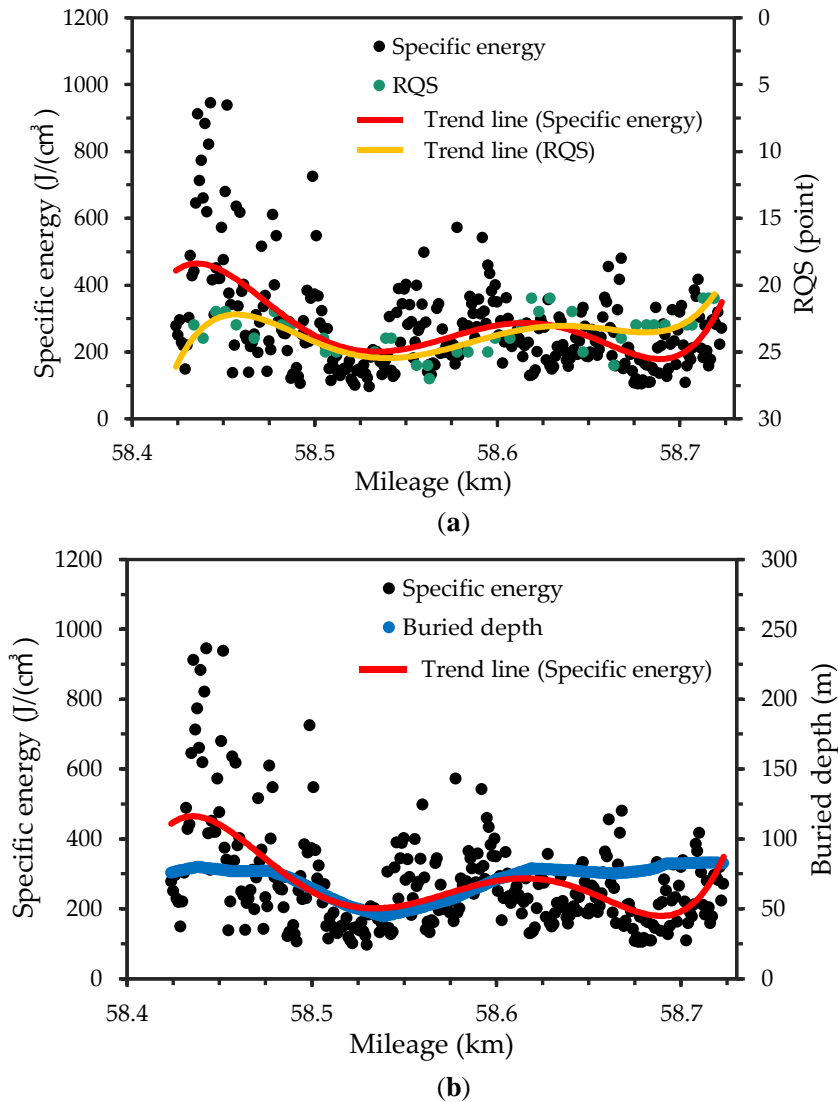


Fig. 2.9 Distribution of specific energy, RQS, and buried depth with mileage of interval 1. (a) Comparison of distributions between specific energy and RQS; (b) Comparison of distributions between specific energy and buried depth.

Fig. 2.9b shows the distributions of specific energy and buried depth with mileage of interval 1. The relationship between specific energy and buried depth is discussed by comparing Fig. 2.8 with Fig. 2.9b and Fig. 2.10b. Interval 1 has relatively small buried depth among the four intervals; the buried depth of interval 1 is 82.7 m at maximum, 44.3

m at minimum, and 69.64 m on average. Theoretically, as the burial depth increases, the rock mass hardens and the specific energy increases accordingly. The distribution trends of specific energy and buried depth points are basically the same except for the mileage of 58.650–58.724 km as presented in in Fig. 2.9b. Fig. 2.10b shows that lower R^2 values exist at the mileage of 58.650–58.724 km. This result reveals that a certain correlation exists between specific energy and buried depth except for the mileage of 58.650–58.724 km where the deformation is large. It should be noted that the trend lines in Fig. 2.9 are computed by using multiple regression technique. The regression equations between specific energy, RQS, and mileage are all quintic equations. Accordingly, the following Figures 12, 14, and 17 use the same technology to calculate the trend lines.

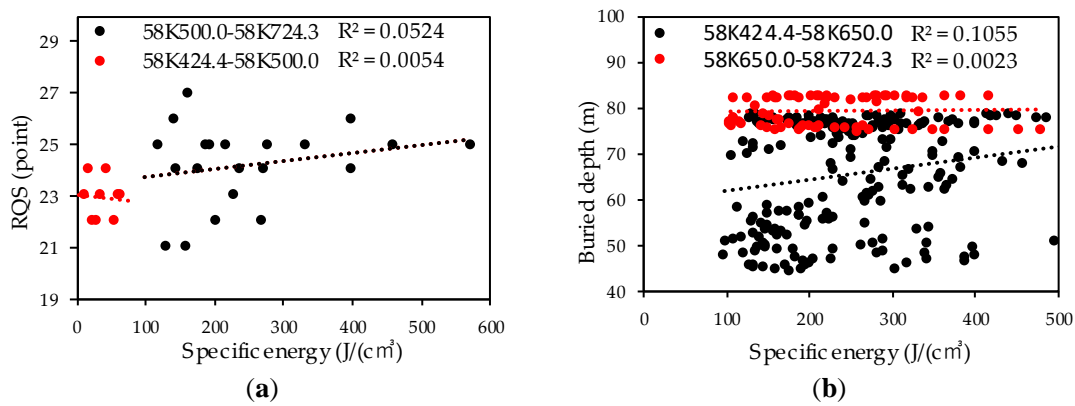


Fig. 2.10 Correlation coefficients of specific energy, RQS, and buried depth with mileage of interval 1. (a) Correlation coefficients of specific energy and RQS; (b) Correlation coefficients of specific energy and buried depth.

2.3.2.2 Interval 2

A large amount of water inrush and poor geological conditions exist in parts of interval 2, which leads to the inability to obtain specific energy data, as presented in Fig. 2.11. From Fig. 2.11, it is considered that the geological conditions are quite deteriorated after 59.32 m mileage. The maximum deformation of the area before 59.32 m mileage is about 120 mm, which can allow us to predict that the geological conditions near this mileage are the worst.

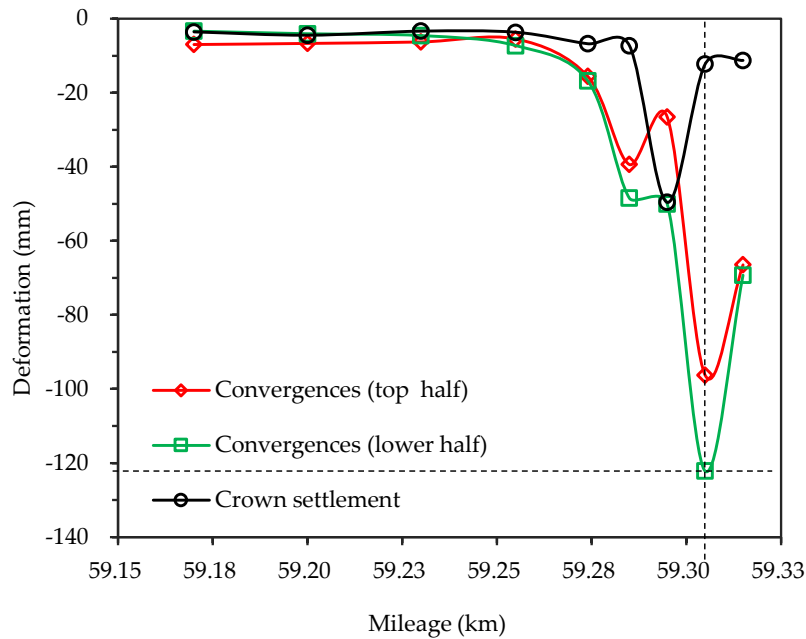


Fig. 2.11 Measured deformation of the convergences and crown settlement of interval 2

The distributions of specific energy and RQS with mileage of interval 2 are shown in Fig. 2.12a. As can be seen, although some mileage in interval 2 cannot obtain specific energy, the specific energy is basically distributed between $100\text{--}500\text{ J/cm}^3$, which is the same value as interval 1 with good geological conditions. In addition, the average value is 280.9 J/cm^3 , which is very close to 273.8 J/cm^3 of interval 1. Although the specific energy of interval 1 and 2 are similar, the geological conditions are totally different. The relationship between specific energy and RQS was analyzed by comparing Fig. 2.11 with Fig. 2.12a and Fig. 2.13a. As displayed in Table 2.2, it can be seen that RQS of interval 2 is 28 points at the highest, 23 points at the lowest, and 25.71 points on average. Although the value of the specific energy is not lowest near the 59.24 km mileage in interval 2, the value of RQS is the highest. In addition, according to the theory that the higher the specific energy, the harder the rock mass and the lower the RQS value will be, the distribution of specific energy is basically similar to the distribution of RQS with mileage in interval 2, so it can be concluded that for interval 2, the specific energy and RQS have a certain correlation (as shown in Fig. 2.13a). It can be seen that although the specific energy is related to RQS, the distribution of deformation changes greatly with mileage (as shown in Fig. 2.11). Therefore, it is difficult to accurately predict the geological conditions of rock mass based only on the relationship between specific energy and RQS.

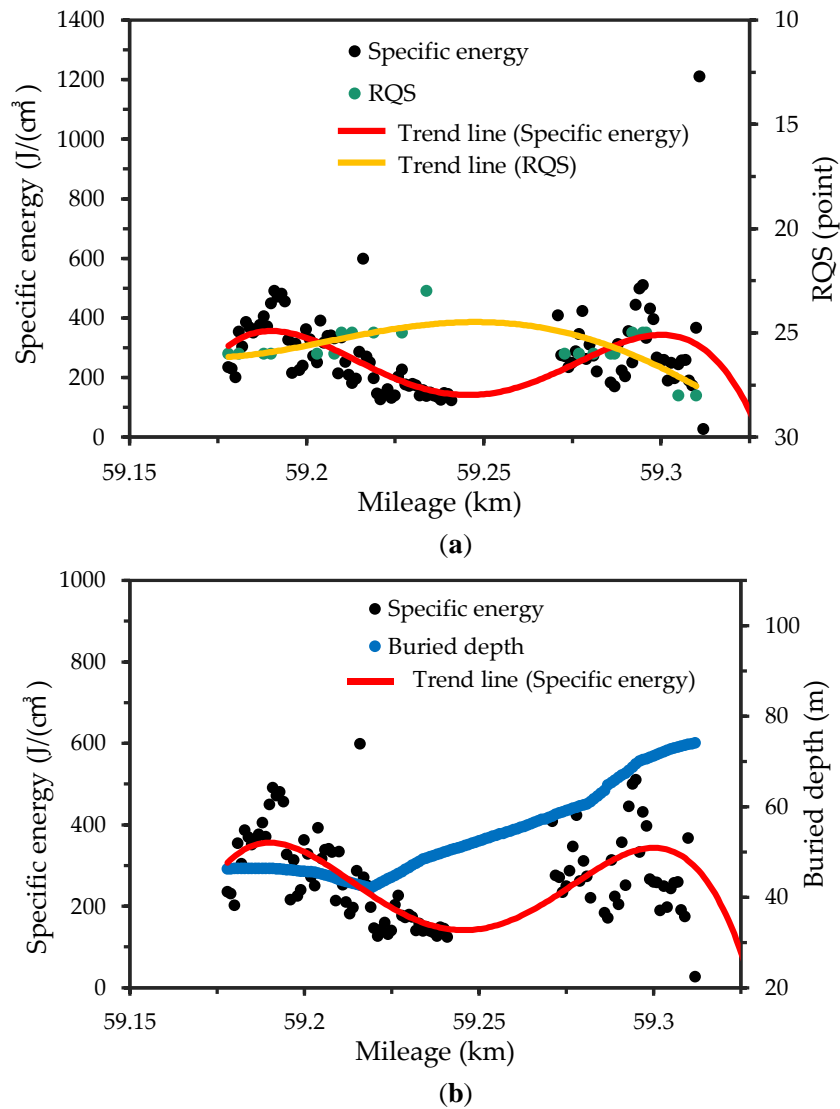


Fig. 2.12 Distribution of specific energy, RQS, and buried depth with mileage of interval 2. (a) Comparison of distributions between specific energy and RQS; (b) Comparison of distributions between specific energy and buried depth.

Fig. 2.12b displays the distributions of specific energy and buried depth with mileage of interval 2. The comparison of the graphs of Fig. 2.11, Fig. 2.12b and Fig. 2.13b was carried out to examine the relationship between specific energy and buried depth. The maximum buried depth of interval 2 is 74.1 m, the minimum is 42 m, and the average is 53.92 m, which is roughly the same as interval 1. From Table 2.2, Fig. 2.12b, the distributions of specific energy and buried depth corresponding to the first half of mileage are very similar; however, the specific energy remains generally constant when the buried

depth of the second half becomes higher. Fig. 2.13b shows that lower R^2 value exists at these mileages. As the deformation becomes larger in the second half (as shown in Fig. 2.11), an assumption that the geological conditions of the area will be worse with higher buried depth and lower specific energy with a higher probability was proposed and carried out to investigate the remaining intervals.

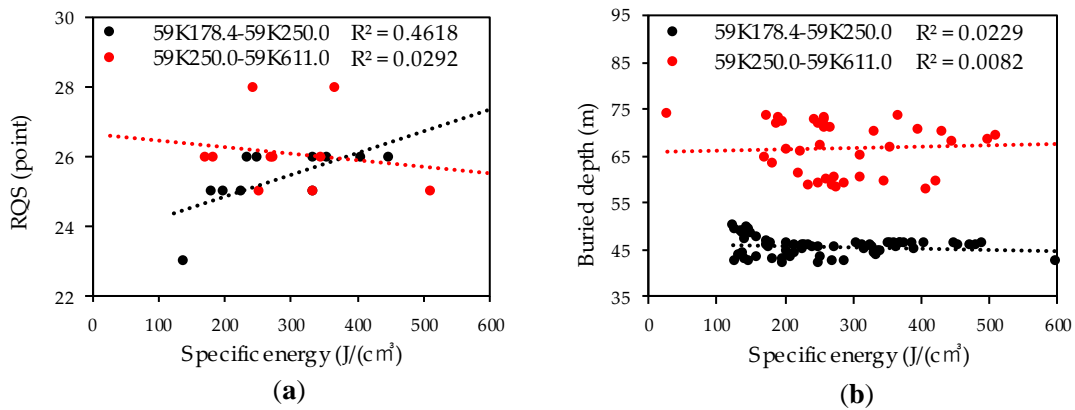


Fig. 2.13 Correlation coefficients of specific energy, RQS, and buried depth with mileage of interval 2. (a) Correlation coefficients of specific energy and RQS; (b) Correlation coefficients of specific energy and buried depth

2.3.2.3 Interval 3

Almost no water inflow exists in the whole part of interval 3; however, the maximum deformation of about 20 mm occurs near the 60.100 km mileage, and the large deformation of about 17 mm occurs near the 60.700 km mileage, as shown in Fig. 2.14.

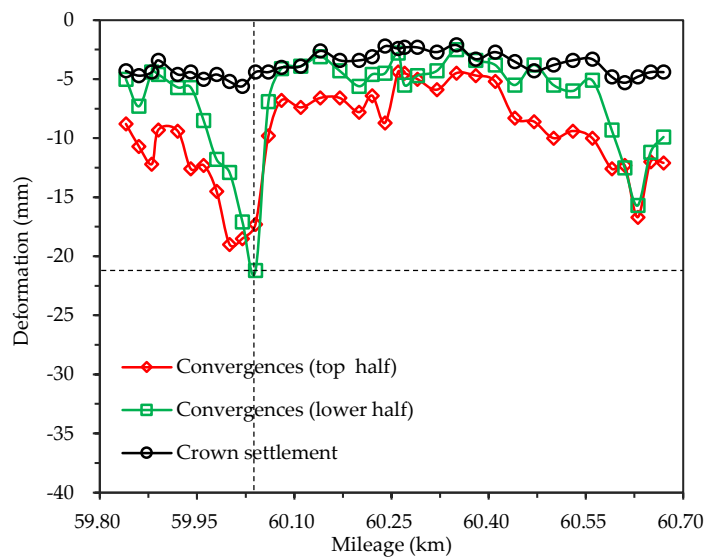


Fig. 2.14 Measured deformation of the convergences and crown settlement of interval 3

Fig. 2.15a depicts the distributions of specific energy and RQS with mileage of interval 3. The average value of specific energy is similar to intervals 1 and 2 (as shown in Table 2.2); however, the distribution of specific energy with mileage fluctuates significantly. The relationship between specific energy and RQS was analyzed by comparing Fig. 2.14 with Fig. 2.15a and Fig. 2.16a. It can be seen that the distributions and the R^2 values of specific energy and RQS with mileage are almost the same. However, it cannot be concluded that the low specific energy values and the low RQS values indicate that the deformation is larger.

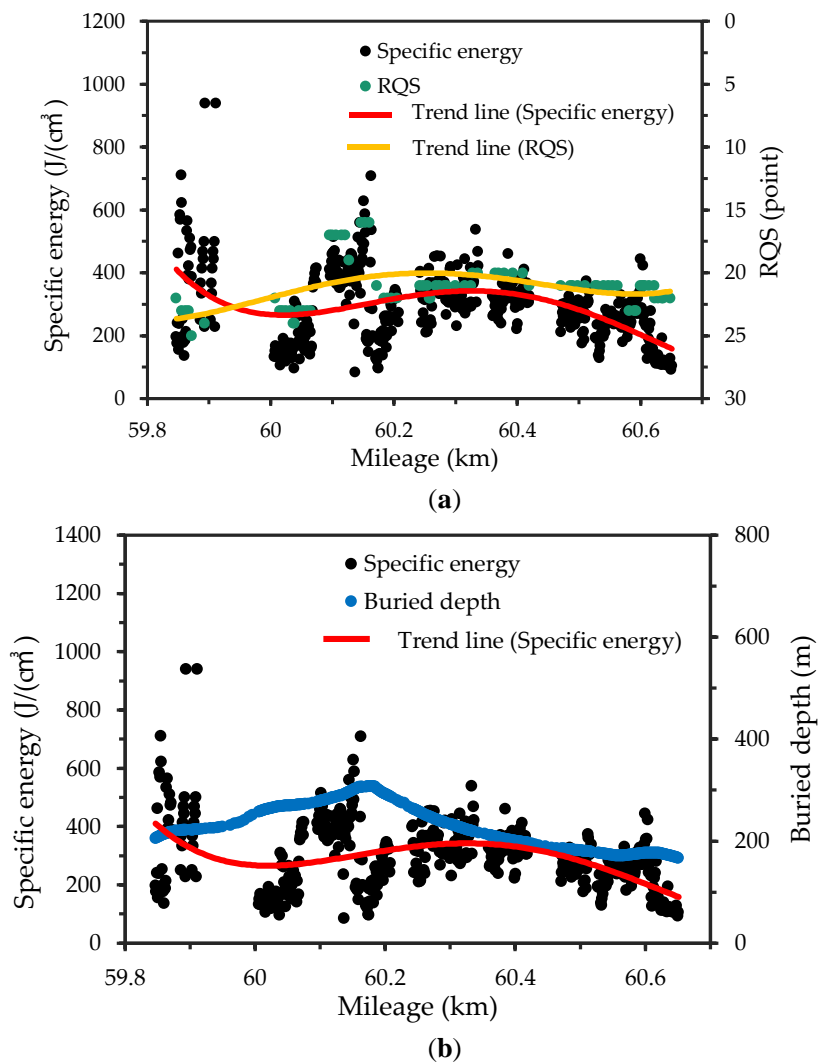


Fig. 2.15 Distribution of specific energy, RQS, and buried depth with mileage of interval 3. (a) Comparison of distributions between specific energy and RQS; (b) Comparison of distributions between specific energy and buried depth

As can be seen from Table 2.2, the maximum burial depth of interval 3 is 306.8 m, the minimum is 166.6 m, and the average is 228.42 m. Interval 3 has the highest burial depth among the four intervals. Fig. 2.15a shows the distributions of specific energy and buried depth with mileage of interval 3. The relationship between specific energy and buried depth was analyzed through the comparison of the graphs of Fig. 2.14, Fig. 2.15b and Fig. 2.16b. The results show that although the distribution of specific energy and buried depth with mileage is very similar, the distribution of specific energy near the 59.847–60.300 km mileage is lower than the buried depth, the lower R^2 value exists at these mileages and it can be seen from Fig. 2.14 that the deformation of this area is larger. These results verify the assumption in interval 2 that the geological conditions of the area are worse with higher buried depth and lower specific energy.

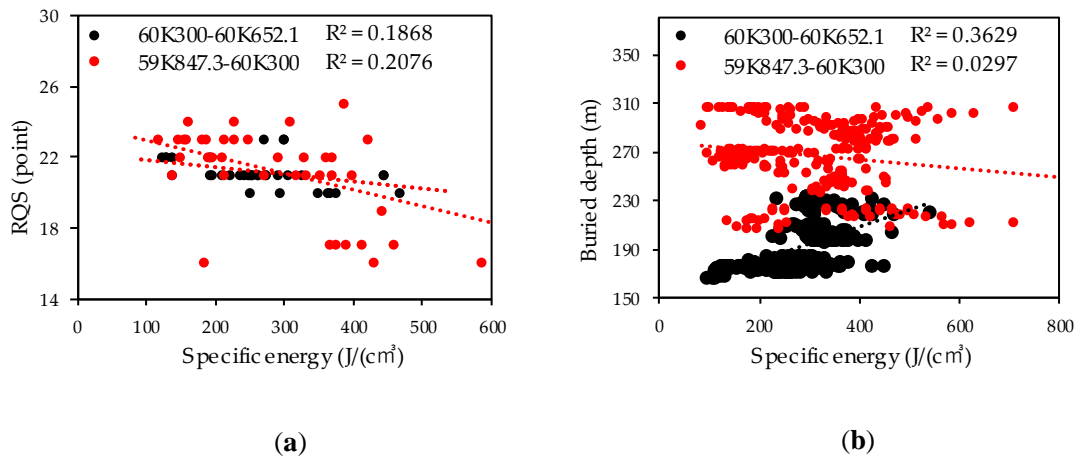


Fig. 2.16 Correlation coefficients of specific energy, RQS, and buried depth with mileage of interval 3. (a) Correlation coefficients of specific energy and RQS; (b) Correlation coefficients of specific energy and buried depth

2.3.2.4 Interval 4

The water inflow exists in the whole section of interval 4, and the deformation of about 10 mm can be seen almost in the whole section, as shown in Fig. 2.17.

The distributions of specific energy and RQS with mileage of interval 4 are expressed in Fig. 2.18a. The specific energy of interval 4 is between 100–400 J/cm³, and the larger specific energy exists near 61.68 km of interval 4. The total variation range of specific energy of interval 4 is very small, the smallest one among the four intervals. The average value of specific energy is also smaller than other intervals, but the specific energy

fluctuates obviously in interval 4, the same as interval 3. The relationship between specific energy and RQS was analyzed by comparing Fig. 2.17 with Fig. 2.18a and Fig. 2.19a. As expressed in Table 2.2, the RQS of interval 4 is 26 points at the highest, 22 points at the lowest, and 24.75 points on average. For the first half of interval 4, the distributions of specific energy and RQS with mileage are approximately the same. However, for the second half, some fluctuations exist in the distribution of specific energy, but the distribution of RQS remains constant. It can also be seen from Fig. 2.19a that the R^2 value of the first half is greater than that of the second half. However, a large amount of deformation exists in these two sections.

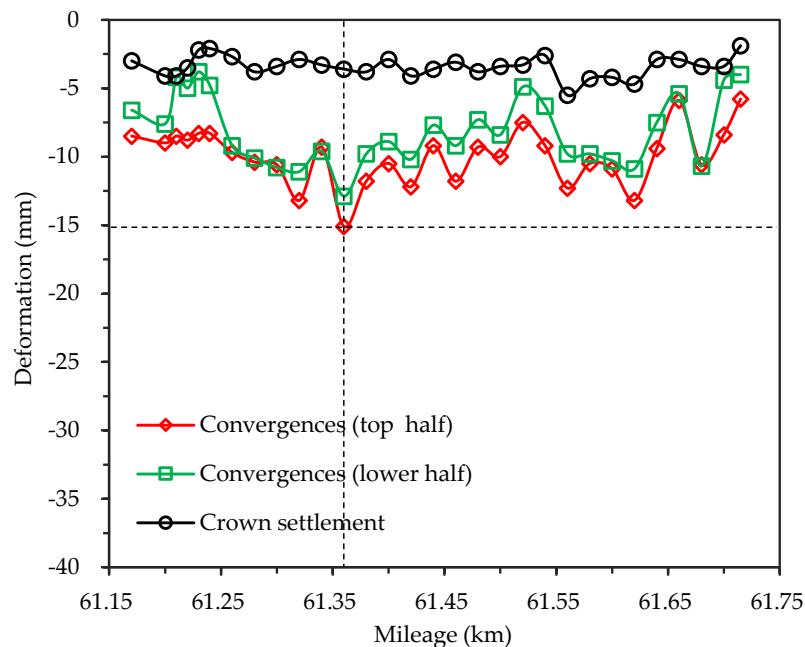


Fig. 2.17 Measured deformation of the convergences and crown settlement of interval 4

As indicated in Table 2.2, the maximum burial depth of interval 4 is 124.2 m, the minimum is 74.5 m, and the average is 102.61 m. The burial depth of interval 4 is slightly higher than that of intervals 1 and 2. Fig. 2.18b depicts the distributions of specific energy and buried depth with mileage of interval 4. The relationship between specific energy and buried depth was analyzed through the comparison of the graphs of Fig. 2.17, Fig. 2.18b and 19b. As shown in Fig. 2.18b, the deformation is relatively large near 61.25–61.40 km mileage and 61.55–61.68 km mileage, which indicates that poor geological conditions exist in these two sections. The lower R^2 values also exist in these two sections (as shown in Fig. 2.19b). Except for the distribution of specific energy of these two sections being

lower than that of buried depth, the distributions of specific energy and buried depth with mileage are basically the same for other parts of interval 4. These results further reveal that the distribution of specific energy in this section is much lower than that of buried depth, which may be due to the poor geological conditions in this area. Therefore, the assumption proposed in interval 2 is verified; that is, the areas with lower specific energy distribution than the buried depth distribution have worse geological conditions with a higher probability.

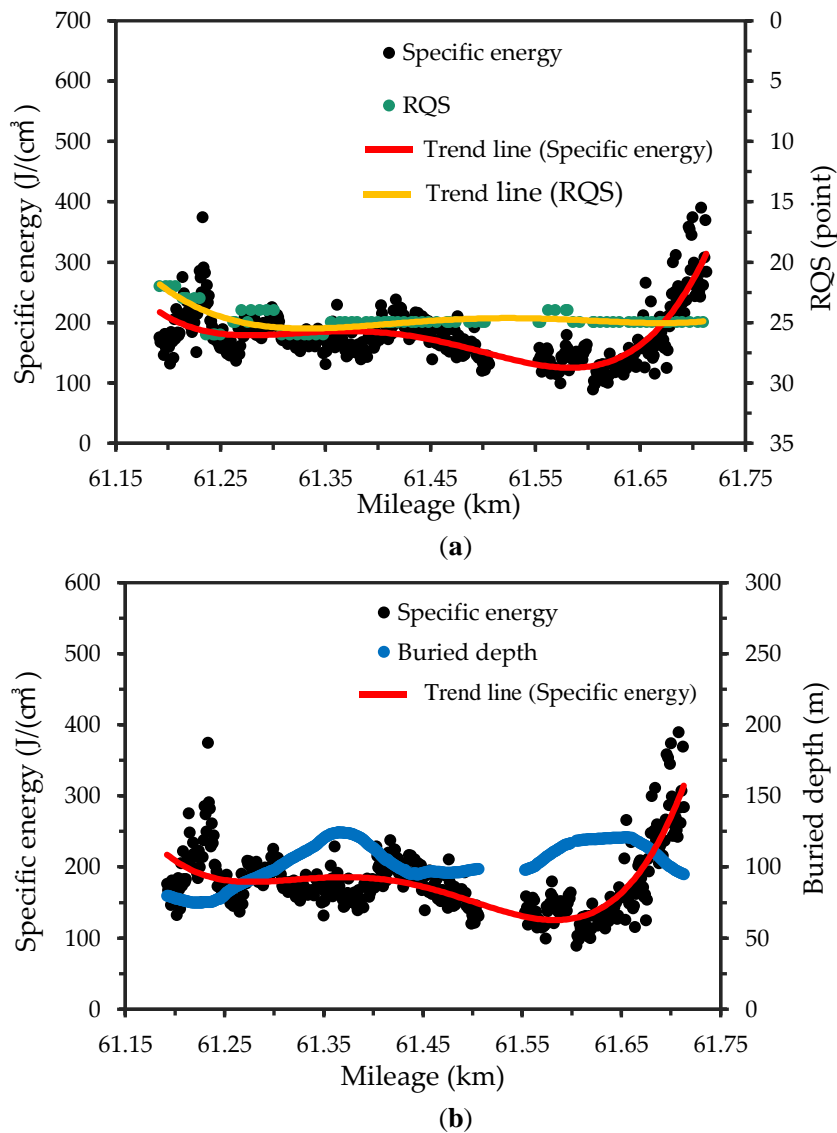


Fig. 2.18 Distribution of specific energy, RQS, and buried depth with mileage of interval 4. (a) Comparison of distributions between specific energy and RQS; (b) Comparison of distributions between specific energy and buried depth

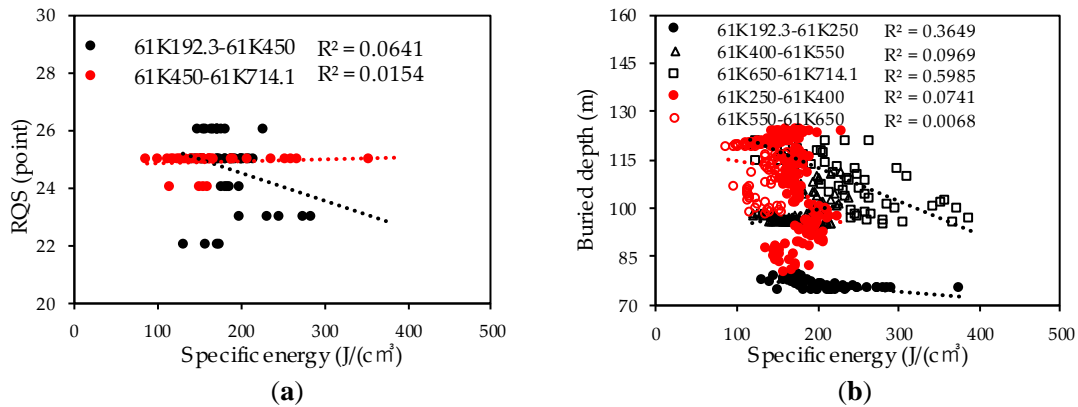


Fig. 2.19 Correlation coefficients of specific energy, RQS, and buried depth with mileage of interval 4. (a) Correlation coefficients of specific energy and RQS; (b) Correlation coefficients of specific energy and buried depth

2.4 Conclusions

The accurate/objective evaluation of geological conditions ahead of a tunnel face is one of the biggest challenges in tunnel building. Serious mistakes in geological condition prediction can cause considerable irreparable damage, i.e., support instability caused by the unexpected anomalies (i.e., cavities or water bearing, fractured or relatively stronger zones). Therefore, in this paper, the feasibility of using mechanical specific energy (a composite parameter of the MWD parameter) in the drilling process to evaluate the geological conditions ahead of tunnel face is analyzed, and the relationship between specific energy, RQS, tunnel buried depth, and tunnel deformation is compared. The specific conclusions from this study are the following:

(1) Although the geological conditions of the four intervals of the new Nagasaki tunnel (east) are different, the difference between the average values of specific energy of these intervals is very small, within 100 J/cm^3 . According to the distributions of specific energy, RQS and buried depth with the mileage of this tunnel, it can be observed that certain correlations exist between these items.

(2) A high correlation exists between specific energy and RQS, but the feasibility of employing this correlation to evaluate the geological conditions ahead of the tunnel face is very limited.

(3) Although the correlation coefficient values obtained are small and widely dispersed, the geological conditions can be evaluated by comparing the correlation coefficient values in different regions and the distribution trend of each variable. Compared with the

distribution of buried depth, a high probability of large tunnel deformation occurs in the region with extensive low specific energy values. The reason behind this view is explained as follows: The specific energy can reflect the strength of rock and the strength state of rock mass; in theory, the strength of the rock mass with larger buried depth is higher, and the corresponding specific energy value is larger. If the buried depth of a certain area is larger, but the specific energy value measured is smaller, it is an abnormal phenomenon with greater probability. Therefore, the objective criterion for evaluating geological conditions can be obtained: If the distribution of the specific energy in some areas deviates from the distribution of buried depth, it is considered that abnormal geological conditions exist in this area with a higher probability.

Although the criterion for evaluating geological conditions ahead of the tunnel face has been determined via comparing the specific energy, the RQS, the tunnel buried depth, and the tunnel deformation, some problems should be considered further. How to establish the quantitative index based on the MWD data to evaluate the geological conditions ahead of a tunnel face is a challenging topic. This is still an open problem and therefore deserves further investigation.

References

- Akagi W, Sano A, Shinji M, Nishi T, Nakagawa K (2001), A new rock mass classification method at tunnel face for tunnel support system. *Doboku Gakkai Ronbunshu*, 2001:121-134. (In Japanese)
- Aoki K, Shirasagi S, Yamamoto T, Inou M, Nishioka K (1999), Examination of the application of drill Logging to predict ahead of the tunnel face. In: *Proceedings of the 54th Annual Conference of the Japan Society of Civil Engineers*, Tokyo, Japan, September 1999. pp 412-413. (In Japanese)
- Ashida Y (2001), Seismic imaging ahead of a tunnel face with three-component geophones. *Int J Rock Mech Min Sci*, 38:823-831. [https://doi.org/10.1016/S1365-1609\(01\)00047-8](https://doi.org/10.1016/S1365-1609(01)00047-8)
- Bellino A, Garibaldi L, Godio A (2013), An automatic method for data processing of seismic data in tunneling. *J Appl Geophys*, 98:243-253. <https://doi.org/10.1016/j.jappgeo.2013.09.007>
- Bizjak KF, Petkovšek B (2004), Displacement analysis of tunnel support in soft rock

- around a shallow highway tunnel at Golovec. *Eng Geol*, 75:89-106.
<https://doi.org/10.1016/j.enggeo.2004.05.003>
- Bu L et al. (2019), Application of the comprehensive forecast system for water-bearing structures in a karst tunnel: a case study. *Bulletin of Engineering Geology the Environment*, 78:357-373. <https://doi.org/10.1007/s10064-017-1114-4>
- Celada B, Galera J, Muñoz C, Tardáguila I The use of the specific drilling energy for rock mass characterisation and TBM driving during tunnel construction. In: *ITA-AITES World Tunnel Congress, 2009. ITA-AITES Budapest*, pp 1-13.
- Chen Z, Shi C, Li T, Yuan Y (2012), Damage characteristics and influence factors of mountain tunnels under strong earthquakes. *Natural Hazards*, 61:387-401.
<https://doi.org/10.1007/s11069-011-9924-3>
- Dix CH (1952), *Seismic prospecting for oil*. Harper New York,
- Djogo M, Vasic M, Cosic M (2011), Engineering geological evaluation of the conditions for constructing a bridge and a tunnel in the zone of the old Petrovaradin Fortress, Serbia. *Bulletin of Engineering Geology the Environment*, 70:139-142.
- Galende-Hernández M, Menéndez M, Fuente MJ, Sainz-Palmero GI (2018), Monitor-While-Drilling-based estimation of rock mass rating with computational intelligence: The case of tunnel excavation front. *Autom Constr*, 93:325-338.
<https://doi.org/10.1016/j.autcon.2018.05.019>
- Gong Q, Yin L, She Q (2013), TBM tunneling in marble rock masses with high in situ stress and large groundwater inflow: a case study in China. *Bull Eng Geol Environ*, 72:163-172.
- Grima MA, Babuška R (1999), Fuzzy model for the prediction of unconfined compressive strength of rock samples. *International Journal of Rock Mechanics Mining Sciences*, 36:339-349.
- Høien AH, Nilsen B (2014), Rock mass grouting in the Løren Tunnel: case study with the main focus on the groutability and feasibility of drill parameter interpretation. *Rock Mech Rock Eng*, 47:967-983. <http://10.1007/s00603-013-0386-7>
- Inaba T, Ishiyama K, Akashi T, Hirano T (1996), Prediction system of geological condition ahead of the tunnel face. *Construction Machinery Equipment*, 32:40-45.
- Janda T, Šejnoha M, Šejnoha J (2018), Applying Bayesian approach to predict deformations during tunnel construction. *International Journal for Numerical*

- Analytical Methods in Geomechanics, 42:1765-1784.
<https://doi.org/10.1002/nag.2810>
- KASA H, IGARI T, YAMAMOTO H, MAEDA N A study on exploration accuracy of tunnel seismic prediction method. In: Proceedings of tunnel engineering, JSCE, 1996. Japan Society of Civil Engineers, pp 95-100.
- Lee IM, Truong QH, Kim DH, Lee JS (2009), Discontinuity detection ahead of a tunnel face utilizing ultrasonic reflection: Laboratory scale application. *Tunnelling Underground Space Technology*, 24:155-163.
- Leung R, Scheduling S (2015), Automated coal seam detection using a modulated specific energy measure in a monitor-while-drilling context. *Int J Rock Mech Min Sci*, 75:196-209. <https://doi.org/10.1016/j.ijrmms.2014.10.012>
- Li L et al. (2014), Cause Analysis of Soft and Hard Rock Tunnel Collapse and Information Management. *Pol J Environ Stud*, 23:1227-1233.
- Li S et al. (2017a), An overview of ahead geological prospecting in tunneling. *Tunnelling Underground Space Technology*, 63:69-94.
- Li SC, Wu J, Xu ZH, Li LP (2017b), Unascertained measure model of water and mud inrush risk evaluation in karst tunnels and its engineering application. *KSCE J Civ Eng*, 21:1170-1182. 10.1007/s12205-016-1569-z
- Lu J, Liu X (2009), Construction Techniques for Water and Sand Gushing Section in Xiushan Tunnel on Yuxi-Mengzi Railway. *Tunnel Construction*, 3
- Mahdevari S, Torabi SR (2012), Prediction of tunnel convergence using artificial neural networks. *Tunnelling Underground Space Technology*, 28:218-228.
<https://doi.org/10.1016/j.tust.2011.11.002>
- Masayuki Y, Ishiyama K, Yumura T, Tsukada J (2001), Application of drilling survey system for weak rock with in-flow water. Paper presented at the the 31st Symposium on Rock Mechanics, Tokyo, Japan, January 2001.
- Robertson JD, Pritchett WC (1985), Direct hydrocarbon detection using comparative P-wave and S-wave seismic sections. 50:383-393. 10.1190/1.1441918
- Sattel G, Sander B, Amberg F, Kashiwa T (1996), Predicting ahead of the face. *Tunnels Tunn Int*
- Schubert W, Steindorfer A, Button EA (2002), Displacement monitoring in tunnels—an overview. *Felsbau*, 20:7-15.

- Schunnesson H (1996), RQD predictions based on drill performance parameters. *Tunn Undergr Space Technol*, 11:345-351.
- Shin HS, Han KC, Sunwoo C, Choi SO, Choi YK (1999), Collapse of a Tunnel In Weak Rock And the Optimal Design of the Support System. Paper presented at the 9th ISRM Congress, Paris, France, 1999.
- Stewart RR, Gaiser JE, Brown RJ, Lawton DC (2002), Converted-wave seismic exploration: Methods. *Geophysics*, 67:1348-1363. 10.1190/1.1512781 %J Geophysics
- Sugawara J, Yue Z, Tham L, Law K, Lee C (2003), Weathered rock characterization using drilling parameters. *Canadian geotechnical journal*, 40:661-668.
- Swinnen G, Thorbecke JW, Drijkoningen GG (2007), Seismic Imaging from a TBM. *Rock Mechanics Rock Engineering*, 40:577-590. <https://doi.org/10.1007/s00603-006-0116-5>
- Teale R (1965), The concept of specific energy in rock drilling. *International Journal of Rock Mechanics and Mining Sciences & Geomechanics Abstracts*, 2:57-73. [https://doi.org/10.1016/0148-9062\(65\)90022-7](https://doi.org/10.1016/0148-9062(65)90022-7)
- Tzavaras J, Buske S, Groß K, Shapiro S (2012), Three-dimensional seismic imaging of tunnels. *Int J Rock Mech Min Sci*, 49:12-20. <https://doi.org/10.1016/j.ijrmms.2011.11.010>
- Yamamoto T, Shirasagi S, Yokota Y, KOIZUMI Y (2011), Imaging geological conditions ahead of a tunnel face using Three-dimensional Seismic Reflector Tracing System. *International Journal of the JCRM*, 6:23-31.
- Yue ZQ, Lee CF, Law KT, Tham LG (2004), Automatic monitoring of rotary-percussive drilling for ground characterization—illustrated by a case example in Hong Kong. *Int J Rock Mech Min Sci*, 41:573-612. <https://doi.org/10.1016/j.ijrmms.2003.12.151>

3 Prediction models of tunnel support patterns using artificial neural network

3.1 Introduction

The selection of tunnel support patterns heavily relies on the detailed detection of engineering rock mass characteristics (Bathke 1997; El-Naqa 2001; Marinos et al. 2006; Kaya et al. 2011; Morelli 2015; Cheng et al. 2019). In the past, the preliminary design of the support patterns was mainly based on empirical calculations and standardized rock mass classification systems. Due to the uncertainties in the rock mass behavior, the final selection of the support patterns was determined in construction process according to the exposed geological characteristics. The instability of such support patterns often occurs because of the sudden change of geological conditions ahead of the tunnel face (Kontogianni et al. 2004; Li et al. 2012; Wang et al. 2019). With the advancement of advanced detection technologies, it is possible to use advanced measure while drilling (MWD) technology for geological evaluation ahead of tunnel face (as shown in Fig. 1) (Schunnesson 1996; Sugawara et al. 2003; Høien and Nilsen 2014; Galende-Hernández et al. 2018). At the same time, applications of artificial neural networks (ANN) in decision-making and prediction of engineering problems have been attracted substantial interest to various computation sciences and engineering disciplines, since neural networks have the strong non-linear analysis capabilities and can provide engineers with scientific methods for optimal decision-making (Cai et al. 1998; Caglar and Arman 2007; Sarkar et al. 2010; Adoko et al. 2013; Gordan et al. 2016; Ozer et al. 2019).

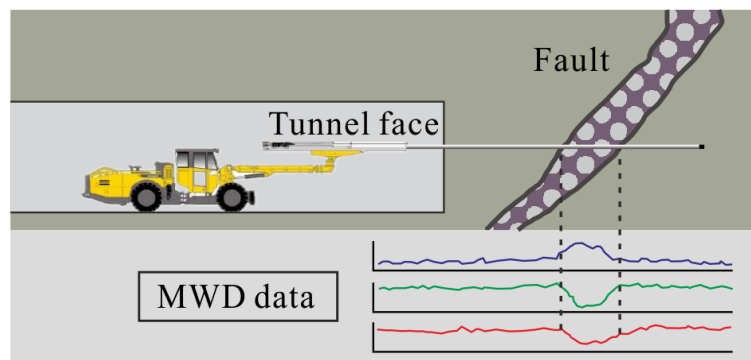


Fig. 3.1 Diagram of direct drilling method

In tunnel construction, although the site survey including rough prediction of rock mass structural properties is generally carried out, unexpected anomalies (i.e., cavities or water bearing, fractured, or relatively stronger zones) that may influence construction safety often exist (Otto et al. 2002; Ryu et al. 2011; Park et al. 2017; Liu et al. 2018; Ren et al. 2019; Han et al. 2020). Such anomalies can be detected by MWD system (Schunnesson 1997), which records the data information of operational parameters involved in drilling. For rotary drilling, Teale (1965) defined the concept of specific energy (SE) as the energy required to excavate unit volume of rock. Rabia (1985) compared different bit selections based on both cost per foot and SE and presented a simplified approach to bit selection that uses the principle of SE. Zhou et al. (2011) proposed an adaptive unsupervised approach based on MWD data to predict the rock types and demonstrated that the proposed approach has a satisfactory performance in identification of rock types by experiments on actual data. Leung and Scheduling (2015) proposed a novel measure called modulated specific energy (SEM) for characterizing drilled material in open-pit coal mining, which can overcome the problems of low specificity and high variability observed in existing MWD approaches. Khorzoughi et al. (2018) correlated drill performance variables (MWD data) with measured fracture logs and identified that drill performance variables can accurately determine open versus closed fractures. In relation to studies developed for percussive and rotary-percussive drilling, Aoki et al. (1999) reported that a drill logging system had been developed in 1995 to evaluate the ground conditions at various depths by the data obtained while boring through the rock with a hydraulic drill. Yue et al. (2004) presented a methodology for identifying zones of volcanic weathering and decomposition grades in the ground through the MWD data monitored from rotary-percussive drilling. Factual data showed that the penetration rate parameter had a close correlation with decomposition grades in the ground. Peng et al. (2005) and Tang (2006) investigated the characteristics of void/fracture and the rock mass properties in roof rocks. The clear correlation between such geological properties and drilling parameters was confirmed. They found that the feed pressure can be used to detect the anomalies or discontinuities in the rock and to predict the rock mass strength. Laudanski et al. (2012) evaluated the drilling measurements individually as well as combined into compound parameters to further enhance the ability of MWD to identify strata characteristics. It demonstrated that MWD can clearly provide qualitative evaluation of soil types, density and permeability using both rotary and percussion drilling methods. Ghosh et al. (2015) used MWD data to evaluate data trends among

logged parameters and calculated average SE. They found that the prediction of SE through penetration rate and feed force was affected greatly by the hole length. From the correlation of MWD data with rock mass geo-mechanical features, Ghosh et al. (2017) suggested a method for distinguishing solid rock, fracture zones, cavities and damaged rock, based on the responses from the drill monitoring system. Navarro et al. (2018) investigated the mutual relation between MWD parameters. They determined that the feed pressure is a lead parameter that drives the adjustment of other parameters. The MWD method is usually implemented to quantify and visualize the geological conditions ahead of the tunnel face, yet directly estimating the support pattern selection is absent because of the difficulty of carrying out the MWD detection during the whole length of tunnel construction.

Furthermore, in the last few years, artificial neural network (ANN) has been proved to be a powerful tool to settle geotechnical engineering problems (Alimoradi et al. 2008; Yilmaz 2009; Ocak and Seker 2012; Dantas Neto et al. 2017; Elkatatny 2019). Kanamoto et al. (2005) and Kimura et al. (2005) accurately predicted the different rock mass rating of a part of one tunnel using ANN based on partial MWD parameters. Guan et al. (2009) proposed a rheological parameter prediction technique using error backpropagation neural network (BPNN) and genetic algorithm, which was proved that the proposed technique can provide an optimal prediction of the rheological parameters and predict the long-term deformations of mountain tunnels in the future. Mahdevari and Torabi (2012) developed a method based on ANN for prediction of convergence in tunnels and carried out a correlation analysis of the convergence data sets with geo-mechanical and geological parameters. They determined that cohesion, internal friction angle, Young's modulus and uniaxial compressive strength are the most effective factors and uniaxial tensile strength is the least effective one. Avunduk et al. (2014) suggested a model for prediction of the roadheaders based on ANN and concluded that the prediction capacity of ANN is better than the empirical models developed previously. Hasanipanah et al. (2016) proposed a new hybrid model of ANN optimized by particle swarm for estimating the maximum surface settlement caused by tunneling. Ghorbani and Firouzi Niavol (2017) applied ANN and evolutionary polynomial regressions to propose a method which can accurately reflect both static and coupled static-dynamic settlements. Ghorbani et al. (2018) used two different classes of ANNs to predict the prediction of the support pressure of circular tunnels in elasto-plastic, strain-softening rock mass. There were many studies focused on geological and geo-mechanical interpretation of rock mass using

MWD data and on solution of geotechnical engineering problems by using ANN. However, the studies involving the prediction of support patterns ahead of tunnel face based on MWD data using ANN, especially for the different support pattern selection under the same rock mass rating, have seldom been reported.

This paper aims at proposing an ANN model, based on the MWD data, to predict the support pattern selection according to the rock mass condition ahead of the tunnel face. A total of 318, 649 MWD data sets along the whole length of a tunnel were used for this assignment by BPNN algorithm. Also, the feasibility of using ANN to predict the support pattern selection was investigated. The effects of different input sample sizes and different neural network structures on the prediction performance of the ANN for tunnel support patterns were analyzed. Finally, the ANN model with optimal prediction performance was recommended.

3.2 Case description

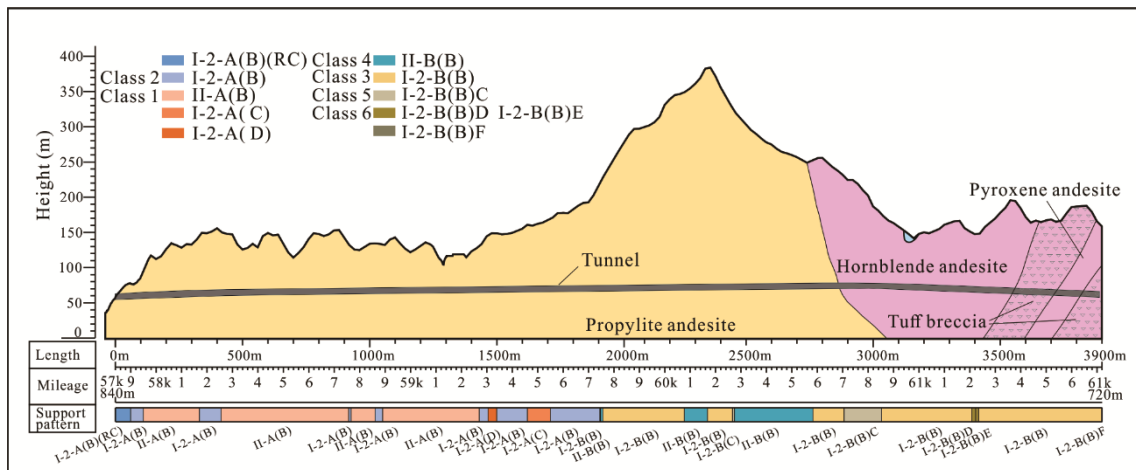


Fig. 3.2 General view of the tunnel support patterns

The data sets used in the study were obtained from the new Nagasaki (east) tunnel project in Japan. The new Nagasaki (east) tunnel is located within the Nagasaki City in the southern part of Japan with an East-Westward trend. The tunnel is in the form of Single-Arch with a length of 3.88 kilometers. The approximate project cost is 60 million USD. The project started in 2013 and has finished in 2017. The tunnel was excavated using the new austrian tunnelling method. In this tunnel construction, many support patterns were applied, namely I-2-A(RC)(B), I-2-A(B), I-2-A(C), I-2-A(D), I-2-B(B), I-2-B(B) C, I-2- B(B) D [I-2-B (B) E], I-2- B (B) F, II-A-B(B) and II-B(B). It should be

noted that due to the lack of part of the drilling data [corresponding to the tunnel with support patterns I-2-A(RC)(B), I-2-A(C), I-2-A(D) and I-2-B(B)F, totaling about 190 meters] collected from the construction site, the selection of the remaining six tunnel support patterns was predicted and analyzed in this study. A general view of the tunnel support patterns used in the on-site construction is shown in Fig. 3.2. Six support patterns were analyzed in this study. The class number of support patterns is shown in Table 3.1. The details of the six support patterns are exhibited in Fig. 3.3 and Table 3.2.

Table 3.1 The classification number of support patterns

Mileage	Distance (m)	Support pattern	Class No.
57K840.0~57K900.0	60.0	I-2-A(RC) (B)	-
57K900.0~57K948.0	48.0	I-2-A(B)	-
57K948.0~58K150.0	202.0	II-A(B)	1
58K150.0~58K167.0	17.0	II-A-B (B)	1
58K167.0~58K259.4	92.4	I-2-A(B)	2
58K259.4~58K750.9	491.5	II-A(B)	1
58K750.9~58K766.5	15.6	I-2-A(B)	2
58K766.5~58K860.4	93.9	II-A(B)	1
58K860.4~58K890.4	30.0	I-2-A(B)	2
58K890.4~59K269.9	379.5	II-A(B)	1
59K269.9~59K303.5	33.6	I-2-A(B)	2
59K303.5~59K339.5	36.0	I-2-A(D)	-
59K339.5~59K460.1	120.6	I-2-A(B)	2
59K460.1~59K555.1	95.0	I-2-A(C)	-
59K555.1~59K746.1	191.0	I-2-A(B)	2
59K746.1~59K747.1	1.0	I-2-B(B)	3
59K747.1~59K756.1	9.0	II-B(B)	-
59K756.1~60K077.7	321.6	I-2-B(B)	3
60K077.7~60K168.4	90.7	II-B(B)	4
60K168.4~60K269.2	100.8	I-2-B(B)	3
60K269.2~60K275.2	6.0	I-2-B(B)C	5
60K275.2~60K582.7	307.5	II-B(B)	4
60K582.7~60K705.1	122.4	I-2-B(B)	3
60K705.1~60K856.3	151.2	I-2-B(B)C	5
60K856.3~61K206.7	350.4	I-2-B(B)	3
61K206.7~61K222.3	15.6	I-2-B(B)D	6
61K222.3~61K234.3	12.0	I-2-B(B)E	6
61K234.3~61K719.1	484.8	I-2-B(B)	3
61K719.1~61K720.0	0.9	I-2-B(B)F	-

Note: The mark "-" represents no drilling data

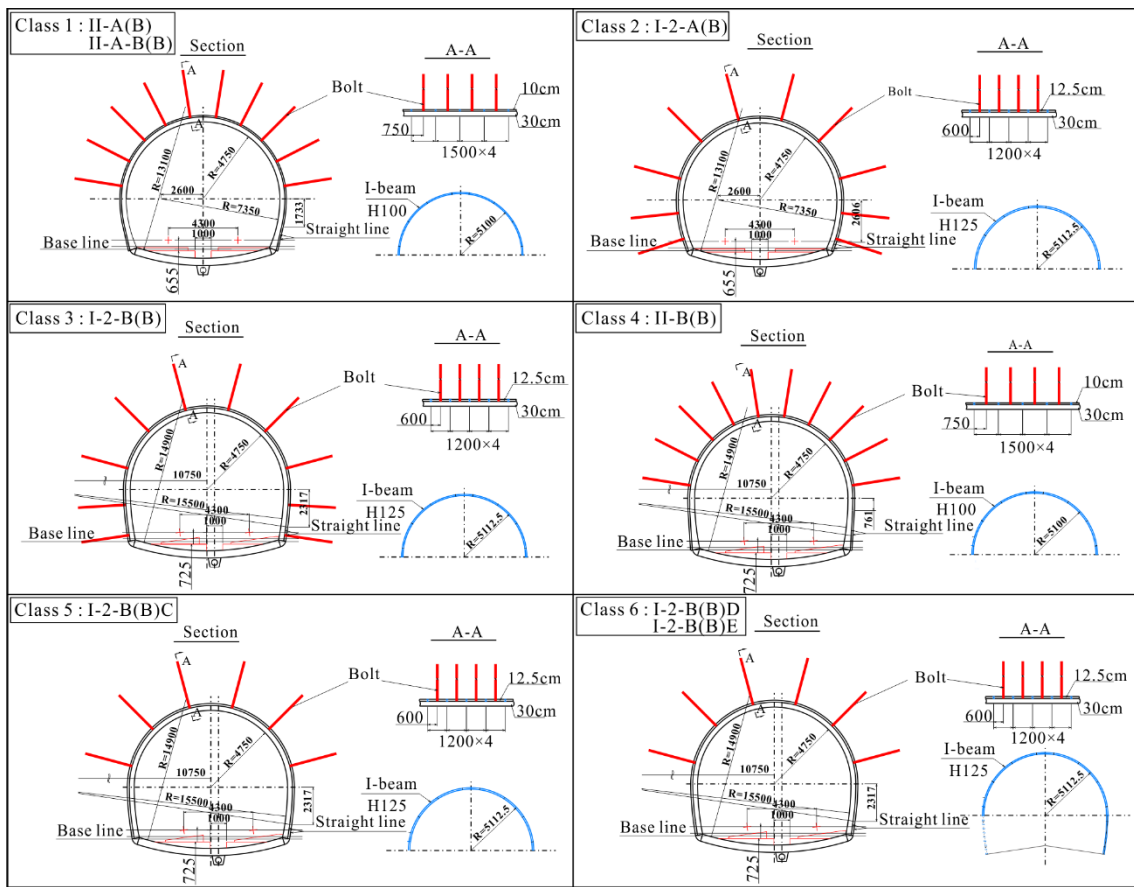


Fig. 3.3 The details of the six support patterns

Table 3.2 The comparison of details of the six support patterns

Parameter	Uite	Class 1	Class 2	Class 3	Class 4	Class 5	Class 6
Number of bolts	-	10	10	10	10	6	6
Space of bolts	mm	1500	1200	1200	1500	1200	1200
Type of I-beam	-	H100	H125	H125	H100	H125	H125
Shape of I-beam	-						
Eccentric or not	logic	N	N	Y	Y	Y	Y
Initial lining thickness	cm	10	12.5	12.5	10	12.5	12.5
Secondary lining thickness	cm	30	30	30	30	30	30

The hydraulic rotary-percussive drill was used for drilling investigation ahead of tunnel face. The MWD data as shown in Fig. 3.4 obtained from the data collection device include penetration rate (PR), hammer pressure (HP), rotation pressure (RP), feed pressure (FP), hammer frequency (HF) and SE. Each set of these data and the class number of the corresponding support pattern constitute a data set. All MWD data are output from the data recording apparatus in real time approximately every 0.25 seconds. The total number

of all data sets from 97 drill holes is 318, 649.

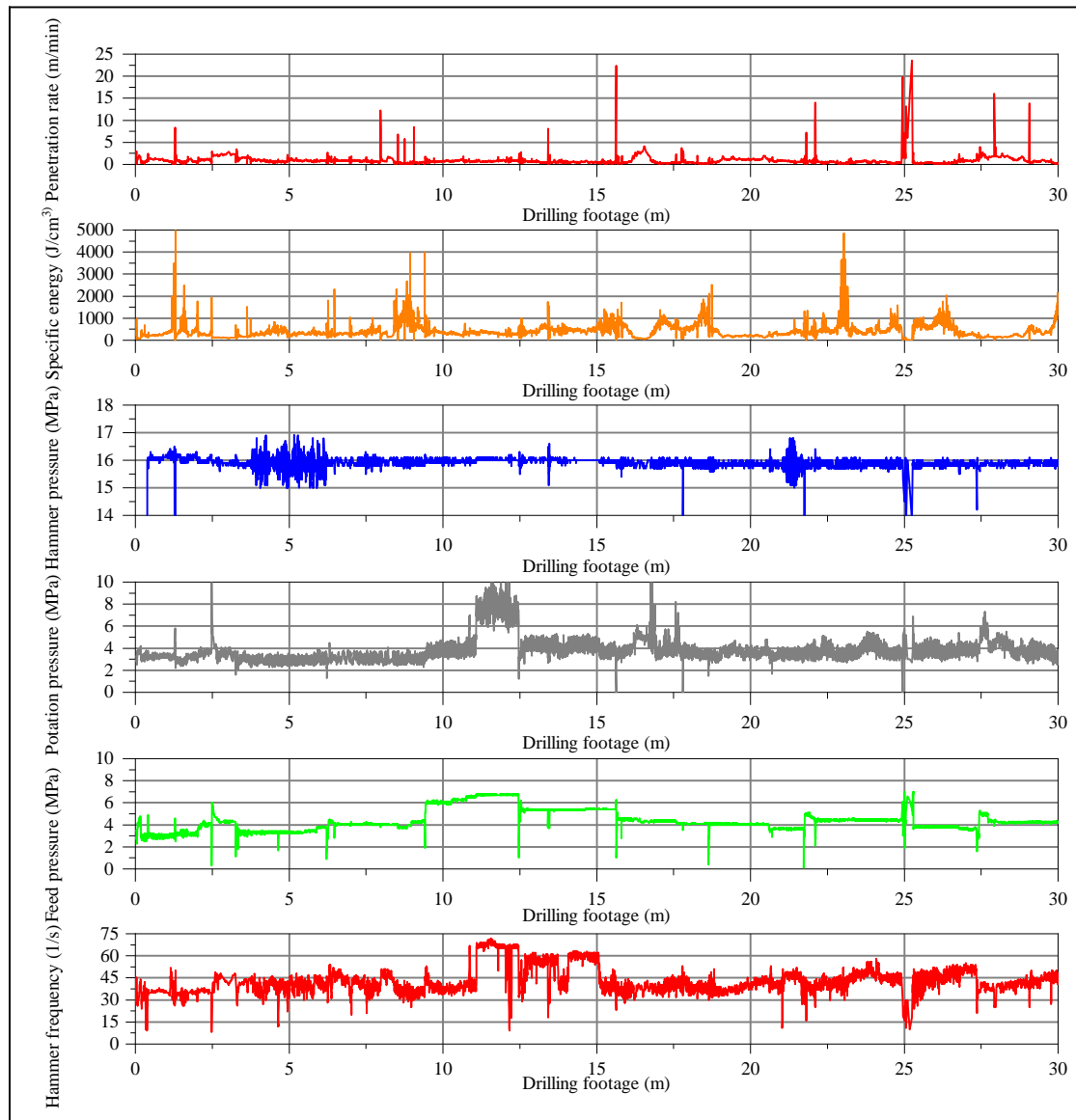


Fig. 3.4 Visualization of the MWD data obtained from a 30 m borehole

In the first stage of the study, an ANN for estimating the class of support patterns was constructed using the numerous data sets. The parameters PR, HP, RP, FP, HF and SE were used as input parameters and the class number was used as output parameter. The range and distribution of the MWD data are tabulated in Table 3.3, in which the data are quite widely distributed.

Table 3.3 Basic descriptive statistics for the original MWD data

Parameter	Symbol	Unit	Class 1			Class 2			
			Class	Support pattern	Number of datasets	Class	Support pattern	Number of datasets	
			1	II-A(B)	66514	2	I-2-A(B)	49228	
			Ave.	Min.	Max.	Ave.	Min.	Max.	
Penetration rate	PR	m/min		0.93	0.02	17.44	0.89	0.00	22.16
Hammer pressure	HP	MPa		15.33	6.00	16.80	14.15	5.10	19.30
Rotation pressure	RP	MPa		4.10	0.00	9.10	3.65	0.00	18.20
Feed pressure	FP	MPa		4.64	0.10	7.70	3.29	0.10	9.40
Hammer frequency	HF	1/s		37.19	0.00	65.00	30.43	0.00	62.00
Specific energy	SE	J/cm ³		378.32	1.00	17028.00	332.69	0.00	13062.80

Parameter	Symbol	Unit	Class 3			Class 4			
			Class	Support pattern	Number of datasets	Class	Support pattern	Number of datasets	
			3	I-2-B(B)	75767	4	II-B(B)	81976	
			Ave.	Min.	Max.	Ave.	Min.	Max.	
Penetration rate	PR	m/min		0.58	0.00	22.58	0.45	0.02	4.99
Hammer pressure	HP	MPa		14.54	5.60	17.80	14.77	5.20	16.80
Rotation pressure	RP	MPa		6.40	0.00	20.00	5.15	0.00	12.50
Feed pressure	FP	MPa		4.39	0.20	9.10	5.00	0.30	7.40
Hammer frequency	HF	1/s		17.82	0.00	66.00	26.66	0.00	57.00
Specific energy	SE	J/cm ³		253.51	0.00	13598.00	332.11	18.30	7013.40

Parameter	Symbol	Unit	Class 5			Class 6			
			Class	Support pattern	Number of datasets	Class	Support pattern	Number of datasets	
			5	I-2-B(B)C	35413	6	I-2-B(B)D	9751	
			Ave.	Min.	Max.	Ave.	Min.	Max.	
Penetration rate	PR	m/min		0.49	0.00	3.01	0.76	0.06	4.99
Hammer pressure	HP	MPa		14.92	6.10	16.00	14.33	12.50	16.00
Rotation pressure	RP	MPa		5.03	2.50	9.90	7.65	3.50	15.10
Feed pressure	FP	MPa		3.98	0.50	6.40	3.83	0.70	6.10
Hammer frequency	HF	1/s		26.84	0.00	55.00	20.10	0.00	56.00
Specific energy	SE	J/cm ³		269.11	0.00	7210.80	182.98	16.90	2389.50

3.3 Model development

ANN is a simplified mathematical model inspired by the biological structure and

functioning of the brain. French and Recknagel (1970) and Park et al. (1991) defined an ANN as a structure consisting of closely connected adaptive processing elements that can perform large-scale parallel computing for data processing. The purpose of ANN studies is to adapt biological neural networks for data processing. Multi-layer perception is a development of the ANN. A typical network topology consists of the input layer, one or more hidden layers and the output layer. The ANN model has a high performance in the modeling of nonlinear multivariable problems, so which is also a powerful tool in geological engineering applications.

The input from the previous layer (x_i) of each processing unit (PE) is multiplied by an adjustable connection weight (w_{ij}) and summed at each PE and then a threshold (θ_j) is added. This summation result is then used as the input (H_j) of the nonlinear transfer function, f , through which the output y_i of the PE is generated. The output of each PE is used as the input of each PE of the next layer. This process is summarized in Eq. 3-1 and Eq. 3-2 (Zurada 1992).

$$H_j = \sum_i^n w_{ij}x_i + \theta_j, \quad (3-1)$$

$$y_j = f(H_j) \quad (3-2)$$

The transfer function, also called the activation function, is designed to map a neuron, or layer, net output to its actual output. The class selection of these transfer functions, including simple linear or nonlinear step functions, depends on the purpose of the ANN. The most common transfer function implemented in the literature is the sigmoid function (Mitchell 1997). The sigmoid function is preferred as the transfer function in this study. The generic formula of the sigmoid function is given in Eq. 3-3.

$$f(x) = \frac{1}{1 + e^{-x}}, \quad (3-3)$$

There are many algorithms that can be applied to ANNs, however the BPNN algorithm is more general technology. It provides an effective learning method for multilayer perception neural networks (Law 2000). One of the purposes of this study is to calculate the best possible values of network weights. In this calculation, the BPNN algorithm is implemented by changing the weights and thresholds according to the results of the output layer. Fig. 3.5 shows the outlook of structure of the error back-propagation neural network (BPNN) model. Each input node of BPNN model represents each MWD parameter, and the output nodes represent six support models. The main flow of BPNN algorithm

includes: Step 1 initialize network, Step 2 calculate outputs of hidden layer, Step 3 calculate outputs of output layer, Step 4 calculate the error, Step 5 update weight and threshold, Step 6 judgment of iteration results. The details of the algorithm are illustrated in Fig. 3.6.

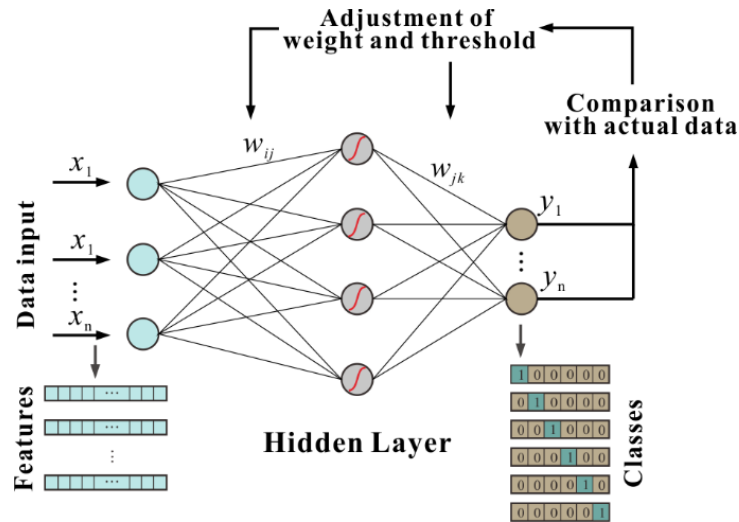


Fig. 3.5 Structure of error back-propagation neural network

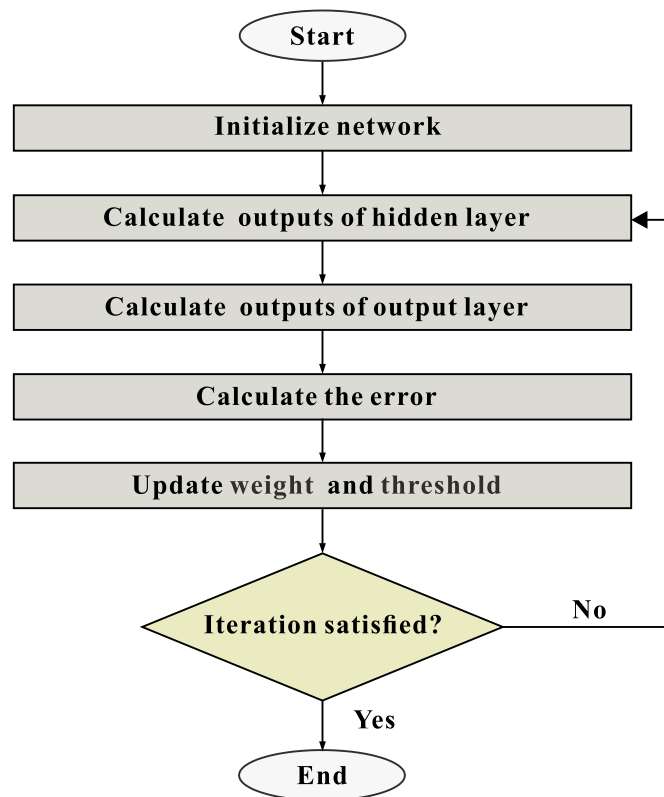


Fig. 3.6 Flow chart of artificial neural network algorithm

3.3.1 *The input and output layer sizes*

The input layer size is equal to the number of input layer nodes multiplied by the number of input samples corresponding to each node. Staufer and Fischer (1997) stated the input layer size is one of the important factors affecting the performance of neural networks. Garson (1998) suggested that input layer size should be 10-30 times the number of input nodes. However, in order to achieve near optimal performance, Hush (1989) recommended to use $[60 \times \text{numbers of input nodes} \times (\text{numbers of input nodes} + 1)]$ training samples in the performance analysis of neural networks for classification problems while Swingler (1996) and Looney (1996) suggested using 20% and 25% of the data for testing, respectively. In the present study, in order to investigate the effect of the input layer size on the prediction performance of neural networks, 3000, 6000, 9000, 12000, 15000, 18000 and 21000 data sets (corresponding to 500, 1000, 1500, 2000, 2500, 3000 and 3500 data sets of each class of support patterns) were used in the training stage, and 600 data sets (corresponding to 100 data sets of the remainder of each class) were used in testing stage.

3.3.2 *The hidden layer sizes*

Determining the number of hidden layers and the number of nodes in these layers is a major task in designing neural networks (Kavzoğlu 2001). Garson (1998) and García-Pedrajas et al. (2005) reported that a single hidden layer is usually sufficient to solve most problems, especially classification issues. Kanellopoulos and Wilkinson (1997) stated that a second hidden layer is recommended when the output layer of the neural network has 20 (or more) nodes. Lippmann (1987) and Rumelhart et al. (1985) indicated that there is rarely an advantage in using more than one hidden layer. Therefore, one hidden layer was preferred in this study. However, the number of nodes in hidden layers is the most critical task in the BPNNs structure. The heuristics proposed for this purpose are summarized in Table 3.4. The number of nodes that may be used in the hidden layer varies between 6 and 18, depending on the proposed heuristics in the literature. However, in order to comprehensively analyze the influence of the number of hidden layer nodes on the classification performance of the neural networks, the number of hidden layer nodes was set as 6, 8, 10, 12, 14, 16, 18, 20, 30, 40, 50, 60, 70, 80, 90 and 100 separately to conduct conducted trials.

Table 3.4 The proposed number of nodes in hidden layer.
(N_i : number of input nodes, N_o : number of output nodes)

Formula	This study ($N_i=6, N_o=6$)	Reference
$\leq 2 \times N_i + 1$	≤ 13	Hecht-Nielsen (1987)
$3N_i$	18	Hush (1989)
$(N_i + N_o)/2$	6	Ripley (1993)
$\frac{2 + N_o \times N_i + 0.5N_o \times (N_o^2 + N_i) - 3}{N_i + N_o}$	13	Paola (1994)
$\sqrt{N_i(N_o + 2)} + 1$	8	Gao (1998)
$\sqrt{N_i \times N_o}$	6	Masters (1993); Kaastra and Boyd (1996)
$2N_i$	12	Kanellopoulos and Wilkinson (1997)

3.3.3 The learning rate and the momentum term

The main disadvantage of the BPNN algorithm is the slow convergence rate, which is mainly related to the selected learning rate (η). If the selected η values is larger, the modification of the weight will be greater and the network convergence will be faster. However, the too large η values will cause oscillations of updating process of weights. And, too small η values will slow the convergence of the network and make the weight difficult to stabilize. The momentum term (α) has a stabilizing effect in the BPNN algorithm (Attoh-Okine 1999). It can be used to improve the convergence while reducing the oscillations of updating process of weights. Refenes et al. (1994) reported that for a layer and a two-layer network, $\eta = 0.2$ and the momentum term of $0.3 < \alpha \leq 0.5$ is the best combination of convergence. Wythoff (1993) set the momentum term between 0.4 and 0.9. After several trials, η values = 0.01 and $\alpha = 0.5$ were set to ensure the convergence of the algorithm before 500 iterations.

3.4 Results and discussion

In this study, different BPNN models were set up applying MATLAB software according to the combination of different numbers of training samples and different network structures defined above to search for the most effective ANN architecture. This study used MATLAB software to develop its own code, without using built-in ANN tool

of the software. In these trials, η of 0.01 and α of 0.5 were used. Testing and validation of the BPNN models were done with date sets shown above. These date sets were randomly selected from the total data sets. The results are presented to demonstrate the performance of the networks. Average accuracy (\bar{A} , \bar{A} = the correctly predicted number of output samples / total number of output samples) and average computing time (\bar{T}) were taken as the performance measures to assess the performance and stability of neural networks. And, average accuracy (\bar{A} , $\bar{A} = A / 10$) and average computing time (\bar{T}) ($\bar{T} = T / 10$) were obtained from 10 trials under the same experimental conditions.

The results obtained for these models are listed in Appendix (A) and shown in Fig. 3.7 and Fig. 3.8. Fig. 3.7 shows a graph with variations in \bar{A}_s with different numbers of training samples and hidden layer nodes. For all training samples, the \bar{A}_s of the predicted results of the BPNN models increase with the increase in the number of hidden layer nodes. The growth curves become horizontal, until the hidden layer node equals 30. In addition, the \bar{A}_s are lowest as the number of samples is 3000, and the difference is small when the number of samples is 6000, 9000, 12000, 15000, 18000 and 21000. For example, when the number of the hidden layer node equals 30, the \bar{A}_s equal to 0.839, 0.839, 0.843, 0.841, 0.847 and 0.844 respectively (as the number of training samples is 6000, 9000, 12000, 15000, 18000 and 21000, respectively).

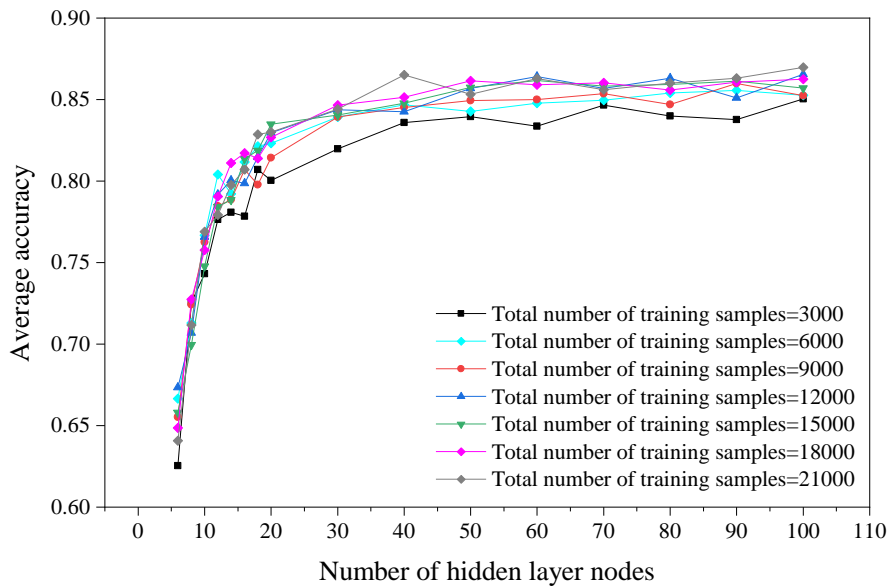


Fig. 3.7 Variations of the average accuracies with different number of training samples and nodes in hidden layer

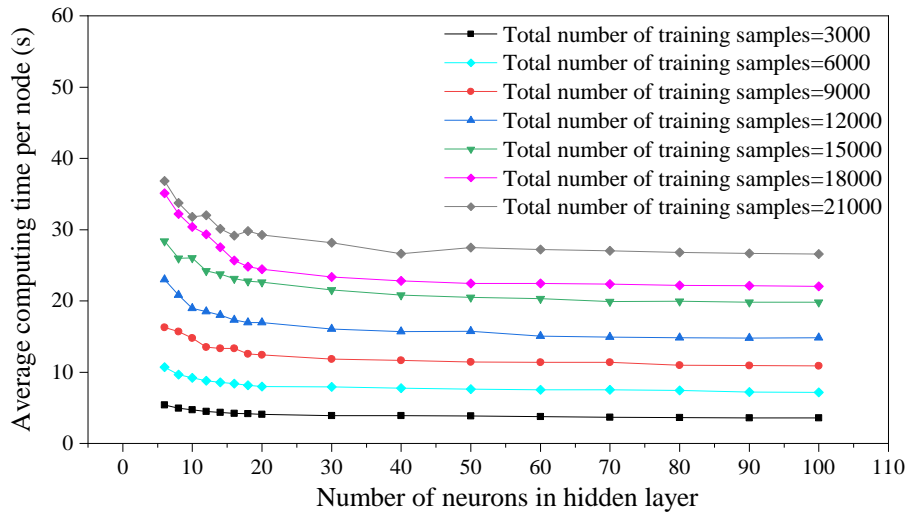


Fig. 3.8 Variations of the average computing time per node

Fig. 3.8 illustrates variations in the \bar{T} per node (\bar{T} per node = \bar{T} / the number of nodes in hidden layer) with different numbers of training samples and hidden layer nodes. For different training samples, when the number of nodes in hidden layer is more than 30, the \bar{T} per node value tend to fixed values of 4, 8, 11, 15, 20, 23 and 27 (as the number of training samples is 3000, 6000, 9000, 12000, 15000, 18000 and 21000, respectively). When the number of nodes in hidden layer is more than 30, the \bar{T} value can be calculated by the formula: $\bar{T} = \bar{T}_f \cdot N_h$ (where, \bar{T}_f = the fixed value of the \bar{T} per node, N_h = the number of nodes in hidden layer), but the performance of the network does not improve. Thus, observing Fig. 3.7, Fig. 3.10, and Appendix (A) and considering the less \bar{T} and the guaranteed performance, the optimal neural network model is proposed with the number of training samples of 6000 and the hidden layer nodes of 30. The prediction results of six classes of the support patterns for the preferred BPNN model have relatively high \bar{A}_s , as shown in Table 3.5.

Fig. 3.9 illustrates variations in \bar{A}_s of prediction results for each class of support patterns in 10 trials based on the preferred BPNN model. The \bar{A}_s of prediction results of the six support patterns have a high robustness, especially for class 1 and class 2. In addition, the comparison between the prediction results and the real classes of the fourth experiment is shown in Fig. 3.10. The \bar{A} values of 0.840, 0.870, 0.840, 0.720, 0.860 and 0.910 (corresponding to six classes of support patterns, respectively). Except for the \bar{A} value of class 4 is less than 0.8, the other classes obtain a higher \bar{A} value. This result

indicates that the MWD data can characterize the rock mass condition ahead of tunnel face and there is a high correlation between predicted and measured values.

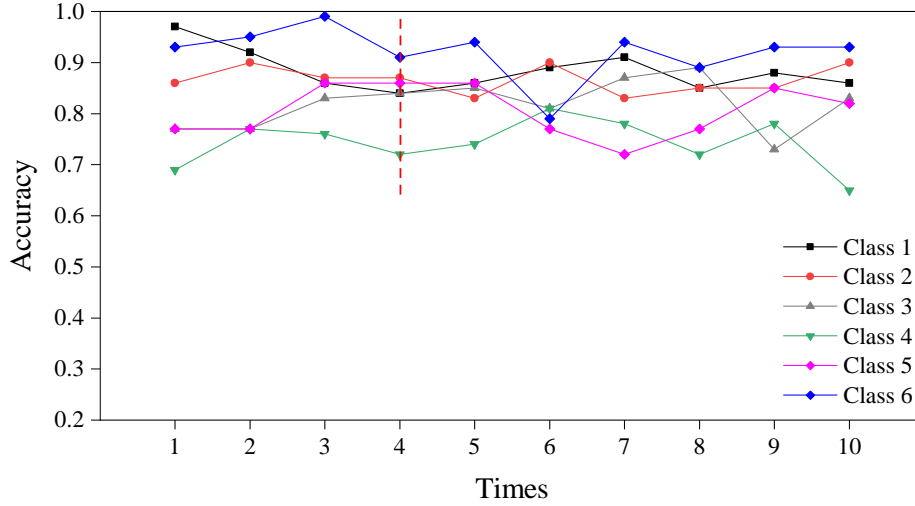


Fig. 3.9 Variations of the accuracies of prediction with each support pattern in 10 trials

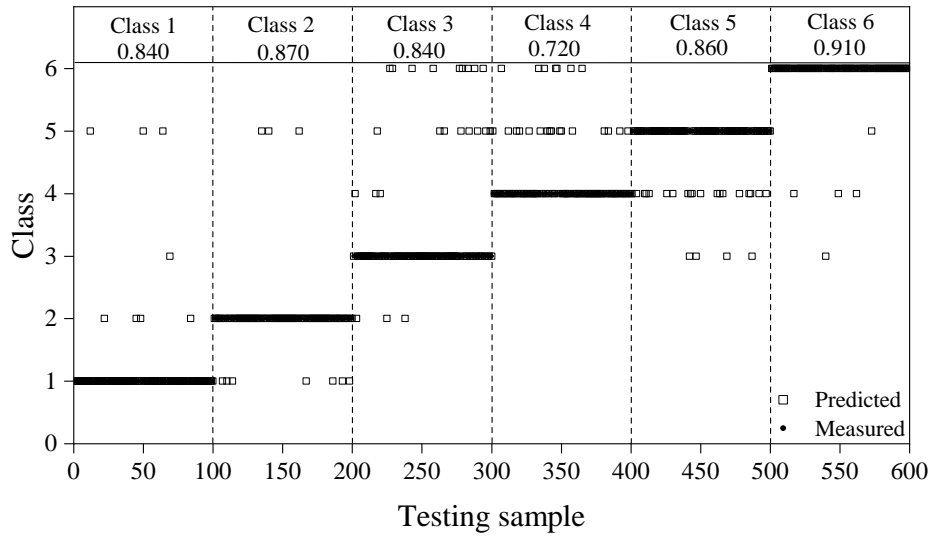


Fig. 3.10 Predicted results for the test sample

Table 3.5 The average accuracy rates of prediction of support pattern selections (with the number of nodes in hidden layer =30, the number of training samples =6000)

Parameter	Class 1	Class 2	Class 3	Class 4	Class 5	Class 6
\bar{A}_s	0.884	0.866	0.819	0.742	0.805	0.920

3.5 Conclusions

This study presented an artificial neural network (ANN) model to predict support pattern selection ahead of tunnel face based on measure while drilling (MWD) data. The MWD data was obtained from 97 drill holes of a high-speed railway tunnel project carried out along 3.88 kilometers long in Japan. In order to obtain the optimal neural network model, controlled trials are conducted considering different input sample sizes and hidden layer sizes. An ANN with 6 inputs (penetration rate (PR), hammer pressure (HP), rotation pressure (RP), feed pressure (FP), hammer frequency (HF) and specific energy (SE)) and 6 outputs (6 dimensions correspond to 6 classes of support patterns) is designed for estimating the selection of support patterns. The architecture of the error backpropagation neural network (BPNN) consists of 1 hidden layer. Numerous training trials are performed starting from a single node to 100 nodes in the hidden layer. Accuracy and computing time of each trial are recorded to obtain the performance index.

The results show that strong correlation exists between MWD data and support patterns, with the optimal prediction results of the average accuracy (\bar{A}) values corresponding to six classes of support patterns are, respectively, 0.884, 0.866, 0.819, 0.742, 0.805 and 0.920. The selection of tunnel support patterns is mainly influenced by the geotechnical condition of the rock mass. The prediction performance of ANN is affected by the input sample sizes and the hidden layer sizes. An input sample size greater than 6000 samples and a hidden layer size greater than 30 neurons do not have an optimizing effect on the performance. An optimal ANN model is obtained with 6000 samples in input layer and 1 hidden layer with 30 nodes. The ANN draws an excellent performance using only 2% of the total samples as training samples and is a convenient tool for estimating tunnel support pattern selection ahead of tunnel face. It can be stated that the prediction of tunnel support pattern selection using ANN can be used as an essential knowledge of project engineers for improving the safety and reliability of tunnel engineering.

In the present study, the commonly used BPNN model is utilized to demonstrate the correlation between the MWD data and the support pattern selection. As a prior work, the ANN models with other outstanding algorithms are not adopted but will be considered in the future studies. The present study established the BPNN models with all the MWD data parameters, which is therefore merely an initial step to explore the concerned topic. More combinatorial and complex parameters based on the MWD data parameters need to be considered to improve the prediction performance of the ANN. Besides, more

verification and analysis based on other tunnel projects under similar geological conditions should be carried out to understand the adaptability of the proposed ANN prediction model in the future works.

References

- Adoko AC, Jiao YY, Wu L, Wang H, Wang ZH (2013), Predicting tunnel convergence using multivariate adaptive regression spline and artificial neural network. *Tunn Undergr Space Technol*, 38:368-376. <https://doi.org/10.1016/j.tust.2013.07.023>
- Alimoradi A, Moradzadeh A, Naderi R, Salehi MZ, Etemadi A (2008), Prediction of geological hazardous zones in front of a tunnel face using TSP-203 and artificial neural networks. *Tunn Undergr Space Technol*, 23:711-717. <https://doi.org/10.1016/j.tust.2008.01.001>
- Aoki K, Shirasagi S, Yamamoto T, Inou M, Nishioka K (1999), Examination of the application of drill Logging to predict ahead of the tunnel face. In: Proceedings of the 54th Annual Conference of the Japan Society of Civil Engineers, Tokyo, Japan, September 1999. pp 412-413. (In Japanese)
- Attoh-Okine NO (1999), Analysis of learning rate and momentum term in backpropagation neural network algorithm trained to predict pavement performance. *Adv Eng Software*, 30:291-302. [https://doi.org/10.1016/S0965-9978\(98\)00071-4](https://doi.org/10.1016/S0965-9978(98)00071-4)
- Avunduk E, Tumac D, Atalay AK (2014), Prediction of roadheader performance by artificial neural network. *Tunn Undergr Space Technol*, 44:3-9. <https://doi.org/10.1016/j.tust.2014.07.003>
- Bathke CG (1997), Systems analysis in support of the selection of the ARIES-RS design point. *Fusion Eng Des*, 38:59-86. [https://doi.org/10.1016/S0920-3796\(97\)00112-9](https://doi.org/10.1016/S0920-3796(97)00112-9)
- Caglar N, Arman H (2007), The applicability of neural networks in the determination of soil profiles. *Bull Eng Geol Environ*, 66:295-301. 10.1007/s10064-006-0075-9
- Cai J, Zhao J, Hudson J (1998), Computerization of rock engineering systems using neural networks with an expert system. *Rock Mech Rock Eng*, 31:135-152.
- Cheng Z, Yang S, Li L, Zhang L (2019), Support working resistance determined on top-coal caving face based on coal-rock combined body. *Geomechanics Engineering*, 19:255-268. <https://doi.org/10.12989/gae.2019.19.3.255>
- Dantas Neto SA, Indraratna B, Oliveira DAF, de Assis AP (2017), Modelling the shear

- behaviour of clean rock discontinuities using artificial neural networks. *Rock Mech Rock Eng*, 50:1817-1831. <http://10.1007/s00603-017-1197-z>
- El-Naqa A (2001), Application of RMR and Q geomechanical classification systems along the proposed Mujib Tunnel route, central Jordan. *Bull Eng Geol Environ*, 60:257-269.
- Elkhatatny S (2019), Development of a new rate of penetration model using self-adaptive differential evolution-artificial neural network. *Arabian J Geosci*, 12:19. <https://doi.org/10.1007/s12517-018-4185-z>
- French M, Recknagel F (1970), Modeling of algal blooms in freshwaters using artificial neural networks. *WIT Trans Ecol Environ*, 6
- Galende-Hernández M, Menéndez M, Fuente MJ, Sainz-Palmero GI (2018), Monitor-While-Drilling-based estimation of rock mass rating with computational intelligence: The case of tunnel excavation front. *Autom Constr*, 93:325-338. <https://doi.org/10.1016/j.autcon.2018.05.019>
- Gao D (1998), On structures of supervised linear basis function feedforward three-layered neural networks. *Chinese Journal of Computers*, 1
- García-Pedrajas N, Hervás-Martínez C, Ortiz-Boyer D (2005), Cooperative Coevolution of Artificial Neural Network Ensembles for Pattern Classification. *IEEE Trans Evol Comput*, 9:271-302.
- Garson GD (1998), *Neural networks: An introductory guide for social scientists*. Sage, London.
- Ghorbani A, Firouzi Niavol M (2017), Evaluation of induced settlements of piled rafts in the coupled static-dynamic loads using neural networks and evolutionary polynomial regression. *Applied Computational Intelligence and Soft Computing*, 2017
- Ghorbani A, Hasanzadehshooiili H, Sadowski Ł (2018), Neural prediction of tunnels' support pressure in elasto-plastic, strain-softening rock mass. *Applied Sciences*, 8:841.
- Ghosh R, Danielsson M, Gustafson A, Falksund H, Schunnesson H (2017), Assessment of rock mass quality using drill monitoring technique for hydraulic ITH drills. *Int J Min Miner Process Eng*, 8:169-186.
- Ghosh R, Schunnesson H, Kumar U (2015), The use of specific energy in rotary drilling: the effect of operational parameters. In: *Proceedings of the 37th International Symposium, May 2015. Application of Computers and Operations Research in the*

- Mineral Industry. pp 713-723.
- Gordan B, Jahed Armaghani D, Hajihassani M, Monjezi M (2016), Prediction of seismic slope stability through combination of particle swarm optimization and neural network. *Eng Comput*, 32:85-97. <http://10.1007/s00366-015-0400-7>
- Guan Z, Jiang Y, Tanabashi Y (2009), Rheological parameter estimation for the prediction of long-term deformations in conventional tunnelling. *Tunn Undergr Space Technol*, 24:250-259. <https://doi.org/10.1016/j.tust.2008.08.001>
- Han W, Li G, Sun Z, Luan H, Liu C, Wu X (2020), Numerical investigation of a foundation pit supported by a composite soil nailing structure. *Symmetry*, 12:252. <https://doi.org/10.3390/sym12020252>
- Hasanipanah M, Noorian-Bidgoli M, Jahed Armaghani D, Khamesi H (2016), Feasibility of PSO-ANN model for predicting surface settlement caused by tunneling. *Eng Comput*, 32:705-715. <http://10.1007/s00366-016-0447-0>
- Hecht-Nielsen R Kolmogorov's mapping neural network existence theorem. In: *Proceedings of the international conference on Neural Networks*, 1987. IEEE Press New York, pp 11-14.
- Høien AH, Nilsen B (2014), Rock mass grouting in the Løren Tunnel: case study with the main focus on the groutability and feasibility of drill parameter interpretation. *Rock Mech Rock Eng*, 47:967-983. <http://10.1007/s00603-013-0386-7>
- Hush DR (1989), Classification with neural networks: a performance analysis. In: *Proceedings of the IEEE International Conference on Systems Engineering*, August 1989. pp 277-280.
- Kaastra I, Boyd M (1996), Designing a neural network for forecasting financial and economic time series. *Neurocomputing*, 10:215-236. [https://doi.org/10.1016/0925-2312\(95\)00039-9](https://doi.org/10.1016/0925-2312(95)00039-9)
- Kanamoto T, Ohnishi Y, Nishiyama S, Uehara S, Kimura T, Yamashita M (2005), Study on application of neural network to evaluation of geological condition using drilling survey system. Paper presented at the Proceedings of the 60th JSCE Annual Meeting, 2005.
- Kanellopoulos I, Wilkinson GG (1997), Strategies and best practice for neural network image classification. *Int J Remote Sens*, 18:711-725.
- Kavzoğlu T (2001), An investigation of the design and use of feed-forward artificial

- neural networks in the classification of remotely sensed images. Dissertation, University of Nottingham.
- Kaya A, Bulut F, Sayin A (2011), Analysis of support requirements for a tunnel portal in weak rock: A case study from Turkey. *Scientific Research and Essays*, 6:6566-6583.
- Khorzoughi MB, Hall R, Apel D (2018), Rock fracture density characterization using measurement while drilling (MWD) techniques. *International Journal of Mining Science and Technology*, 28:859-864. <https://doi.org/10.1016/j.ijmst.2018.01.001>
- Kimura T, Ohnishi Y, Nishiyama S, Ishiyama K (2005), Study on prediction ahead of tunnel face by using drilling survey method. *Geoinformatics*, 16:191.
- Kontogianni V, Tzortzis A, Stiros S (2004), Deformation and failure of the Tymfristos tunnel, Greece. *J Geotech Geoenviron Eng*, 130:1004-1013.
- Laudanski G, Reiffsteck P, Tacita J, Desanneaux G, Benoît J (2012), Experimental study of drilling parameters using a test embankment. In: *Proceedings of the Fourth International Conference on Geotechnical and Geophysical Site Characterization, Pernambuco, Brazil, September 2012*. CRC Press Porto de Galinhas-Pernambuco, pp 435-440.
- Law R (2000), Back-propagation learning in improving the accuracy of neural network-based tourism demand forecasting. *Tourism Management*, 21:331-340. [https://doi.org/10.1016/S0261-5177\(99\)00067-9](https://doi.org/10.1016/S0261-5177(99)00067-9)
- Leung R, Scheduling S (2015), Automated coal seam detection using a modulated specific energy measure in a monitor-while-drilling context. *Int J Rock Mech Min Sci*, 75:196-209. <https://doi.org/10.1016/j.ijrmms.2014.10.012>
- Li L et al. (2012), Spatial deformation mechanism and load release evolution law of surrounding rock during construction of super-large section tunnel with soft broken surrounding rock masses. *Chin J Rock Mechan Eng*, 10:2109-2118.
- Lippmann RP (1987), An introduction to computing with neural nets. *IEEE Assp magazine*, 4:4-22.
- Liu B, Chen L, Li S, Xu X, Liu L, Song J, Li M (2018), A new 3D observation system designed for a seismic ahead prospecting method in tunneling. *Bull Eng Geol Environ*, 77:1547-1565. 10.1007/s10064-017-1131-3
- Looney CG (1996), Advances in feedforward neural networks: demystifying knowledge acquiring black boxes. *IEEE Transactions on Knowledge & Data Engineering*:211-226.

- Mahdevari S, Torabi SR (2012), Prediction of tunnel convergence using artificial neural networks. *Tunn Undergr Space Technol*, 28:218-228. <https://doi.org/10.1016/j.tust.2011.11.002>
- Marinos P, Hoek E, Marinos V (2006), Variability of the engineering properties of rock masses quantified by the geological strength index: the case of ophiolites with special emphasis on tunnelling. *Bull Eng Geol Environ*, 65:129-142. <http://10.1007/s10064-005-0018-x>
- Masters T (1993), *Practical neural network recipes in C++*. Morgan Kaufmann, San Francisco.
- Mitchell TM (1997), Evaluating hypotheses. *Machine Learning*:128-153.
- Morelli GL (2015), Variability of the GSI index estimated from different quantitative methods. *Geotech Geol Eng*, 33:983-995. <http://10.1007/s10706-015-9880-x>
- Navarro J, Sanchidrian JA, Segarra P, Castedo R, Paredes C, Lopez LM (2018), On the mutual relations of drill monitoring variables and the drill control system in tunneling operations. *Tunn Undergr Space Technol*, 72:294-304. <https://doi.org/10.1016/j.tust.2017.10.011>
- Ocak I, Seker SE (2012), Estimation of elastic modulus of intact rocks by artificial neural network. *Rock Mech Rock Eng*, 45:1047-1054. <http://10.1007/s00603-012-0236-z>
- Otto R, Button E, Bretterebner H, Schwab P (2002), The application of TRT-true reflection tomography-at the Unterwald Tunnel. *Felsbau*, 20:51-56.
- Ozer U, Karadogan A, Ozyurt MC, Sahinoglu UK, Sertabipoglu Z (2019), Environmentally sensitive blasting design based on risk analysis by using artificial neural networks. *Arabian J Geosci*, 12:60. 10.1007/s12517-018-4218-7
- Paola J (1994), *Neural network classification of multispectral imagery*. Dissertation, The University of Arizona.
- Park DC, El-Sharkawi M, Marks R, Atlas L, Damborg M (1991), Electric load forecasting using an artificial neural network. *IEEE Trans Power Syst*, 6:442-449.
- Park J, Lee KH, Kim BK, Choi H, Lee IM (2017), Predicting anomalous zone ahead of tunnel face utilizing electrical resistivity: II. Field tests. *Tunn Undergr Space Technol*, 68:1-10. <https://doi.org/10.1016/j.tust.2017.05.017>
- Peng S, Tang D, Sasaoka T, Luo Y, Finfinger G, Wilson G (2005), A method for quantitative void/fracture detection and estimation of rock strength for underground

- mine roof. In: Proceedings of 24th International Conference on Ground Control in Mining, Morgantown, USA, August 2005. pp 195-197.
- Rabia H (1985), Specific energy as a criterion for bit selection. *Journal of petroleum technology*, 37:1,225-221,229.
- Refenes AN, Zapranis A, Francis G (1994), Stock performance modeling using neural networks: a comparative study with regression models. *Neural networks*, 7:375-388.
- Ren F, Zhu C, He M (2019), Moment Tensor Analysis of Acoustic Emissions for Cracking Mechanisms During Schist Strain Burst. *Rock Mechanics Rock Engineering*:1-12. <https://doi.org/10.1007/s00603-019-01897-3>
- Ripley BD (1993), Statistical aspects of neural networks. *Networks and chaos—statistical and probabilistic aspects*, 50:40-123.
- Rumelhart DE, Hinton GE, Williams RJ (1985), Learning internal representations by error propagation. *California Univ San Diego La Jolla Inst for Cognitive Science*,
- Ryu HH, Cho GC, Yang SD, SHIN HK (2011), Development of tunnel electrical resistivity prospecting system and its applicaton. *Geoelectric Monitoring*:179.
- Sarkar K, Tiwary A, Singh TN (2010), Estimation of strength parameters of rock using artificial neural networks. *Bull Eng Geol Environ*, 69:599-606. 10.1007/s10064-010-0301-3
- Schunnesson H (1996), RQD predictions based on drill performance parameters. *Tunn Undergr Space Technol*, 11:345-351.
- Schunnesson H (1997), Drill process monitoring in percussive drilling for location of structural features, lithological boundaries and rock properties, and for drill productivity evaluation. *Dissertation, Luleå tekniska universitet*.
- Staufer P, Fischer MM (1997), Spectral pattern recognition by a two-layer perceptron: effects of training set size. In: *Neurocomputation in Remote Sensing Data Analysis*. Springer, Berlin, pp 105-116.
- Sugawara J, Yue Z, Tham L, Law K, Lee C (2003), Weathered rock characterization using drilling parameters. *Canadian geotechnical journal*, 40:661-668.
- Swingler K (1996), *Applying neural networks: a practical guide*. Morgan Kaufmann, San Francisco.
- Tang X (2006), Development of real time roof geology detection system using drilling parameters during roof bolting operation. *Dissertations, West Virginia University*.

- Teale R (1965), The concept of specific energy in rock drilling. In: International Journal of Rock Mechanics and Mining Sciences & Geomechanics Abstracts, 1965. vol 1. Elsevier, pp 57-73.
- Wang J, Li S-c, Li L-p, Lin P, Xu Z-h, Gao C-l (2019), Attribute recognition model for risk assessment of water inrush. Bull Eng Geol Environ, 78:1057-1071. <https://doi.org/10.1007/s10064-017-1159-4>
- Wythoff BJ (1993), Backpropagation neural networks: a tutorial. Chemometrics and Intelligent Laboratory Systems, 18:115-155.
- Yilmaz I (2009), A case study from Koyulhisar (Sivas-Turkey) for landslide susceptibility mapping by artificial neural networks. Bull Eng Geol Environ, 68:297-306. <https://doi.org/10.1007/s10064-009-0185-2>
- Yue ZQ, Lee CF, Law KT, Tham LG (2004), Automatic monitoring of rotary-percussive drilling for ground characterization—illustrated by a case example in Hong Kong. Int J Rock Mech Min Sci, 41:573-612. <https://doi.org/10.1016/j.ijrmms.2003.12.151>
- Zhou H, Hatherly P, Ramos F, Nettleton E An adaptive data driven model for characterizing rock properties from drilling data. In: 2011 IEEE International Conference on Robotics and Automation, Shanghai, China, May 2011. IEEE, pp 1909-1915.
- Zurada JM (1992), Introduction to artificial neural systems, West, St. Paul, Minn

Appendix (A)

The results obtained for different models (N_{ts} : Number of training samples \bar{A} : average accuracies \bar{T} : average computing times)

No.	N_{ts}	Network structure	\bar{A}	\bar{T}	No.	N_{ts}	Network structure	\bar{A}	\bar{T}
1	3000	6-6-6	0.625	32.52	57	12000	6-30-6	0.844	481.93
2	3000	6-8-6	0.726	39.60	58	12000	6-40-6	0.843	627.40
3	3000	6-10-6	0.743	46.99	59	12000	6-50-6	0.857	785.90
4	3000	6-12-6	0.777	53.73	60	12000	6-60-6	0.864	902.55
5	3000	6-14-6	0.781	61.04	61	12000	6-70-6	0.857	1044.66
6	3000	6-16-6	0.778	67.79	62	12000	6-80-6	0.863	1185.99
7	3000	6-18-6	0.807	75.32	63	12000	6-90-6	0.851	1329.98
8	3000	6-20-6	0.801	81.85	64	12000	6-100-6	0.866	1482.69
9	3000	6-30-6	0.820	117.16	65	15000	6-6-6	0.658	170.31
10	3000	6-40-6	0.836	156.77	66	15000	6-8-6	0.700	207.90
11	3000	6-50-6	0.840	191.76	67	15000	6-10-6	0.748	260.11
12	3000	6-60-6	0.834	226.58	68	15000	6-12-6	0.784	290.86
13	3000	6-70-6	0.847	258.01	69	15000	6-14-6	0.789	332.43
14	3000	6-80-6	0.840	288.74	70	15000	6-16-6	0.814	370.22
15	3000	6-90-6	0.838	323.84	71	15000	6-18-6	0.819	409.76
16	3000	6-100-6	0.850	358.32	72	15000	6-20-6	0.835	452.75
17	6000	6-6-6	0.667	64.34	73	15000	6-30-6	0.841	646.23
18	6000	6-8-6	0.713	77.29	74	15000	6-40-6	0.848	832.62
19	6000	6-10-6	0.767	92.09	75	15000	6-50-6	0.858	1025.32
20	6000	6-12-6	0.804	105.59	76	15000	6-60-6	0.862	1217.78
21	6000	6-14-6	0.792	119.72	77	15000	6-70-6	0.858	1393.02
22	6000	6-16-6	0.812	133.91	78	15000	6-80-6	0.859	1594.97
23	6000	6-18-6	0.821	146.61	79	15000	6-90-6	0.861	1785.53
24	6000	6-20-6	0.823	160.08	80	15000	6-100-6	0.857	1982.60
25	6000	6-30-6	0.839	238.43	81	18000	6-6-6	0.649	210.49
26	6000	6-40-6	0.847	310.50	82	18000	6-8-6	0.728	257.58
27	6000	6-50-6	0.843	380.44	83	18000	6-10-6	0.758	304.03
28	6000	6-60-6	0.848	451.46	84	18000	6-12-6	0.791	351.97
29	6000	6-70-6	0.850	527.90	85	18000	6-14-6	0.811	385.43
30	6000	6-80-6	0.854	594.81	86	18000	6-16-6	0.817	410.93
31	6000	6-90-6	0.856	647.51	87	18000	6-18-6	0.814	446.27

No.	N_{ts}	Network structure	\bar{A}	\bar{T}	No.	N_{ts}	Network structure	\bar{A}	\bar{T}
32	6000	6-100-6	0.853	715.04	88	18000	6-20-6	0.827	488.55
33	9000	6-6-6	0.655	97.71	89	18000	6-30-6	0.847	701.35
34	9000	6-8-6	0.724	125.41	90	18000	6-40-6	0.852	912.10
35	9000	6-10-6	0.763	147.86	91	18000	6-50-6	0.862	1121.67
36	9000	6-12-6	0.785	162.22	92	18000	6-60-6	0.859	1346.63
37	9000	6-14-6	0.789	186.46	93	18000	6-70-6	0.860	1564.15
38	9000	6-16-6	0.807	213.57	94	18000	6-80-6	0.856	1775.91
39	9000	6-18-6	0.798	226.23	95	18000	6-90-6	0.861	1992.42
40	9000	6-20-6	0.814	248.16	96	18000	6-100-6	0.863	2202.52
41	9000	6-30-6	0.839	354.97	97	21000	6-6-6	0.641	264.03
42	9000	6-40-6	0.845	466.27	98	21000	6-8-6	0.712	269.94
43	9000	6-50-6	0.849	570.81	99	21000	6-10-6	0.769	317.92
44	9000	6-60-6	0.850	681.77	100	21000	6-12-6	0.779	384.37
45	9000	6-70-6	0.854	795.41	101	21000	6-14-6	0.798	421.30
46	9000	6-80-6	0.847	879.06	102	21000	6-16-6	0.807	466.45
47	9000	6-90-6	0.860	984.95	103	21000	6-18-6	0.829	536.72
48	9000	6-100-6	0.853	1089.28	104	21000	6-20-6	0.830	585.45
49	12000	6-6-6	0.673	137.86	105	21000	6-30-6	0.844	845.34
50	12000	6-8-6	0.707	166.43	106	21000	6-40-6	0.865	1064.07
51	12000	6-10-6	0.766	189.64	107	21000	6-50-6	0.853	1374.39
52	12000	6-12-6	0.792	221.92	108	21000	6-60-6	0.863	1631.82
53	12000	6-14-6	0.800	251.86	109	21000	6-70-6	0.856	1890.87
54	12000	6-16-6	0.799	277.25	110	21000	6-80-6	0.860	2144.15
55	12000	6-18-6	0.815	305.10	111	21000	6-90-6	0.863	2401.31
56	12000	6-20-6	0.830	339.63	112	21000	6-100-6	0.870	2655.73

4 Influence of different combinations of MWD parameters on prediction of tunnel support patterns

4.1 Introduction

As a mountainous country, in most cases, mountain tunnels are indispensable for transportation such as railways and highways in Japan. The stability of such tunnels is generally affected by hazardous geological conditions such as cavities or water bearing, fractured, or relatively stronger zones (Miura 2003; Gong et al. 2013; Mikaeil et al. 2016; Liu et al. 2020; Zhou et al. 2020). In the mountain tunnel design process, engineers perform a geotechnical investigation generally by means of surface exploration e.g., borehole drilling, geophysical exploration, and geologic mapping, to yield predicts of overall geological profiles (Dahlin et al. 1999; Soupios et al. 2008; Kun and Onargan 2013; Park et al. 2017). Unexpected geological conditions may occur if only depending on the crude drawings of overall geological profiles, which seriously threaten the tunnel support stability (Kontogianni et al. 2004; Li et al. 2012; Wang and Meng 2018). During the excavation, advanced Measure While Drilling (MWD) technology (Schunnesson 1997) implemented in construction site can provide more accurate geological condition information ahead of tunnel face (Friant et al. 1997; Lindén 2005; Nilsen 2015; Navarro et al. 2018; van Eldert et al. 2019). Furthermore, numerous successful applications of artificial neural network (ANN) technology in engineering cases make it possible to predict the selection of support patterns ahead of tunnel face (Yang and Zhang 1997; Rafiq et al. 2001; Guan et al. 2009; Zhang et al. 2017; Ghorbani et al. 2018; Kwon and Lee 2018; Koopialipoor et al. 2019).

It is necessary to grasp precisely the geological conditions ahead of tunnel face to ensure the effectiveness of the selected tunnel support pattern (Singh et al. 1992; El-Naqa 2001; Bizjak and Petkovšek 2004; Kaya et al. 2011; Elyasi et al. 2016). In geological engineering, many researchers have carried out the study of evaluating geological conditions by MWD method. Schunnesson (1998) has focused on MWD extensively and analyzed the correlation between the MWD data and the characteristics of specific rock class. The potential of for RQD (Rock Quality Designation) classification ahead of the tunnel face from MWD data was pointed out. Segui and Higgins (2002) concluded that

with the elimination of human errors in classification and the development of automated logging systems, MWD data can provide an accurate description of the rock mass. Ghosh et al. (2015) evaluated data trends among logged parameters and calculated average specific energy (SE) by MWD data. It demonstrated that there is a significant hole length dependency for penetration rate (PR) and feed pressure (FP) affecting the predicted specific energy. Galende-Hernández et al. (2018) introduced an MWD based methodology for support tunnel construction: Rock Mass Rating (RMR) prediction was provided by excavation surface features and expert knowledge based on MWD data. The results showed a good and serviceable performance. The above researches confirm that the MWD data can characterize the geological condition of rocks. However, the possibility of using such measured data directly to predict the support patterns ahead of tunnel face requires further investigate.

Artificial neural network (ANN) is one artificial intelligence (AI) application which imitates the structure and behavior of neurons in the human brain and can be trained to recognize and categorize complex patterns (Ben Ali et al. 2015; Xue 2019). Pattern recognition is carried out by training and adjusting the parameters of the ANN through error minimization process (Lo et al. 1995; Basu et al. 2010). They can be calibrated using any class of input data, such as MWD data and corresponding rock quality designation (RQD) and the output can be classified into any given number of categories (Kumar et al. 2019). ANN has been recently applied to tunnel engineering problems, such as classification of rock mass rating (Qiu et al. 2014; Nikafshan Rad et al. 2015; Hussain et al. 2016), prediction of tunnel convergence (Yi et al. 2006; Mahdevari and Torabi 2012; Mahdevari et al. 2012) and surface settlement (Kim et al. 2001; Suwansawat and Einstein 2006; Ocak and Seker 2013). For rock support, Utt (1999) pointed out that based on the ANN technology, the MWD data can be converted into the characteristics of appropriate proportion, and the strength of the formation can be classified. In 2002, the real-time monitoring system using ANN to predict the strength of continuous strata was reported in detail by Utt et al. (2002), and the feasibility of the system was verified in the laboratory. Leu et al. (2001) proposed a data mining method for the prediction of tunnel support stability by ANN, and the results showed that ANN is superior to the traditional discriminant analysis and multiple nonlinear regression method in the prediction of tunnel support stability. Based on machine learning and computational intelligence technology, Galende-Hernández et al. (2018) used MWD data to predict rock mass rating. The results indicated that the accuracy of this method is high, and the error is about 3%. However,

the studies involving the prediction of support patterns ahead of tunnel face based on MWD data using ANN, have not been reported.

In this study, the ANN was used to predict the support patterns ahead of the tunnel face based on the MWD data. A total of 318, 649 MWD data sets obtained along the whole length of a tunnel were used for this assignment. Also, the feasibility of using ANN to predict the support patterns based on the MWD data was investigated. The effects of different neural network structures on the prediction performance of the ANN for tunnel support patterns were analyzed. Furthermore, all possible combinations of the six MWD parameters were used to evaluate the prediction performance. The sensitivity of each feature to the prediction performance of the ANN was compared. The stability of the prediction performance of the superior ANN models were analyzed as well. Finally, the ANN model with optimal prediction performance was recommended.







4.2 Data collection

The new Nagasaki tunnel is the longest (7.46 km) tunnel of West Kyushu Line in Japan, which is divided into two working areas: east and west. The tunnel is constructed by 3.885 km in the east and 3.575 km in the west. Among them, the new Nagasaki tunnel (east) was completed in 2017. In the present study, 318, 649 drilling data sets were obtained in the tunnel project from 97 drill holes. The tunnel was excavated by the method of New Austrian Tunneling Method. In this tunnel construction, many support patterns were applied, namely I-2-A(RC)(B), I-2-A(B), I-2-A(C), I-2-A(D), I-2-B(B), I-2-B (B) C, I-2-B(B) D [I-2-B (B) E], I-2- B (B) F, II-A-B(B) and II-B(B). It should be noted that except for part of the data [comprising the support patterns I-2-A(RC)(B), I-2-A(C), I-2-A(D) and I-2- B (B) F, totaling about 190 meters] cannot be collected, the support patterns corresponding to the remaining data sets were divided into six classes according to number of bolts, space of bolts, Class and shape of I-beam, initial and secondary lining thickness and eccentric or not. The comparison of details of the six support patterns are listed in Table 4.1. Fig. 4.1 shows the section diagram of support pattern of class 1.

The MWD technology can provide accurate and objective description of rock mass characteristics and be used to design the final rock support. The recorded MWD data is the response of different rock mass characteristics. It has proved to be an objective and reliable method to evaluate the rock mass conditions ahead of a tunnel face (Schunnesson 1996; Schunnesson et al. 2011; Humstad et al. 2012; van Eldert et al. 2017). Hydraulic percussion drill was used in this study for drilling investigation ahead of tunnel face. This

drilling equipment is equipped with drilling data logging system to measure and record the drilling data. The model of drilling rig is JTH3200R-III with the number of booms of 3. The drilling mode is semi-automatic. The length of drill pipe is 3m and the diameter of drill bit is 65mm. The length of standard sampling borehole is 30-45m. All MWD data are output from the data collection device in approximately every 0.25 seconds. The MWD data is collected and recorded by a data collection device connected to the drilling equipment which can record the oil pressure data when drilling. The excavation of the tunnel needs to be stopped before the drilling procedure starts. The drilling procedure includes adjusting the position of the drilling equipment and the drill pipe, drilling, data recording, connecting the drill pipe, and withdrawing the drill pipe. The MWD data obtained from the data collection device include PR, Hammer pressure (HP), rotation pressure (RP), FP, hammer frequency (HF) and SE. The RP represents the speed of the drill pipe during drilling, which can be used to judge whether it is fragile or soft geology. The HP is the force transmitted from drill pipe to rock during drilling, which is sensitive to the hardness of rock. The RP is a kind of pressure applied to rotate the drill pipe. When the pressure increases, it can be judged that there are some geological changes such as the appearance of weak layer and clay layer. The FP is the hydraulic oil pressure applied when the drill pipe rotates and impacts, which is generally affected by the strength of the rock. The HF represents the frequency of the drill pipe hitting the rock, and the higher frequency generally means that the broken rock is harder. The SE is a composite parameter, which refers to the energy consumed to destroy the rock per unit volume.

Table 4.1 Description details for the six support patterns

Class No.	Support patterns	Number of bolts	Space of bolts (mm)	Class of I-beam	Shape of I-beam	Eccentric or not	Initial lining thickness (cm)	Secondary lining thickness (cm)
Class 1	II-A(B)	10	1500	H100		N	10	30
Class 2	I-2-A(B)	10	1200	H125		N	12.5	30
Class 3	I-2-B(B)	10	1200	H125		Y	12.5	30
Class 4	II-B(B)	10	1500	H100		Y	10	30
Class 5	I-2-B(B)C	6	1200	H125		Y	12.5	30
Class 6	I-2-B(B)D I-2-B(B)E	6	1200	H125		Y	12.5	30

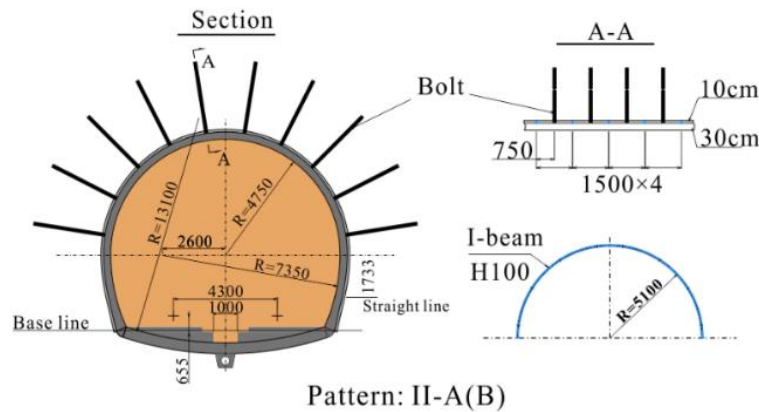


Fig. 4.1 Section diagram of support pattern of class 1

In the process of drilling, the working environment must be close to the ideal state. However, because the parameters obtained by the drilling system are not stable, there are many influencing factors, such as: the conditions with bit shape, flushing fluid, slag discharge state, bit diameter, etc., as well as the technical level difference of the drilling operator. In the actual drilling process, the ideal state does not exist, so the response between the MWD parameters obtained by the drilling equipment and the physical properties of the rock is not high from the visual point of view. Therefore, this paper aims to use a powerful ANN technology to analyze the relationship between these data and the physical properties of the rock.

In the first stage of the study, an ANN for estimating the class of tunnel support patterns was constructed by using the recorded MWD data. The MWD data parameters (PR, HP, RP, FP, HF and SE) have been used as input feature parameters and the class numbers have been used as output parameters. The statistics of the maximum, minimum and average value of each parameter of different classes are presented in Table 3.3. As can be seen in Table 3.3, there is a difference in the average value of the MWD parameters related to each Class. It should be noted that a small number of singular values exist in the MWD data in Table 3.3, which is due to the original data collected by the project. In order to investigate the robustness of ANN, the original data are not filtered in this paper. This is also for the development of real-time prediction system based on ANN technology as a preliminary study. In order to reduce the influence of the order of magnitude difference among the feature parameters on the prediction performance of ANN, the input data was normalized to the range of 0-1 by the following Eq. 4-1. This normalization process is a

common practice before the establishment of ANN model.

$$X_{norm} = \frac{x - x_{min}}{x_{max} - x_{min}} \quad (4-1)$$

where X_{norm} and x are normalized and measured data, respectively. x_{min} and x_{max} are the minimum and maximum value, respectively, of x .

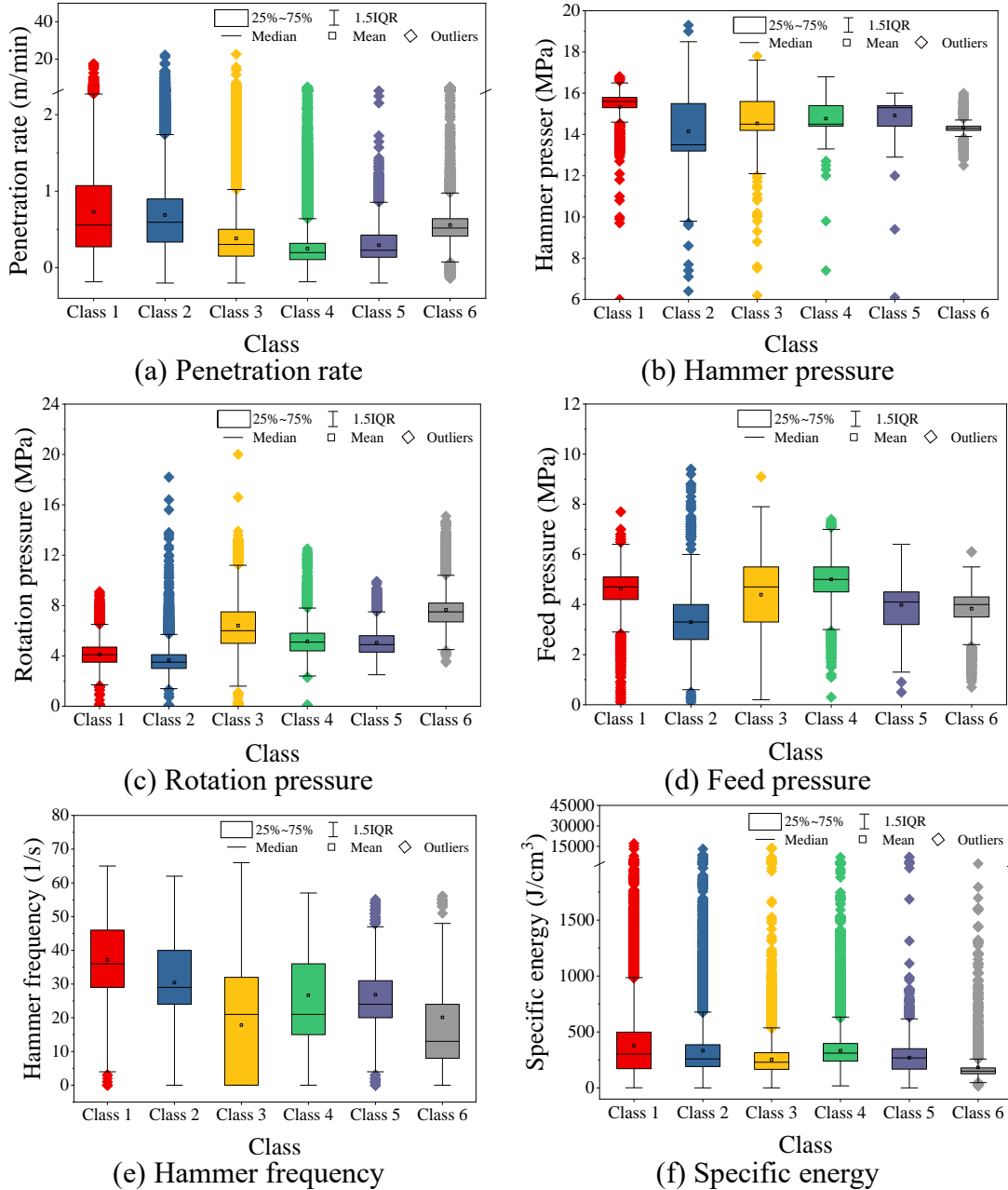


Fig. 4.2 Distribution of feature parameters of the input data

Additionally, Fig. 4.2 compares the distribution of feature parameters. It can also be seen from the figure that the average values of the MWD parameters are different for each Class. However, it is indispensable to further study the correlation of the six feature

parameters and whether there is information redundancy in the case when all six feature parameters are used as input data of the neural network. In the remaining subsections, neural network structure optimization and the input feature selection problem will be analyzed.

4.3 Experimental setup

ANN is an information processing pattern developed by McCulloch and Pitts (1943) by simulating human brain. It consists of three layers: input layer, hidden layer and output layer. Each layer consists of nodes, which are sets of interconnected processor elements. The output of each layer is used as the input of the next layer. The output of any layer could be connected to the next layer using weighting factors based on their strengths or weaknesses. Moreover, linear or sigmoid colon functions are used as activation functions to calculate the output of neurons in each layer (Hsu et al. 1995).

For input and output layer, it should be noted that the number of nodes is determined by the number of variables in these layers. For the hidden layer, many researches (Hecht-Nielsen 1987; Hush 1989; Ripley 1993; Paola 1994; Kanellopoulos and Wilkinson 1997) have proposed heuristic methods to determine the number of nodes. However, there is no definite standard. To train ANNs, the most commonly adapted algorithm is error back-propagation algorithm (Dreyfus 2005; Togholi et al. 2014). For minimizing the model error between goal standards and output, back-propagation algorithm is extremely suitable. Whenever the error of model is greater than predefined error, the network weights are adjusted by the system through back propagation. Consequently, in this study, the error back-propagation algorithm was employed for training. Fig. 3.5 shows the outlook of structure of the error back-propagation neural network (BPNN) model. Each input node of BPNN model represents each MWD parameter, and the output nodes represent six support models. The main flow of BPNN algorithm includes: Step 1 initialize network, Step 2 calculate outputs of hidden layer, Step 3 calculate outputs of output layer, Step 4 calculate the error, Step 5 update weight and threshold, Step 6 judgment of iteration results. The details of the algorithm are illustrated in Fig. 3.6.

4.3.1 Basic ANN parameter setting

In this study, MATLAB software has been used for development of BPNN model. It should be noted that in order to automate the processing as much as possible this study

develops the code of the BPNN model, without using built-in ANN tool of the software. For model training, if the selected learning rate value is larger, the modification of the weight will be greater and the network convergence will be faster. However, too small learning rate value will slow the convergence of the network and make the weight difficult to stabilize. The momentum term can be used to improve the convergence while reducing the oscillations of updating process of weights. In this study, after several trials, learning rate of 0.01 and momentum factor of 0.5 have been set to ensure the convergence of the algorithm. For the number of hidden layers, Kanellopoulos and Wilkinson (1997) stated that a second hidden layer is recommended when the output layer of the neural network has 20 (or more) nodes. Garson (1998) and García-Pedrajas et al. (2005) reported that a single hidden layer is usually sufficient to solve most problems, especially classification tasks. Thus, one hidden layer was preferred in this study. For the number of nodes in the input layer, it was equal to the number of feature parameters. Therefore, the input layer size can be calculated by multiplying the number of input layer nodes by the number of corresponding training sample data of each node. In order to evaluate the effect of different combinations of feature parameters as input data on the prediction performance of ANN models, different combinations of feature parameters and different number of hidden layer nodes were set up. In all cases, the number of nodes in output layer was equal to 6 corresponding to six tunnel support patterns. Sigmoidal activation function was used for modeling the transformation of values across the layers. In addition, randomly selected 6000 data sets (corresponding to 1000 data sets of each class of support patterns) from the total data sets were used in the training stage as training samples, and randomly selected 600 data sets (corresponding to 100 data sets of each class) were used in testing stage as testing samples.

4.3.2 *Setting of the experiments*

To ensure selection of the optimal combination of feature parameters, an analysis was performed with the data sets obtained from the tunnel construction site described in section 2. In this subsection, various experiment cases on 63 datasets were implemented. These cases aim to evaluate the performance of the BPNN with the different combinations of the feature parameters and the different number of hidden layer nodes. It must be pointed out that the marks P1, P2, ..., P6 refer to the six feature parameters as shown in Table 4.2. In order to avoid the influence of different hardware specifications on the

calculation time of the same code, all these cases were performed on the same PC with the same specification. The detailed specification parameters are presented in Table 4.3. Also, it must be highlighted that ID1-1, ID1-2, ..., ID6 in Table 4.4 refer to the full combinations of the six feature parameters. In order to ensure the accuracy of the experiment, each experiment case was conducted 10 times under the same experimental conditions (the same combination of the feature parameters, the same number of hidden layer nodes). Accuracy (A , $A = \text{the correctly predicted number of output samples} / \text{total number of output samples}$), computing-time (T), sensitivity and stability were taken as the performance indices. And, average accuracy (\bar{A} , $\bar{A} = A / 10$) and average computing-time (\bar{T} , $\bar{T} = T / 10$) were obtained from 10 experiment cases under the same experimental conditions.

Table 4.2 The marks the six feature parameters

Feature parameters	Penetration rate	Hammer pressure	Rotation pressure	Feed pressure	Hammer frequency	Specific energy
Symbol	PR	HP	RP	FP	HF	SE
No.	P1	P2	P3	P4	P5	P6

Table 4.3 PC specification

	Penetration rate
CPU	Core (TM) i7
Frequency	4.00GHZ
RAM	20GB
Operating system	Windows 10

4.4 Results and discussion

4.4.1 Performance of ANN with different experimental conditions

A comparison between using whole feature length and using subset of it with different number of hidden layer nodes is shown in Fig. 4.3 and Fig. 4.4. In Fig. 4.3, as it can be seen, for all cases, the \bar{A} s of the BPNN models increases with the number of hidden layer nodes. The growth curves become flat as the number of nodes increases to a certain value. For features 1 to 6, the certain value of the number of nodes is 30, 20, 20, 15, 10 and 10,

respectively. In addition, it can be noticed that for different combinations of the feature parameters, optimal average accuracy (\bar{A}_{op} , \bar{A}_{op} is calculated as the average of the \bar{A}_s corresponding to the number of hidden layer nodes after the inflection point) of the neural network model is different as shown in Table 4.4.

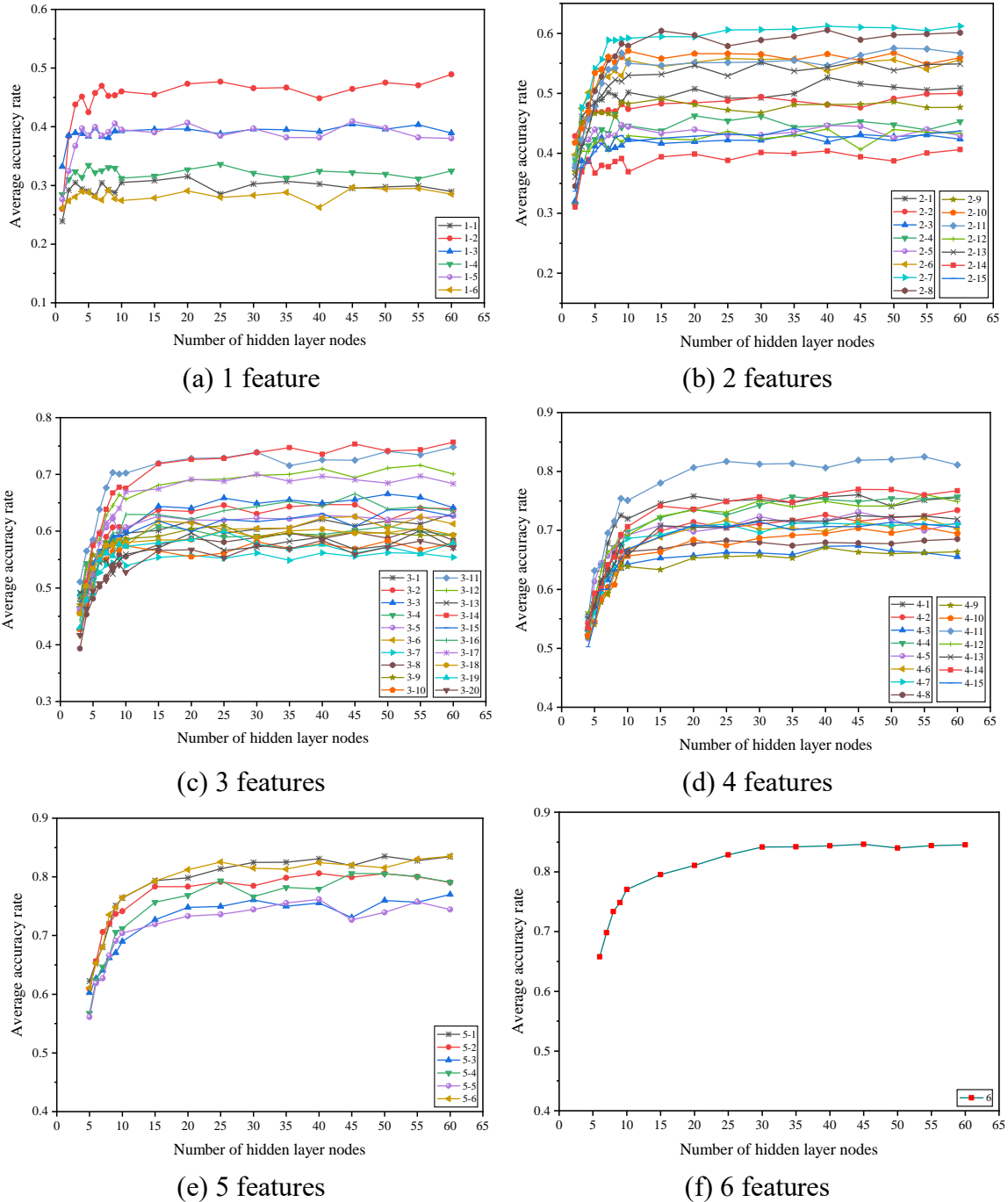


Fig. 4.3 Variations of the average accuracies with the different number of hidden layer nodes and different number of the feature parameters

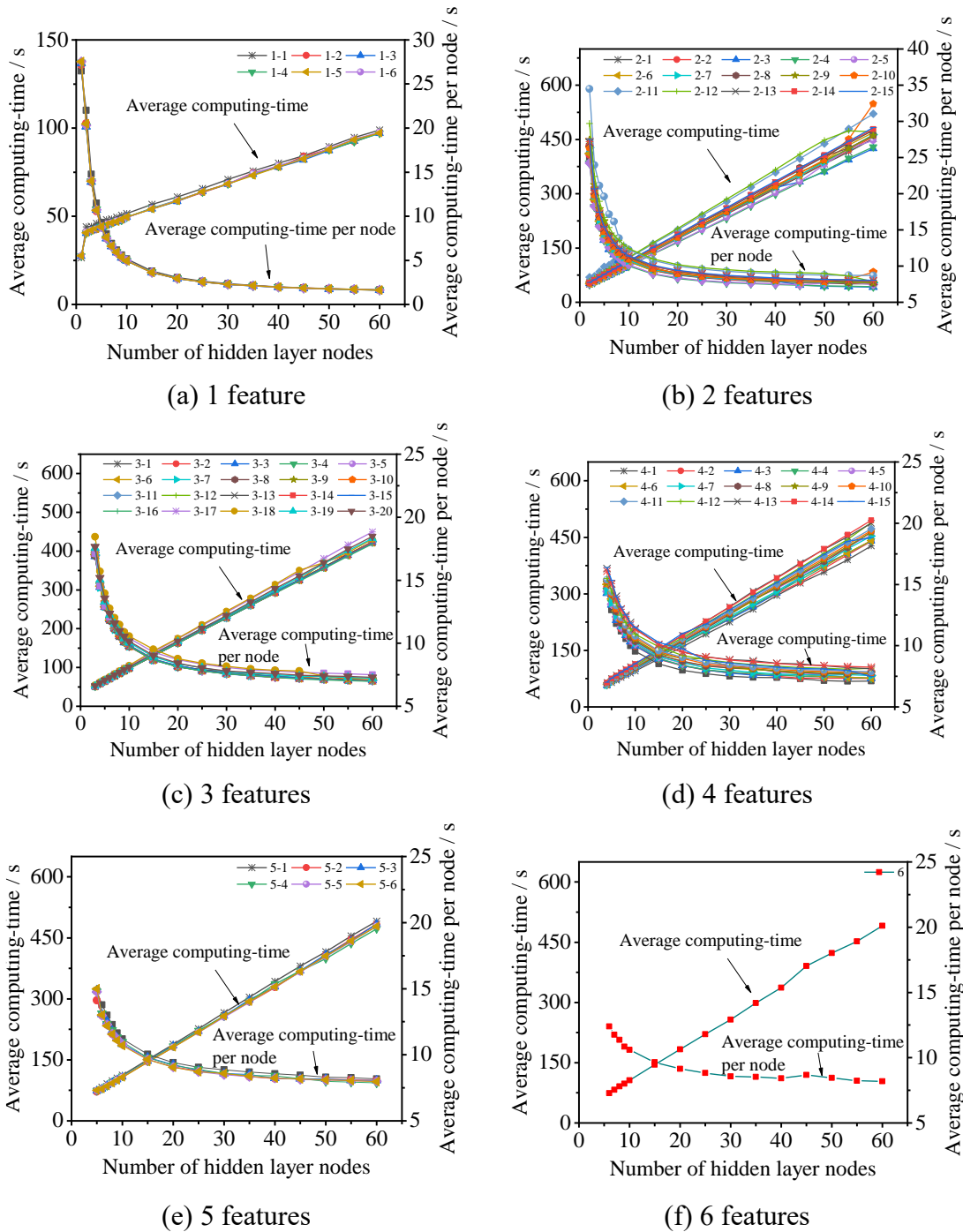


Fig. 4.4 Variations of the average computing-times and the average computing-times per node with the different number of hidden layer nodes and the different number of the feature parameters

Fig. 4.4 illustrates variations of the \bar{T} and the \bar{T} per node with the different number of hidden layer nodes and the different combinations of the feature parameters. As shown, for the combinations with the same number of features, the \bar{T} s increase linearly and the \bar{T} s per node tend to be a fixed value after a sharp drop. This means that when the number

of hidden layer nodes is more than the fixed value, the \bar{T} per node value can be calculated by the formula: the $\bar{T} = \text{the fixed value} \times \text{the number of hidden layer nodes}$, but the performance of the network does not increase. In addition, the rates of increase of the \bar{T} s, the \bar{T} s and the fixed values of the \bar{T} s per node are approximately the same with the combinations at the same number of features. Moreover, further comparison of \bar{T} with different feature combinations as the number of hidden layer nodes = 20 as shown in Fig. 4.6 and Table 4.4. As it can be seen, \bar{T} increases with the number of features. The case of 1 feature obtains the minimum value of \bar{T} . Additionally, \bar{T} value shows that there is no huge difference for 2 features, 3 features, 4 features, 5 features and 6 features.

Fig. 4.5 compares \bar{A}_{op} for all combinations of the feature parameters. As it can be seen from this figure, \bar{A}_{op} is different with the same number of features. However, \bar{A}_{op} increases with the number of features. The case of 6 features obtains the highest results. The case of 1 feature obtains the worst results. This is due to the significant influence of the number of features on the performance of BPNN. Also, it can be observed, the results of the combination ID 6, ID 5-1, ID 5-6 and ID 4-11 of the feature parameters are comparable with each other.

4.4.2 Sensitivity analysis of each feature parameter

In this subsection, the sensitivity of each feature parameter for prediction performance has been compared. Sensitivity has been measured by counting occurrence times of each parameter in the corresponding combinations of feature parameters of the experiment cases with superior prediction performance. The sensitivity is defined as the contribution of each parameter to the prediction performance. Fig. 4.7 shows the excellent combinations of feature parameters with a prediction $\bar{A} > 0.700$, which are ID 6, ID 5-1, ID 5-6, ID 4-11, ID 5-2, ID 5-4, ID 4-14, ID 4-1, ID 5-3, ID 4-4, ID 4-12, ID 5-5, ID 3-14, ID 3-11, ID 4-2, ID 4-13, ID 4-5, ID 4-7, ID 4-6 and ID 4-15, respectively. Table 4.5 counts the occurrence times of the feature parameters corresponding to the superior combinations. It must be pointed out that in order to distinguish the sensitivity better, the sum of the occurrence times of the feature parameters when the \bar{A} is greater than 0.7 and 0.8 will be taken as the final score. As it can be observed, the scores of parameters P1, P2, P3, P4, P5 and P6 are 15, 21, 18, 20, 19 and 14, respectively. Thus, the sensitivity of the six parameters is ordered as $P2 > P4 > P5 > P3 > P1 > P6$ (HP > FP > HF > RP > PR > SE). The SE is a comprehensive parameter measured indirectly, which represents the

energy needed to destroy the rock per unit volume. The PR can also be regarded as a comprehensive parameter, which is affected by the mechanical properties of rock and the drilling equipment. HP, FP, HF and RP are directly measured parameters, which are the direct response of drilling equipment to rock performance. The selection of support pattern is mainly determined by the properties of rock. From the sensitivity analysis results of prediction performance, it shows that the sensitivity of the parameters directly measured to the prediction results is higher than the parameters indirectly measured. The HF parameter has the highest sensitivity to the prediction performance of support pattern, while the SE parameter is the lowest.

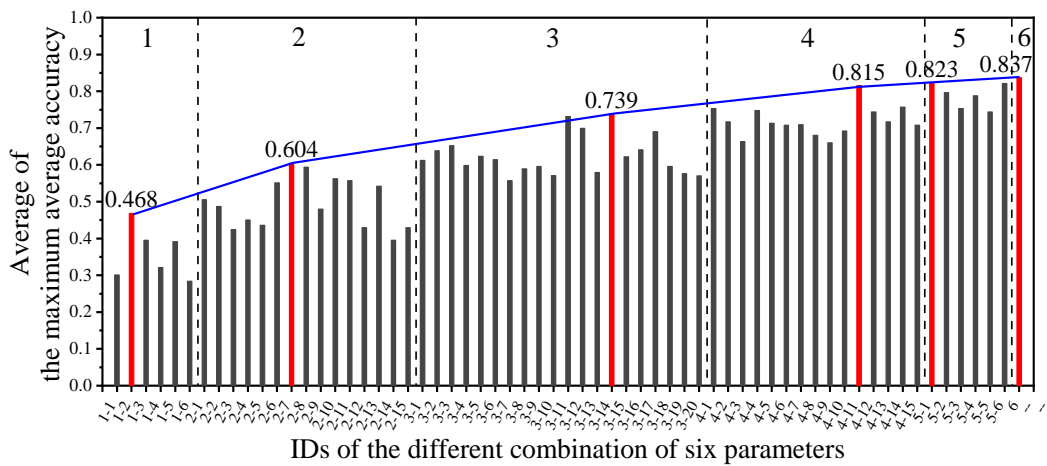


Fig. 4.5 The optimal average accuracies with the different combinations of six parameters

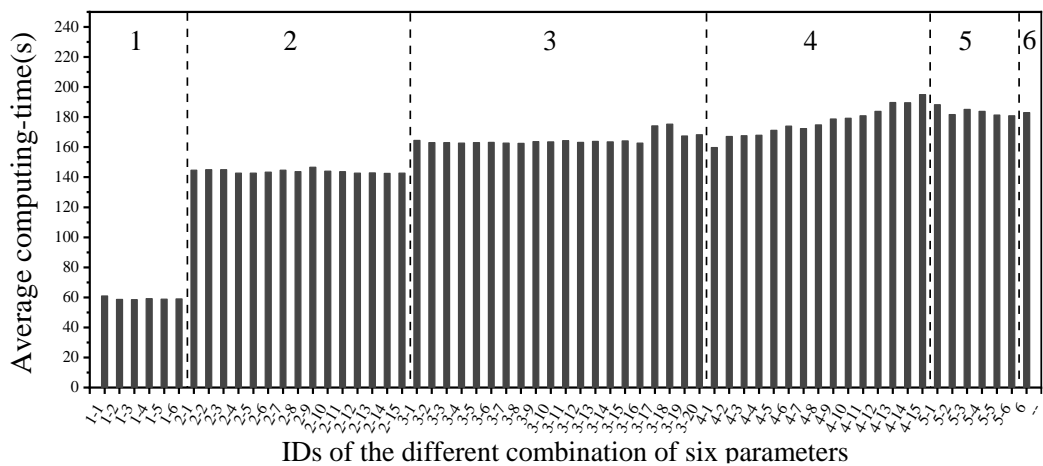


Fig. 4.6 The average computing-time with the different combinations of six parameters

Table 4.4 IDs and prediction results of different parameter combinations

Feature numbers	Combination	ID	\bar{A}_{op}	\bar{T} (20 nodes)	
1	P1	1-1	0.301	60.98	
	P2	1-2	0.468	58.63	
	P3	1-3	0.395	58.46	
	P4	1-4	0.321	59.08	
	P5	1-5	0.391	58.74	
	P6	1-6	0.284	58.90	
2	P1-P2	2-1	0.505	144.61	
	P1-P3	2-2	0.487	144.92	
	P1-P4	2-3	0.424	144.99	
	P1-P5	2-4	0.450	142.74	
	P1-P6	2-5	0.436	142.72	
	P2-P3	2-6	0.551	143.36	
	P2-P4	2-7	0.604	144.66	
	P2-P5	2-8	0.594	143.69	
	P2-P6	2-9	0.480	146.56	
	P3-P4	2-10	0.562	144.00	
	P3-P5	2-11	0.557	143.70	
	P3-P6	2-12	0.429	142.67	
	P4-P5	2-13	0.542	142.89	
	P4-P6	2-14	0.395	142.50	
	P5-P6	2-15	0.429	142.62	
3	P1-P2-P3	3-1	0.612	164.53	
	P1-P2-P4	3-2	0.638	162.94	
	P1-P2-P5	3-3	0.652	163.01	
	P1-P2-P6	3-4	0.598	162.65	
	P1-P3-P4	3-5	0.623	163.01	
	P1-P3-P5	3-6	0.614	163.18	
	P1-P3-P6	3-7	0.557	162.62	
	P1-P4-P5	3-8	0.589	162.45	
	P1-P4-P6	3-9	0.596	163.64	
	P1-P5-P6	3-10	0.571	163.42	
	P2-P3-P4	3-11	0.731	164.34	
	P2-P3-P5	3-12	0.699	163.10	
	P2-P3-P6	3-13	0.579	163.83	
	P2-P5-P6	3-16	0.641	162.63	
	P3-P4-P5	3-17	0.690	174.13	
	P3-P4-P6	3-18	0.596	175.30	
	P3-P5-P6	3-19	0.576	167.35	
	P4-P5-P6	3-20	0.570	168.25	
	4	P1-P2-P3-P4	4-1	0.753	159.73
		P1-P2-P3-P5	4-2	0.717	167.05
P1-P2-P3-P6		4-3	0.663	167.58	
P1-P2-P4-P5		4-4	0.748	167.87	
P1-P2-P4-P6		4-5	0.713	171.21	
P1-P2-P5-P6		4-6	0.708	174.04	
P1-P3-P4-P5		4-7	0.709	172.30	
P1-P3-P4-P6		4-8	0.680	174.80	
P1-P3-P5-P6		4-9	0.660	178.72	
P1-P4-P5-P6		4-10	0.692	179.29	
P2-P3-P4-P5		4-11	0.815	180.88	
P2-P3-P4-P6		4-12	0.744	183.86	
P2-P3-P5-P6		4-13	0.717	189.77	
P2-P4-P5-P6		4-14	0.757	189.60	
P3-P4-P5-P6		4-15	0.708	195.00	
5	P1-P2-P3-P4-P5	5-1	0.823	188.30	
	P1-P2-P3-P4-P6	5-2	0.796	181.75	
	P1-P2-P3-P5-P6	5-3	0.753	185.20	
	P1-P2-P4-P5-P6	5-4	0.788	183.83	
	P1-P3-P4-P5-P6	5-5	0.744	181.33	
	P2-P3-P4-P5-P6	5-6	0.821	180.90	
6	P1-P2-P3-P4-P5-P6	6	0.843	183.00	

Table 4.5 The occurrence times of different parameter combinations

ID	P1 (PR)	P2 (HP)	P3 (RP)	P4 (FP)	P5 (HF)	P6 (SE)
6	●	●	●	●	●	●
5-1	●	●	●	●	●	○
5-6	●	●	●	●	●	●
4-11	○	●	●	●	●	○
Subtotal ($\bar{A} > 0.800$)	3	4	4	4	4	2
5-2	●	●	●	●	○	●
5-4	●	●	○	●	●	●
4-14	○	●	○	●	●	●
4-1	●	●	●	●	○	○
5-3	●	●	●	○	●	●
4-4	●	●	○	●	●	○
4-12	○	●	●	●	○	●
5-5	●	○	●	●	●	●
3-14	○	●	○	●	●	○
3-11	○	●	●	●	○	○
4-2	●	●	●	○	●	○
4-13	○	●	●	○	●	●
4-5	●	●	○	●	○	●
4-7	●	○	●	●	●	○
4-6	●	●	○	○	●	●
4-15	○	○	●	●	●	●
Subtotal ($\bar{A} > 0.700$)	12	17	14	16	15	12
Total	15	21	18	20	19	14

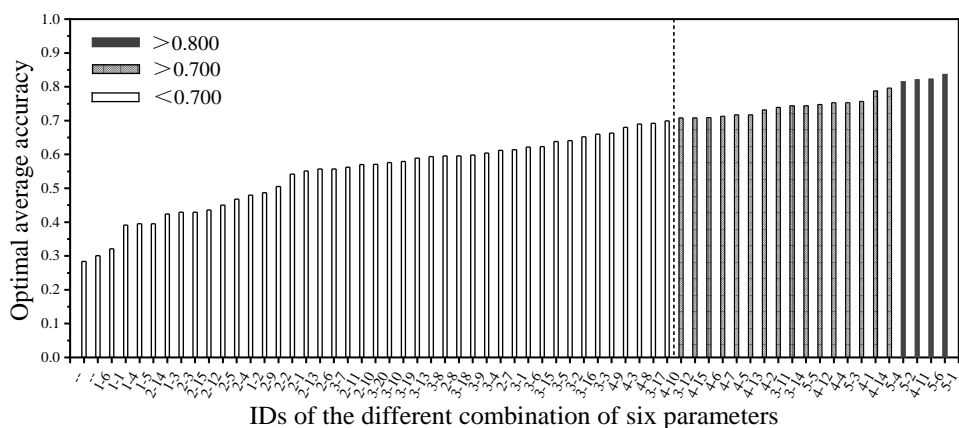


Fig. 4.7 The order of the optimal average accuracies with the different combinations of six parameters

4.4.3 Stability of prediction performance

For further comparison of the prediction performance of the BPNN algorithm with different combinations of the feature parameters, stability of the prediction performance with four optimal combinations of feature parameters (combination ID 6, ID 5-1, ID 5-6 and ID 4-11) were analyzed as well. The average of standard deviation (SD) of the A_s of six class support patterns in 10 experiment cases was counted as index to measure the stability of prediction performance as shown in Table 4.6. Fig. 4.8 illustrates variations of the A_s of prediction results for each class of support patterns in 10 experiments with optimal combinations of feature parameters. In addition, the comparison between the predicted results and the real classes of one of the 10 experiments is shown in Fig. 4.8. As it can be seen from Table 4.6, Fig. 4.8 and Fig. 4.9, the optimal stability score to 0.066 was obtained by the combination ID 6. The result obtained with the combination ID 4-11 was worst by 0.094. The stability of the prediction performance with four combinations of feature parameters is ordered as ID 6 > ID 5-1 > ID 5-6 > ID 4-11. It can be observed that the order of \bar{A} is the same as the stability.

Table 4.6 Statistics of the average accuracy rates and standard deviation of prediction of support pattern selections with the combination ID 6, 5-1, 5-6 and 4-11

ID	Class 1	Class 2	Class 3	Class 4	Class 5	Class 6
6	0.887	0.870	0.835	0.745	0.812	0.902
5-1	0.838	0.884	0.858	0.713	0.753	0.901
5-6	0.843	0.879	0.822	0.726	0.778	0.904
4-11	0.826	0.900	0.794	0.699	0.769	0.914

Through the above analysis, the best predicted results (\bar{A}) for six classes of support patterns were 0.887, 0.870, 0.835, 0.745, 0.812 and 0.902, respectively, which were obtained under the combination of six feature parameters (ID=6). These obtained results prove the superiority of the combination with six feature parameters. These selected features can be used further for improving the clustering performance. Although in the literature of the subject, the clusters built by a subset of salient features are more practical and interpretable than clusters built all of the features in most cases, in this study, the clusters built by a subset of salient features has no advantage, which is probably due to the small number of feature parameters. Therefore, for this study, the cluster built by the

whole feature parameters has stronger performance, and it can help in better data understanding and interpretation.

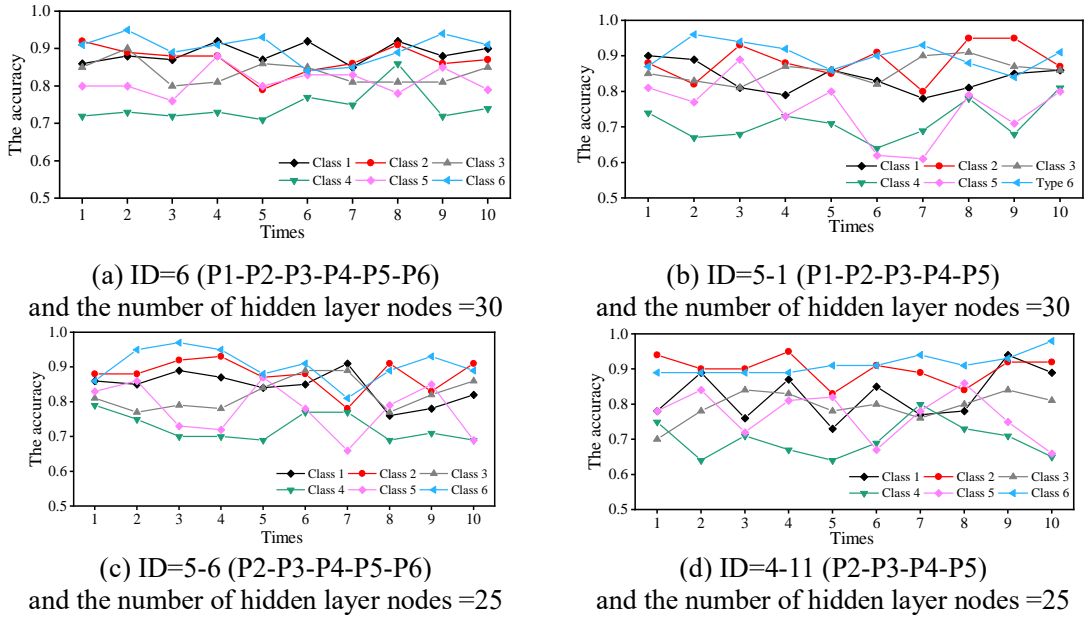


Fig. 4.8 Variations of the accuracy rates of prediction of support pattern selections in 10 experiments with the combination ID 6, ID 5-1, ID 5-6 and ID 4-11

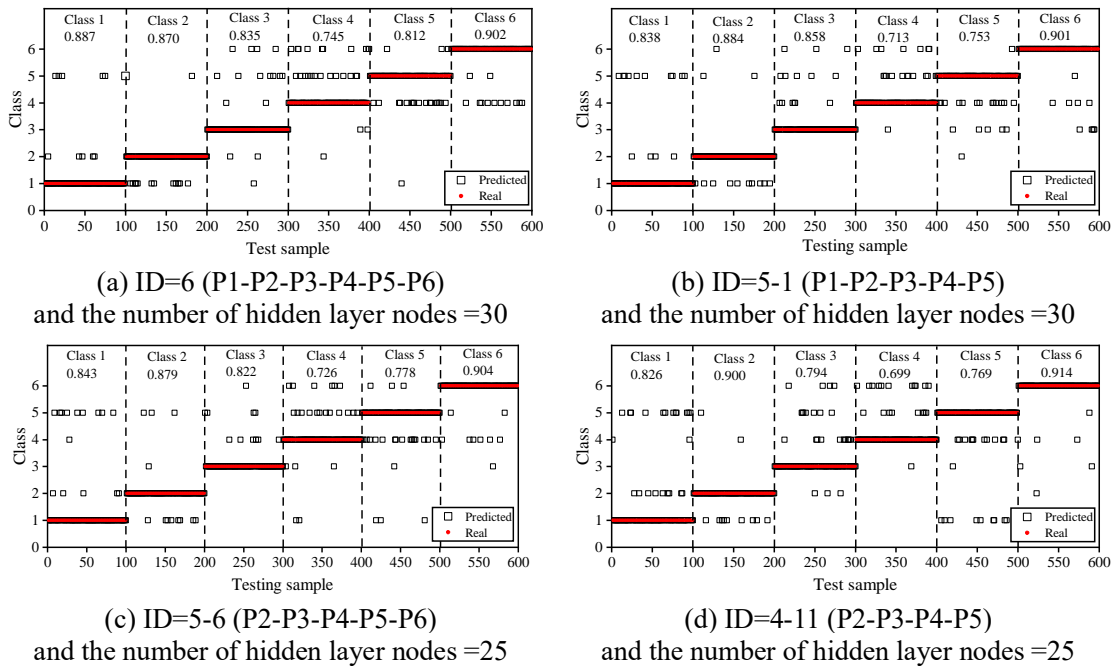


Fig. 4.9 Predicted results of the test sample with the combination ID 6, ID 5-1, ID 5-6 and ID 4-11

4.5 Conclusions

In this study, an artificial neural network (ANN) model is proposed to predict the selection of support patterns ahead of tunnel face using measure while drilling (MWD) data including penetration rate (PR), Hammer pressure (HP), rotation pressure (RP), feed pressure (FP), hammer frequency (HF) and specific energy (SE). The proposed ANN model is validated by 318, 649 MWD data obtained from 97 drill holes of a 3.88 km high-speed railway tunnel in Japan. ANN models with different input feature parameters and different hidden layer sizes are constructed for pursuing the best prediction performance. The sensitivity of each feature parameter to the prediction performance of the ANN is compared. The stability of the prediction performance of the ANN models with better performance are analyzed as well. Four different evaluation indices including average accuracy (\bar{A}), computing-time (\bar{T}), sensitivity and stability are adopted in this study.

The results show that it is feasible to predict the selection of support patterns ahead of tunnel face using the ANN by the MWD data. The prediction performance of the ANN is affected by the input layer sizes and hidden layer sizes. The combination of 6 feature parameters outperforms the subset of the entire feature parameters in terms of \bar{A} , sensitivity and stability.

As a reminder, although \bar{T} increases with the number of feature parameters, there is on huge difference for 2 to 6 feature parameters. A hidden layer size greater than 30 neurons has no optimizing effect on the prediction performance.

The sensitivity of the 6 feature parameters is ordered as $HP > FP > HF > RP > PR > SE$. The stability of the prediction performance with four better combinations of feature parameters is ordered as $ID\ 6 > ID\ 5-1 > ID\ 5-6 > ID\ 4-11$ (ID 6: combination of PR, HP, RP, FP, HF and SE; ID 5-1: combination of PR, HP, RP, FP and HF; ID 5-6: combination of HP, RP, FP, HF and SE; ID 4-11: combination of PR, HP, RP and FP). The \bar{A} is the same order as the stability.

Although it has a slightly larger \bar{T} , the ANN model with 6 feature parameters and the 30 hidden layer nodes is proposed as optimal model considering all indices. The results confirm that the proposed combination with six feature parameters is effective for tunnel support pattern prediction. Prediction of the selection of support patterns ahead of tunnel face in advance using the ANN technology can improve the safety of tunnel excavation and bring considerable benefits in time and cost.

In the present study, the commonly used the error back-propagation neural network

(BPNN) algorithm is utilized to demonstrate the correlation between the MWD data and the support patterns. As a preliminary work, the ANN models with other outstanding algorithms are not adopted but will be considered in the future studies. The present study established the BPNN models with all the MWD data parameters, which is therefore merely an initial step to explore the concerned topic. Composition of parameters based on the MWD data need to be considered to improve the prediction performance of the ANN. Besides, more verification and analysis based on other tunnel projects under similar geological conditions should be carried out to understand the adaptability of the proposed ANN prediction model in the future works.

References

- Basu JK, Bhattacharyya D, Kim T (2010), Use of artificial neural network in pattern recognition. *International journal of software engineering and its applications*, 4
- Ben Ali J, Fnaiech N, Saidi L, Chebel-Morello B, Fnaiech F (2015), Application of empirical mode decomposition and artificial neural network for automatic bearing fault diagnosis based on vibration signals. *Applied Acoustics*, 89:16-27. <https://doi.org/10.1016/j.apacoust.2014.08.016>
- Bizjak KF, Petkovšek B (2004), Displacement analysis of tunnel support in soft rock around a shallow highway tunnel at Golovec. *Eng Geol*, 75:89-106. <https://doi.org/10.1016/j.enggeo.2004.05.003>
- Dahlin T, Bjelme L, Svensson C (1999), Use of electrical imaging in site investigations for a railway tunnel through the Hallandsås Horst, Sweden. *Q J Eng Geol Hydrogeol*, 32:163-172.
- Dreyfus G (2005), *Neural networks: methodology and applications*. Springer Science & Business Media,
- El-Naqa A (2001), Application of RMR and Q geomechanical classification systems along the proposed Mujib Tunnel route, central Jordan. *Bull Eng Geol Environ*, 60:257-269.
- Elyasi A, Javadi M, Moradi T, Moharrami J, Parnian S, Amrac M (2016), Numerical modeling of an umbrella arch as a pre-support system in difficult geological conditions: a case study. *Bull Eng Geol Environ*, 75:211-221. <https://doi.org/10.1007/s10064-015-0738-5>

- Friant JE, Bauer RA, Gross DL, May M, Lach J (1997), Pipetron Tunnel Construction Issues. Fermi National Accelerator Lab.(FNAL), Batavia, IL (United States),
- Galende-Hernández M, Menéndez M, Fuente MJ, Sainz-Palmero GI (2018), Monitor-While-Drilling-based estimation of rock mass rating with computational intelligence: The case of tunnel excavation front. *Autom Constr*, 93:325-338. <https://doi.org/10.1016/j.autcon.2018.05.019>
- García-Pedrajas N, Hervás-Martínez C, Ortiz-Boyer D (2005), Cooperative Coevolution of Artificial Neural Network Ensembles for Pattern Classification. *IEEE Trans Evol Comput*, 9:271-302.
- Garson GD (1998), *Neural networks: An introductory guide for social scientists*. Sage, London.
- Ghorbani A, Hasanzadehshooiili H, Sadowski Ł (2018), Neural Prediction of Tunnels' Support Pressure in Elasto-Plastic, Strain-Softening Rock Mass. *Applied Sciences*, 8:841.
- Ghosh R, Schunnesson H, Kumar U (2015), The use of specific energy in rotary drilling: the effect of operational parameters. In: *Proceedings of the 37th International Symposium, May 2015. Application of Computers and Operations Research in the Mineral Industry*. pp 713-723.
- Gong Q, Yin L, She Q (2013), TBM tunneling in marble rock masses with high in situ stress and large groundwater inflow: a case study in China. *Bull Eng Geol Environ*, 72:163-172.
- Guan Z, Jiang Y, Tanabashi Y (2009), Rheological parameter estimation for the prediction of long-term deformations in conventional tunnelling. *Tunn Undergr Space Technol*, 24:250-259. <https://doi.org/10.1016/j.tust.2008.08.001>
- Hecht-Nielsen R Kolmogorov's mapping neural network existence theorem. In: *Proceedings of the international conference on Neural Networks*, 1987. IEEE Press New York, pp 11-14.
- Hsu KI, Gupta HV, Sorooshian S (1995), Artificial neural network modeling of the rainfall-runoff process. *Water Resour Res*, 31:2517-2530.
- Humstad T, Høien AH, Kveen A, Hoel JE (2012), Complete Software Overview of Rock Mass And Support In Norwegian Road Tunnels. Paper presented at the ISRM International Symposium - EUROCK 2012, Stockholm, Sweden, May.

- Hush DR (1989), Classification with neural networks: a performance analysis. In: Proceedings of the IEEE International Conference on Systems Engineering, August 1989. pp 277-280.
- Hussain S, Mohammad N, Khan M, Rehman ZU, Tahir M (2016), Comparative analysis of rock mass rating prediction using different inductive modeling techniques. International Journal of Mining Engineering and Mineral Processing, 5:9-15.
- Kanellopoulos I, Wilkinson GG (1997), Strategies and best practice for neural network image classification. Int J Remote Sens, 18:711-725.
- Kaya A, Bulut F, Sayin A (2011), Analysis of support requirements for a tunnel portal in weak rock: A case study from Turkey. Scientific Research and Essays, 6:6566-6583.
- Kim CY, Bae GJ, Hong SW, Park CH, Moon HK, Shin HS (2001), Neural network based prediction of ground surface settlements due to tunnelling. Comput Geotech, 28:517-547. [https://doi.org/10.1016/S0266-352X\(01\)00011-8](https://doi.org/10.1016/S0266-352X(01)00011-8)
- Kontogianni V, Tzortzis A, Stiros S (2004), Deformation and failure of the Tymfristos tunnel, Greece. J Geotech Geoenviron Eng, 130:1004-1013.
- Koopialipour M, Ghaleini EN, Tootoonchi H, Jahed Armaghani D, Haghghi M, Hedayat A (2019), Developing a new intelligent technique to predict overbreak in tunnels using an artificial bee colony-based ANN. Environmental Earth Sciences, 78:165. <https://doi.org/10.1007/s12665-019-8163-x>
- Kumar R, Kumaraswamidhas LA, Murthy VMSR, Vettivel SC (2019), Experimental investigations on machine vibration in blast-hole drills and optimization of operating parameters. Measurement, 145:803-819. <https://doi.org/10.1016/j.measurement.2019.05.069>
- Kun M, Onargan T (2013), Influence of the fault zone in shallow tunneling: A case study of Izmir Metro Tunnel. Tunn Undergr Space Technol, 33:34-45.
- Kwon S, Lee C (2018), THM analysis for an in situ experiment using FLAC3D-TOUGH2 and an artificial neural network. Geotech Eng, 16:363-373. <http://doi.org/10.12989/GAE.2018.16.4.363>
- Leu S-S, Chen C-N, Chang S-L (2001), Data mining for tunnel support stability: neural network approach. Autom Constr, 10:429-441. [https://doi.org/10.1016/S0926-5805\(00\)00078-9](https://doi.org/10.1016/S0926-5805(00)00078-9)
- Li L et al. (2012), Spatial deformation mechanism and load release evolution law of

- surrounding rock during construction of super-large section tunnel with soft broken surrounding rock masses. *Chin J Rock Mech Eng*, 10:2109-2118.
- Lindén P (2005), Val av borrhklass kopplat till MWD, bergklass samt vattenflöde vid projektet Hallandsås.
- Liu J, Sakaguchi O, Ishizu S, Luan H, Han W, Jiang Y (2020), Application of Specific Energy in Evaluation of Geological Conditions Ahead of Tunnel Face. *Energies*, 13:909. <https://doi.org/10.3390/en13040909>
- Lo SCB, Chan HP, Lin JS, Li H, Freedman MT, Mun SK (1995), Artificial convolution neural network for medical image pattern recognition. *Neural networks*, 8:1201-1214.
- Mahdevari S, Torabi SR (2012), Prediction of tunnel convergence using artificial neural networks. *Tunn Undergr Space Technol*, 28:218-228. <https://doi.org/10.1016/j.tust.2011.11.002>
- Mahdevari S, Torabi SR, Monjezi M (2012), Application of artificial intelligence algorithms in predicting tunnel convergence to avoid TBM jamming phenomenon. *Int J Rock Mech Min Sci*, 55:33-44. <https://doi.org/10.1016/j.ijrmms.2012.06.005>
- McCulloch WS, Pitts W (1943), A logical calculus of the ideas immanent in nervous activity. *The bulletin of mathematical biophysics*, 5:115-133.
- Mikaeil R, Haghshenas SS, Shirvand Y, Hasanluy MV, Roshanaei V (2016), Risk assessment of geological hazards in a tunneling project using harmony search algorithm (case study: Ardabil-Mianeh railway tunnel). *Civil Engineering Journal*, 2:546-554.
- Miura K (2003), Design and construction of mountain tunnels in Japan. *Tunn Undergr Space Technol*, 18:115-126. [https://doi.org/10.1016/S0886-7798\(03\)00038-5](https://doi.org/10.1016/S0886-7798(03)00038-5)
- Navarro J, Sanchidrian JA, Segarra P, Castedo R, Paredes C, Lopez LM (2018), On the mutual relations of drill monitoring variables and the drill control system in tunneling operations. *Tunn Undergr Space Technol*, 72:294-304. <https://doi.org/10.1016/j.tust.2017.10.011>
- Nikafshan Rad H, Jalali Z, Jalalifar H (2015), Prediction of rock mass rating system based on continuous functions using Chaos-ANFIS model. *Int J Rock Mech Min Sci*, 73:1-9. <https://doi.org/10.1016/j.ijrmms.2014.10.004>
- Nilsen B (2015), Main challenges for deep subsea tunnels based on norwegian experience. *Journal of Korean Tunnelling and Underground Space Association*, 17:563-573.

- Ocak I, Seker SE (2013), Calculation of surface settlements caused by EPBM tunneling using artificial neural network, SVM, and Gaussian processes. *Environmental Earth Sciences*, 70:1263-1276. <https://doi.org/10.1007/s12665-012-2214-x>
- Paola J (1994), Neural network classification of multispectral imagery. Dissertation, The University of Arizona.
- Park J, Lee KH, Kim BK, Choi H, Lee IM (2017), Predicting anomalous zone ahead of tunnel face utilizing electrical resistivity: II. Field tests. *Tunn Undergr Space Technol*, 68:1-10. <https://doi.org/10.1016/j.tust.2017.05.017>
- Qiu D, Li S, Xu Y, Tian H, Yan M (2014), Advanced prediction of surrounding rock classification based on digital drilling technology and QGA-RBF neural network. *Rock and Soil Mechanics (China)*:2013-2018.
- Rafiq MY, Bugmann G, Easterbrook DJ (2001), Neural network design for engineering applications. *Computers & Structures*, 79:1541-1552. [https://doi.org/10.1016/S0045-7949\(01\)00039-6](https://doi.org/10.1016/S0045-7949(01)00039-6)
- Ripley BD (1993), Statistical aspects of neural networks. *Networks and chaos—statistical and probabilistic aspects*, 50:40-123.
- Schunnesson H (1996), RQD predictions based on drill performance parameters. *Tunn Undergr Space Technol*, 11:345-351. [https://doi.org/10.1016/0886-7798\(96\)00024-7](https://doi.org/10.1016/0886-7798(96)00024-7)
- Schunnesson H (1997), Drill process monitoring in percussive drilling for location of structural features, lithological boundaries and rock properties, and for drill productivity evaluation. Dissertation, Luleå tekniska universitet.
- Schunnesson H (1998), Rock characterisation using percussive drilling. *Int J Rock Mech Min Sci*, 35:711-725. [https://doi.org/10.1016/S0148-9062\(97\)00332-X](https://doi.org/10.1016/S0148-9062(97)00332-X)
- Schunnesson H, Elsrud R, Rai P (2011), Drill monitoring for ground characterization in tunnelling operations Paper presented at the International Symposium on Mine Planning and Equipment Selection, National Center on Complex Processing of Mineral Raw Materials of the Republic of Kazakhstan, Almaty, Kazakhstan, October.
- Segui J, Higgins M (2002), Blast design using measurement while drilling parameters. *Fragblast*, 6:287-299.
- Singh B, Jethwa J, Dube A, Singh B (1992), Correlation between observed support pressure and rock mass quality. *Tunn Undergr Space Technol*, 7:59-74.
- Soupios P, Loupasakis C, Vallianatos F (2008), Reconstructing former urban

- environments by combining geophysical electrical methods and geotechnical investigations—an example from Chania, Greece. *J Geophys Eng*, 5:186-194.
- Suwansawat S, Einstein HH (2006), Artificial neural networks for predicting the maximum surface settlement caused by EPB shield tunneling. *Tunn Undergr Space Technol*, 21:133-150. <https://doi.org/10.1016/j.tust.2005.06.007>
- Toghroli A, Mohammadhassani M, Suhatri M, Shariati M, Ibrahim Z (2014), Prediction of shear capacity of channel shear connectors using the ANFIS model. *Steel Compos Struct*, 17:623-639.
- Utt WK Neural network technology for strata strength characterization. In: International Joint Conference on Neural Networks, Middleton, WI, 10-16 July 1999 1999. International Neural Network Society, pp 3806-3809. 10.1109/IJCNN.1999.830760
- Utt WK, Miller GG, Howie WL, Woodward CC (2002), Drill monitor with strata strength classification in near-real time. *National Institute for Occupational Safety and Health* 9658:No. 2002-2141.
- van Eldert J, Schunnesson H, Johansson D (2017), The History and Future of Rock Mass Characterisation by Drilling in Drifting : From sledgehammer to PC-tablet. Paper presented at the 26th International Symposium on Mine Planning and Equipment Selection, Luleå, Sweden, August 29-31.
- van Eldert J, Schunnesson H, Johansson D, Saiang D (2019), Application of Measurement While Drilling Technology to Predict Rock Mass Quality and Rock Support for Tunnelling. *Rock Mech Rock Eng*:1-10. <https://doi.org/10.1007/s00603-019-01979-2>
- Wang X, Meng F (2018), Statistical analysis of large accidents in China's coal mines in 2016. *Natural Hazards*, 92:311-325. <https://doi.org/10.1007/s11069-018-3211-5>
- Xue X (2019), Application of a support vector machine for prediction of piping and internal stability of soils. *Geotech Eng*, 18:493-502. <http://doi.org/10.12989/GAE.2019.18.5.493>
- Yang Y, Zhang Q (1997), A hierarchical analysis for rock engineering using artificial neural networks. *Rock Mech Rock Eng*, 30:207-222.
- Yi X, Chen W, Li S, Dai Y (2006), Application of bp neural network to back analysis of forked tunnel displacement. *Chinese Journal of Rock Mechanics and Engineering*, 25:3927-3932.
- Zhang S, Li Y, Xu C (2017), Application of black box model for height prediction of the

fractured zone in coal mining. *Geotech Eng*, 13:997-1010.

<http://doi.org/10.12989/GAE.2017.13.6.997>

Zhou F, Sun W, Shao J, Kong L, Geng X (2020), Experimental study on nano silica modified cement base grouting reinforcement materials. *Geotech Eng*, 20:67.

<https://doi.org/10.12989/gae.2020.20.1.067>

5 Optimized artificial neural network model for predicting of rock mass quality ahead of tunnel face

5.1 Introduction

Assessment of rock mass quality is one of the main issues that affect the support design and operation cost of tunnel engineering (Lowson and Bieniawski 2013; Rehman et al. 2018). Inaccurate evaluation may cause the failure of support, and even lead to irreparable disasters such as water and mud gushing (Lu and Liu 2009; Li et al. 2017) and sudden collapse of a tunnel (Shin et al. 1999). Accurate, effective and objective rock mass quality assessment can reduce the cost and improve safety for tunnel engineering .

In recent decades, the most commonly employed rock mass quality assessment system is the rock quality designation (RQD) system (Deere 1964), Norwegian geotechnical institute Q-system (Q) (Barton et al. 1974), rock mass rating (RMR) system (Bieniawski 1973) and geological strength index (GSI) system (Hoek and Brown 1997). In Japan, the Japan Highway Public Corporation (JH) system, which is based on the RMR system, is commonly used to quantitatively evaluate the rock mass quality (Masahiro et al. 1999; Akagi et al. 2001; Yuji et al. 2006). Similar to other assessment systems (e.g., Q system, RMR system, and GSI system), when the JH system is utilized, the rock mass quality score (RQS), the scores of tunnel face observation items (e.g., compressive strength, weathering, and spacing of joints), is utilized to evaluate and grade the rock mass quality. Although these proposed assessment systems are extensively employed in rock engineering and tunnel engineering, the objectivity of the evaluation is insufficient due to subjective judgments that are based on the engineers' experience observation items (Palmstrom 2005; Rahmati et al. 2014; Zolfaghari et al. 2015).

Over the last decades, with the development of measure-while-drilling (MWD) technology, this technology can be used to predict and evaluate rock mass quality in broad tunneling projects (Lear and Dareing 1990; Nilsen 2015; Navarro et al. 2018). Aoki et al. (1999) proposed to use MWD data to evaluate the geological conditions of different drilling depths. Yue et al. (2004) used the MWD data to study decomposition grades in the ground, and confirmed that there is a certain relationship between the drilling speed and decomposition. Zhou et al. (2011) developed an unsupervised method to predict rock

types based on MWD data, who verified that the method is effective in rock type recognition. Leung and Scheduling (2015) adopted a modulation specific energy to overcome the low specificity and high variability of existing MWD methods. Considering hundreds of thousands or more MWD data, the more efficient prediction method of fitting these MWD data to a rock mass quality index should be further developed.

With the development of artificial neural network (ANN) technology, application of ANN in rock mass quality prediction has been successful (Sousa et al. 2012). Xu et al. (2007) used a back-propagation neural network to assess the rock mass quality. The RMR values were predicted by Hussain et al. (2016), who compared ANN technology with multiple regression technology. Karlaftis (2018) proposed an ANN model to classify rock masses using data from tunnels in Greece. The results demonstrated that the ANN can place a rock mass in the classification ratings very quickly and with very high accuracy with a smaller number of input variables. The applicability of ANN technology for an automatic online classification of rock mass was explored by Erharter et al. (2019). This research obtained a final classification accuracy of 74.4%.

ANN is one of the most innovative research fields in the field of science and engineering, with strong nonlinear mapping ability (Mohamad et al. 2012; Momeni et al. 2015). However, slow learning speed and easy to fall into local minima are some defects of ANN (Armaghani et al. 2018; Armaghani et al. 2019). Applications of population-based evolutionary algorithms, such as genetic algorithm (GA), particle swarm optimization (PSO) and imperialist competitive algorithm (ICA), are helpful to overcome these shortcomings. Using these algorithms to optimize artificial neural network can solve complex engineering problems and become a research hotspot (Hasanipanah et al. 2017; Khandelwal et al. 2017; Liu et al. 2020).

Although the feasibility of traditional rock mass quality assessment system has been identified, research on the development of more objective, intelligent and efficient evaluation methods require further study. The purpose of this research is to introduce hybrid ANN technologies, including GA-ANN, PSO-ANN and ICA-ANN, to predict the RQS (a rock mass quality index used in Japan) using the MWD data obtained from the new Nagasaki tunnel (east) of the West Kyushu line of the high-speed railway project in Japan. A conventional regression model and simple ANN model are developed. Subsequently, three hybrid ANNs are established and compared with the developed regression model and ANN model. Through comparative analysis, the best model to predict RQS value is selected. This method can evaluate rock mass quality accurately,

effectively and objectively.

5.2 Case study and dataset collection

A case study of the new Nagasaki tunnel in Japan was carried out. Excavation of the tunnel, which connects Nagasaki city and Isahaya city in southeastern Nagasaki province and central Nagasaki province, respectively, commenced in March 2013. The MWD data of this study were obtained from the Nagasaki tunnel (east), with a length of 3.885 km, and adjacent to it is the new Nagasaki tunnel (west), with a length of 3.575 km. The New Austrian Tunneling Method was employed. The stratum exposed by this tunnel is mainly volcanic rock. The type of rock passing from west to east is propylite andesite, hornblende andesite, tuff breccia, pyroxene andesite and tuff breccia. Among them, propylite andesite accounts for the largest proportion, about 3 km. The geological condition of surrounding rock is poor, and the measured compressional wave velocity (P-wave) ranges from 2.5 km/s to 3.5 km/s.

Table 5.1 **Grading configuration of each item of rock masses**

Item	Description	Evaluation score			
		1	2	3	4
1	Total state	Stable	Rock fall	Pressed	Collapse or outflow
2	Self-stability	Able	Gradual instability	Unable, primary support	Unable, pre-support
3	Unconfined compressive strength, MPa	> 100	20-100	5-20	< 5
4	Weathering	Unweathered	Slightly weathered	Moderately weathered	Highly weathered
5	Joints proportion	< 5%	5%-20%	20%-50%	> 50%
6	Spacing of joints	> 1 m	0.2-1 m	50-200 mm	< 50 mm
7	Joint aperture	Highly closed	Moderately closed	Slightly closed	Unclosed
8	Morphology of joints	Random square	Columnar	Layered	Psammitic
9	Ground water inflow	None	Slight	Moderate	Heavy
10	Ground Water deterioration	Uncorroded	Slightly deteriorated	Moderate deteriorated	Heavy deteriorated

During tunnel excavation, the JH method based on the observation report of tunnel face

was adopted to evaluate the rock mass exposed by the tunnel. This method uses ten rock parameters of total state, self-stability, unconfined compressive strength, weathering, joints proportion, spacing of joints, joint aperture, distribution of joints, ground water inflow and ground water deterioration to evaluate the rock mass quality. As shown in Table 5.1, when using the JH method for rock mass classification, all observation items are configured with four values from 1 to 4. The sum of each item value is the final rock rating score, which is called RQS value. The larger RQS value represents the worse geological conditions of the tunnel and the higher support strength is required.

At the same time of tunnel excavation, the MWD data of drilling in advance working face were recorded. The parameters of MWD data include the penetration rate (PR), hammer pressure (HP), rotation pressure (RP), feed pressure (FP), hammer frequency (HF) and specific energy (SE). The MWD data and the corresponding RQS constitute one dataset.

Table 5.2 Distribution statistics of dataset parameters

Parameter	Description	Symbol	Mean	Min	Max	Std. Dev
Input	Penetration rate	PR	1.00	0.08	4.44	0.62
	Hammer presser	HP	14.88	9.41	16.80	0.90
	Rotation pressure	RP	4.45	0.50	12.50	1.46
	Feed pressure	FP	3.87	0.90	8.70	1.31
	Hammer frequency	HF	32.14	0.00	60.00	13.70
	Specific energy	SE	285.49	34.90	3281.00	212.01
Output	Rock mass quality score	RQS	23.86	16.00	31.00	4.53

In the process of tunneling, a total of 1270 datasets were collected in the new Nagasaki tunnel (east). To model and predict the RQS value, six parameters of MWD data were considered as the input parameters. The RQS value was calculated from the observation report of tunnel face. As shown in Table 5.2, descriptive statistics of parameters in the datasets were carried out. Their visual statistic distribution is provided in Fig. 5.1. The statistical results show that the values are extensively distributed. In addition, the correlation between each MWD parameter and their corresponding RQS was investigated. Fig. 5.2 shows the distribution trend of each MWD parameter and RQS value along the tunnel chainage. The coefficient of determination (R^2) of each MWD parameter and corresponding RQS were calculated, as shown in Fig. 5.3. As shown in Fig. 5.2 and Fig.

5.3, a positive correlation exists among RQS and PR, HP, HF and FE, while a negative correlation exists for RP and FP. The correlation between RQS and FP is better than that of other parameters; however, a low correlation factor ($R^2 = 0.395$) is obtained. These results show a low correlation between MWD data and the RQS. The proportion of R^2 value obtained by calculating each MWD parameter in the total R^2 value obtained by all parameters is taken as the influence weight for each MWD parameter on the prediction of RQS. Through calculation, parameters PR, HP, RP, FP, HF and SE respectively obtain weight values of 0.26, 0.01, 0.11, 0.36, 0.05 and 0.20. The results show that parameter FP has the greatest influence on the prediction of RQS, while parameter HP has the least. At the same time, correlation analysis between input parameters was carried out. The correlation results of parameters evaluated by power, exponential and linear equations are shown in Fig. 5.4. Considering the evaluation index of R^2 , the equation is evaluated. Figure 6 shows a high correlation between PR and SE; however, not too much R^2 value ($R^2 = 0.739$) is obtained. These results show that the correlation between the parameters is low. Therefore, using all of the MWD parameters to develop prediction model requires further study. The above analysis shows that the prediction ability of the model developed with single MWD parameter is weak, and the modeling analysis of multiple MWD parameters needs to be carried out. In the following Sections, the attempt to apply an advanced hybrid ANN technology to develop the RQS prediction models by multiple MWD parameters will be carried out.

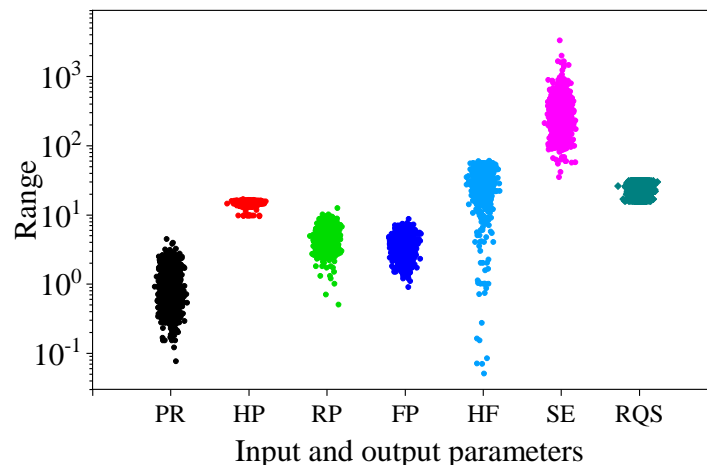


Fig. 5.1 Distribution of the parameters of the input data and output data

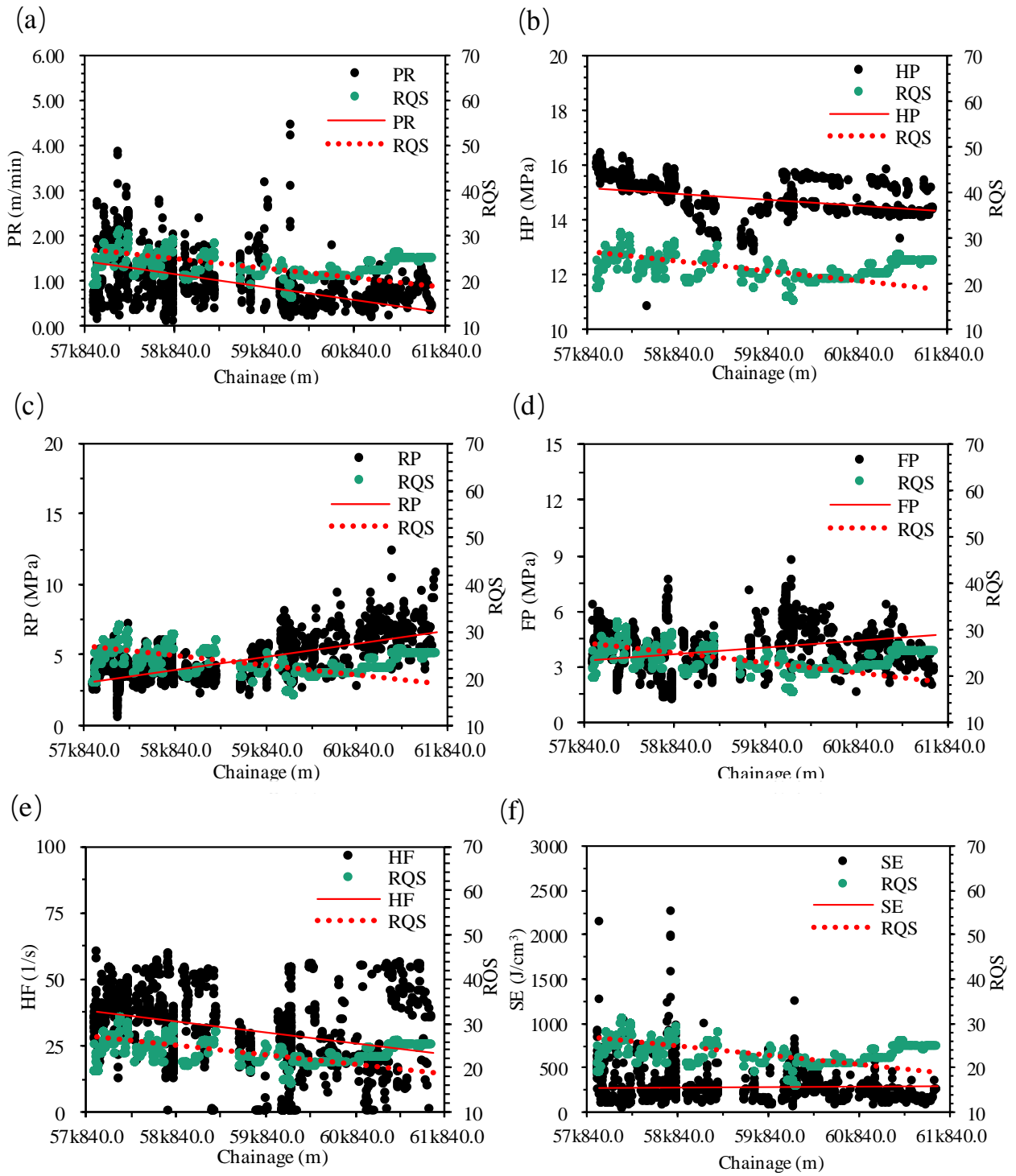


Fig. 5.2 Distribution trend of among RQS and MWD parameters. (a) PR; (b) HP; (c) RP; (d) FP; (e) HF; (f) SE

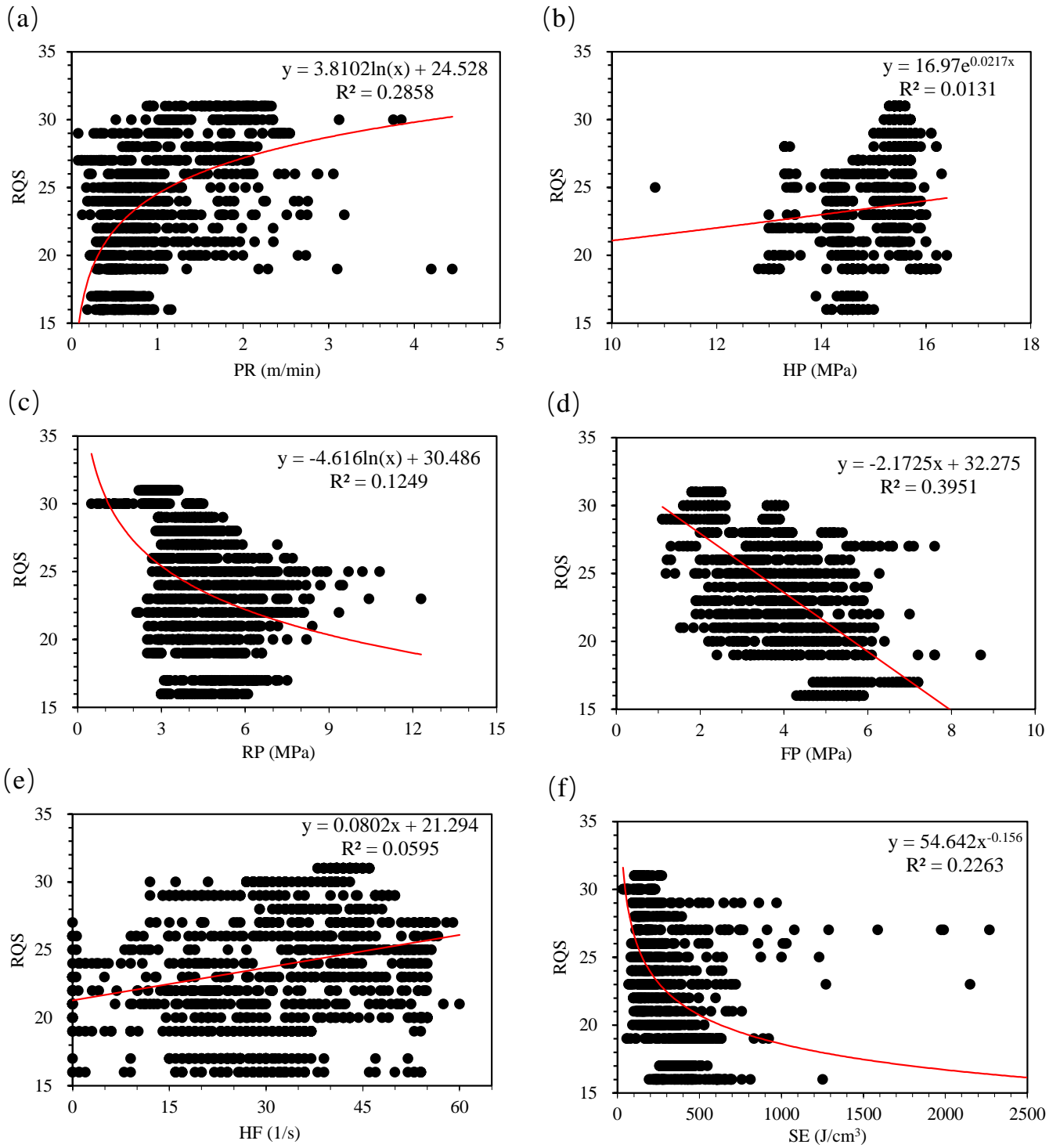


Fig. 5.3 The correlation among RQS and MWD parameters. (a) PR; (b) HP; (c) RP; (d) FP;(e) HF; (f) SE

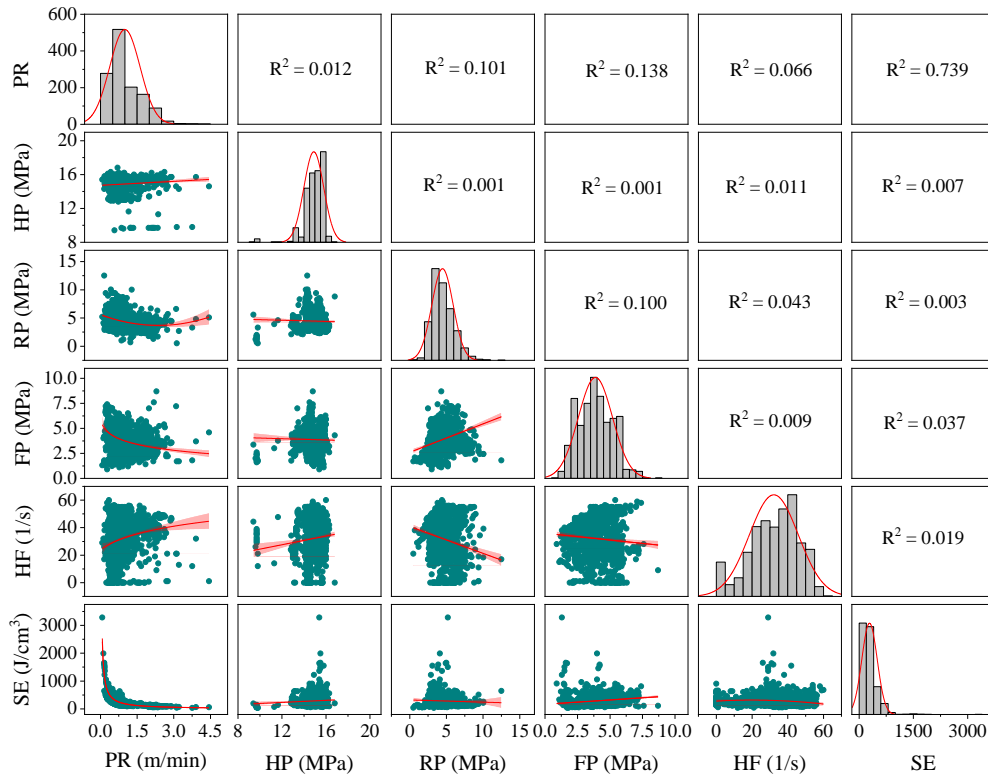


Fig. 5.4 Correlation analysis among the input parameters

To reduce the influence of the order of magnitude, the datasets were normalized by Eq.4-1:

The established datasets were divided into training set and testing set, to establish and evaluate the created networks. In order to train these datasets, Swinger (1996), Looney (1996) and Nelson and Illingworth (1991) proposed 80%, 75% and 70-80% of the whole datasets as training sets respectively. In this study, the ratio of training set and testing set was set to 8:2, which means that there are 1016 datasets for training prediction models, 254 datasets for testing the predictability of the developed prediction model.

5.3 Methods

5.3.1 Multiple linear/nonlinear regression

Multiple regression analysis is a statistical analysis method that considers one variable as a dependent variable and at least two other variable as independent variables to establish a linear or nonlinear mathematical relationship among multiple variables

(Knofczynski and Mundfrom 2008). Multiple regression techniques are commonly used to predict the dependent variable by the independent variables. The multiple linear regression (MLR) equation is $Y=b_1x_1+b_2x_2+\dots+b_nx_n+c$, where b_i is a regression coefficient, x_i is the independent variables, Y is the dependent variable and c is the intercept. The form of multiple nonlinear regression (MNR) equation is generally determined by the relationship between each independent variable and dependent variable.

5.3.2 Artificial neural network

ANN was invented by McCulloch and Pitts (McCulloch and Pitts 1943), who show that, in principle, ANNs can calculate any arithmetic or logic function. The work of these researchers is often regarded as the origin of the field of ANN. Rosenblatt (1958) invented a perceptron network and associated learning rules and demonstrated its ability of pattern recognition, which marked the first practical application of ANN. The successful application of a neural network generated substantial interest in the research of the ANN. However, subsequent research showed that the performance of the basic perceptron network was limited. ANNs became a research hotspot in the late 1980s as information processing structures that were inspired by a biological neural organization structure and operation mode. An ANN is a system composed of several nodes (neurons). These basic nodes are connected and work in parallel to complete certain processing tasks. ANNs can automatically derive general rules by provided pairs of input and output signals. Using this rule, an ANN can generate prediction output for previously unused signals.

The traditional nonlinear regression technique is a highly fitting method for general nonlinear functions, which is based on the nonlinear structure of each element that is linearly combined. As a "universal approximation" technology, ANN is proved to be an "Input-Hidden-Output" hierarchical structure, which enables it to fit almost all functions (including nonlinear functions) (Hornik 1991; Back and Chen 2002; Monjezi et al. 2013). The nonlinear fitting ability of ANN is mainly attributed to the ability to express the properties of each element and the organizational structure between elements. In this research, a typical three-layer neural network is adopted to developed ANN models (Fig. 5.5). Fig. 5.5 also shows the processing flow of ANN, including training stage and testing stage. In the training stage, the input and output of training data set are input to the input layer of ANN in pairs. Then, the relationship between the training datasets was established by one training algorithm. The remainder of the dataset was applied as a testing dataset.

The error back-propagation algorithm is employed as the training algorithm. This algorithm includes two passes: feed-forward pass and backward propagation pass. In the feed-forward pass, the output value of network and the weight and biases of network nodes are random. In the process of the backward propagation pass, the actual values of the outputs are subtracted from the calculated values in a previous pass to generate an error signal. The signal propagates backward to the input layer. According to this signal, the weight and biases are adjusted until the set condition is reached.

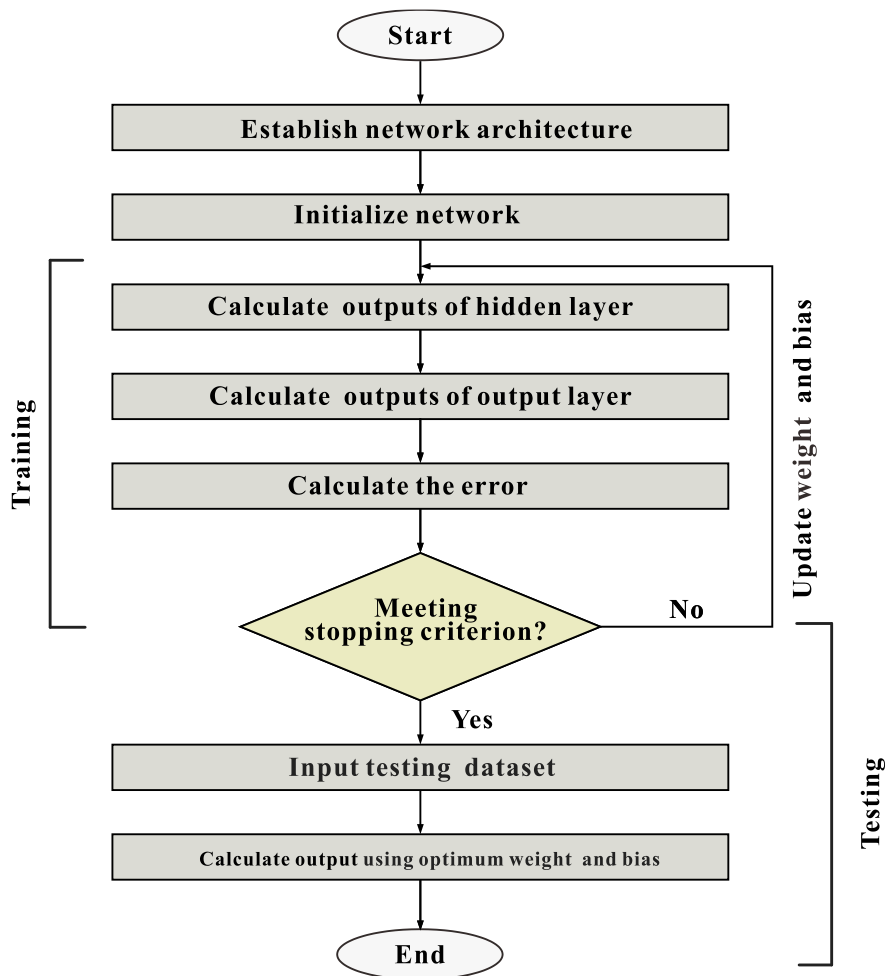


Fig. 5.5 Flowchart of the artificial neural network

5.3.3 Genetic algorithm

The GA was developed by Holland (1992) to find the optimal solution based on the theory of natural evolution. The genetic operation of a GA consists of selection, crossover

and mutation. The GA has many advantages, such as no limit of derivation and function continuity, and better global optimization ability. Despite the advantages of the GA, it has numerous problems. These problems include difficult operator parameter selection, slow search speed and dependence on initial population selection. However, GAs continue to be extensively employed in approximating nonlinear optimization (Yang 2010). In the first stage of the general process of GA, the problem solutions are encoded (e.g., binary encoding or real encoding). In the second stage, the loop process is executed by randomly generating chromosomes. In the final stage, the fitness of each chromosome is calculated. Two individuals are selected from the population for crossover and mutation based on the fitness and selection probability. A crossover operator is used to randomly select two chromosomes of the selected individuals to produce the next generation. A mutation operator is utilized to randomly select the chromosomes of the new generations for the mutation operation. The cycle is repeated until stop condition is satisfied (Dybowski et al. 1996; Nasserri et al. 2008).

5.3.4 Particle swarm optimization

PSO, which is also a heuristic algorithm, is an evolutionary computing technology that was proposed by Kennedy and Eberhart (1995). Particle position and velocity are the core operators of PSO. The motion of particle is the process of individual search. The movement velocity of each particle is adjusted according to the historical optimal position of all particles and the historical optimal position of each particle. The optimal solution that each particle individually searches is referred to as the personal best (p_{best}), and the optimal individual extremum of all particles is the current global best (g_{best}). The velocity and particle position were updated Eq. 5-1 and Eq. 5-2. The optimal solution is obtained by cyclic iteration.

$$v_{\text{new}} = \omega v + c_1 r_1 (p_{\text{best}} - p) + c_2 r_2 (g_{\text{best}} - p), \quad (5-1)$$

$$p_{\text{new}} = p + v_{\text{new}} \quad (5-2)$$

where v_{new} , v , p_{new} , p and w are the new velocity, current velocity, new position, current position, inertia weight, respectively. r_1 and r_2 are random numbers that are usually chosen between $[0,1]$. c_1 is a positive constant, which is referred to as the coefficient of self-adjustment, and c_2 is a positive constant, which is referred to as the coefficient of the social component. p_{best} and g_{best} are the best locations for individuals and the best locations

for all particles. PSO has been widely used in civil engineering, traffic engineering and other engineering fields. A detailed description of PSO and its application in different subjects are provided in the literature (Shi and Eberhart 1998; Gandomi et al. 2013; Nouiri et al. 2018).

5.3.5 Imperialist competition algorithm

Inspired by the colonial competition mechanism of imperialism, Atashpaz-Gargari and Lucas (2007) proposed a new intelligent optimization algorithm, imperialist competitive algorithm (ICA), in 2007. Different from GA, PSO and other swarm intelligence algorithms inspired by biological behavior, ICA is an optimization method inspired by social behavior. ICA is also a population-based optimization algorithm. ICA divided the country into several empires. Within each empire, ICA brought the colonies closer to the imperialist countries through assimilation mechanism. Empire competition mechanism is an important operator of ICA algorithm. One or more weakest empires are annexed by the strongest empires through empire competition mechanism. Through the annexation of the empire, the exchange of information between the empires is completed. More detailed description of the ICA and its application in different subjects is provided in the literature (Gazafroudi et al. 2014; Moayedi and Jahed Armaghani 2018).

5.4 Determination of prediction models

5.4.1 Multiple linear regression statistical model

MLR and MNR prediction models were developed to correlate the RQS by the input parameters of PR, HP, RP, FP, HF and SE of the training datasets. Eq. 5-3 and Eq. 5-4 show the developed MLR and MNR model, respectively. The evaluations of these two models with testing datasets will be carried out in Section of results and discussion.

$$RQS = 13.082 + 1.845PR + 1.034HP - 0.142RP - 1.717FP + 0.032HF - 0.001SE, \quad (5-3)$$

$$RQS = 112.553 - 0.983\ln(PR) + 0.004e^{0.471HP} - 2.165\ln(RP) - 1.514FP + 0.030HF - 69.971SE^{0.037} \quad (5-4)$$

$$RQS = C - 0.983\ln(PR) + 0.004e^{0.471HP} - 2.165\ln(RP) - 1.514FP + 0.030HF - 69.971SE^{0.037}$$

In this study, the coefficient of determination (R^2), root mean square error (RMSE) and variance account for (VAF) indices were calculated to evaluate the prediction capacity of the developed models, as adopted by Yilmaz (2009) and Kayabasi (2012):

$$R^2 = 1 - \frac{\sum_{i=1}^n (y - y')^2}{\sum_{i=1}^n (y - \bar{y})^2} \quad (5-5)$$

$$RMSE = \sqrt{\frac{1}{n} \sum_{i=1}^n (y - y')^2} \quad (5-6)$$

$$VAF = \left[1 - \frac{\text{var}(y - y')}{\text{var}(y)} \right] \quad (5-7)$$

where y is the i^{th} measured value, y' is the i^{th} predicted value, \bar{y} is mean value of the y and n is the number of datasets. High R^2 and VAF values and low RMSE values indicate that the prediction performance is superior. If the R^2 is 1, the RMSE is 0 and the VAF is 100, the model performance will be excellent.

5.4.2 Artificial neural network models

The prediction ANN model was proposed in this Section. As previously mentioned, the Levenberg-Marquardt was employed as training algorithm. Difficulty in establishing ANN model is encountered in selecting the number of hidden layer and nodes.

Many researchers reported that one hidden layer is usually enough to solve most problems. Therefore, the number of hidden layers in this study was set to one. The number of input and output layer nodes was set to 6 and 1, respectively. The prediction performance of ANN is mainly affected by the number of hidden nodes (Kanellopoulos and Wilkinson 1997; Gao 1998; Monjezi et al. 2011) to evaluate the influence of the number of hidden layer nodes on the performance of the ANN model. As shown in Table 5.3, 26 single hidden layer neural network models and 1-80 hidden layer nodes were constructed. Index R^2 and RMSE were used to evaluate the prediction performance of the developed models. However, it is difficult to determine the optimal model. Zorlu et al. (2008) proposed a simple sorting selection method to deal with the above difficulties in selecting the optimal model. The principle of this ranking method is that the highest score means the best performance. For example, R^2 values of 0.542, 0.621, 0.663, 0.724, 0.767, 0.759, 0.759, 0.760, 0.770, 0.796, 0.771, 0.815, 0.825, 0.790, 0.833, 0.819, 0.807, 0.766, 0.727, 0.788, 0.802, 0.803, 0.810, 0.797, 0.832 and 0.811 were obtained for the

training datasets of models 1-26, as shown in Table 5.3. The ratings of the models were assigned 1, 2, 3, 4, 10, 5, 7, 8, 11, 18, 6, 20, 21, 12, 25, 24, 13, 14, 9, 23, 15, 17, 19, 22, 26 and 16, respectively. This method was also used to evaluate RMSE results. Table 5.3 showed the final sorting results. Results revealed that, the network model No. 15, which had one hidden layer with the neural network architecture of 6-15-1, was considered the optimum model for RQS prediction. According to the results in this table, model No. 15 representing the network structure of 6-15-1 was selected as the best prediction mode. Additional discussions regarding the optimum developed model (among 5 runs) is given in Section of results and discussion. It is note that different hybrid models of the neural network structure were developed based on 6-15-1.

5.4.3 *Optimized ANN models by genetic algorithm*

In this section, the hybrid model GA-ANN was established. Fig. 5.6 shows the flowchart. The establishment process of hybrid GA-ANN prediction model for RQS is detailed in the following section.

5.4.3.1 *GA parameters*

The main parameters of GA are population size (S_{pop}), number of generations (N_{gen-GA}), mutation probability and crossover probability. The main task of developing hybrid GA-ANN model is to determine these parameters. The mutation probability proposed by Momeni et al. (2014) was set to 25%, and the crossover probability was set to 70%. Roulette method was used as the selection method of crossover operation.

5.4.3.2 *Value of the S_{pop}*

Different GA-ANN models with population size between 25 and 600 were established to determine the best S_{pop} value, as shown in Table 5.4. It should be noted that these models were all developed with 6-15-1 neural network structure with the maximum generation of 100. Similar to Section of ANN models, the simple sorting method was used to filter out the best S_{pop} . The results show that the model No. 8 has the optimal prediction performance. As a result, the best S_{pop} value was selected as 300.

Table 5.3 The performance index results of different number of hidden nodes for predicting RQS

Model No.	Nodes in hidden layer	Index Result		Average result										Rank value	Total	
		R ²		Run 1		Run 2		Run 3		Run 4		Run 5				
		Training	Testing	Training	Testing	Training	Testing	Training	Testing	Training	Testing	Training	Testing			
1	1	0.543	0.624	0.543	0.616	0.542	0.622	0.542	0.623	0.543	0.620	0.542	0.618	1	1	2
2	2	0.652	0.680	0.639	0.656	0.540	0.611	0.658	0.657	0.627	0.664	0.621	0.652	2	2	4
3	3	0.700	0.700	0.726	0.727	0.720	0.769	0.663	0.712	0.548	0.626	0.663	0.706	3	5	8
4	4	0.690	0.567	0.783	0.803	0.712	0.715	0.622	0.690	0.786	0.796	0.724	0.752	4	8	12
5	5	0.735	0.744	0.758	0.784	0.773	0.775	0.807	0.826	0.761	0.749	0.767	0.777	10	20	30
6	6	0.740	0.762	0.664	0.675	0.788	0.795	0.803	0.834	0.740	0.702	0.759	0.760	5	17	22
7	7	0.753	0.779	0.777	0.802	0.661	0.670	0.820	0.822	0.798	0.804	0.759	0.761	7	22	29
8	8	0.828	0.804	0.748	0.738	0.686	0.707	0.824	0.837	0.733	0.722	0.760	0.765	8	18	26
9	9	0.822	0.835	0.701	0.623	0.810	0.804	0.722	0.701	0.806	0.748	0.770	0.736	11	14	25
10	10	0.786	0.756	0.810	0.824	0.843	0.824	0.790	0.799	0.775	0.751	0.796	0.794	18	23	41
11	11	0.677	0.668	0.843	0.823	0.682	0.694	0.813	0.781	0.751	0.686	0.771	0.733	6	11	17
12	12	0.759	0.693	0.840	0.838	0.830	0.826	0.802	0.814	0.815	0.783	0.815	0.806	20	24	44
13	13	0.797	0.780	0.812	0.781	0.834	0.814	0.872	0.846	0.754	0.657	0.825	0.784	21	21	42
14	14	0.733	0.710	0.840	0.734	0.728	0.670	0.770	0.745	0.792	0.770	0.790	0.749	12	10	22
15	15	0.835	0.825	0.835	0.840	0.825	0.786	0.829	0.758	0.836	0.833	0.833	0.803	25	26	51
16	16	0.784	0.732	0.814	0.724	0.804	0.783	0.853	0.835	0.833	0.765	0.819	0.782	24	19	43
17	17	0.691	0.660	0.770	0.721	0.836	0.838	0.758	0.698	0.836	0.769	0.807	0.762	13	13	26
18	18	0.860	0.815	0.793	0.789	0.807	0.649	0.676	0.704	0.753	0.708	0.766	0.729	14	12	26
19	19	0.834	0.814	0.844	0.813	0.670	0.682	0.745	0.731	0.730	0.701	0.727	0.718	9	16	25
20	20	0.875	0.544	0.767	0.493	0.851	0.828	0.774	0.756	0.811	0.801	0.788	0.707	23	3	26
21	30	0.751	0.678	0.797	0.789	0.860	0.770	0.730	0.669	0.765	0.632	0.802	0.739	15	6	21
22	40	0.782	0.719	0.813	0.757	0.783	0.623	0.783	0.689	0.791	0.702	0.803	0.714	17	4	21
23	50	0.828	0.809	0.855	0.605	0.795	0.718	0.714	0.672	0.837	0.792	0.810	0.720	19	9	28
24	60	0.842	0.824	0.871	0.814	0.761	0.675	0.777	0.649	0.819	0.757	0.797	0.700	22	15	37
25	70	0.843	0.799	0.821	0.757	0.867	0.762	0.821	0.803	0.886	0.840	0.832	0.769	26	25	51
26	80	0.782	0.672	0.771	0.726	0.838	0.777	0.798	0.699	0.750	0.666	0.811	0.702	16	7	23

Table 5.3 (continued)

Model No.	Nodes in hidden layer	Index	Result										Average result		Rank value	Total	
			Run 1		Run 2		Run 3		Run 4		Run 5		Training	Testing			
			Training	Testing	Training	Testing	Training	Testing	Training	Testing	Training	Testing					
1	1	RMSE	3.023	2.948	3.024	2.988	3.026	2.959	3.025	2.962	3.023	2.965	3.026	2.978	1	1	2
2	2		2.640	2.704	2.690	2.813	3.034	2.992	2.617	2.802	2.740	2.751	2.752	2.816	2	3	5
3	3		2.452	2.618	2.342	2.484	2.365	2.292	2.596	2.564	3.008	2.938	2.584	2.593	3	7	10
4	4		2.488	3.222	2.085	2.111	2.403	2.549	2.751	2.672	2.073	2.155	2.340	2.366	4	9	13
5	5		2.302	2.435	2.200	2.204	2.130	2.251	1.964	1.986	2.189	2.365	2.157	2.233	9	21	30
6	6		2.282	2.335	2.591	2.718	2.057	2.152	1.985	1.930	2.281	2.629	2.182	2.316	5	17	22
7	7		2.225	2.254	2.112	2.120	2.603	2.729	1.895	2.007	2.016	2.135	2.180	2.313	7	20	27
8	8		1.855	2.100	2.255	2.470	2.506	2.567	1.879	1.923	2.311	2.514	2.181	2.297	8	18	26
9	9		1.890	1.957	2.445	2.947	1.950	2.095	2.359	2.620	1.970	2.409	2.136	2.438	12	14	26
10	10		2.090	2.413	1.950	2.000	1.771	1.979	2.051	2.148	2.121	2.364	2.016	2.152	18	24	42
11	11		2.550	2.728	1.773	2.009	2.530	2.670	1.936	2.213	2.232	2.672	2.128	2.452	6	12	18
12	12		2.196	2.651	1.790	1.914	1.845	1.988	2.001	2.095	1.925	2.218	1.927	2.099	20	25	45
13	13		2.014	2.237	1.944	2.245	1.822	2.049	1.598	1.867	2.219	2.828	1.862	2.203	22	22	44
14	14		2.314	2.562	1.789	2.528	2.334	2.734	2.145	2.429	2.042	2.319	2.041	2.397	11	10	21
15	15		1.817	1.997	1.819	1.888	1.881	2.232	1.850	2.341	1.814	1.945	1.828	2.110	25	26	51
16	16		2.087	2.466	1.942	2.584	2.003	2.220	1.714	1.938	1.825	2.324	1.910	2.233	23	19	42
17	17		2.504	2.793	2.145	2.510	1.816	1.941	2.205	2.613	1.814	2.306	1.957	2.324	13	13	26
18	18		1.677	2.077	2.033	2.177	1.967	3.004	2.561	2.574	2.223	2.572	2.160	2.494	14	11	25
19	19		1.830	2.035	1.770	2.070	2.569	2.687	2.259	2.471	2.324	2.600	2.325	2.515	10	16	26
20	20		1.579	3.808	2.162	3.833	1.730	1.977	2.126	2.369	1.943	2.124	2.052	2.626	24	2	26
21	30		2.232	2.710	2.025	2.221	1.675	2.320	2.324	2.743	2.167	2.955	1.976	2.436	15	5	20
22	40		2.090	2.516	1.933	2.391	2.083	3.022	2.095	2.704	2.043	2.609	1.983	2.573	17	4	21
23	50		1.900	2.092	1.726	3.270	2.023	2.533	2.393	2.713	1.804	2.184	1.940	2.550	19	8	27
24	60		1.787	1.984	1.608	2.059	2.187	2.738	2.110	2.874	1.915	2.333	2.006	2.608	21	15	36
25	70		1.774	2.137	1.894	2.352	1.640	2.418	1.892	2.112	1.518	1.930	1.824	2.299	26	23	49
26	80		2.090	2.761	2.157	2.532	1.802	2.249	2.013	2.649	2.238	2.756	1.926	2.680	16	6	22

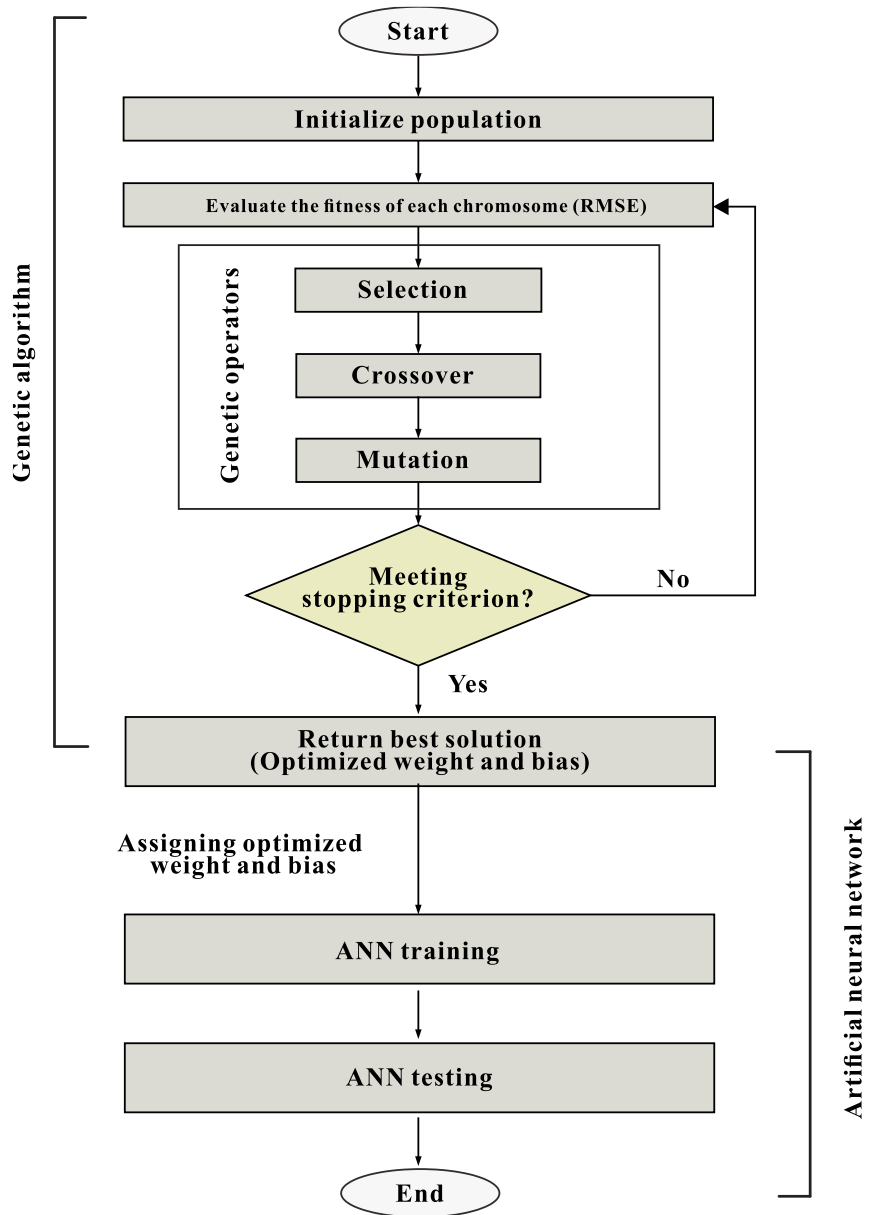


Fig. 5.6 Flowchart of the optimized artificial neural network by the genetic algorithm

Table 5.4 RQS prediction performance index results of the GA-ANN for different population size

No.	Population size	GA-ANN				Rank value				Total
		Training		Testing		Training		Testing		
		R ²	RMSE	R ²	RMSE	R ²	RMSE	R ²	RMSE	
1	25	0.801	1.975	0.786	2.191	3	3	4	6	16
2	50	0.840	1.787	0.792	2.179	12	12	10	10	44
3	75	0.800	1.991	0.771	2.259	2	2	1	1	6
4	100	0.844	1.765	0.791	2.186	14	14	9	9	46
5	150	0.822	1.882	0.787	2.196	8	7	6	5	26
6	200	0.813	1.924	0.782	2.243	5	5	3	2	15
7	250	0.837	1.804	0.808	2.083	11	11	13	13	48
8	300	0.844	1.770	0.818	2.036	13	13	14	14	54
9	350	0.831	1.825	0.788	2.230	10	10	7	3	30
10	400	0.822	1.879	0.807	2.086	7	8	12	12	39
11	450	0.805	1.970	0.787	2.188	4	4	5	7	20
12	500	0.797	2.003	0.781	2.212	1	1	2	4	8
13	550	0.816	1.913	0.789	2.187	6	6	8	8	28
14	600	0.823	1.859	0.800	2.130	9	9	11	11	40

5.4.3.3 Value of the N_{gen-GA}

Many GA-ANN models were established to determine the most appropriate N_{gen-GA} with the maximum number of 1000 and S_{pop} values of 25-600. Other parameters of GA-ANN used in these models were set as the parameters determined in the previous steps.

As shown in Fig. 5.7, after 700 generations, the RMSE value no longer continues to decline and remains constant. Thus, a value of 700 was chosen as the optimum N_{gen-GA} .

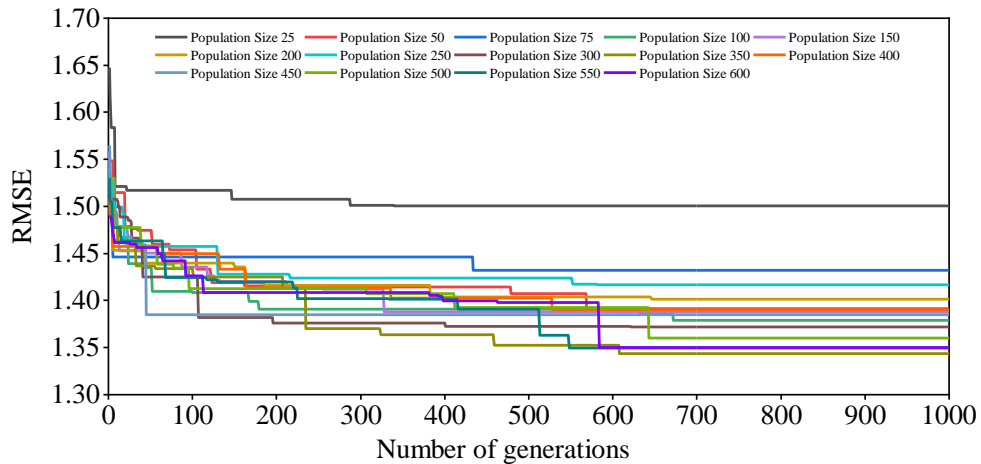


Fig. 5.7 Performance comparison of the GA-ANN models with the different number of generations

5.4.3.4 Network modelling

Using the best parameters obtained in the above steps, the final hybrid GA-ANN model was established, and 5 times of training were carried out. The performance index values obtained of the development models are shown in Table 5.9. Further comparative analysis will be performed in Section of results and discussion.

5.4.4 Optimized ANN models by particle swarm optimization

Similar to the GA, several researchers have successfully employed the PSO to optimize ANN (Hoballah and Erlich 2009; Vasumathi and Moorthi 2012; Moayedi et al. 2019). In this section, the optimal parameters of the hybrid PSO-ANN model will be determined. Fig. 5.8 shows the flowchart of the hybrid PSO-ANN algorithm.

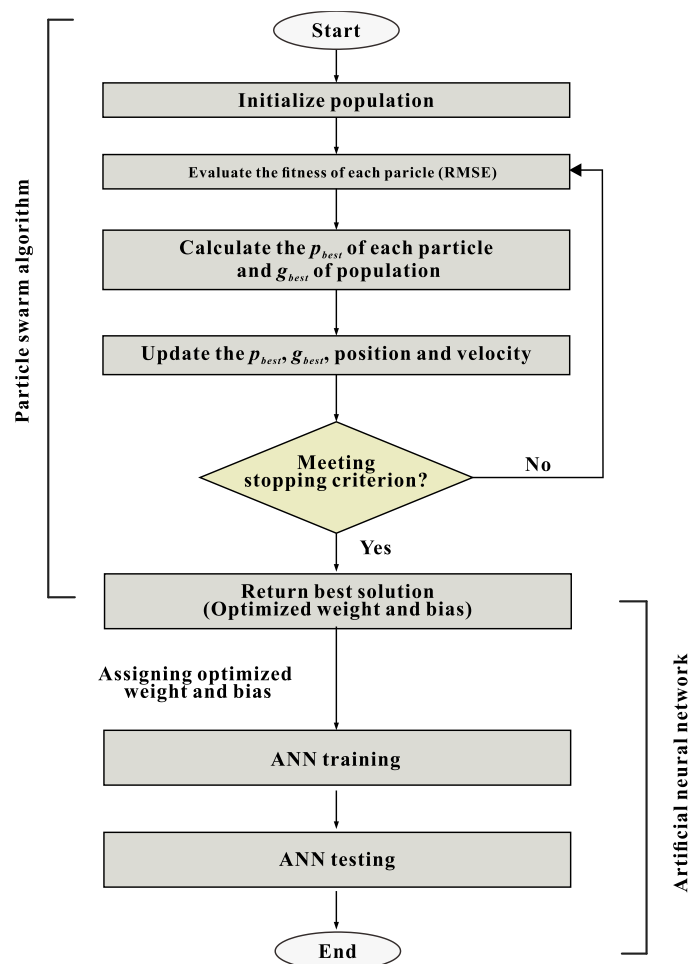


Fig. 5.8 Flowchart of the particle swarm optimization algorithm

5.4.4.1 PSO parameters

For PSO algorithm, the main parameters are the coefficient of velocity equation, number of particles (N_{par}), number of generations ($N_{gen-PSO}$), c_1 , c_2 and w . It should be emphasized that in the establishment of all PSO-ANN models, the values of c_1 , c_2 and w were all set to $c_1=c_2=2$ and $w=0.25$ recommended by Kennedy and Eberhart (1997) and Clerc and Kennedy (2002).

5.4.4.2 Value of the N_{par}

Several PSO-ANN models were established with a range of N_{par} from 25 to 600 to select the optimal N_{par} value, as presented in Table 5.5. The architecture of 6-15-1 and maximum generation of 100 were utilized, and the performance indices of R^2 and RMSE were employed to assess the developed models. As discussed in the previous sections, the performance indexes of the established models were sorted. According to Table 5.5, model No. 11 with 450 particles obtained the highest sorting value. As a result, 450 was determined to be the best N_{par} value.

5.4.4.3 Value of the $N_{gen-PSO}$

Different models with a fixed number of generations of 1000 and N_{par} in the range of 25-600 were developed to choose the optimum $N_{gen-PSO}$. Fig. 5.9 shows that the values of the RMSE do not change after the $N_{gen-PSO}$ value of 800. Therefore, the optimum $N_{gen-PSO}$ was set to 800 in this study.

Table 5.5 Effect of the swarm size on the hybrid PSO-ANN in predicting RQS

No.	Swarm size	PSO-ANN				Rank value				Total
		Training		Testing		Training		Testing		
		R^2	RMSE	R^2	RMSE	R^2	RMSE	R^2	RMSE	
1	25	0.821	1.878	0.782	2.238	6	7	5	5	23
2	50	0.807	1.952	0.760	2.331	1	1	1	1	4
3	75	0.833	1.822	0.805	2.105	11	10	10	10	41
4	100	0.839	1.793	0.777	2.313	13	13	4	2	32
5	150	0.824	1.878	0.776	2.274	8	8	3	3	22
6	200	0.819	1.899	0.795	2.169	4	4	7	7	22
7	250	0.809	1.943	0.792	2.172	2	2	6	6	16
8	300	0.832	1.820	0.817	2.041	9	12	12	12	45
9	350	0.845	1.751	0.802	2.113	14	14	8	8	44
10	400	0.833	1.822	0.812	2.068	10	11	11	11	43
11	450	0.834	1.824	0.820	2.017	12	9	14	14	49
12	500	0.821	1.884	0.803	2.112	7	6	9	9	31
13	550	0.820	1.891	0.775	2.261	5	5	2	4	16
14	600	0.819	1.906	0.817	2.018	3	3	13	13	32

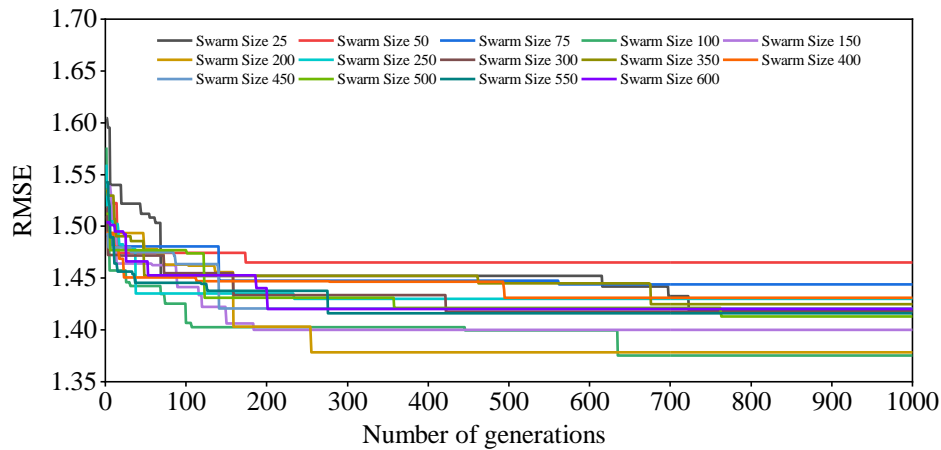


Fig. 5.9 Performance comparison of the PSO-ANN models with the different number of generations

5.4.4.4 Network modelling

Similarly, the PSO-ANN model was developed with ANN architecture of 6-15-1 and the obtained optimum parameters of PSO and was also trained five times. The performance index values of the final model were recorded in Table 5.9. The developed PSO-ANN model will be evaluated further in Section of results and discussion.

5.4.5 Optimized ANN models by imperialist competition algorithm

The hybrid ICA-ANN model was also established to predict RQS. The hybrid ICA-ANN algorithm flowchart is shown in Fig. 5.10. The establishment process of the hybrid PSO-ANN prediction model will be discussed in the following.

5.4.5.1 ICA parameters

The main parameters of the ICA are the number of countries (N_{cou}), number of imperialists (N_{imp}), number of decades (N_{dec}), β (number greater than 1), θ (random number) and ζ (positive number less than 1). As previously mentioned, before establishing the hybrid model, the parameters β , θ and ζ were selected as 1.5, $\pi/4$ and 0.2, respectively, according to the recommendations in the literature (Ahmadi et al. 2013; Marto et al. 2014). The remaining parameters of the N_{cou} , the N_{imp} and the N_{dec} are determined in the following Sections.

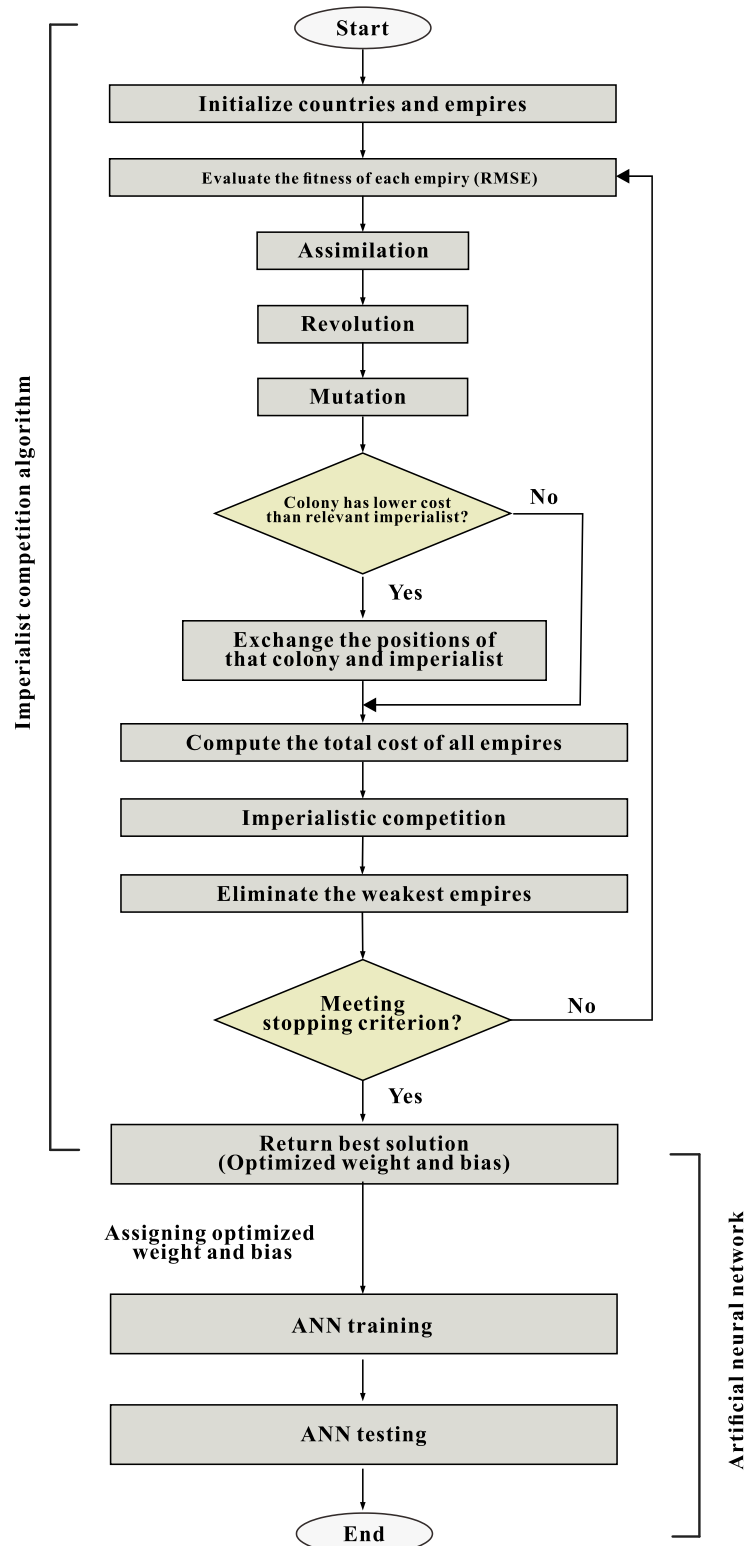


Fig. 5.10 Flowchart of the imperialist competitive algorithm

5.4.5.2 Value of N_{cou}

To select the optimal N_{cou} , different ICA-ANN models were developed with a range of N_{cou} from 50 to 600, as presented in Table 5.6. The ANN architecture of 6-15-1 and maximum decade of 100 were employed. Table 5.6 records the ranking results of the prediction performance indexes of the established prediction models. The results show that model No. 10, which represents 450 countries, has the largest ranking value. Thus, 450 was selected as the best N_{cou} value.

Table 5.6 RQS prediction performance index results of the hybrid ICA-ANN for the different number of countries

No.	No. of country	ICA-ANN				Rank value				Total
		Training		Testing		Training		Testing		
		R ²	RMSE	R ²	RMSE	R ²	RMSE	R ²	RMSE	
1	50	0.816	1.913	0.801	2.114	5	5	7	8	25
2	75	0.836	1.801	0.778	2.255	9	10	2	2	23
3	100	0.794	2.019	0.784	2.190	1	2	4	3	10
4	150	0.826	1.867	0.816	2.025	6	6	10	13	35
5	200	0.831	1.833	0.802	2.120	7	7	8	7	29
6	250	0.859	1.667	0.813	2.049	13	13	9	10	45
7	300	0.805	1.967	0.784	2.185	3	3	3	4	13
8	350	0.831	1.819	0.817	2.028	8	8	13	12	41
9	400	0.796	2.020	0.791	2.175	2	1	5	5	13
10	450	0.844	1.758	0.816	2.042	12	12	12	11	47
11	500	0.837	1.809	0.816	2.050	10	9	11	9	39
12	550	0.813	1.929	0.768	2.295	4	4	1	1	10
13	600	0.840	1.786	0.794	2.173	11	11	6	6	34

5.4.5.3 Value of N_{imp}

In this Section, different ICA-ANN models were constructed with N_{imp} ranging from 50 to 200 and N_{cou} of 450. Table 5.8 shows that the No. 5 model representing $N_{imp} = 90$ has the highest sorting value. Therefore, 90 was set as the best N_{imp} value.

5.4.5.4 Value of the N_{dec}

As shown in Fig. 5.11. Different models were developed to determine the best N_{dec} value with the fixed N_{dec} values of 1000 and the N_{cou} values between 50-600. The results show that the RMSE values of all models do not continue to decline after $N_{dec} = 800$. Therefore, 800 was determined as the best N_{dec} value of ICA-ANN prediction model.

Table 5.7 RQS prediction performance index results of the hybrid ICA-ANN for the different number of imperialists

No.	No. of imperialist	ICA-ANN				Rank value				Total
		Training		Testing		Training		Testing		
		R ²	RMSE	R ²	RMSE	R ²	RMSE	R ²	RMSE	
1	50	0.818	1.919	0.785	2.196	4	4	1	1	10
2	60	0.833	1.809	0.802	2.146	11	11	10	6	38
3	70	0.820	1.895	0.810	2.068	5	5	14	14	38
4	80	0.833	1.820	0.802	2.100	10	10	11	12	43
5	90	0.854	1.704	0.834	1.940	16	16	16	16	64
6	100	0.796	2.011	0.797	2.147	1	1	4	5	11
7	110	0.824	1.879	0.808	2.075	6	6	13	13	38
8	120	0.853	1.714	0.820	2.041	15	15	15	15	60
9	130	0.852	1.718	0.797	2.182	14	14	5	2	35
10	140	0.830	1.830	0.799	2.126	8	9	7	9	33
11	150	0.836	1.805	0.803	2.116	12	12	12	10	46
12	160	0.840	1.783	0.795	2.156	13	13	3	4	33
13	170	0.814	1.932	0.790	2.179	2	2	2	3	9
14	180	0.825	1.864	0.801	2.114	7	7	9	11	34
15	190	0.832	1.836	0.799	2.141	9	8	8	7	32
16	200	0.814	1.921	0.798	2.130	3	3	6	8	20

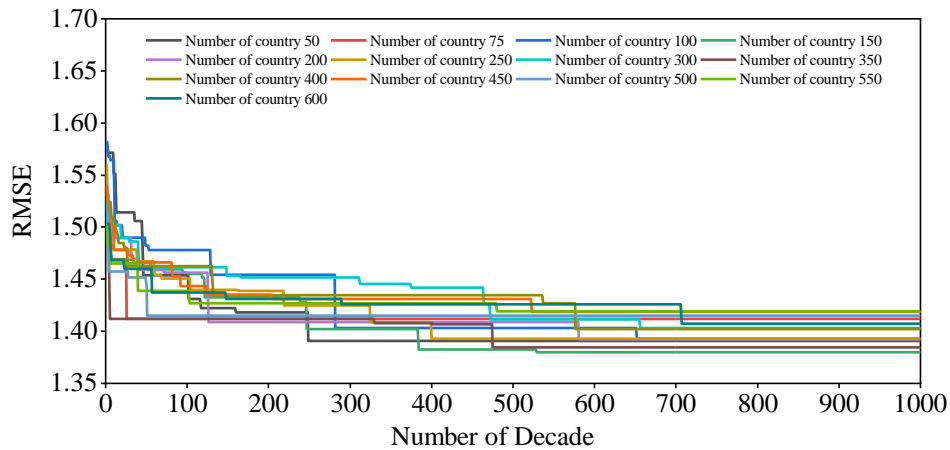


Fig. 5.11 Performance comparison of the ICA -ANN models with the different number of decades

5.4.5.5 Network modelling

As before with the developments of the GA-ANN and PSO-ANN models, the final ICA-ANN model was developed with the ANN architecture of 6-15-1 and determined optimal ICA parameters. The final ICA-ANN model was also trained five times. The performance index results of development models were shown in Table 5.9. All final prediction models established above will be discussed in next Section.

Table 5.8 RQS prediction performance index results of the hybrid ICA-ANN for the different number of imperialists

No.	No. of imperialist	ICA-ANN				Rank value				Total
		Training		Testing		Training		Testing		
		R ²	RMSE	R ²	RMSE	R ²	RMSE	R ²	RMSE	
1	50	0.818	1.919	0.785	2.196	4	4	1	1	10
2	60	0.833	1.809	0.802	2.146	11	11	10	6	38
3	70	0.820	1.895	0.810	2.068	5	5	14	14	38
4	80	0.833	1.820	0.802	2.100	10	10	11	12	43
5	90	0.854	1.704	0.834	1.940	16	16	16	16	64
6	100	0.796	2.011	0.797	2.147	1	1	4	5	11
7	110	0.824	1.879	0.808	2.075	6	6	13	13	38
8	120	0.853	1.714	0.820	2.041	15	15	15	15	60
9	130	0.852	1.718	0.797	2.182	14	14	5	2	35
10	140	0.830	1.830	0.799	2.126	8	9	7	9	33
11	150	0.836	1.805	0.803	2.116	12	12	12	10	46
12	160	0.840	1.783	0.795	2.156	13	13	3	4	33
13	170	0.814	1.932	0.790	2.179	2	2	2	3	9
14	180	0.825	1.864	0.801	2.114	7	7	9	11	34
15	190	0.832	1.836	0.799	2.141	9	8	8	7	32
16	200	0.814	1.921	0.798	2.130	3	3	6	8	20

5.5 Results and discussion

In this section, the final model previously developed will be compared to select the model with the highest predictive performance. In the last stage of the developing models, except MLR and MNR models, other models were trained five times to predict the RQS. The indices of R², RMSE and VAF are utilized to assess the performance of these developed models.

Table 5.9 displays the obtained results of the developed models. Determining the optimal model is not easy because the results are similar. The method of ranking, as previously mentioned, was employed to select the optimal model in the same way. The total rank of all developed models is indicated in Table 5.10. The results show that ANN model No. 5, GA-ANN model No. 3, PSO-ANN model No. 2 and ICA-ANN model No. 1 have a total rank of 27, 27, 30 and 27, respectively, which indicates the optimal performance. For a certain training dataset, note that only one prediction formula can be fitted using the MLR method. Therefore, only one prediction model of the MLR was developed in this study.

Table 5.11 shows the best performance index results of the 6 final prediction models of MLR, MNR, GA-ANN, PSO-ANN and ICA-ANN. The results revealed that the performance level of the regression models can be increased from approximately 0.60 (for MLR and MNR models) to approximately 0.83 (for ANN models) based on R^2 by developing the ANN model. The performance level of the ANN model can be increased based on R^2 by developing a hybrid model, i.e., PSO-ANN and ICA-ANN from approximately 0.83 (for ANN models) to approximately 0.86 (for PSO-ANN and ICA-ANN models).

The measured and predicted RQS values of RQS obtained by the five optimal models are shown in Fig. 5.12. The comparison between measured RQS and predicted RQS using all five models with testing datasets are shown in Fig. 5.13. In addition, the weight of prediction effect of each model (Table 5.11) is obtained by calculating the proportion of R^2 value obtained by each model at the test stage in the total R^2 value of all models.

It should be noted that the test stage is an important part of the evaluation of the prediction performance and It should be emphasized that the test stage is an important part of the evaluation of the prediction effect and the change trend of the three evaluation indexes (R^2 , RMSE and VAF) is basically the same. Therefore, only R^2 value of the test stage is considered when calculating the weight value of each model. Table 5.11 shows that MLR, MNR, ANN, GA-ANN, PSO-ANN and ICA-ANN obtain weight values of 0.133, 0.141, 0.178, 0.180, 0.185, and 0.183 respectively. The results reveal that the hybrid models of PSO-ANN and ICA-ANN are better than the MLR, MNR, ANN, GA-ANN models. When both the training dataset and testing dataset are considered, R^2 values of 0.875 and 0.862 and R^2 values of 0.873 and 0.857 for the PSO-ANN technique and ICA-ANN technique, respectively, indicate that the PSO-ANN model has slightly higher performance compared with other models.

Table 5.9 RQS prediction performance index results of the MLR, ANN, GA-ANN, PSO-ANN and ICA-ANN models

Method	Stage	Model No.	R ²	RMSE	VAF	Rank value			Total
						R ²	RMSE	VAF	
MLR	Training	1	0.543	3.024	0.543	1	1	1	1
	Testing	1	0.621	2.964	0.615	1	1	1	1
MNR	Training	1	0.583	2.889	0.583	1	1	1	1
	Testing	1	0.659	2.800	0.654	1	1	1	1
ANN	Training	1	0.835	1.817	0.835	3	4	4	11
		2	0.835	1.819	0.835	4	3	3	10
		3	0.825	1.881	0.825	1	1	1	3
		4	0.829	1.850	0.829	2	2	2	6
		5	0.836	1.814	0.835	5	5	5	15
	Testing	1	0.825	1.997	0.824	3	3	3	9
		2	0.840	1.888	0.840	5	5	5	15
		3	0.786	2.232	0.779	2	2	2	6
		4	0.758	2.341	0.755	1	1	1	3
		5	0.833	1.945	0.833	4	4	4	12
GA-ANN	Training	1	0.830	1.863	0.828	3	3	3	9
		2	0.839	1.792	0.839	5	5	5	15
		3	0.833	1.828	0.833	4	4	4	12
		4	0.827	1.864	0.826	2	2	2	6
		5	0.820	1.899	0.820	1	1	1	3
	Testing	1	0.828	1.960	0.827	3	3	2	8
		2	0.816	2.038	0.814	1	1	1	3
		3	0.840	1.905	0.839	5	5	5	15
		4	0.827	1.980	0.827	2	2	3	7
		5	0.833	1.932	0.833	4	4	4	12
PSO-ANN	Training	1	0.836	1.815	0.835	2	2	3	9
		2	0.875	1.584	0.875	5	5	5	12
		3	0.868	1.629	0.867	4	4	4	15
		4	0.830	1.843	0.830	1	1	2	3
		5	0.866	1.638	0.829	3	3	1	6
	Testing	1	0.846	1.871	0.829	1	1	1	3
		2	0.862	1.782	0.861	5	5	5	9
		3	0.855	1.814	0.852	4	4	4	15
		4	0.849	1.834	0.849	3	3	3	6
		5	0.848	1.864	0.845	2	2	2	12
ICA-ANN	Training	1	0.873	1.592	0.873	4	4	4	12
		2	0.852	1.723	0.852	2	2	2	6
		3	0.876	1.574	0.876	5	5	5	15
		4	0.862	1.661	0.862	3	3	3	9
		5	0.839	1.796	0.839	1	1	1	3
	Testinging	1	0.857	1.812	0.855	5	5	5	15
		2	0.852	1.816	0.852	3	3	3	9
		3	0.845	1.868	0.844	2	2	2	6
		4	0.853	1.814	0.853	4	4	4	12
		5	0.840	1.899	0.840	1	1	1	3

Table 5.10 Results of total rank values of all stages of the developed final models

Method	Model No.	Total rank
MLR	1	1
MNR	1	1
ANN	1	20
	2	25
	3	9
	4	9
	5	27
GA-ANN	1	17
	2	18
	3	27
	4	13
	5	15
PSO-ANN	1	10
	2	30
	3	24
	4	13
	5	13
ICA-ANN	1	27
	2	15
	3	21
	4	21
	5	6

Table 5.11 Results of the best performance indices of the developed final models

Method	No.	Training			Testing			Weight
		R ²	RMSE	VAF	R ²	RMSE	VAF	R ² of Testing
MLR	1	0.543	3.024	0.543	0.621	2.964	0.615	0.133
MNR	1	0.583	2.889	0.583	0.659	2.800	0.654	0.141
ANN	5	0.836	1.814	0.835	0.833	1.945	0.833	0.178
GA-ANN	3	0.833	1.828	0.833	0.840	1.905	0.839	0.180
PSO-ANN	2	0.875	1.584	0.875	0.862	1.782	0.861	0.185
ICA-ANN	1	0.873	1.592	0.873	0.857	1.812	0.855	0.183

Table 5.12 Results of the comparative test of the prediction performance for four intervals

Interval	Geological conditions	Average R ²
Interval 1	Good	0.689
Interval 2	Poor	0.536
Interval 3	Good	0.638
Interval 4	Fair	0.182

The comparison results of learning rates of ANN, GA-ANN, PSO-ANN and ICA-ANN algorithms were shown in Fig. 5.14. ANN obtains the lowest RMSE value of 0.292 when epoch are about 160 steps. However, for GA-ANN, PSO-ANN and ICA-ANN get the

lowest RMSE values when epoch are 80 steps, which are 0.212, 0.193 and 0.201, respectively. The results show that GA, PSO and ICA can improve the learning rate of ANN and get better training effect.

To investigate the influence of geological conditions on the prediction performance of RQS, comparative test were carried out for four intervals. It should be noted that the best prediction model that has been determined above, the PSO-ANN model, was used in this comparative test and the average value of the R^2 calculated for 10 times was applied as the evaluation index. The comparison result is shown in Table 5.12. The result shows that the prediction performance of intervals 1 and 3 with good geological conditions is higher, and the R^2 values obtained are 0.689 and 0.638, respectively. On the contrary, the prediction performance of intervals 2 and 4 with poor geological conditions is lower, with R^2 values of 0.548 and 0.273, respectively. The reason for this result is that for the tunnel face with good geological conditions, the single MWD data can better reflect the whole face condition. Therefore, it can be concluded that when using optimized ANN to predict RQS, the prediction performance is affected by geological conditions so that it cannot reach 100%. In addition, due to the reduction of the number of training samples, compared with the total datasets of four intervals, the prediction performance of each interval is reduced.

It should be noted that the best prediction model is determined as PSO-ANN hybrid model, and the corresponding ANN structure is 6-15-1. In this structure, all six variables were taken as input variables. According to the results of relative influence of each input variable on RQS in Chapter Dataset Collection and Analysis, the weight values of 0.26, 0.01, 0.11, 0.36, 0.05 and 0.20 were obtained for PR, HP, RP, FP, HF, and SE respectively. In practical application, the weight values can be used to determine the final required input variables.

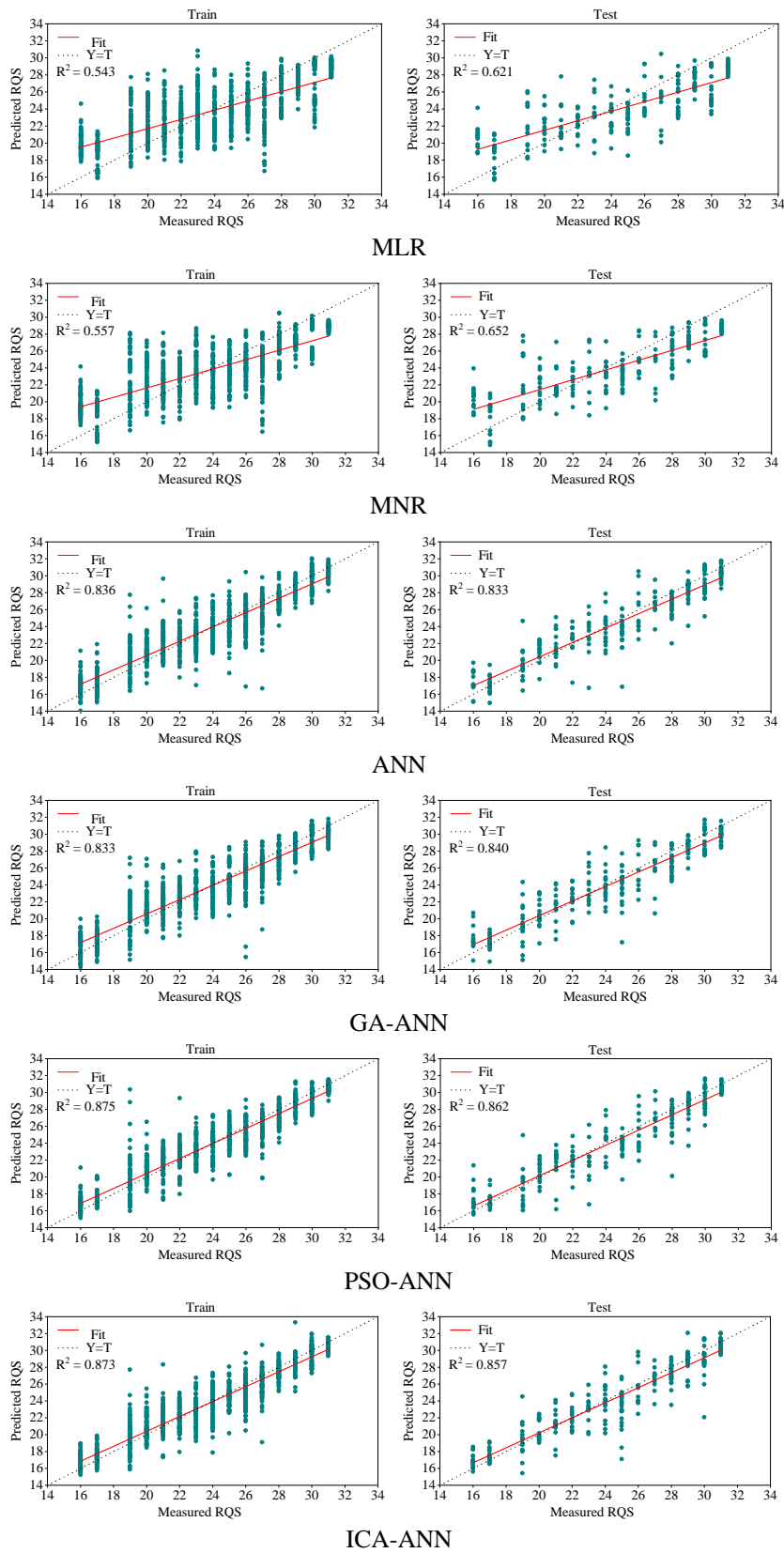
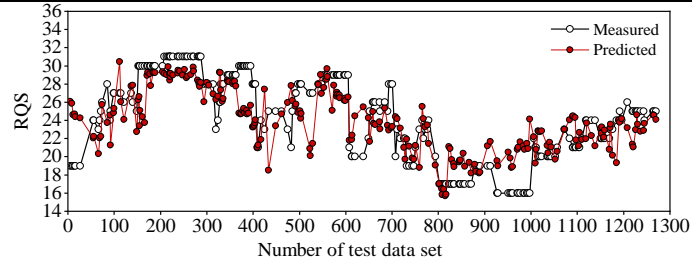
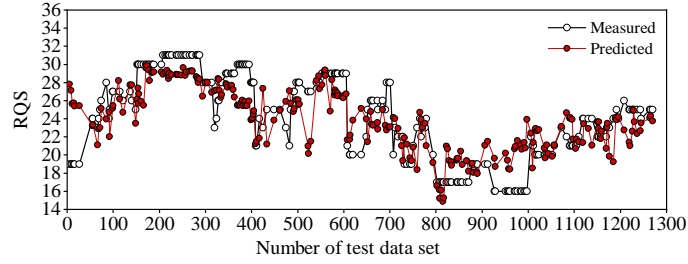


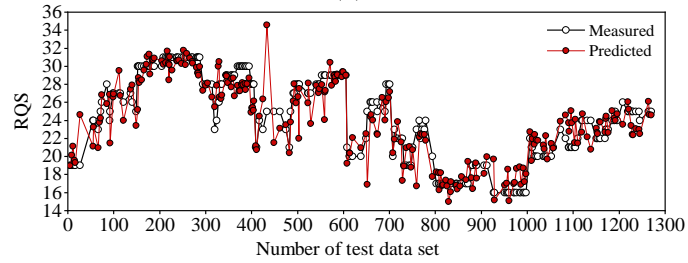
Fig. 5.12 The coefficient of determination of measured and predicted QRS values of five developed final models for training and testing datasets. (a) MLR; (b) MNR; (c) ANN; (d) The GA-ANN; (e) PSO-ANN; (f) ICA-ANN



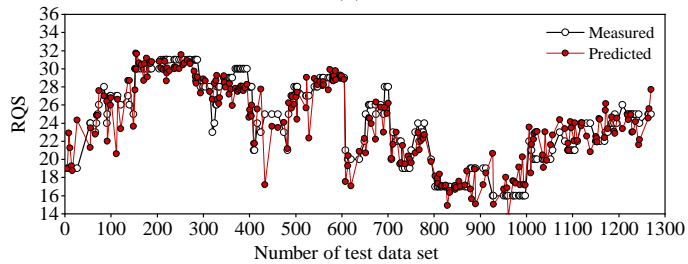
(a)



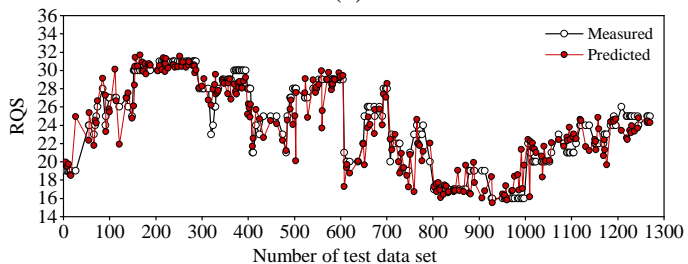
(b)



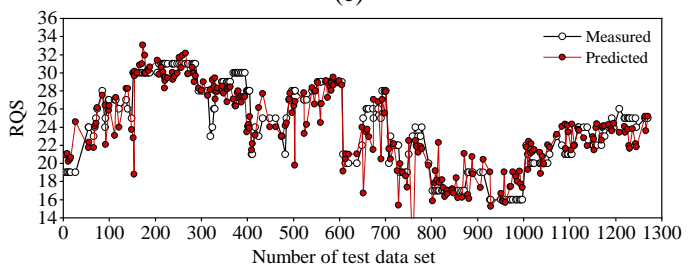
(c)



(d)



(e)



(f)

Fig. 5.13 Comparison of measured and predicted RQS values of five developed final models for training and testing datasets. (a) MLR; (b) MNR; (c) ANN; (d) The GA-ANN; (e) PSO-ANN; (f)

ICA-ANN

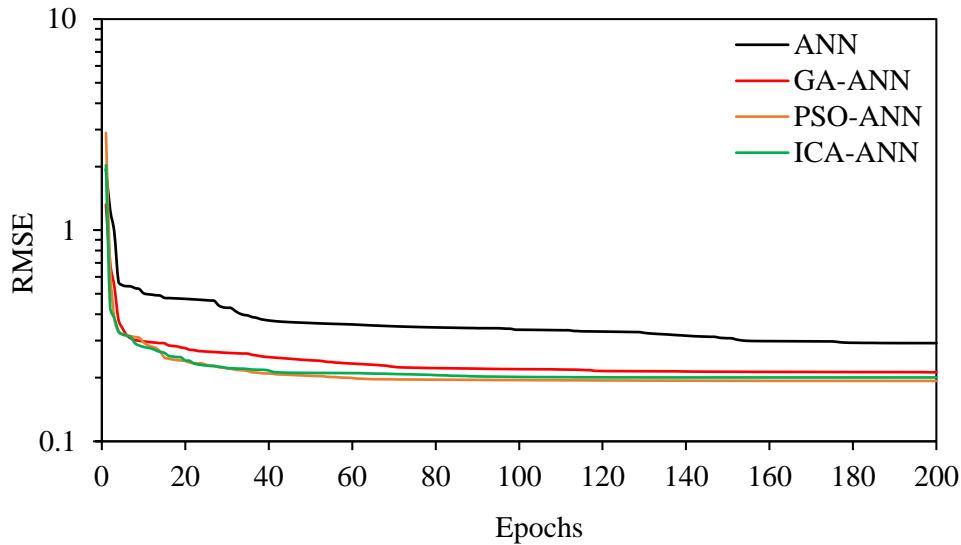


Fig. 5.14 Comparison of learning rates of ANN, GA-ANN, PSO-ANN and ICA-ANN algorithms at training stage

5.6 Conclusion

The accurate/objective prediction of the rock mass quality score (RQS) utilizing measure-while-drilling (MWD) data is one of the greatest challenges in tunneling operations. An advantage of artificial neural network (ANN) methods is that they can address complex multivariate nonlinear mapping problems. However, it is required to overcome the shortcomings of slow training speed and minimum layout through optimization ANN, so as to produce more reliable results in the prediction of RQS. Therefore, three optimization algorithms of the genetic algorithm (GA), particle swarm optimization (PSO) and imperialist competition algorithm (ICA), were employed to develop hybrid models of GA-ANN, PSO-ANN and ICA-ANN to predict the RQS value. For this purpose, 1270 datasets, including six measure-while-drilling parameters of penetration rate (PR), hammer pressure (HP), rotation pressure (RP), feed pressure (FP), hammer frequency (HF) and specific energy (SE), were acquired from the new Nagasaki tunnel (east) of the West Kyushu Line high-speed railway in Japan and considered as input parameters, while their corresponding RQS were considered as output parameters. To compare the performance of the hybrid models, MLR and ANN models were also developed to predict the RQS.

Three performance indexes R^2 , RMSE and VAF are used to compare the developed prediction model. The results show that the developed PSO-ANN and ICA-ANN models

have higher accuracy and efficiency than other models. However, among the two hybrid models, PSO-ANN hybrid model has slightly higher performance in predicting RQS. The results of $R^2 = 0.875$ and 0.862 , $RMSE=1.584$ and 1.782 and $VAF = 0.875$ and 0.861 for the training dataset and testing dataset, and the results of $R^2 = 0.873$ and 0.857 , $RMSE=1.592$ and 1.812 and $VAF = 0.873$ and 0.855 for the training dataset and testing dataset were obtained for the PSO-ANN model and ICA-ANN model, respectively. In addition, the comparative results show that the prediction performance is affected by geological conditions.

Note that the models established in this paper are specific to the West Kyushu Line of the high-speed railway region and the parameters of the final prediction model need to be modified according to their conditions for other regions and other tunnel construction methods.

References

- Ahmadi MA, Ebadi M, Shokrollahi A, Majidi SMJ (2013), Evolving artificial neural network and imperialist competitive algorithm for prediction oil flow rate of the reservoir. *Appl Soft Comput*, 13:1085-1098.
<https://doi.org/10.1016/j.asoc.2012.10.009>
- Akagi W, Sano A, Shinji M, Nishi T, Nakagawa K (2001), A new rock mass classification method at tunnel face for tunnel support system. *Doboku Gakkai Ronbunshu*, 2001:121-134
- Aoki K, Shirasagi S, Yamamoto T, Inou M, Nishioka K (1999), Examination of the application of drill Logging to predict ahead of the tunnel face. In: *Proceedings of the 54th Annual Conference of the Japan Society of Civil Engineers*, Tokyo, Japan, September 1999. pp 412-413
- Armaghani DJ, Hasanipanah M, Mahdiyar A, Abd Majid MZ, Bakhshandeh Amnieh H, Tahir MMD (2018), Airblast prediction through a hybrid genetic algorithm-ANN model. *Neural Computing and Applications*, 29:619-629.
<https://doi.org/10.1007/s00521-016-2598-8>
- Armaghani DJ, Koopialipour M, Marto A, Yagiz S (2019), Application of several optimization techniques for estimating TBM advance rate in granitic rocks. *J Rock Mech Geotech Eng*, 11:779-789. <https://doi.org/10.1016/j.jrmge.2019.01.002>

- Atashpaz-Gargari E, Lucas C Imperialist competitive algorithm: An algorithm for optimization inspired by imperialistic competition. In: 2007 IEEE Congress on Evolutionary Computation, 25-28 Sept. 2007 2007. pp 4661-4667.
<https://doi.org/10.1109/CEC.2007.4425083>
- Back AD, Chen T (2002), Universal Approximation of Multiple Nonlinear Operators by Neural Networks. *Neural Comput*, 14:2561-2566
- Barton N, Lien R, Lunde J (1974), Engineering classification of rock masses for the design of tunnel support. *Rock mechanics*, 6:189-236.
<https://doi.org/10.1007/bf01239496>
- Bieniawski Z (1973), Engineering classification of jointed rock masses. *Civil Engineer in South Africa*, 15
- Clerc M, Kennedy J (2002), The particle swarm-explosion, stability, and convergence in a multidimensional complex space. *IEEE Trans Evol Comput*, 6:58-73
- Deere DU (1964), Technical description of rock cores for engineering purpose. *Rock Mechanics and Engineering Geology*, 1:17-22
- Dybowski R, Gant V, Weller P, Chang R (1996), Prediction of outcome in critically ill patients using artificial neural network synthesised by genetic algorithm. *The Lancet*, 347:1146-1150. [https://doi.org/10.1016/S0140-6736\(96\)90609-1](https://doi.org/10.1016/S0140-6736(96)90609-1)
- Erharter GH, Marcher T, Reinhold C Artificial Neural Network Based Online Rockmass Behavior Classification of TBM Data. In: Cham, 2019. *Information Technology in Geo-Engineering*. Springer International Publishing, pp 178-188
- Gandomi AH, Yun GJ, Yang X-S, Talatahari S (2013), Chaos-enhanced accelerated particle swarm optimization. *Commun Nonlinear Sci Numer Simul*, 18:327-340.
<https://doi.org/10.1016/j.cnsns.2012.07.017>
- Gao D (1998), On structures of supervised linear basis function feedforward three-layered neural networks. *Chinese Journal of Computers*, 1
- Gazafroudi AS, Bigdeli N, Ramandi MY, Afshar K A hybrid model for wind power prediction composed of ANN and imperialist competitive algorithm (ICA). In: 2014 22nd Iranian Conference on Electrical Engineering (ICEE), 20-22 May 2014 2014. pp 562-567. [10.1109/IranianCEE.2014.6999606](https://doi.org/10.1109/IranianCEE.2014.6999606)
- Hasanipanah M, Jahed Armaghani D, Bakhshandeh Amnieh H, Majid MZA, Tahir MMD (2017), Application of PSO to develop a powerful equation for prediction of flyrock

- due to blasting. *Neural Computing Applications*, 28:1043-1050.
<https://doi.org/10.1007/s00521-016-2434-1>
- Hoballah A, Erlich I PSO-ANN approach for transient stability constrained economic power generation. In: 2009 IEEE Bucharest PowerTech, 28 June-2 July 2009 2009. pp 1-6. <https://doi.org/10.1109/PTC.2009.5281926>
- Hoek E, Brown ET (1997), Practical estimates of rock mass strength. *Int J Rock Mech Min Sci*, 34:1165-1186. [https://doi.org/10.1016/S1365-1609\(97\)80069-X](https://doi.org/10.1016/S1365-1609(97)80069-X)
- Holland JH (1992), *Adaptation in natural and artificial systems: an introductory analysis with applications to biology, control, and artificial intelligence*. MIT press.
- Hornik K (1991), Approximation capabilities of multilayer feedforward networks. *Neural Networks*, 4:251-257. [https://doi.org/10.1016/0893-6080\(91\)90009-T](https://doi.org/10.1016/0893-6080(91)90009-T)
- Hussain S, Mohammad N, Khan M, Rehman ZU, Tahir M (2016), Comparative analysis of rock mass rating prediction using different inductive modeling techniques. *International Journal of Mining Engineering Mineral Processing*, 5:9-15
- Kanellopoulos I, Wilkinson GG (1997), Strategies and best practice for neural network image classification. *Int J Remote Sens*, 18:711-725
- Karlaftis A (2018), Classifying rock masses using artificial neural networks. In: *Geocology and Computers*. Routledge, pp 279-284
- Kayabasi A (2012), Prediction of pressuremeter modulus and limit pressure of clayey soils by simple and non-linear multiple regression techniques: a case study from Mersin, Turkey. *Environmental earth sciences*, 66:2171-2183
- Kennedy J, Eberhart R Particle swarm optimization (PSO). In: *Proc. IEEE International Conference on Neural Networks*, Perth, Australia, 1995. pp 1942-1948
- Kennedy J, Eberhart RC A discrete binary version of the particle swarm algorithm. In: 1997 IEEE International Conference on Systems, Man, and Cybernetics. *Computational Cybernetics and Simulation*, 12-15 Oct. 1997 1997. pp 4104-4108 vol.4105. <https://doi.org/10.1109/ICSMC.1997.637339>
- Khandelwal M, Mahdiyar A, Armaghani DJ, Singh TN, Fahimifar A, Faradonbeh RS (2017), An expert system based on hybrid ICA-ANN technique to estimate macerals contents of Indian coals. *Environmental Earth Sciences*, 76:399.
<https://doi.org/10.1007/s12665-017-6726-2>

- Knofczynski GT, Mundfrom D (2008), Sample sizes when using multiple linear regression for prediction. *Educational psychological measurement*, 68:431-442
- Lear WE, Dareing DW (1990), Effect of Drillstring Vibrations on MWD Pressure Pulse Signals. *J Energy Res Technol*, 112:84
- Leung R, Scheduling S (2015), Automated coal seam detection using a modulated specific energy measure in a monitor-while-drilling context. *Int J Rock Mech Min Sci*, 75:196-209. <https://doi.org/10.1016/j.ijrmms.2014.10.012>
- Li SC, Wu J, Xu ZH, Li LP (2017), Unascertained measure model of water and mud inrush risk evaluation in karst tunnels and its engineering application. *KSCE J Civ Eng*, 21:1170-1182. 10.1007/s12205-016-1569-z
- Liu J, Luan H, Zhang Y, Sakaguchi O, Jiang Y (2020), Prediction of unconfined compressive strength ahead of tunnel face using Measurement-While-Drilling data based on hybrid genetic algorithm. *Geotech Eng*, 22. <https://doi.org/10.12989/gae.2020.22.1.000>
- Looney CG (1996), Advances in feedforward neural networks: demystifying knowledge acquiring black boxes. *IEEE Transactions on Knowledge Data Engineering*:211-226
- Lowson A, Bieniawski Z Critical assessment of RMR based tunnel design practices: a practical engineer's approach. In: *Proceedings of the SME, Rapid Excavation and Tunnelling Conference*, Washington, DC, USA, 2013. pp 23-26
- Lu J, Liu X (2009), Construction Techniques for Water and Sand Gushing Section in Xiushan Tunnel on Yuxi-Mengzi Railway. *Tunnel Construction*, 3
- Marto A, Hajihassani M, Jahed Armaghani D, Tonnizam Mohamad E, Makhtar AM (2014), A novel approach for blast-induced flyrock prediction based on imperialist competitive algorithm and artificial neural network. *The Scientific World Journal*, 2014
- Masahiro N, Koji M, Hiroshi Y, Takuro N, Kazuo N, Koji N (1999), A New Proposal of Evaluation System for Tunnel Face Based on the Analysis of the Observation Records. *Journal of Japan Society of Civil Engineers*, 623:131-141
- McCulloch WS, Pitts W (1943), A logical calculus of the ideas immanent in nervous activity. *The bulletin of mathematical biophysics*, 5:115-133. <https://doi.org/10.1007/bf02478259>
- Moayed H, Jahed Armaghani D (2018), Optimizing an ANN model with ICA for

- estimating bearing capacity of driven pile in cohesionless soil. *Eng Comput*, 34:347-356. <https://doi.org/10.1007/s00366-017-0545-7>
- Moayed H, Mehrabi M, Mosallanezhad M, Rashid ASA, Pradhan B (2019), Modification of landslide susceptibility mapping using optimized PSO-ANN technique. *Eng Comput*, 35:967-984. <https://doi.org/10.1007/s00366-018-0644-0>
- Mohamad ET, Hajihassani M, Armaghani DJ, Marto A (2012), Simulation of blasting-induced air overpressure by means of artificial neural networks. *Int Rev Modell Simulations*, 5:2501-2506
- Momeni E, Nazir R, Armaghani DJ, Maizir H (2015), Application of Artificial Neural Network for Predicting Shaft and Tip Resistances of Concrete Piles *Earth Sci Res J*, 19:85-93
- Momeni E, Nazir R, Jahed Armaghani D, Maizir H (2014), Prediction of pile bearing capacity using a hybrid genetic algorithm-based ANN. *Measurement*, 57:122-131. <https://doi.org/10.1016/j.measurement.2014.08.007>
- Monjezi M, Ghafurikalajahi M, Bahrami A (2011), Prediction of blast-induced ground vibration using artificial neural networks. *Tunn Undergr Space Technol*, 26:46-50. <https://doi.org/10.1016/j.tust.2010.05.002>
- Monjezi M, Hasanipanah M, Khandelwal M (2013), Evaluation and prediction of blast-induced ground vibration at Shur River Dam, Iran, by artificial neural network. *Neural Computing Applications and Applied Mathematics*, 22:1637-1643
- Nasseri M, Asghari K, Abedini MJ (2008), Optimized scenario for rainfall forecasting using genetic algorithm coupled with artificial neural network. *Expert Syst Appl*, 35:1415-1421. <https://doi.org/10.1016/j.eswa.2007.08.033>
- Navarro J, Sanchidrián J, Segarra P, Castedo R, Costamagna E, López L (2018), Detection of potential overbreak zones in tunnel blasting from MWD data. *Tunn Undergr Space Technol*, 82:504-516. [10.1016/j.tust.2018.08.060](https://doi.org/10.1016/j.tust.2018.08.060)
- Nelson MM, Illingworth WT (1991), *A practical guide to neural nets*.
- Nilsen B (2015), Main challenges for deep subsea tunnels based on norwegian experience. *Journal of Korean Tunnelling and Underground Space Association*, 17:563-573. [10.9711/KTAJ.2015.17.5.563](https://doi.org/10.9711/KTAJ.2015.17.5.563)
- Nouiri M, Bekrar A, Jemai A, Niar S, Ammari AC (2018), An effective and distributed particle swarm optimization algorithm for flexible job-shop scheduling problem.

- Journal of Intelligent Manufacturing, 29:603-615. <https://doi.org/10.1007/s10845-015-1039-3>
- Palmstrom A (2005), Measurements of and correlations between block size and rock quality designation (RQD). *Tunn Undergr Space Technol*, 20:362-377. <https://doi.org/10.1016/j.tust.2005.01.005>
- Rahmati A, Faramarzi L, Sanei M (2014), Development of a new method for RMR and Q classification method to optimize support system in tunneling. *Frontiers of Structural Civil Engineering*, 8:448-455. <https://doi.org/10.1007/s11709-014-0262-x>
- Rehman H, Naji AM, Kim J-j, Yoo H-K (2018), Empirical Evaluation of Rock Mass Rating and Tunneling Quality Index System for Tunnel Support Design. *Applied Sciences*, 8:782
- Rosenblatt F (1958), The perceptron: a probabilistic model for information storage and organization in the brain. *Psychological review*, 65:386
- Shi Y, Eberhart RC Parameter selection in particle swarm optimization. In, Berlin, Heidelberg, 1998. *Evolutionary Programming VII*. Springer Berlin Heidelberg, pp 591-600
- Shin HS, Han KC, Sunwoo C, Choi SO, Choi YK (1999), Collapse of a Tunnel In Weak Rock And the Optimal Design of the Support System. Paper presented at the 9th ISRM Congress, Paris, France, 1999
- Sousa LR, Miranda T, Roggenthen W, Sousa RL (2012), Models For Geomechanical Characterization of the Rock Mass Formations At DUSEL Using Data Mining Techniques. Paper presented at the 46th U.S. Rock Mechanics/Geomechanics Symposium, Chicago, Illinois, 2012
- Swingler K (1996), *Applying neural networks: a practical guide*. Morgan Kaufmann,
- Vasumathi B, Moorthi S (2012), Implementation of hybrid ANN–PSO algorithm on FPGA for harmonic estimation. *Eng Appl Artif Intell*, 25:476-483. <https://doi.org/10.1016/j.engappai.2011.12.005>
- Xu J, Wang J, Ma Y (2007), Rock mass quality assessment based on BP artificial neural network (ANN) A case study of borehole BS03 in Jiujiang segment of Beishan, Gansu. *Uranium Geology*, 23:243,249-256
- Yang X-S (2010), *Engineering optimization: an introduction with metaheuristic applications*. John Wiley & Sons,

- Yilmaz I (2009), A new testing method for indirect determination of the unconfined compressive strength of rocks. *International Journal of Rock Mechanics Mining Sciences*, 46:1349-1357
- Yue ZQ, Lee CF, Law KT, Tham LG (2004), Automatic monitoring of rotary-percussive drilling for ground characterization—illustrated by a case example in Hong Kong. *Int J Rock Mech Min Sci*, 41:573-612. <https://doi.org/10.1016/j.ijrmms.2003.12.151>
- Yuji W, Tatsuo K, Masaki K, Kenichi H (2006), Solution with modified perceptron to tunnel cutting face evaluation problems. *Geoinformatics*, 17:61-70
- Zhou H, Hatherly P, Ramos F, Nettleton E An adaptive data driven model for characterizing rock properties from drilling data. In: 2011 IEEE International Conference on Robotics and Automation, Shanghai, China, May 2011. IEEE, pp 1909-1915
- Zolfaghari A, Sohrabi Bidar A, Maleki Javan MR, Haftani M, Mehinrad A (2015), Evaluation of rock mass improvement due to cement grouting by Q-system at Bakhtiary dam site. *Int J Rock Mech Min Sci*, 74:38-44. <https://doi.org/10.1016/j.ijrmms.2014.12.004>
- Zorlu K, Gokceoglu C, Ocakoglu F, Nefeslioglu HA, Acikalin S (2008), Prediction of uniaxial compressive strength of sandstones using petrography-based models. *Eng Geol*, 96:141-158. <https://doi.org/10.1016/j.enggeo.2007.10.009>

6 Prediction models of unconfined compressive strength ahead of tunnel face using machine learning technology

6.1 Introduction

The measurement of the unconfined compressive strength (UCS) of the rock is one of the important influencing factors in assessment of the geological conditions ahead of a tunnel face (Bieniawski 1974; Yilmaz 2009c; Nazir et al. 2013). The UCS standard test of the rock is directly determined in the laboratory by the measurement of compression characteristics of rock specimen under the axial load. This test is standardized by the American Society for Testing and Materials (ASTM 2006) and the International Society for Rock Mechanics (ISRM and Hudson 2007). Nevertheless, some shortcomings exist in this kind of direct laboratory test. It is not easy to obtain a sufficiently perfect core sample if the rock of interest is weak, thinly bedded, or densely fractured. In addition, the direct laboratory test is time-consuming and costly (Zorlu et al. 2008; Dehghan et al. 2010; Mohamad et al. 2015; Wang et al. 2020). Some researchers report that due to standard UCS test methods require costly equipment, it is economical and convenient to use the indirect test methods to measure UCS (Yagiz et al. 2012; Othman et al. 2018; Mokhtari and Behnia 2019).

In indirect test methods, in order to avoid the difficulties in preparing and testing core samples by direct method, many researchers have developed some prediction methods, such as schmidt hammer rebound number, point load index, p-wave velocity and physical properties to related with the UCS using regression techniques or artificial intelligence techniques (Shakoor and Bonelli 1991; Kahraman 2001; Yılmaz and Sendir 2002; Tsiambaos and Sabatakakis 2004; Toghrolı et al. 2018; Yagiz 2019). Compared with the UCS direct test, these index tests need relatively few samples, which have the advantages of quick and easy fast operation, portability and low costs. Nevertheless, Zhang (2016) pointed out that when considering different rock types, different strength values can be calculated by different empirical formulas. Moreover, Meulenkamp and Grima (1999) described that statistical regression methods have the disadvantage of predicting only the

average value; Therefore, over prediction of low UCS value and under prediction of high UCS value may occur. At the same time, many scholars also proposed that the regression analysis technology has limitations on the prediction accuracy of solving complex nonlinear tasks (Baykasoğlu et al. 2004). In addition, according to the research of Meulenkamp and Grima (1999), in contrast to the statistical regression analysis, the UCS value predicted by artificial neural network (ANN) is not force to be the average value, so the existing variance of measurement data can be retained and employed. For the assessment of the rock mass quality ahead of a tunnel face, although these existing direct and indirect test techniques can be applied to measure the UCS of the exposed rock, it is very difficult to predict the UCS values of the unexposed rocks ahead of the tunnel face.

Recently, with the rapid development of measurement-while-drilling (MWD) technology, the evaluation technology of rock mass quality ahead of a tunnel face has been improved (Schunnesson 1996; Sugawara et al. 2003; Høien and Nilsen 2014; Galende-Hernández et al. 2018); Therefore, as long as the original data is properly processed and effectively analyzed, the MWD technology can be regarded as a robust method for detailed characterization of large rock mass. Many scholars have done a lot of research in this field. By analyzing the change of drilling parameters, Scoble et al. (1989) determined different geological structures. The original MWD system was developed by Aoki et al. (1999); The geological conditions of different ground depths were evaluated by analyzing the data obtained by drilling in rock with a hydraulic drill. Peck (1989) verified that MWD parameters can be used to estimate the compressive and shear strength of rocks. Teale (1965) introduced specific energy as a composite MWD parameter, and connected the bit performance parameters in rotary drilling with the concept of energy required to excavate rock per unit volume. Hatherly et al. (2015) described that the wear of the bit affects the recognition accuracy of rock mass characteristics. Schunnesson et al. (2012) proposed a method to estimate the range of rock strength values based on the MWD hardness parameter index recorded by Atlas Copco software. Celada et al. (2009) investigated the correlation between specific energy and rock mechanical parameters through laboratory tests, and demonstrated that the specific energy value has a certain correlation with rock mass rating index. Kahraman et al. (2016) evaluated the feasibility of estimating UCS, Brazilian tensile strength, point load strength and Schmidt hammer test value by penetration rate parameter. However, limited by the difficulty of efficient analysis and processing of the MWD data, the technology of predicting UCS ahead of a tunnel face using the MWD data has not been effectively

applied in the field.

In recent decades, the ANN has been applied to solve geotechnical engineering problems as a powerful tool (Alimoradi et al. 2008; Yilmaz 2009a; Ocak and Seker 2012; Kwon and Lee 2018; Xue 2019). However, the disadvantages of slow learning speed and easy to fall into local minima exist in the realization of ANN (Jadav and Panchal 2012; Momeni et al. 2014). In order to solve these problems, optimization algorithms such as genetic algorithm (GA) can be used to enhance the performance of ANN (Bhatti et al. 2011; Karimi and Yousefi 2012; Khandelwal et al. 2018). In addition, ANN is a black-box model, which can not estimate the importance of each input feature to the prediction results of the model, and the interaction between different features can not be understood; while the classification and regression tree (CART) is a white box model, it usually has better interpretability and its internal working principle is easier to explain. (Tayyebi and Pijanowski 2014; Hasanipanah et al. 2017; Hamze-Ziabari and Bakhshpoori 2018; Samadi et al. 2020).

The purpose of this paper is to propose a machine learning method: artificial neural network (ANN) and classification and regression tree (CART), to predict of UCS utilizing the Measurement-While-Drilling (MWD) data acquired from the new Nagasaki tunnel (east) of the West Kyushu line of the high-speed railway project in Japan. Subsequently, as a contrast, the traditional multiple linear regression (MLR) and multiple nonlinear regression (MNR) model will be developed to evaluate the prediction performance of machine learning models. Finally, the best prediction model is selected by comparing the results of these models. The results can contribute to the accurate, effective and objective assessment of rock mass quality ahead of a tunnel face.

6.2 Data collection and regression analysis

6.2.1 *Project description*

As a mountainous country, if the construction of roads and railways in Japan adopts the construction around mountains, the project cost will be huge. Therefore, it is inevitable to need a lot of tunnel excavation in highway and railway construction. The complicated and dangerous geological conditions such as water gushing, mud bursting and cavity are very common in mountain tunnels, which is more common in southern Japan. The new Nagasaki tunnel is part of Japan's West Kyushu line with a total length of

7.46 km. The New Nagasaki tunnel is divided into two parts, namely, the new Nagasaki tunnel (east) and the new Nagasaki tunnel (west). As the research object of this study, the new Nagasaki tunnel (east) was started in March 2013 and completed in 2017. The length of the two tunnels is 3.885 km and 3.575 km respectively. The New Austrian Tunneling Method is the main method of tunnel excavation. The shape of the tunnel is a horseshoe with a height of 9.3 m and a width of 10.4 m. The main rock type that the tunnel passes through is pyroxene andesite with poor surrounding rock geological conditions and elastic wave velocity range of 2.5 - 3.5 km/sec.

6.2.2 Data collection

In the field measurement, important parameters including the MWD data and the UCS values were recorded. Situ tests, i.e., advanced drilling data (the MWD data) and Schmidt hammer rebound number were recorded at the same time in the same tunnel section. It should be noted that due to the reason that some field measurements are difficult to carry out, the MWD data used in this paper have not been obtained from all tunnel sections.

The MWD data of this study comes from the hydraulic rotary percussion drill, which carries out drilling operation ahead of the tunnel face. In order to eliminate the influence of the error, the drilling data of a certain location is processed averagely within one meter. The parameters of MWD data including the penetration rate (PR), hammer pressure (HP), rotation pressure (RP), feed pressure (FP), hammer frequency (HF) and specific energy (SE). Among these MWD parameters, the specific energy is a composite parameter, which refers to the energy consumed to destroy the rock per unit volume.

Considering the time-consuming and high cost of the standard uniaxial compression test, Schmidt hammer test is generally employed to measure the UCS of rock as an indirect method. This indirect method has the advantages of simple operation, no sample preparation and convenient field application (Goudie 2006; Demirdag et al. 2009; Hoseinie et al. 2012). The operation procedure of Schmidt hammer test is as follows:

- Press on the surface of the rock material with a Schmidt hammer. After the switch is turned, the piston in Schmidt hammer hits the plunger.
- The hammer test should be carried out at five different representative points perpendicular to the core samples, and the spacing between these representative points should be at least twice the diameter of the plunger.

In the construction of the new Nagasaki tunnel (east), detailed observation report of the

exposed tunnel face is used to comprehensively evaluate the surrounding rock of the tunnel. The UCS is one of the important terms in the observation report, which is calculated indirectly by schmidt hammer rebound number based on conversion Table 6.1.

Table 6.1 Conversion of schmidt hammer rebound number and unconfined compressive strength

Schmidt hammer rebound number (X)	UCS (MPa) (Y)	Schmidt hammer rebound number (X)	UCS (MPa) (Y)
10	51	36	321
11	55	37	345
12	59	38	370
13	63	39	397
14	68	40	426
15	73	41	457
16	78	42	491
17	84	43	527
18	90	44	565
19	97	45	607
20	104	46	651
21	111	47	700
22	119	48	750
23	128	49	805
24	138	50	864
25	148	51	927
26	158	52	995
27	170	53	1068
28	182	54	1146
29	196	55	1230
30	210	56	1321
31	226	57	1417
32	242	58	1521
33	260	59	1633
34	279	60	1752
35	299		

Note: When the schmidt hammer rebound number is greater than 60, the UCS value is calculated according to the following equation. $\log Y = 0.307X + 1.4016$.

In this study, MWD data, and UCS were collected in situ in the new Nagasaki tunnel (east phase). A total of 1350 datasets from 1350 sections of the tunnel were recorded and collected. To predict the UCS value, the MWD data (PR, HP, RP, FP, HF and SE) are regarded as input parameters of the ANN, and the UCS values are regarded as output parameters. Table 1 summarizes the descriptive statistical distribution of all parameters in the database. Their visual statistic distribution is provided in Fig. 6.1. According to the

analysis in Table 6.2 and Fig. 6.1, the values of these parameters are widely distributed. It should be noted that a small number of singular values exist in the MWD data. In order to investigate the robustness of ANN, the original data are not filtered in this paper.

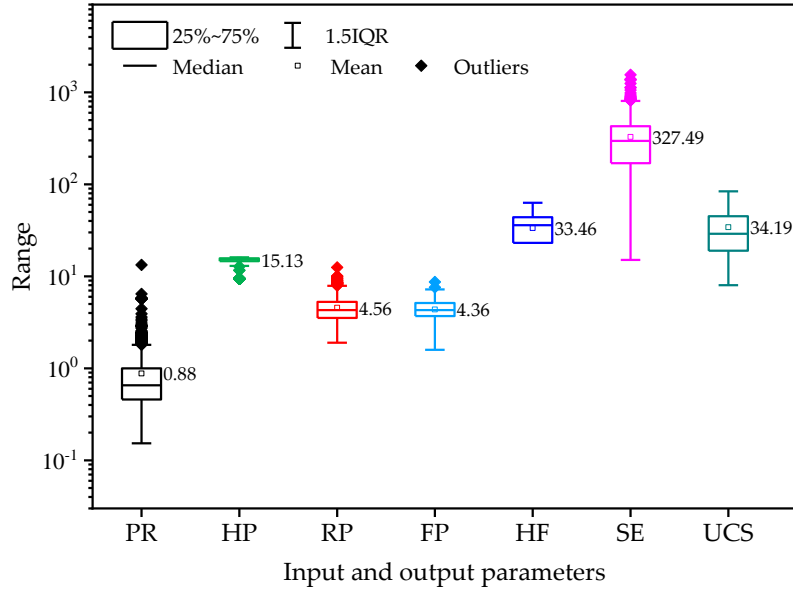


Fig. 6.1 Distribution of the parameters of the input data and output data

Table 6.2 Basic statistics of dataset parameters

Item	Symbol	Unit	Mean	Min	Max	Std. Dev
Input	PR	m/min	0.88	0.15	13.30	0.80
	HP	MPa	15.13	9.40	16.10	0.97
	RP	MPa	4.56	1.90	12.50	1.35
	FP	MPa	4.36	1.59	8.70	1.05
	HF	1/s	33.46	0.00	63.00	13.96
	SE	J/cm ³	327.49	15.10	1549.80	191.40
Output	UCS	MPa	34.19	8.00	84.00	19.16

6.2.3 Regression analysis

In addition, the correlation between each MWD parameter and their corresponding UCS was investigated. Fig. 6.2 summarizes the input datasets used and shows the relationship matrix between all data.

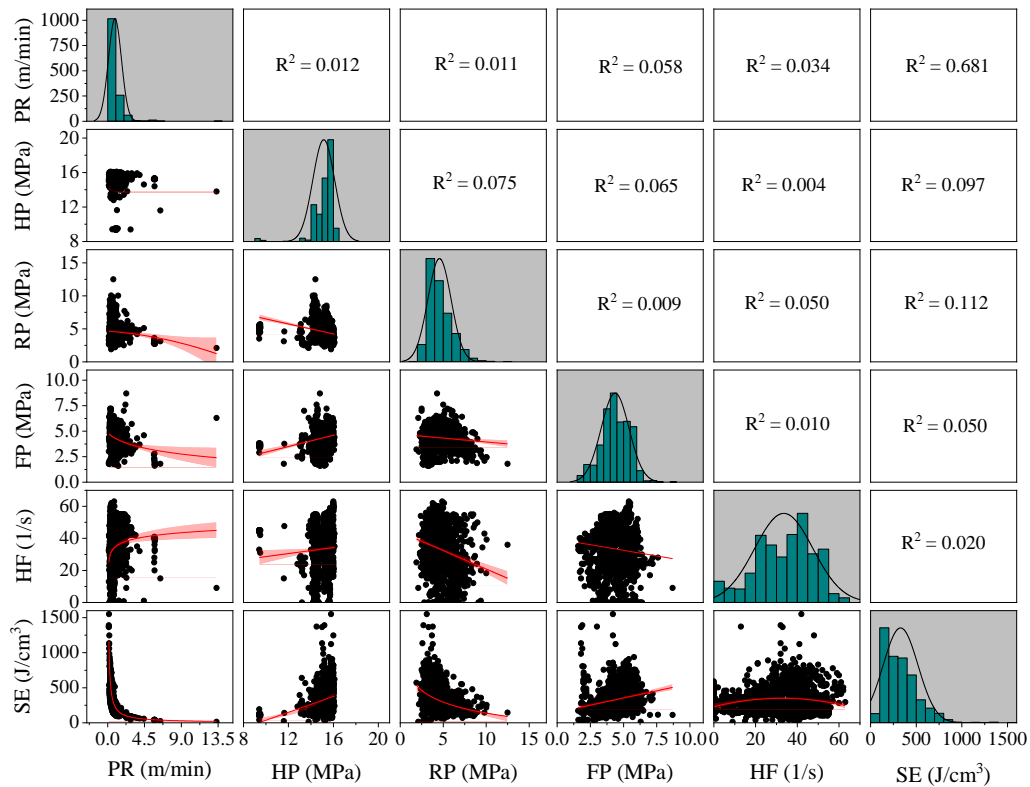


Fig. 6.2 General information related to the input parameter

The correlations between input parameters (PR, HP, RP, FP, HF and SE) and output parameters (UCS) were determined by simple regression models. For the linear fitting problem, the correlation coefficient (R^2), root mean square error (RMSE) and variance account for (VAF) are often used as evaluation indexes to evaluate the performance of the developed models, as employed by Grima and Babuška (1999), Yilmaz (2009b), Kayabasi (2012). The equations were evaluated with taking into consideration an evaluation index of R^2 . The most suitable equation types for predicting UCS were evaluated and selected by power, exponential and linear equations based on the values of R^2 . The equations used for the prediction of UCS are listed in Fig. 6.3. As shown in Fig. 6.3, the results of R^2 was calculated as 0.082, 0.198, 0.173, 0.117, 0.003, and 0.276, for PR, HP, RP, FP, HF and SE, respectively. The correlation between UCS and SE is better than the correlation among the other parameters; however, a low coefficient of determination ($R^2 = 0.276$) is obtained. These results show a low correlation between a single MWD parameter and the UCS. Therefore, using all or part of the MWD parameters to develop prediction model requires further study. In the following sections, attempt for applying an advanced hybrid ANN technology to predict the UCS based on multiple MWD parameters will be carried out.

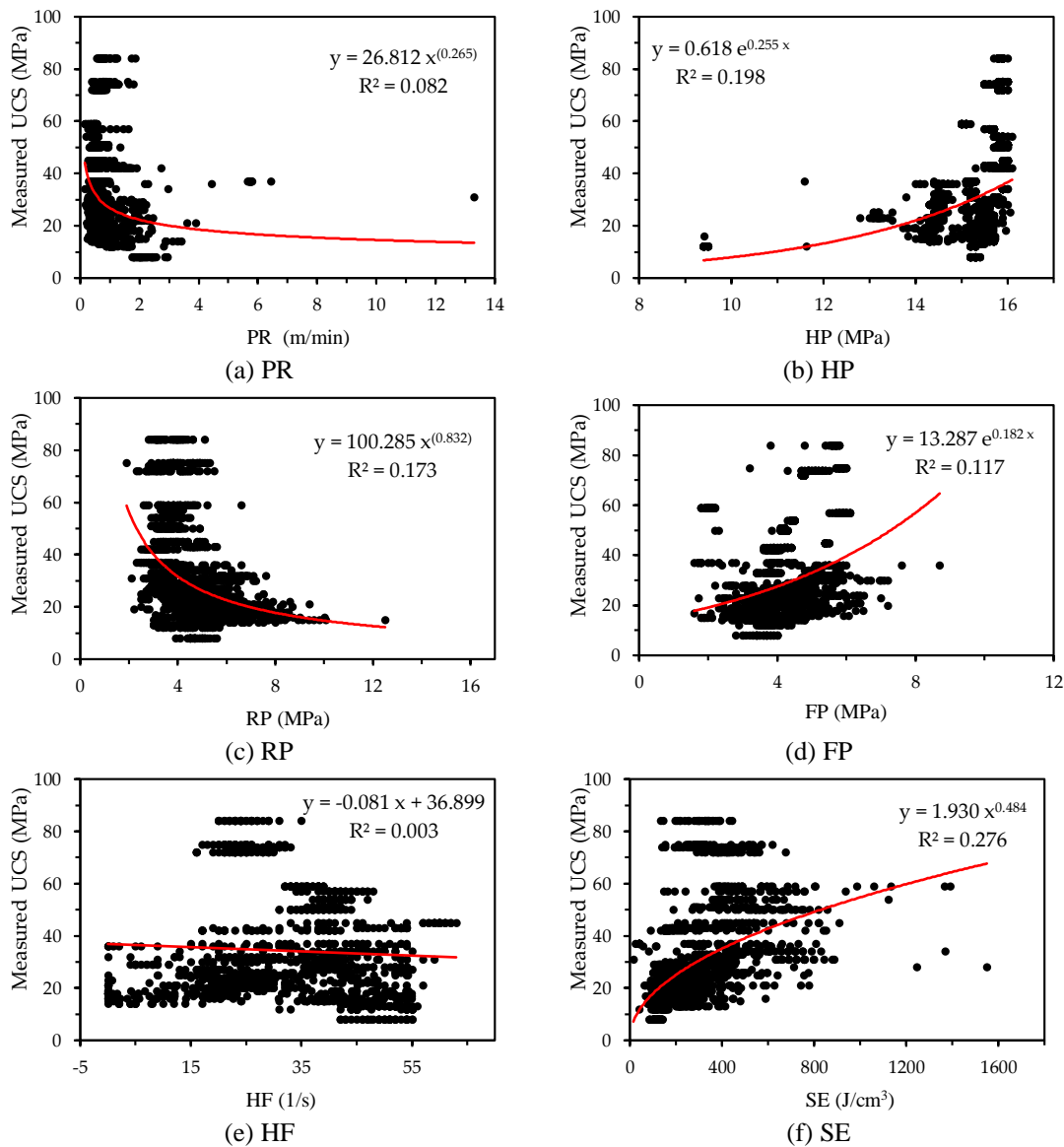


Fig. 6.3 The best simple regression model of each input parameter

The correlations between input parameters (PR, HP, RP, FP, HF and SE) and output parameters (UCS) were determined by simple regression models. The most suitable equation types for predicting UCS were evaluated and selected by power, exponential and linear equations. The equations were evaluated with taking into consideration an evaluation index of the correlation coefficient (R^2). The equations used for the prediction of UCS are listed in Fig. 6.3. As shown in Fig. 6.3, the results of R^2 was calculated as 0.082, 0.198, 0.173, 0.117, 0.003, and 0.276, for PR, HP, RP, FP, HF and SE, respectively. The correlation between UCS and SE is better than the correlation among the other parameters; however, a low coefficient of determination ($R^2 = 0.276$) is obtained. These

results show a low correlation between a single MWD parameter and the UCS. Therefore, using all or part of the MWD parameters to develop prediction model requires further study. In the following sections, attempt for applying an advanced hybrid ANN technology to predict the UCS based on multiple MWD parameters will be carried out.

Before developing the prediction models, to minimize the influence of order of magnitude on the prediction results, the database was normalized to the range of 0-1 by Eq.4-1:

The datasets were divided into training set and testing set to develop and evaluate the established networks. Swingler (1996), Looney (1996) and Nelson and Illingworth (1991) suggested that 80%, 75% and 70-80% , respectively, of the whole datasets should be used as training set. Therefore, in this research, 1350 data sets were divided into training set and testing set by 80% and 20% ratio, respectively. A total of 1080 training sets and 270 testing sets were conducted to develop the UCS prediction models.

6.3 Establish prediction models

6.3.1 Multiple regression

MLR is based on the development of simple linear regression technology, attempting to find an equation through measured data to describe the relationship between two or more interpretive variables (characteristics) and dependent variables (output). MLR is widely used in various branches of science and technology (Preacher et al. 2006; Nathans et al. 2012; Khademi et al. 2017). The mathematical form of MLR is as follows:

$$y = b_1x_1 + b_2x_2 + \dots + b_nx_n + c \quad (6-1)$$

Where, x_i , y , c and b_i are the i^{th} independent variable, i^{th} dependent variable, a constant (intercept) and the vector of regression coefficients (slope).

The form of multiple nonlinear regression (MNR) equation is generally determined by the relationship between each independent variable and dependent variable.

In this research, training datasets were applied to calculate the MLR and MNR models to correlate the UCS to the input parameters of PR, HP, RP, FP, HF and SE of the training datasets. Eq.6-2 shows the results obtained from the linear regression analysis. Eq.6-3 shows the MNR model.

$$\begin{aligned} \text{UCS} = & -36.498 - 0.381\text{PR} + 5.052\text{HP} - 4.022\text{RP} \\ & + 2.776\text{FP} - 0.181\text{HF} + 0.021\text{SE} \end{aligned} \quad (6-2)$$

$$UCS = e^{-2.879-0.025PR+0.443HP-0.141RP+0.095FP-0.007HF+0.0002SE} \quad (6-3)$$

The evaluation of the developed MLR and MNR models with testing datasets will be discussed in Sect. 6.4.

6.3.2 Artificial neural network models

As an information processing program, ANN was first proposed by McCulloch and Pitts (McCulloch and Pitts 1943). Three layers, input layer, hidden layer and output layer, constitute a typical ANN. Groups of processor elements (or nodes) exist in each layer, which relates to each other between layers. The input signal of the previous layer is weighted to get the output signal as the next layer input. The activation function exists in each node of the hidden layer and the output layer. These activation functions are used to calculate the output of each node. The number of nodes in the input and output layer is determined by the dimension of their respective variables. However, it is difficult to determine the number of the hidden layer nodes. Generally, according to the problem to be solved, the optimal number of hidden layer nodes is determined by trial and error procedure. There are several training algorithms for ANN. The error back-propagation algorithm is the well-known and often used training algorithm. In this algorithm, the continuous adjustment of the connection weight between nodes is to reduce the error between the measured and the predicted output through the neural network iteration, and the error will spread to the input layer. If the error level between the output and the expected value is high, the adjustment of weight and deviation will continue. Therefore, the back-propagation algorithm was selected as a training algorithm in this research. Fig. 6.4 shows the ANN model of predicted UCS with six input and one output variables in this study.

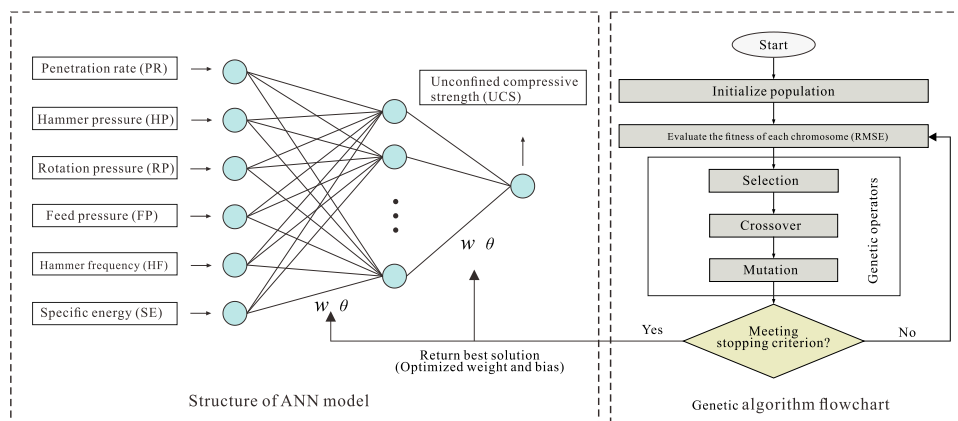


Fig. 6.4 Framework of the ANN model and the flowchart of GA

The construction of ANN model was carried out in this section. As previously mentioned, the multi-layer perceptron was applied for predicting the UCS. The parameters of PR, HP, RP, FP, HF and SE were designated as the inputs, and the parameter of UCS was designated as the outputs.

6.3.2.1 ANN parameters

The most effective parameters of ANN are training function, learning rate (η), momentum term (α), number of hidden layers and number of hidden layer nodes. The establishment of the ANN prediction model is to determine these main parameters. In order to predict the UCS accurately, these parameters were studied in detail to determine the optimal ANN parameters. According to the suggestion of Hasanipanah et al. (2016), Levenberg Marquardt algorithm is used to train neural network prediction model. As many researchers (Hecht-Nielsen 1987; Hornik et al. 1989; Garson 1998) introduced, the ANN with one hidden layer has enough performance to solve overwhelming majority engineering prediction tasks. Therefore, in this study, all the prediction models are designed with a hidden layer. To develop the ANN model, the difficulty is encountered in determining the learning rate, the momentum term and the number of hidden layer nodes.

6.3.2.2 Training function

The training function is generally divided into two types: one is a heuristic algorithm using the steepest descent method, such as resilient back-propagation (trainrp) and variable learning rate algorithms (traingdx); the other is a standard numerical algorithm, such as Scaled Conjugate Gradient (trainscg) and Levenberg–Marquardt (trainlm). To select the optimal training function, several models were developed using these four training functions. The ANN architecture of 6–15–1, the η of 0.01 and α of 0.5 were utilized, and the performance indices of RMSE were employed to assess the developed models. The results of various ANN experiments with 1-30 nodes trained by traingdx, trainrp, trainscg and trainlm are shown in Fig. 6.5. Fig. 6.5 illustrates that in all functions, traingdx had the weakest performance. Among them, the trainlm fluctuation reduces the errors during nodes and shows the best performance in both training and testing stage. Thus, the trainlm was chosen as the optimum the best training function.

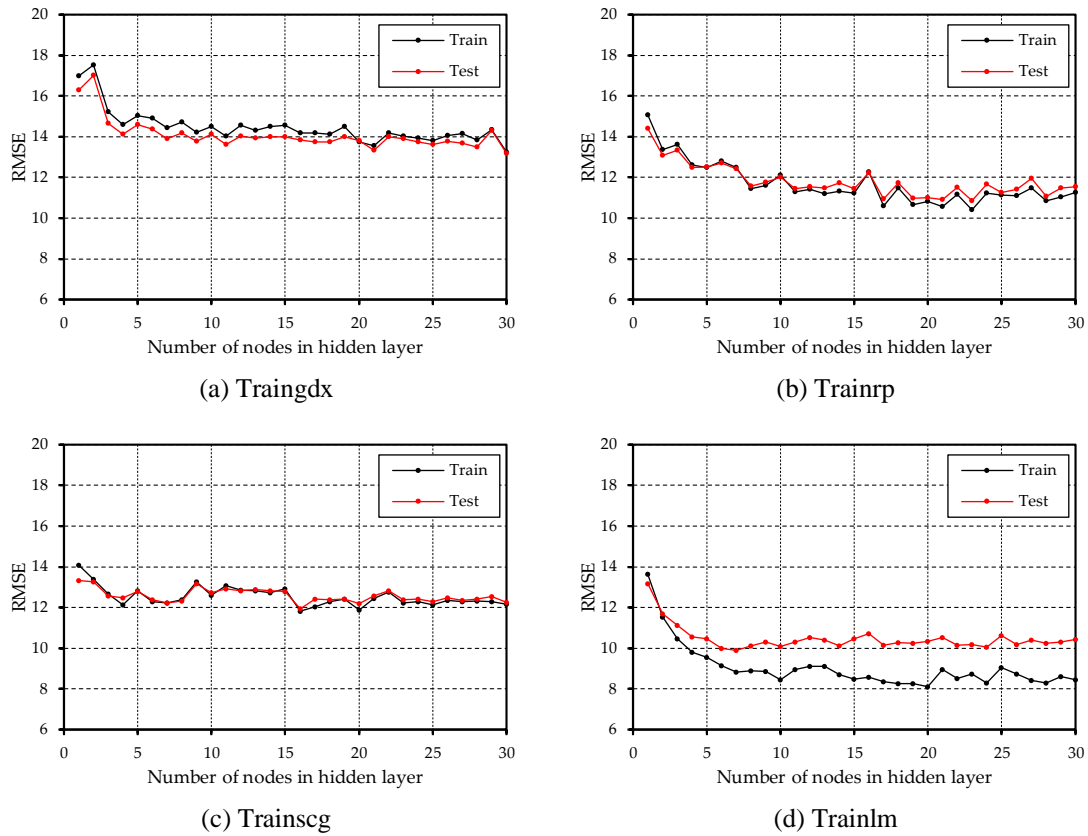


Fig. 6.5 The various trials with 1-30 nodes with four training functions

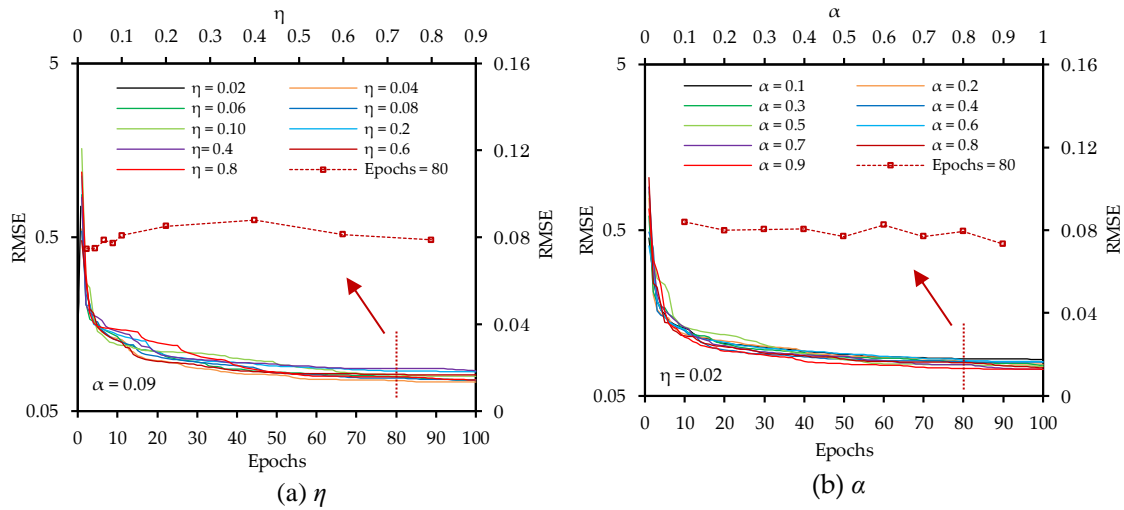


Fig. 6.6 Effects of learning rate and momentum parameters on ANN

6.3.2.3 Parameters of η and α

To choose the best values of η and α , several ANN models were constructed with η values of 0.02, 0.04, 0.06, 0.08, 0.1, 0.2, 0.4, 0.6 and 0.8, respectively, and α values of 0.1, 0.2, 0.3, 0.4, 0.5, 0.6, 0.7, 0.8 and 0.9, respectively. The ANN architecture of 6-15-1

and `trainlm` training function were applied. RMSE values were applied to evaluate the capacity of these models. Based on the evaluation, the optimal η and α values were chosen as 0.02 and 0.9, respectively, as shown in Fig. 6.6. Therefore, these values were chosen as the optimal value of η and α .

6.3.2.4 The number of hidden layer nodes

The number of hidden layer nodes has a great influence on the prediction performance of ANN (Kanellopoulos and Wilkinson 1997; Gao 1998; Monjezi et al. 2011). To evaluate this influence, different experiments of artificial neural network model with hidden layer nodes in 1-60, input layer nodes and output layer nodes in 1 and 6 respectively were set up, as shown in Appendix (A).

6.3.2.5 The number of hidden layer nodes

The number of hidden layer nodes has a great influence on the prediction performance of ANN (Kanellopoulos and Wilkinson 1997; Gao 1998; Monjezi et al. 2011). To evaluate this influence, different experiments of artificial neural network model with hidden layer nodes in 1-60, input layer nodes and output layer nodes in 1 and 6 respectively were set up, as shown in Appendix (A). The prediction performance of the developed models was assessed by performance index RMSE and R^2 . Superior models have lower value of RMSE and higher values of R^2 . However, it is difficult to choose the optimal prediction model. For this reason, Zorlu et al. (2008) recommended a easier method based on sorting method to realize this choice. On the basis of this method, each performance index was sorted, and the sorting value indicates the strength of performance. For example, RMSE values of 13.72, 11.87, 10.42, 9.86, 9.22, 9.75, 9.48, 9.22, 9.06, 8.42, 9.02, 7.98, 8.84, 8.87, 9.09, 8.30, 9.78, 7.95, 8.66, 8.64, 8.15, 8.50, 8.68, 7.81, 8.18 and 8.39 were obtained from training sets of models 1-26 shown in Appendix (A), respectively. Therefore, the sorting result value were 1, 2, 3, 4, 9, 6, 7, 8, 11, 19, 12, 24, 14, 13, 10, 21, 5, 25, 16, 17, 23, 18, 15, 26, 22 and 20, respectively. The result value of R^2 was also carried out in this way. After that, the training stage and testing stage were sorted respectively, and the total rank was the sum of the sorting values of the two stages, as shown in Appendix (A). As the results shown in Appendix (A), the No.12 model was selected as the model with the best performance in all the developed models. The average RMSE was 7.98 and 10.11, respectively, and R^2 was 0.827 and 0.721, respectively. Therefore, the ANN structure of 6–12–1 was finally determined as the optimum model for UCS value prediction. The

optimal prediction model of ANN (run 5 times) will be further discussed in Sect. 6.3.3. In Sects. 6.3.3, note that GA-ANN hybrid model of the neural network structure was developed based on 6–12–1, and indices of RMSE and R^2 were also used to evaluate the developed prediction models.

6.3.3 Optimized ANN models by genetic algorithm

GA was developed by professor Holland of the university of Michigan (Holland 1992). As an algorithm in the computer science field, GA is a heuristic search algorithm for solving optimization problems. This algorithm is often used in optimization and search solutions. Heredity, mutation, natural selection and hybridization are used in GA. It has the advantages of simple principle and operation, strong generality, unlimited constraints, implicit parallelism and global solution searching ability, and is widely employed in combinatorial optimization problems. However, the biggest disadvantage is that when the selection of activation function is not appropriate, the GA may only converge to the local optimal, but not the global optimal (Mohamad et al. 2017). The GA program is divided into three stages: chromosome fitness evaluation, parental chromosome selection, and the application of genetic operators on parental chromosomes. The new chromosome produced becomes the next generation population, and the process is iterated until the stop condition is reached. GA has a large number of application cases in civil engineering, traffic engineering and other engineering fields due to its excellent performance. The detailed description of genetic algorithm and its application can be acquired from the studies (Whitley 1994; Kosakovsky Pond et al. 2006; Kumar et al. 2010; Qiu et al. 2015; Jahed Armaghani et al. 2018).

To solve the problems of slow convergence and local optimization, many researchers employed GA to optimize the weights and biases of ANN, and successfully complete many engineering tasks (Balasubramanian et al. 2008; Yazdanmehr et al. 2009; Benyelloul and Aourag 2013; Khandelwal and Armaghani 2016). The hybrid GA-ANN algorithm flowchart is shown in Fig. 6.4. The steps of structuring the hybrid GA-ANN predictive model for UCS is detailed in the following section.

6.3.3.1 GA parameters

To developing GA models, population size (S_{pop}), methods of selection, number of generations (N_{gen}), mutation probability and crossover probability are the critical parameters set by the user. In this study, after the trial and error procedure, the mutation

probability was determined as 25 % and the crossover probability was used with 70%. For the selection of crossover operation methods, the roulette method is often used to create two offspring from parents (Yu et al. 2010). Hence, in this study, the roulette wheel method was utilized for crossover operations.

6.3.3.2 Value of the S_{pop}

As shown in Table 6.3, many GA-ANN models were developed to select the optimal population size. The population size (S_{pop}) was set as 25-600, the ANN structure was set at 6–12–1, and the maximum generation was set as 100. As in the previous section, performance indexes R^2 and RMSE are applied to evaluate the developed models and the optimal model was selected using a simple ranking process. As shown in the total rank results in Table 6.3, model No. 12 has the highest prediction performance compared with other models. Hence, the value of 500 was determined as the optimal S_{pop} .

Table 6.3 Effect of the population size on the hybrid GA-ANN in predicting UCS

No.	Population size	GA-ANN results				Rank value				Total rank
		Training		Testing		Training		Testing		
		R^2	RMSE	R^2	RMSE	R^2	RMSE	R^2	RMSE	
1	25	0.797	8.636	0.711	10.226	1	1	4	4	10
2	50	0.807	8.434	0.700	10.452	2	2	2	3	9
3	75	0.833	7.821	0.742	9.736	8	8	7	7	30
4	100	0.844	7.596	0.733	9.947	10	10	5	5	30
5	150	0.830	7.924	0.753	9.487	7	6	12	12	37
6	200	0.817	8.195	0.748	9.535	4	4	9	11	28
7	250	0.836	7.770	0.698	10.718	9	9	1	1	20
8	300	0.829	7.913	0.761	9.300	6	7	14	14	41
9	350	0.821	8.085	0.746	9.567	5	5	8	9	27
10	400	0.848	7.495	0.737	9.849	12	12	6	6	36
11	450	0.846	7.520	0.749	9.593	11	11	11	8	41
12	500	0.854	7.334	0.755	9.467	14	14	13	13	54
13	550	0.808	8.369	0.704	10.560	3	3	3	2	11
14	600	0.851	7.412	0.748	9.562	13	13	10	10	46

6.3.3.3 Value of the N_{gen}

In order to determine the optimal N_{gen} , different GA-ANN models were also developed with a fixed value of 1000 as the N_{gen} and the values of 25-600 of the S_{pop} . As shown in

Fig. 6.7, the RMSE values for all models remains constant after more than 700 generations. Based on this, the value 700 is determined as the optimal N_{gen} .

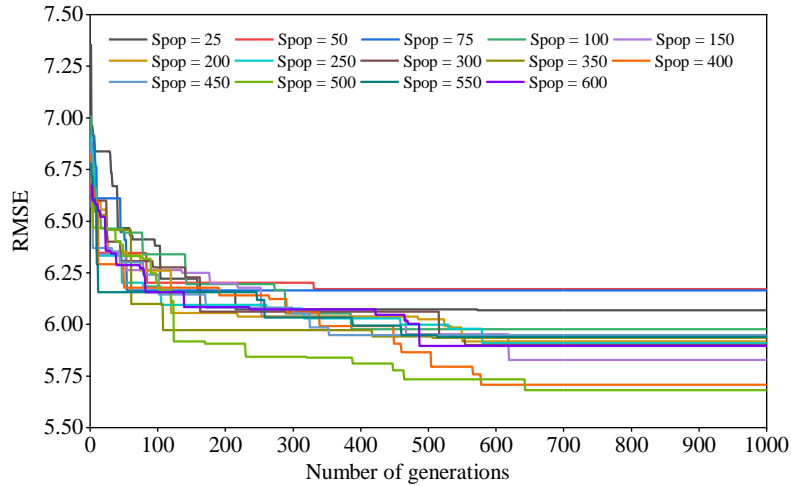


Fig. 6.7 The results of RMSE of different the GA-ANN models with different values of S_{pop}

6.3.3.4 Network modelling

In this step, predicted GA-ANN models were developed with the structure of 6–12–1 and the optimal GA parameters and trained 5 times. The prediction performance indices of the developed models are listed in Table 3. More valuation of the developed models will be carried out in Sect. 6.4.

6.3.4 Classification and regression tree models

Decision tree is a prediction model and a kind of machine learning algorithm (Friedl and Brodley 1997; Buhrman and de Wolf 2002; Sarker et al. 2020). It represents a mapping relationship between object attributes and object values. Each node in the tree represents an object, each fork path represents a possible attribute value, and each leaf node corresponds to the value of the object represented by the path from the root node to the leaf node. CART is a classic decision tree algorithm, which can be applied for classification and regression (Schilling et al. 2016; Choubin et al. 2018). The main steps of CART tree classification are: generation of decision tree; pruning of decision tree. In this paper, Matlab software was utilized to build CART model to predict the value of UCS. Fig. 6.8 shows the final tree prediction model established to predict the UCS value. Based on the final CART model, the testing sets were predicted, and the prediction results are shown in Table 6.4.

Table 6.4 The performance indices of the final developed models

Type	Phase	No.	R ²	RMSE	VAF	Rank value			Total rank
						R ²	RMSE	VAF	
MLR	Training	1	0.365	15.324	0.365	1	1	1	1
	Testing	1	0.405	14.536	0.405	1	1	1	1
MNR	Training	1	0.456	14.222	0.453	1	1	1	1
	Testing	1	0.490	13.505	0.487	1	1	1	1
ANN	Training	1	0.846	7.538	0.846	5	5	5	15
		2	0.842	7.658	0.841	3	3	3	9
		3	0.774	9.149	0.774	1	1	1	3
		4	0.845	7.567	0.845	4	4	4	12
		5	0.828	7.968	0.828	2	2	2	6
	Testing	1	0.784	8.768	0.783	5	5	5	15
		2	0.770	9.120	0.767	4	4	4	12
		3	0.677	10.909	0.666	2	2	2	6
		4	0.764	9.174	0.763	3	3	3	9
		5	0.610	12.555	0.556	1	1	1	3
GA-ANN	Training	1	0.865	7.056	0.865	3	3	3	9
		2	0.881	6.629	0.881	5	5	5	15
		3	0.881	6.641	0.881	4	4	4	12
		4	0.845	7.600	0.844	2	2	2	6
		5	0.841	7.677	0.841	1	1	1	3
	Testing	1	0.802	8.430	0.800	3	3	4	10
		2	0.818	8.175	0.697	4	4	1	9
		3	0.819	8.102	0.815	5	5	5	15
		4	0.793	8.629	0.791	2	2	3	7
		5	0.783	8.892	0.779	1	1	2	4
CART	Training	1	0.938	4.77	0.938	1	1	1	1
	Testing	1	0.800	8.851	0.785	1	1	1	1

6.4 Results and discussion

In the last stage of prediction model development, the ANN and the GA-ANN model were trained five times. The final MLR, MNR, and CART models have been developed as above. The indices of R², RMSE and VAF are utilized to assess these models.

Table 6.4 displays the results of the developed models. A larger total rank value indicates stronger prediction performance, and the optimal model is determined based on this principle. The total rank of all developed models is indicated in Table 6.5. As shown, ANN model No. 1 and GA-ANN model No. 3, have a total rank of 30 and 27, respectively, which indicates the highest performance for the modelling techniques.

Table 6.5 The total rank of all phases of the final developed models

Type	No.	Total rank
MLR	1	1
MNR	1	1
ANN	1	30
	2	21
	3	9
	4	21
	5	9
GA-ANN	1	19
	2	24
	3	27
	4	13
	5	7
CART	1	1

Table 6.6 The best performance indices of the optimal models

Type	No.	Training			Testing		
		R ²	RMSE	VAF	R ²	RMSE	VAF
MLR	1	0.365	15.324	0.365	0.405	14.536	0.405
MNR	1	0.456	14.222	0.453	0.490	13.505	0.487
ANN	1	0.846	7.538	0.846	0.784	8.768	0.783
GA-ANN	3	0.881	6.641	0.881	0.819	8.102	0.815
CART	1	0.938	4.77	0.938	0.800	8.851	0.785

The best performance indices of the optimal models are expressed in Table 6.6. The results depict that the performance level of the multiple regression models can be increased from approximately 0.40 (for MLR model) to approximately 0.78 (for ANN models) based on R² by developing the ANN model. The performance level of the ANN model can be increased based on R² by developing a hybrid GA-ANN model from approximately 0.78 (for ANN models) to approximately 0.82 (for GA-ANN models). The performance level of the ANN model can be increased based on R² by developing a CART model from approximately 0.78 (for ANN models) to approximately 0.80 (for CART models). The results of MLR (with R², RMSE, and VAF values of 0.365, 15.324, and 0.365 for training, respectively, and R², RMSE and VAF values of 0.405, 14.536, and 0.405 for testing, respectively); MNR (with R², RMSE and VAF values of 0.456, 14.222, and 0.453, respectively, for training and R², RMSE and VAF values of 0.490, 13.505, and 0.487 for testing, respectively); ANN (with R², RMSE, and VAF values of 0.846, 7.538,

and 0.846, respectively, for training and R^2 , RMSE and VAF values of 0.784, 8.768 and 0.783 for testing, respectively); GA-ANN (with R^2 , RMSE and VAF values of 0.881, 6.641 and 0.881, respectively, for training and R^2 , RMSE and VAF values of 0.819, 8.102 and 0.815, respectively, for testing), and CART (with R^2 , RMSE and VAF values of 0.938, 4.77, and 0.938, respectively, for training and R^2 , RMSE and VAF values of 0.800, 8.851, and 0.785, respectively, for testing) are obtained for each optimal model of the developed MLR, MNR, ANN, GA-ANN and CART models. Moreover, the correlation index values of R^2 between the measured values of UCS and the predicted values predicted by the optimal MLR, MNR, ANN, GA-ANN and CART models are graphically shown in Fig. 6.9. The comparison between measured UCS and predicted UCS using all three models with testing datasets are shown in Fig. 6.10. The results show that the ANN, GA-ANN, and CART models have better prediction ability than the MLR and MNR models, and the GA-ANN model has slightly higher prediction performance compared with other models.

Table 6.7 Results of the comparative test of the prediction performance for four intervals

Interval	Geological conditions	Average R^2
Interval 1	Good	0.762
Interval 2	Poor	0.548
Interval 3	Good	0.732
Interval 4	Fair	0.273

Finally, comparative tests were set up for four intervals to investigate the influence of geological conditions on UCS prediction performance. The prediction model used in the comparative test is the best GA-ANN model determined for this study, and the average value of R^2 predicted 10 times is utilized as the evaluation index. Table 6.7 shows the comparison result that the prediction performance of intervals 1 and 3 with good geological conditions is better than that of intervals 2 and 4 with poor geological conditions. The reason for this result is that the better the geological conditions of tunnel face, the more complete the rock mass is, and the MWD data of a single borehole can better reflect the geological conditions of the whole tunnel face. Therefore, it can be concluded that when using machine learning algorithms to predict UCS, its prediction performance is affected by geological conditions of the tunnel face. In addition, due to the reduction of the number of training samples, compared with the total datasets of four intervals, the prediction performance of each interval is reduced.

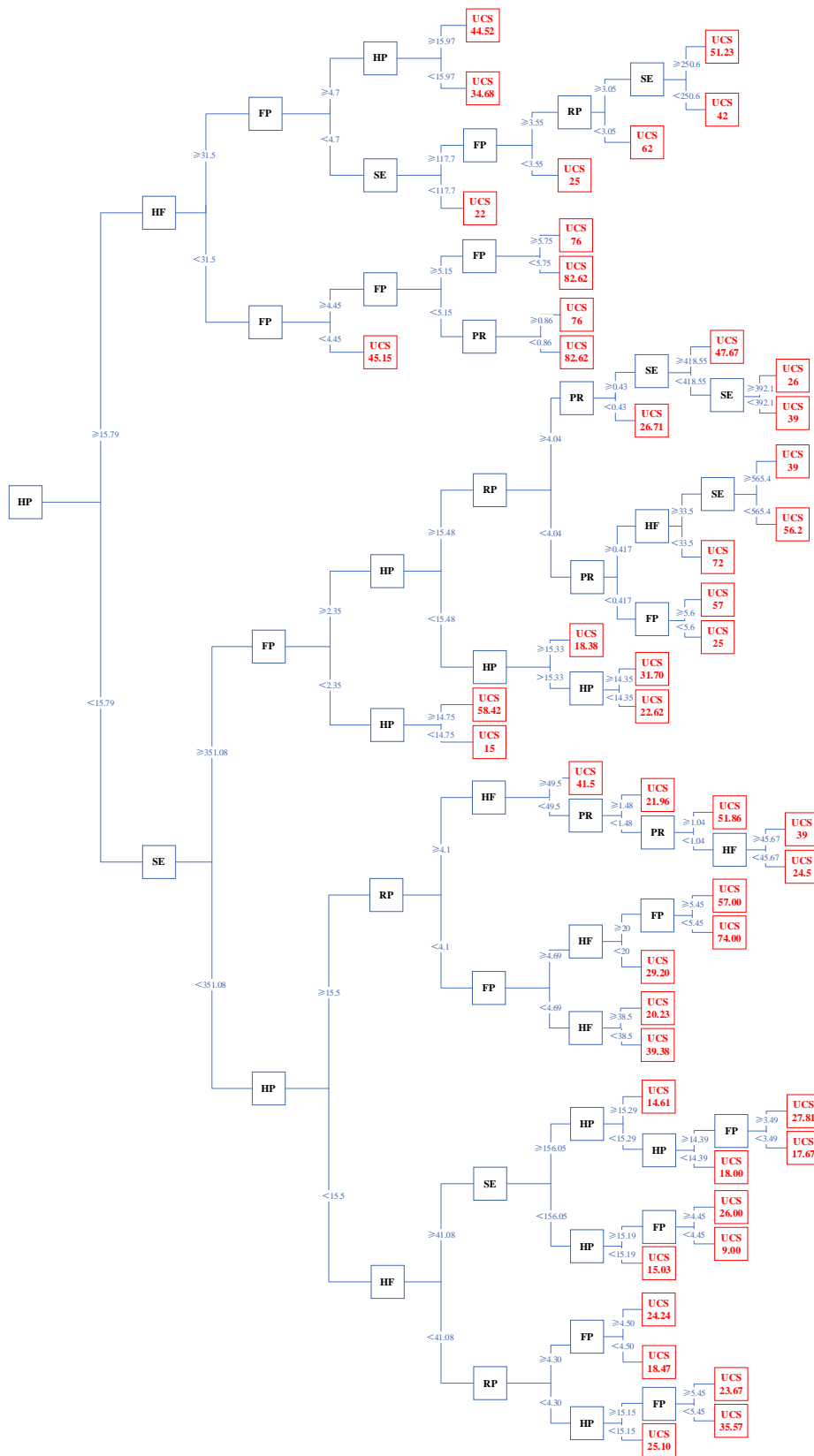
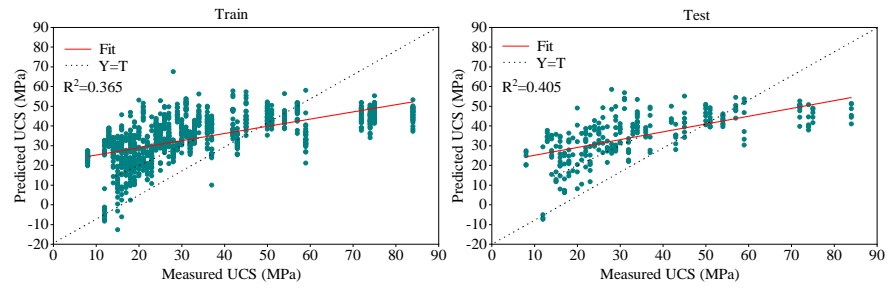
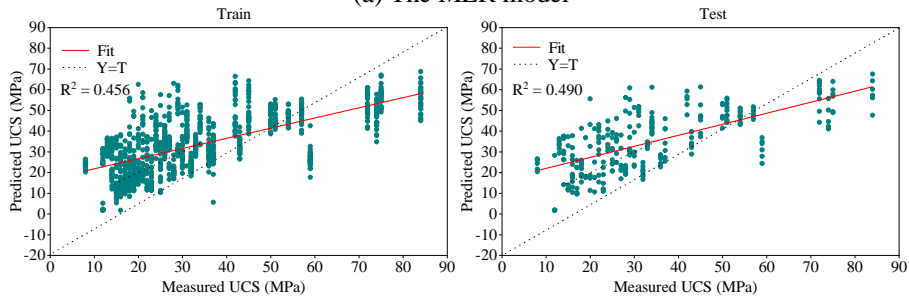


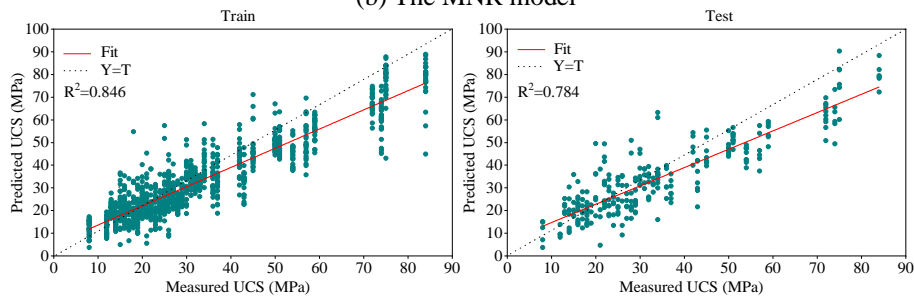
Fig. 6.8 The developed CART model



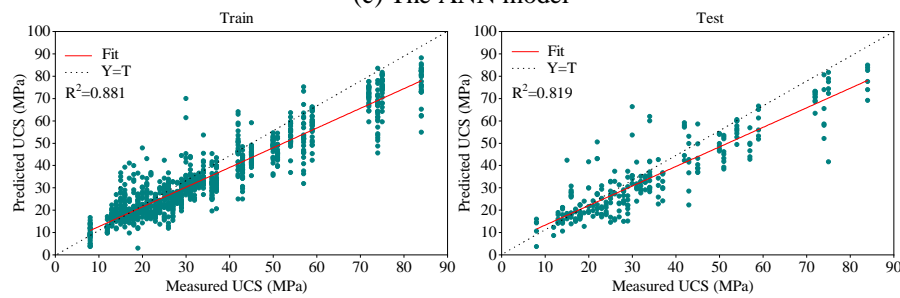
(a) The MLR model



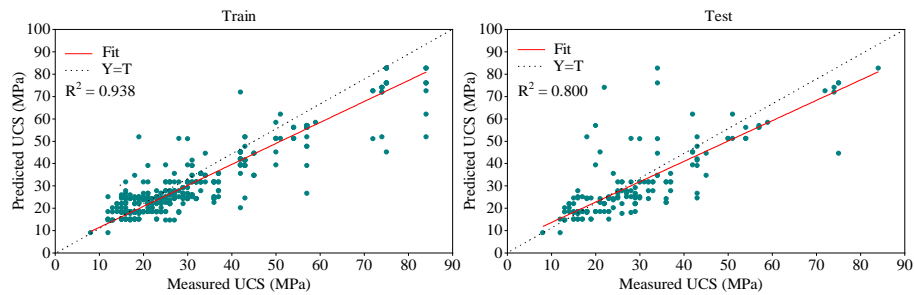
(b) The MNR model



(c) The ANN model

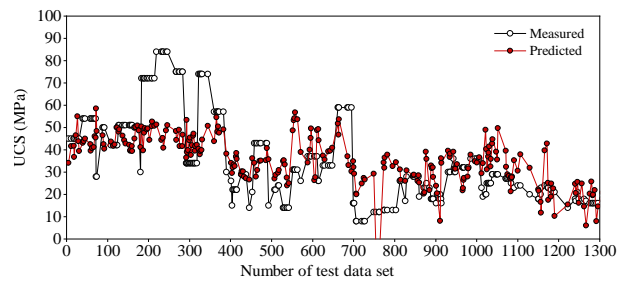


(d) The GA-ANN model

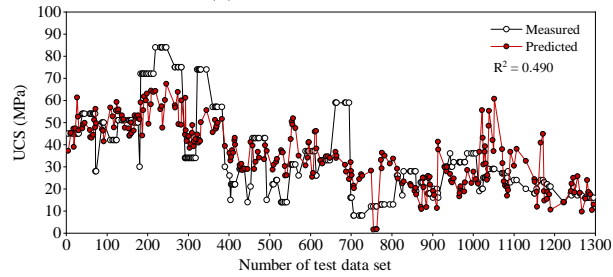


(e) The CART model

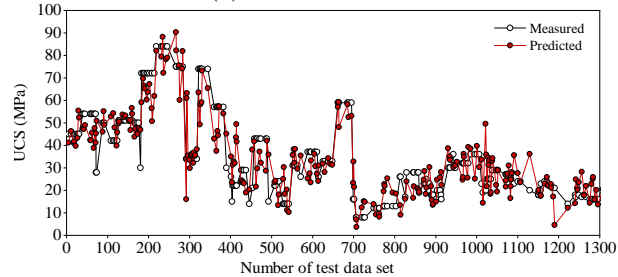
Fig. 6.9 Correlation coefficients of the optimal models



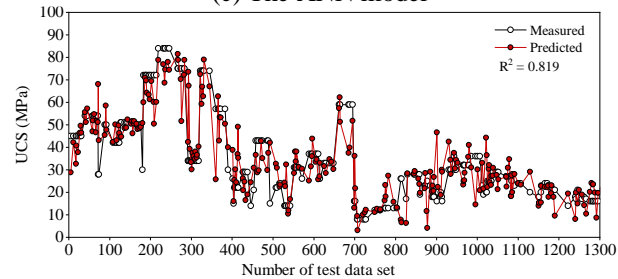
(a) The MLR model



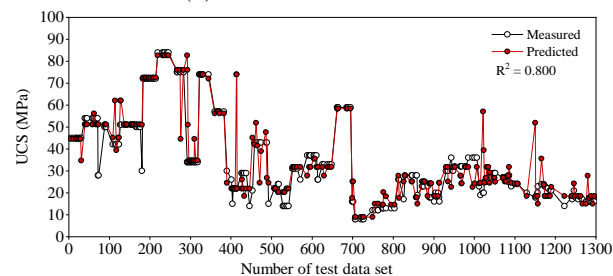
(b) The MNR model



(c) The ANN model



(d) The GA-ANN model



(e) The CART model

Fig. 6.10 Comparison of the predicted and measured UCS in the optimal models with testing data sets

6.5 Conclusions

The accurate prediction of the unconfined compressive strength (UCS) utilizing measurement-while-drilling (MWD) data is one of the important influencing factors in tunnel safety construction. One of the most important advantages of artificial neural network (ANN) methods is that they can solve complex multivariate nonlinear mapping problems. However, ANN methods have significant drawbacks: the disadvantages of slow learning speed and easy to fall into local minima. In this study, therefore, an optimization algorithm of the genetic algorithm (GA), was employed to develop hybrid model of GA-ANN to estimate the UCS value ahead of tunnel face. In addition, ANN is a black-box model, which can not estimate the importance of each input feature to the prediction results of the model, and the interaction between different features can not be understood; while the classification and regression tree (CART) is a white box model, it usually has better interpretability and its internal working principle is easier to explain. The CART model have also been developed. 1350 datasets, including six measure-while-drilling parameters of penetration rate (PR), hammer pressure (HP), rotation pressure (RP), feed pressure (FP), hammer frequency (HF) and specific energy (SE), were collected from the new Nagasaki tunnel (east) of the West Kyushu Line high-speed railway in Japan and set as inputs, while the UCS was set as output. To evaluate the prediction performance of the hybrid models, MLR and MNR models were also developed to estimate the UCS.

A comparison among these developed models was performed by three performance indices, i.e., R^2 , RMSE and VAF. The results indicate that the GA-ANN and CART models have a high degree of accuracy and efficiency. However, the hybrid GA-ANN model has slightly higher prediction performance for predicting the UCS compared with other models. The results of $R^2 = 0.881$ and 0.819 , RMSE = 6.641 and 8.102 and VAF = 0.881 and 0.815 for the training sets and testing sets were obtained for the GA-ANN model, respectively. The findings demonstrate that the GA-ANN model is better than other models. The comparative tests were set up for four intervals to investigate the influence of geological conditions on UCS prediction performance. The comparison result shows that the prediction performance is affected by geological conditions of the tunnel face. It should be noted that the proposed prediction models, especially CART method, can provide reasonable UCS prediction, however, in order to ensure a higher credibility in the process of making the final prediction, it is recommended to use a

combination of different models to evaluate comprehensively.

Although the UCS of the rocks ahead of the tunnel face can be estimated via the MWD data using optimized ANN model, some problems should be considered further. How to apply stronger optimization techniques to further improve the accuracy of prediction. What is the effect of different combination of MWD parameters on prediction results. These are still outstanding issues, so it is necessary to study these further.

References

- Alimoradi A, Moradzadeh A, Naderi R, Salehi MZ, Etemadi A (2008), Prediction of geological hazardous zones in front of a tunnel face using TSP-203 and artificial neural networks. *Tunn Undergr Space Technol*, 23:711-717.
<https://doi.org/10.1016/j.tust.2008.01.001>
- Aoki K, Shirasagi S, Yamamoto T, Inou M, Nishioka K (1999), Examination of the application of drill Logging to predict ahead of the tunnel face. In: *Proceedings of the 54th Annual Conference of the Japan Society of Civil Engineers*, Tokyo, Japan, September 1999. pp 412-413. (In Japanese)
- ASTM D (2006), Standard test method for unconfined compressive strength of cohesive soil. ASTM standard D2166,
- Balasubramanian M, Paglicawan MA, Zhang Z-X, Lee SH, Xin Z-X, Kim JK (2008), Prediction and Optimization of Mechanical Properties of Polypropylene/Waste Tire Powder Blends using a Hybrid Artificial Neural Network-Genetic Algorithm (GA-ANN). *J Thermoplast Compos Mater*, 21:51-69.
<https://doi.org/10.1177/0892705707084543>
- Baykasoğlu A, Dereli T, Tanış S (2004), Prediction of cement strength using soft computing techniques. *Cem Concr Res*, 34:2083-2090.
<https://doi.org/10.1016/j.cemconres.2004.03.028>
- Benyelloul K, Aourag H (2013), Bulk modulus prediction of austenitic stainless steel using a hybrid GA-ANN as a data mining tools. *Comput Mater Sci*, 77:330-334.
<https://doi.org/10.1016/j.commatsci.2013.04.058>
- Bhatti MS, Kapoor D, Kalia RK, Reddy AS, Thukral AK (2011), RSM and ANN modeling for electrocoagulation of copper from simulated wastewater: Multi objective optimization using genetic algorithm approach. *Desalination*, 274:74-80.

- <https://doi.org/10.1016/j.desal.2011.01.083>
- Bieniawski ZT (1974), Estimating the strength of rock materials. *J S Afr Inst Min Metall*, 74:312-320.
- Buhrman H, de Wolf R (2002), Complexity measures and decision tree complexity: a survey. *Theoretical Computer Science*, 288:21-43. [https://doi.org/10.1016/S0304-3975\(01\)00144-X](https://doi.org/10.1016/S0304-3975(01)00144-X)
- Celada B, Galera J, Muñoz C, Tardáguila I The use of the specific drilling energy for rock mass characterisation and TBM driving during tunnel construction. In: *ITA-AITES World Tunnel Congress, 2009. ITA-AITES Budapest*, pp 1-13.
- Choubin B, Zehtabian G, Azareh A, Rafiei-Sardooi E, Sajedi-Hosseini F, Kişi Ö (2018), Precipitation forecasting using classification and regression trees (CART) model: a comparative study of different approaches. *Environmental Earth Sciences*, 77:314. <https://doi.org/10.1007/s12665-018-7498-z>
- Dehghan S, Sattari G, Chehreh Chelgani S, Aliabadi MA (2010), Prediction of uniaxial compressive strength and modulus of elasticity for Travertine samples using regression and artificial neural networks. *Mining Science and Technology*, 20:41-46. [https://doi.org/10.1016/S1674-5264\(09\)60158-7](https://doi.org/10.1016/S1674-5264(09)60158-7)
- Demirdag S, Yavuz H, Altindag R (2009), The effect of sample size on Schmidt rebound hardness value of rocks. *Int J Rock Mech Min Sci*, 46:725-730. <https://doi.org/10.1016/j.ijrmms.2008.09.004>
- Friedl MA, Brodley CE (1997), Decision tree classification of land cover from remotely sensed data. *Remote Sens Environ*, 61:399-409. [https://doi.org/10.1016/S0034-4257\(97\)00049-7](https://doi.org/10.1016/S0034-4257(97)00049-7)
- Galende-Hernández M, Menéndez M, Fuente MJ, Sainz-Palmero GI (2018), Monitor-While-Drilling-based estimation of rock mass rating with computational intelligence: The case of tunnel excavation front. *Autom Constr*, 93:325-338. <https://doi.org/10.1016/j.autcon.2018.05.019>
- Gao D (1998), On structures of supervised linear basis function feedforward three-layered neural networks. *Chinese Journal of Computers*, 1
- Garson GD (1998), *Neural networks: An introductory guide for social scientists*. Sage,
- Goudie AS (2006), The Schmidt Hammer in geomorphological research. 30:703-718. <https://doi.org/10.1177/0309133306071954>

- Grima MA, Babuška R (1999), Fuzzy model for the prediction of unconfined compressive strength of rock samples. *International Journal of Rock Mechanics Mining Sciences*, 36:339-349.
- Hamze-Ziabari SM, Bakhshpoori T (2018), Improving the prediction of ground motion parameters based on an efficient bagging ensemble model of M5' and CART algorithms. *Appl Soft Comput*, 68:147-161.
<https://doi.org/10.1016/j.asoc.2018.03.052>
- Hasanipanah M, Faradonbeh RS, Amnieh HB, Armaghani DJ, Monjezi M (2017), Forecasting blast-induced ground vibration developing a CART model. *Eng Comput*, 33:307-316.
- Hasanipanah M, Noorian-Bidgoli M, Jahed Armaghani D, Khamesi H (2016), Feasibility of PSO-ANN model for predicting surface settlement caused by tunneling. *Eng Comput*, 32:705-715. <https://doi.org/10.1007/s00366-016-0447-0>
- Hatherly P, Leung R, Scheduling S, Robinson D (2015), Technical Note. *Int J Rock Mech Min Sci*, 78:144-154. <https://doi.org/10.1016/j.ijrmms.2015.05.006>
- Hecht-Nielsen R (1987), Kolmogorov's mapping neural network existence theorem. In: the international conference on Neural Networks, New York, 1987. IEEE Press New York, New York, pp 11-14.
- Høien AH, Nilsen B (2014), Rock mass grouting in the Løren Tunnel: case study with the main focus on the groutability and feasibility of drill parameter interpretation. *Rock Mech Rock Eng*, 47:967-983. <http://10.1007/s00603-013-0386-7>
- Holland JH (1992), *Adaptation in natural and artificial systems: an introductory analysis with applications to biology, control, and artificial intelligence*. MIT press,
- Hornik K, Stinchcombe M, White H (1989), Multilayer feedforward networks are universal approximators. *Neural networks*, 2:359-366.
- Hoseinie SH, Ataei M, Mikael R (2012), Comparison of Some Rock Hardness Scales Applied in Drillability Studies. *Arabian Journal for Science Engineering*, 37:1451-1458. <https://doi.org/10.1007/s13369-012-0247-9>
- ISRM UR, Hudson J (2007), *The complete ISRM suggested methods for rock characterization, testing and monitoring: 1974–2006*. Ankara.
- Jadav K, Panchal M (2012), Optimizing weights of artificial neural networks using genetic algorithms. *Int J Adv Res Comput Sci Electron Eng*, 1:47-51.

Jahed Armaghani D, Hasanipanah M, Mahdiyar A, Abd Majid MZ, Bakhshandeh Amnieh H, Tahir MMD (2018), Airblast prediction through a hybrid genetic algorithm-ANN model. *Neural Computing and Applications*, 29:619-629.

<https://doi.org/10.1007/s00521-016-2598-8>

Kahraman S (2001), Evaluation of simple methods for assessing the uniaxial compressive strength of rock. *Int J Rock Mech Min Sci*, 38:981-994. [https://doi.org/10.1016/S1365-1609\(01\)00039-9](https://doi.org/10.1016/S1365-1609(01)00039-9)

Kahraman S, Rostami J, Naeimipour A (2016), Review of Ground Characterization by Using Instrumented Drills for Underground Mining and Construction. *Rock Mechanics Rock Engineering*, 49:585-602. <https://doi.org/10.1007/s00603-015-0756-4>

Kanellopoulos I, Wilkinson GG (1997), Strategies and best practice for neural network image classification. *Int J Remote Sens*, 18:711-725.

Karimi H, Yousefi F (2012), Application of artificial neural network–genetic algorithm (ANN–GA) to correlation of density in nanofluids. *Fluid Phase Equilib*, 336:79-83. <https://doi.org/10.1016/j.fluid.2012.08.019>

Kayabasi A (2012), Prediction of pressuremeter modulus and limit pressure of clayey soils by simple and non-linear multiple regression techniques: a case study from Mersin, Turkey. *Environmental earth sciences*, 66:2171-2183.

Khademi F, Akbari M, Jamal SM, Nikoo M (2017), Multiple linear regression, artificial neural network, and fuzzy logic prediction of 28 days compressive strength of concrete. *Frontiers of Structural Civil Engineering*, 11:90-99.

Khandelwal M, Armaghani DJ (2016), Prediction of Drillability of Rocks with Strength Properties Using a Hybrid GA-ANN Technique. *Geotechnical Geological Engineering*, 34:605-620. <https://doi.org/10.1007/s10706-015-9970-9>

Khandelwal M, Marto A, Fatemi SA, Ghorogi M, Armaghani DJ, Singh TN, Tabrizi O (2018), Implementing an ANN model optimized by genetic algorithm for estimating cohesion of limestone samples. *Eng Comput*, 34:307-317.

<https://doi.org/10.1007/s00366-017-0541-y>

Kosakovsky Pond SL, Posada D, Gravenor MB, Woelk CH, Frost SDW (2006), GARD: a genetic algorithm for recombination detection. *Bioinformatics*, 22:3096-3098. <https://doi.org/10.1093/bioinformatics/btl474>

- Kumar M, Husian M, Upreti N, Gupta D (2010), Genetic algorithm: Review and application. *International Journal of Information Technology Knowledge Management*, 2:451-454.
- Kwon S, Lee C (2018), THM analysis for an in situ experiment using FLAC3D-TOUGH2 and an artificial neural network. *Geotech Eng*, 16:363-373.
<http://doi.org/10.12989/GAE.2018.16.4.363>
- Looney CG (1996), Advances in feedforward neural networks: demystifying knowledge acquiring black boxes. *IEEE Transactions on Knowledge Data Engineering*:211-226.
- McCulloch WS, Pitts W (1943), A logical calculus of the ideas immanent in nervous activity. *The bulletin of mathematical biophysics*, 5:115-133.
<https://doi.org/10.1007/bf02478259>
- Meulenkamp F, Grima MA (1999), Application of neural networks for the prediction of the unconfined compressive strength (UCS) from Equotip hardness. *Int J Rock Mech Min Sci*, 36:29-39. [https://doi.org/10.1016/S0148-9062\(98\)00173-9](https://doi.org/10.1016/S0148-9062(98)00173-9)
- Mohamad ET, Faradonbeh RS, Armaghani DJ, Monjezi M, Majid MZA (2017), An optimized ANN model based on genetic algorithm for predicting ripping production. *Neural Computing Applications*, 28:393-406. <https://doi.org/10.1007/s00521-016-2359-8>
- Mohamad ET, Jahed Armaghani D, Momeni E, Alavi Nezhad Khalil Abad SV (2015), Prediction of the unconfined compressive strength of soft rocks: a PSO-based ANN approach. *Bulletin of Engineering Geology the Environment*, 74:745-757.
<https://doi.org/10.1007/s10064-014-0638-0>
- Mokhtari M, Behnia M (2019), Comparison of LLNF, ANN, and COA-ANN Techniques in Modeling the Uniaxial Compressive Strength and Static Young's Modulus of Limestone of the Dalan Formation. *Nat Resour Res*, 28:223-239.
<https://doi.org/10.1007/s11053-018-9383-6>
- Momeni E, Nazir R, Jahed Armaghani D, Maizir H (2014), Prediction of pile bearing capacity using a hybrid genetic algorithm-based ANN. *Measurement*, 57:122-131.
<https://doi.org/10.1016/j.measurement.2014.08.007>
- Monjezi M, Ghafurikalajahi M, Bahrami A (2011), Prediction of blast-induced ground vibration using artificial neural networks. *Tunn Undergr Space Technol*, 26:46-50.
<https://doi.org/10.1016/j.tust.2010.05.002>

- Nathans LL, Oswald FL, Nimon K (2012), Interpreting multiple linear regression: A guidebook of variable importance. *Practical Assessment, Research Evaluation*, 17
- Nazir R, Momeni E, Armaghani DJ, Amin MM (2013), Prediction of unconfined compressive strength of limestone rock samples using L-type Schmidt hammer. *Electron J Geotech Eng*, 18:1767-1775.
- Nelson MM, Illingworth WT (1991), A practical guide to neural nets.
- Ocak I, Seker SE (2012), Estimation of elastic modulus of intact rocks by artificial neural network. *Rock Mech Rock Eng*, 45:1047-1054. <http://10.1007/s00603-012-0236-z>
- Othman BS, Özcan NT, Kalender A, Sönmez H Multivariate Artificial Neural Network (ANN) models for predicting uniaxial compressive strength from index tests. In: *Geomechanics and Geodynamics of Rock Masses, Volume 1: Proceedings of the 2018 European Rock Mechanics Symposium, 2018*. CRC Press, p 345.
- Peck JP (1989), Performance monitoring of rotary blasthole drills. McGill University Libraries.
- Preacher KJ, Curran PJ, Bauer D (2006), Computational tools for probing interactions in multiple linear regression, multilevel modeling, and latent curve analysis. *Journal of educational behavioral statistics*, 31:437-448.
- Qiu M, Ming Z, Li J, Gai K, Zong Z (2015), Phase-Change Memory Optimization for Green Cloud with Genetic Algorithm. *IEEE Trans Comput*, 64:3528-3540. <https://doi.org/10.1109/TC.2015.2409857>
- Samadi M, Afshar MH, Jabbari E, Sarkardeh H (2020), Prediction of current-induced scour depth around pile groups using MARS, CART, and ANN approaches. *Marine Georesources & Geotechnology*:1-12. 10.1080/1064119X.2020.1731025
- Sarker IH, Colman A, Han J, Khan AI, Abushark YB, Salah K (2020), BehavDT: A Behavioral Decision Tree Learning to Build User-Centric Context-Aware Predictive Model. *Mobile Networks and Applications*, 25:1151-1161. <https://doi.org/10.1007/s11036-019-01443-z>
- Schilling C, Mortimer D, Dalziel K, Heeley E, Chalmers J, Clarke P (2016), Using Classification and Regression Trees (CART) to Identify Prescribing Thresholds for Cardiovascular Disease. *PharmacoEconomics*, 34:195-205. <https://doi.org/10.1007/s40273-015-0342-3>
- Schunnesson H (1996), RQD predictions based on drill performance parameters. *Tunn*

- Undergr Space Technol, 11:345-351.
- Schunnesson H, Pouloupoulos V, Bastis K, Pettersen N, Shetty A Application of computerized drill jumbos at the Chenani-Nashri tunnelling site in Jammu-Kashmir, India. In: Proceedings of 21st International Symposium on Mine Planning and Equipment Selection. New Delhi, India, 2012. pp 729-751.
- Scoble MJ, Peck J, Hendricks C (1989), Correlation between rotary drill performance parameters and borehole geophysical logging. *Mining Science and Technology*, 8:301-312. [https://doi.org/10.1016/S0167-9031\(89\)90448-9](https://doi.org/10.1016/S0167-9031(89)90448-9)
- Shakoor A, Bonelli RE (1991), Relationship Between Petrographic Characteristics, Engineering Index Properties, and Mechanical Properties of Selected Sandstones. *Environ Eng Geosci*, xxviii:55-71. <https://doi.org/10.2113/gsegeosci.xxviii.1.55>
- Sugawara J, Yue Z, Tham L, Law K, Lee C (2003), Weathered rock characterization using drilling parameters. *Canadian geotechnical journal*, 40:661-668.
- Swingler K (1996), Applying neural networks: a practical guide. Morgan Kaufmann,
- Tayyebi A, Pijanowski BC (2014), Modeling multiple land use changes using ANN, CART and MARS: Comparing tradeoffs in goodness of fit and explanatory power of data mining tools. *Int J Appl Earth Obs Geoinf*, 28:102-116. <https://doi.org/10.1016/j.jag.2013.11.008>
- Teale R (1965), The concept of specific energy in rock drilling. *International Journal of Rock Mechanics and Mining Sciences & Geomechanics Abstracts*, 2:57-73. [https://doi.org/10.1016/0148-9062\(65\)90022-7](https://doi.org/10.1016/0148-9062(65)90022-7)
- Toghroli A et al. (2018), Evaluation of the parameters affecting the Schmidt rebound hammer reading using ANFIS method. *Computers and Concrete*, 21 <https://doi.org/10.12989/cac.2018.21.5.525>
- Tsiambaos G, Sabatakakis N (2004), Considerations on strength of intact sedimentary rocks. *Eng Geol*, 72:261-273. <https://doi.org/10.1016/j.enggeo.2003.10.001>
- Wang X, Yuan W, Yan Y, Zhang X (2020), Scale effect of mechanical properties of jointed rock mass: A numerical study based on particle flow code. *Geomech Eng*, 21:259-268.
- Whitley D (1994), A genetic algorithm tutorial. *Statistics Computing*, 4:65-85. <https://doi.org/10.1007/bf00175354>
- Xue X (2019), Application of a support vector machine for prediction of piping and internal stability of soils. *Geotech Eng*, 18:493-502.

<http://doi.org/10.12989/GAE.2019.18.5.493>

Yagiz S (2019), Comments on: The Effects of Density and Porosity on the Correlation Between Uniaxial Compressive Strength and P-wave Velocity by Amin Jamshidi, Hasan Zamanian, Reza Zarei Sahamieh, *Rock Mechanics and Rock Engineering* (2018) 51:1279–1286. *Rock Mechanics and Rock Engineering*, 52:635-638.

<https://doi.org/10.1007/s00603-018-1678-8>

Yagiz S, Sezer EA, Gokceoglu C (2012), Artificial neural networks and nonlinear regression techniques to assess the influence of slake durability cycles on the prediction of uniaxial compressive strength and modulus of elasticity for carbonate rocks. *36:1636-1650*. <https://doi.org/10.1002/nag.1066>

Yazdanmehr M, Anijdan SHM, Bahrami A (2009), Using GA–ANN algorithm to optimize soft magnetic properties of nanocrystalline mechanically alloyed Fe–Si powders. *Comput Mater Sci*, 44:1218-1221.

<https://doi.org/10.1016/j.commatsci.2008.08.003>

Yilmaz I (2009a), A case study from Koyulhisar (Sivas-Turkey) for landslide susceptibility mapping by artificial neural networks. *Bull Eng Geol Environ*, 68:297-306. <https://doi.org/10.1007/s10064-009-0185-2>

Yilmaz I (2009b), A new testing method for indirect determination of the unconfined compressive strength of rocks. *International Journal of Rock Mechanics Mining Sciences*, 46:1349-1357.

Yilmaz I (2009c), A new testing method for indirect determination of the unconfined compressive strength of rocks. *Int J Rock Mech Min Sci*, 46:1349-1357.

<https://doi.org/10.1016/j.ijrmms.2009.04.009>

Yilmaz I, Sendir H (2002), Correlation of Schmidt hardness with unconfined compressive strength and Young's modulus in gypsum from Sivas (Turkey). *Eng Geol*, 66:211-219.

[https://doi.org/10.1016/S0013-7952\(02\)00041-8](https://doi.org/10.1016/S0013-7952(02)00041-8)

Yu S, Guo X, Zhu K, Du J (2010), A neuro-fuzzy GA-BP method of seismic reservoir fuzzy rules extraction. *Expert Syst Appl*, 37:2037-2042.

<https://doi.org/10.1016/j.eswa.2009.06.074>

Zhang L (2016), *Engineering properties of rocks*. Butterworth-Heinemann, Wellington Square, Oxford, UK.

Zorlu K, Gokceoglu C, Ocakoglu F, Nefeslioglu HA, Acikalin S (2008), Prediction of

uniaxial compressive strength of sandstones using petrography-based models. Eng Geol, 96:141-158. <https://doi.org/10.1016/j.enggeo.2007.10.009>

Appendix (A) The results of the developed ANN models with different number of hidden layer nodes

Model No.	Nodes in hidden layer	Index	Result										Average result		Rank value		Total rank
			Iteration 1		Iteration 2		Iteration 3		Iteration 4		Iteration 5		Train	Test	Train	Test	
			Train	Test	Train	Test	Train	Test	Train	Test	Train	Test					
1	1		0.445	0.465	0.498	0.522	0.508	0.531	0.507	0.524	0.508	0.535	0.493	0.516	1	1	2
2	2		0.695	0.646	0.598	0.619	0.591	0.542	0.626	0.647	0.583	0.606	0.619	0.612	2	2	4
3	3		0.679	0.597	0.729	0.704	0.711	0.681	0.726	0.688	0.686	0.623	0.706	0.658	3	3	6
4	4		0.752	0.694	0.738	0.731	0.717	0.643	0.750	0.699	0.733	0.658	0.738	0.685	4	6	10
5	5		0.811	0.781	0.751	0.705	0.731	0.602	0.777	0.711	0.778	0.737	0.770	0.707	9	18	27
6	6		0.749	0.681	0.772	0.739	0.700	0.663	0.686	0.674	0.803	0.759	0.742	0.703	6	17	23
7	7		0.718	0.643	0.751	0.706	0.798	0.692	0.789	0.713	0.728	0.678	0.757	0.686	7	8	15
8	8		0.813	0.727	0.754	0.689	0.759	0.669	0.794	0.729	0.726	0.601	0.769	0.683	8	5	13
9	9		0.798	0.698	0.702	0.655	0.783	0.695	0.809	0.714	0.790	0.683	0.776	0.689	11	9	20
10	10		0.843	0.732	0.808	0.711	0.710	0.665	0.870	0.762	0.796	0.691	0.805	0.712	20	20	40
11	11		0.842	0.743	0.826	0.715	0.696	0.619	0.737	0.644	0.783	0.708	0.777	0.686	12	7	19
12	12		0.846	0.784	0.842	0.770	0.774	0.677	0.845	0.764	0.828	0.610	0.827	0.721	24	25	49
13	13	R ²	0.764	0.711	0.793	0.710	0.785	0.666	0.799	0.696	0.803	0.709	0.789	0.698	14	13	27
14	14		0.791	0.715	0.803	0.700	0.779	0.713	0.780	0.655	0.785	0.664	0.788	0.689	13	10	23
15	15		0.795	0.697	0.636	0.641	0.815	0.697	0.815	0.740	0.808	0.735	0.774	0.702	10	16	26
16	16		0.748	0.683	0.799	0.717	0.840	0.778	0.883	0.556	0.792	0.734	0.812	0.693	21	12	33
17	17		0.708	0.659	0.608	0.600	0.782	0.704	0.804	0.722	0.790	0.696	0.738	0.676	5	4	9
18	18		0.844	0.720	0.787	0.718	0.888	0.721	0.804	0.697	0.813	0.733	0.827	0.718	25	23	48
19	19		0.743	0.666	0.820	0.704	0.743	0.680	0.842	0.756	0.828	0.765	0.795	0.714	16	21	37
20	20		0.761	0.691	0.892	0.739	0.785	0.703	0.762	0.695	0.776	0.675	0.795	0.701	15	15	30
21	30		0.849	0.772	0.842	0.722	0.856	0.715	0.741	0.676	0.803	0.706	0.818	0.718	23	24	47
22	40		0.747	0.664	0.789	0.710	0.801	0.753	0.849	0.758	0.829	0.687	0.803	0.714	19	22	41
23	50		0.771	0.690	0.801	0.698	0.762	0.665	0.807	0.713	0.838	0.730	0.796	0.699	17	14	31
24	60		0.844	0.742	0.798	0.706	0.845	0.780	0.803	0.685	0.879	0.635	0.834	0.710	26	19	45
25	70		0.868	0.771	0.898	0.739	0.725	0.685	0.805	0.725	0.774	0.699	0.814	0.724	22	26	48
26	80		0.803	0.719	0.641	0.646	0.918	0.631	0.801	0.732	0.844	0.726	0.801	0.691	18	11	29

Appendix (A) Continue

Model No.	Nodes in hidden layer	Index	Result	Average result										Rank value		Total rank		
				Iteration 1		Iteration 2		Iteration 3		Iteration 4		Iteration 5		Train	Test	Train	Test	
				Train	Test	Train	Test	Train	Test	Train	Test	Train	Test					
1	1			14.499	13.944	13.633	13.152	13.485	12.943	13.507	13.058	13.489	12.916	13.723	13.202	1	1	2
2	2			10.618	11.291	12.197	11.751	12.373	12.779	11.763	11.234	12.414	11.876	11.873	11.786	2	2	4
3	3			10.919	12.036	10.014	10.312	10.340	10.736	10.060	10.591	10.774	11.790	10.421	11.093	3	3	6
4	4			9.597	10.439	9.850	9.781	10.231	11.393	9.637	10.346	9.968	11.334	9.857	10.659	4	10	14
5	5			8.368	8.829	9.602	10.333	9.982	12.205	9.081	10.266	9.063	9.718	9.219	10.270	9	20	29
6	6			9.638	10.728	9.217	9.683	10.587	10.967	10.779	10.846	8.542	9.307	9.753	10.306	6	18	24
7	7			10.260	11.557	9.590	10.237	8.636	10.657	8.843	10.250	10.048	10.731	9.476	10.686	7	8	15
8	8			8.322	9.998	9.544	10.624	9.440	11.032	8.728	9.887	10.070	12.369	9.221	10.782	8	7	15
9	9			8.647	10.405	10.497	11.155	8.950	10.503	8.410	10.253	8.813	10.678	9.063	10.599	11	11	22
10	10			7.628	9.993	8.443	10.413	10.404	11.092	6.937	9.330	8.696	10.620	8.422	10.290	19	19	38
11	11			7.640	9.649	8.036	10.256	10.608	11.731	9.867	11.340	8.963	10.335	9.023	10.662	12	9	21
12	12			7.538	8.768	7.658	9.120	9.149	10.909	7.567	9.174	7.968	12.555	7.976	10.106	24	25	49
13	13	RMSE		9.346	10.277	8.748	10.418	8.923	11.132	8.624	10.432	8.536	10.307	8.835	10.513	14	13	27
14	14		8.799	10.113	8.526	10.429	9.047	10.099	9.023	11.203	8.959	11.143	8.871	10.598	13	12	25	
15	15		8.764	10.532	11.701	11.461	8.277	10.613	8.290	9.739	8.430	9.816	9.092	10.432	10	16	26	
16	16		9.827	10.955	8.638	10.239	7.697	8.970	6.580	14.303	8.768	9.802	8.302	10.854	21	6	27	
17	17		10.421	11.234	12.158	11.987	8.982	10.347	8.509	10.070	8.840	10.688	9.782	10.865	5	5	10	
18	18		7.590	10.276	8.885	10.158	6.434	10.482	8.520	10.544	8.328	9.879	7.952	10.268	25	21	46	
19	19		9.756	10.989	8.170	10.555	9.745	10.800	7.645	9.436	7.972	9.151	8.658	10.186	16	23	39	
20	20		9.410	10.629	6.334	9.991	8.917	10.348	9.421	10.506	9.123	10.921	8.641	10.479	17	15	32	
21	30		7.477	9.079	7.641	10.135	7.298	10.506	9.784	10.796	8.529	10.366	8.146	10.176	23	24	47	
22	40		9.666	11.066	8.835	10.276	8.581	9.425	7.481	9.306	7.949	10.931	8.503	10.201	18	22	40	
23	50	9.207	10.616	8.576	10.598	9.394	11.018	8.456	10.262	7.778	10.032	8.682	10.505	15	14	29		
24	60	7.603	9.742	8.648	10.450	7.581	8.858	8.542	10.749	6.691	12.347	7.813	10.429	26	17	43		
25	70	7.002	9.278	6.154	10.052	10.095	10.648	8.488	10.003	9.150	10.425	8.178	10.081	22	26	48		
26	80	8.534	10.118	11.702	11.401	5.518	12.929	8.577	9.851	7.601	10.182	8.386	10.896	20	4	24		

7 Summaries

In this thesis, the predication performance of geological conditions and support pattern ahead of tunnel face using intelligent algorithm based on Measurement-While-Drilling (MWD) data. is investigated. The main conclusions are summarized in this chapter.

In chapter 2, the feasibility of using specific energy (a composite parameter of the MWD parameter) in the drilling process to evaluate the geological conditions ahead of tunnel face was analyzed and the relationship between specific energy, rock mass quality score (RQS, an index used in Japan to evaluate the quality of tunnel rock mass), tunnel buried depth and tunnel deformation were compared. As indicated by the results, although the geological conditions of the four intervals of the new Nagasaki tunnel (east) are different, the difference between the average values of specific energy of these intervals is not very large, within 100 J/cm^3 . According to the distributions of specific energy, RQS and buried depth with the mileage of this tunnel, it can be observed that certain correlations exist between these items. In addition, a high correlation exists between specific energy and RQS but the feasibility of employing this correlation to evaluate the geological conditions ahead of the tunnel face is limited. Additionally, although the correlation coefficient values obtained are small and widely dispersed, the geological conditions can be evaluated by comparing the correlation coefficient values and the distribution trend of each variable. The results of comparative analysis show that compared with the distribution of buried depth, a high probability of large tunnel deformation occurs in the region with extensive low specific energy values. The specific energy can reflect the strength of rock and the strength state of rock mass. If the distribution of the specific energy in some areas deviates from the distribution of buried depth, it is considered that abnormal geological conditions exist in this area with a higher probability.

In chapter 3, the feasibility of using artificial neural network (ANN) based on MWD data to predict the support patterns ahead of tunnel face is investigated. Contrast models with different input sample sizes and different ANN structures are developed to analyze the influence of the number of input sample and the hidden layer nodes on prediction performance. The results show that strong correlation exists between MWD data and

support patterns, with the optimal prediction results of the average accuracy (\bar{A}) values corresponding to six classes of support patterns are, respectively, 0.884, 0.866, 0.819, 0.742, 0.805 and 0.920. The selection of tunnel support patterns is mainly influenced by the geotechnical condition of the rock mass. The prediction performance of ANN is affected by the input sample sizes and the hidden layer sizes. An input sample size greater than 6000 samples and a hidden layer size greater than 30 neurons do not have an optimizing effect on the performance. An optimal ANN model is obtained with 6000 samples in input layer and 1 hidden layer with 30 nodes. The ANN draws an excellent performance using only 2% of the total samples as training samples and is a convenient tool for estimating tunnel support pattern selection ahead of tunnel face. It can be stated that the prediction of tunnel support pattern selection using ANN can be used as an essential knowledge of project engineers for improving the safety and reliability of tunnel engineering.

In chapter 4, the effects of all possible combinations of different MWD parameters on the prediction performance were investigated. Four different evaluation indices including average accuracy (\bar{A}), computing-time (\bar{T}), sensitivity and stability were adopted in this study. The results show that the prediction performance of the ANN is affected by the input layer sizes and hidden layer sizes. The combination of 6 feature parameters outperforms the subset of the entire feature parameters in terms of \bar{A} , sensitivity and stability. As a reminder, although \bar{T} increases with the number of feature parameters, there is on huge difference for 2 to 6 feature parameters. A hidden layer size greater than 30 neurons has no optimizing effect on the prediction performance. The sensitivity of each MWD parameter to the prediction performance of the ANN was compared. The sensitivity of the 6 feature parameters is ordered as hammer pressure > feed pressure > hammer frequency > rotation pressure > penetration rate > specific energy. The stability of the prediction performance with four better combinations of feature parameters is ordered as ID 6 > ID 5-1 > ID 5-6 > ID 4-11 (ID 6: combination of PR, HP, RP, FP, HF and SE; ID 5-1: combination of PR, HP, RP, FP and HF; ID 5-6: combination of HP, RP, FP, HF and SE; ID 4-11: combination of PR, HP, RP and FP). The \bar{A} is the same order as the stability. In addition, the stability of the prediction performance of the superior ANN models are analyzed as well. Although it has a slightly larger \bar{T} , the ANN model with 6

feature parameters and the 30 hidden layer nodes is proposed as optimal model considering all indices. The results confirm that the proposed combination with six feature parameters is effective and stable for tunnel support pattern prediction.

In chapter 5, three hybrid ANN models, including GA-ANN, PSO-ANN and ICA-ANN, to predict the RQS using the MWD data obtained from the new Nagasaki tunnel (east) of the West Kyushu line of the high-speed railway project in Japan were proposed. A conventional regression model and simple ANN model were developed. Three hybrid ANNs were established and compared with the developed regression model and ANN model. The coefficient of determination (R^2), root mean square error (RMSE) and variance account for (VAF) indices were calculated to evaluate the prediction capacity of the developed models. The results show that the developed PSO-ANN and ICA-ANN models have higher accuracy and efficiency than other models. However, among the two hybrid models, PSO-ANN hybrid model has slightly higher performance in predicting RQS. The results of $R^2 = 0.875$ and 0.862 , $RMSE=1.584$ and 1.782 and $VAF = 0.875$ and 0.861 for the training dataset and testing dataset, and the results of $R^2 = 0.873$ and 0.857 , $RMSE=1.592$ and 1.812 and $VAF = 0.873$ and 0.855 for the training dataset and testing dataset were obtained for the PSO-ANN model and ICA-ANN model, respectively. In addition, comparative experiments were carried out, and the results showed that the prediction performance is affected by geological conditions.

In chapter 6, the feasibility analysis of using MWD data to predict the UCS of rock mass ahead of tunnel face is conducted. For this purpose, the correlation among MWD parameters and the correlation between MWD parameters and UCS are investigated. And, a machine learning method: ANN, GA-ANN, and CART, to predict of UCS utilizing the MWD data is proposed. As a contrast, the traditional multiple linear/nonlinear regressions models are developed to evaluate the prediction performance of machine learning models. The results indicate that the GA-ANN and CART models have a high degree of accuracy and efficiency. However, the hybrid GA-ANN model has slightly higher prediction performance for predicting the UCS compared with other models. The results of $R^2 = 0.881$ and 0.819 , $RMSE = 6.641$ and 8.102 and $VAF = 0.881$ and 0.815 for the training sets and testing sets were obtained for the GA-ANN model, respectively. The findings demonstrate that the GA-ANN model is better than other models. In addition, it has been verified that the prediction performance is affected by geological conditions. It should be

noted that the proposed prediction models, especially CART method, can provide reasonable UCS prediction, however, in order to ensure a higher credibility in the process of making the final prediction, it is recommended to use a combination of different models to evaluate comprehensively.

Chapter 7 summarizes the major conclusions obtained from the studies of this thesis.